Evaluation of Three Risk Factors for Sporadic Alzheimer's Disease in Human and in Immune-Challenged Wild Type Mice

Dissertation

zur
Erlangung der naturwissenschaftlichen Doktorwürde
(Dr. sc. nat.)
vorgelegt der
Mathematisch-naturwissenschaftlichen Fakultät
der
Universität Zürich

von

Tina Fabia Notter

von

Baden, AG

Promotionskomitee:
Prof. Dr. Jean-Marc Fritschy (Vorsitz)
PD Dr. Irene Knuesel
Prof. Dr. Stephan Neuhauss
Prof. Dr. Roland Martin

Zürich, 2015

ACKNOWLEDGEMENTS

During my dissertation I had the opportunity to be guided by two main supervisors. Both gave me tremendous support to successfully accomplishing my PhD thesis.

I hereby would like to sincerely thank Prof. Dr. Jean-Marc Fritschy. He allowed me to perform my PhD thesis in his lab and also made it possible for me to continue the project after Irene Knuesel has left the Institute. Jean-Marc, you adopted me without hesitation and supported me with your excellent knowledge and expertise. I would have not been able to wrap up my project and write the thesis in the time I managed to do so. I would like to thank you for your discussions related to the project as well as carrier planning and life. I am very grateful for your tremendous support in the application processes that had to be managed during the already intense time of writing. It was a true pleasure to work with you and in your well-equipped and organized lab. Thank you.

I especially thank PD. Dr. Irene Knuesel for giving me the opportunity to start my PhD in the fantastic "Reelin group". Working with you and being a member of your group for almost three years was a great experience. Thank you for introducing me into the fascinating as well as complex world of Alzheimer's disease. The excellent atmosphere in our group motivated us all in doing the best research we could.

I would further like to express my gratitude to the members of my thesis committee, Prof. Dr. Stephan Neuhauss and Prof. Dr. Roland Martin for their guidance, scientific inputs and discussions about my project.

At this point I would like to thank our technicians Tatjana Haenggi (for her patience and endurance in the stereological counting), Christina Koester (for her help with the behavioral experiments), Cornelia Schwerdel and Giovanna Bosshard providing me technical support and knowledge. Special thanks go to Romy Gisler for all your efforts in organizing the lab. I owe my profound gratitude to all the animal care takers, particularly Carmen Brazerol and Dennis Boadum who did an excellent work in taking care of my aging mice cohorts. Big thanks go to Nicole Wildner for your incredible organization skills, all your help with the microscopes, and your good mood and jokes.

Very special and warm thanks go to Karen Haenraets and Sandra Pfister. Karen and Sandra, you have become close friends and your support both work and private related are of tremendous

value to me. Sandra, it was the greatest pleasure to work with you in the Reelin group. Thank you so much for everything (including the formatting of this thesis)! Karen, I am very grateful to have been able to share the same office for almost 3 years. You were always there and took your time independent on your own stress level. Thank you so much for all the proof reading you did during the three years including big parts of this thesis. Special thanks go to Dimi Krstic, who became our mentor once Irene has left the Institute. Thank you for introducing me to the biochemical analyses. Especially thank you for all the great discussions and your skill to always find the appropriate words in any given situation. You are a master of motivation. I hereby would like to thank my co-PhDs of our current group Tilo Gschwind and Mariana Zaichuk. It was fantastic working with you and I am very grateful to having met you and spending the last two years working with you. I would like to thank Mimi I could not have imagined a better master student. Thank you for working one year with me. In addition I would like to thank both Dr. Claire de Groot and PD Dr. Dietmar Benke for their help in biochemical analyses.

I would like to thank my collaborators. I owe my sincere gratitude to Charlotte Burger from the Institute of Anatomy UZH for introducing me to paraffin sectioning of human brain blocks and providing me with her excellent hematoxylin according to Ehrlich protocol and solution. I would like to thank Lutz Slomianka from the Institute of Anatomy UZH, who introduced me to and supported me during, stereological analyses of human brain sections giving me full access to their systems. Especially, I would like to thank him for taking his time in answering all my questions. Special thanks go to PD Dr. Stefanie Kraemer from the Animal Imaging Center of ETH Hoenggerberg for giving me the opportunity to perform the FDG-PET imaging measurements in her facility. I would like to sincerely thank PD Dr. Dr. Matthias Wyss who introduced me to FDG-PET imaging in mice. Matthias, it was a great pleasure working with you. Your skill to introduce me into this novel field of research was remarkable. The two intensive weeks and following analyses were a fantastic experience. Not only were they very inspiring on a scientific level but very amusing. I had a great time! In particular, thank you for your patience in the analysis and your time. I would like to express my gratitude to Claudia Keller, the technician from the animal imaging center. Your expertise and organization skills of PET imaging are incredible. It was a great pleasure working with both of you. We were a great team! In addition I would like to thank Philipp Maechler who taught me how to place a catheter into tail vein of mice.

I sincerely thank Prof. Dr. Urs Meyer from the Institute for Veterinary Pharmacology and Toxicology UZH for his unlimited support during the final phase of my PhD. Urs, your expertise and great help in the prenatal immune challenge model were invaluable. Thank you for your generosity and support. In particular thank you for answering all my questions and introducing me into the field of prenatal developmental models from a different point of view. I hereby owe my gratitude to Dr. Stéphanie Vuillérmot, who performed the cytokine measurements in the third study. Very special thanks go to Dr. Sandra Giovanoli. Without hesitation you took your time and introduced me to, helped me performing and analyzing the Y-maze experiments. It was a fantastic experience working with all of you from the Schwerzenbach Lab. You rock!

I would like to thank my past and present colleagues from the "Fritschy group" and also the members of the "Zeilhofer group" and "Weber group" for the unforgettable and inspiring time I spent with you inside and outside the lab. Special thanks go to Louis Scheurer. It was always a pleasure meeting you in the coffee room or corridors. Again thank you all! I would have never been able to finish my dissertation without having such wonderful and helpful people around me.

Big time thanks go to my present (Karen, Rebecca, Sabine, Monika and Sereina) and former (Sandra, Dimi, Mimi, Fabia, Patrick) office mates for the warm, supportive and joyful atmosphere. I would also like to thank all of you who came and drank coffee here, especially Caro and Laeti. Thanks to all "Jogging ladies" for the enjoyable discussions during running.

I would hereby like to thank Rebecca Das Gupta and Carolin von Schoultz for proofreading the abstract and the "Zusammenfassung". I thank Francine Deprez for her help in formatting this thesis. In addition I thank André Bodmer from Bodmer & Rahn, Zurich. Thank you for your financial support during the start of my PhD. Your donation allowed us to buy the highly valuable human tissue for the first study as well as additional essential lab equipment for biochemical analysis.

Finally, I am deeply thankful to my parents Christian and Kathrin, my elder sister Alexandra and my younger brother Niklaus Notter and all friends (in particular Lisa Basler, Stefania Koller, and Stefanie Fischer) and family (special thanks go to my aunt May Boller for proof reading major parts of this thesis and to my grandmother Ruth Boller for all her motivation and great conversation). Your help and support in all different stages of my life is of indescribable value. I

would have never managed to achieve this without you. Last but not least I thank Max Lutz one of my dearest and best friends. You are always here when I need you. Thank you!

TABLE OF CONTENTS

ZUSAMMENFASSUNG

Die sporadische Alzheimer Krankheit (AD, Englisch: Alzheimer's disease) ist die häufigste altersabhängige Demenz. Sie ist durch eine schnell fortschreitende Abnahme kognitiver Fähigkeiten und durch Neurodegeneration gekennzeichnet. Histopathologisch wird sie durch das Vorhandensein von amyloiden Plaques und neurofibrillären Bündeln, wie auch Entzündungen im Gehirngewebe definiert. Bei Krankheitsbeginn werden typischerweise sowohl Veränderungen im Glukosehaushalt und der Energiezufuhr des Gehirns, als auch Störungen in zentralen cholinergen und monoaminergen Neuronen festgestellt. Im Gegensatz zur sehr seltenen, familiären Form – die durch eine einzelne, dominant vererbbare Mutation ausgelöst wird – stellt die sporadische Form eine multifaktorielle Erkrankung dar, bei der mehrere synergistisch wirkende Mechanismen zum Ausbruch der Krankheit führen können. In den letzten Jahrzehnten wurden eine grosse Anzahl genetischer wie auch umweltbedingter Faktoren identifiziert, die das Risiko, an AD zu erkranken, erhöhen und/oder das Fortschreiten der Krankheit beschleunigen können.

Der Fokus dieser Arbeit lag auf drei spezifischen Systemen, die mit einem solchen erhöhten Risiko in Verbindung gebracht werden konnten. Alle drei zeigen altersbedingte Veränderungen, die sich in frühen Stadien von AD stark verschlimmern. Diese beinhalten die Signalwege von Reelin, chronische, zentrale und periphere Entzündungsreaktionen und das zentrale, noradrenerge (NA) System. In jedem dieser drei Systeme wurden genetische Polymorphismen identifiziert, welche mit einem erhöhten Risiko für AD assoziiert wurden. Diese Polymorphismen befinden sich insbesondere in Genen, welche Bestandteile des angeborenen Immunsystems, Reelin, DBH (Dopamin-β-Hydroxylase – das essenzielle Enzym der Noradrenalin (NA) Synthese) und den β_2-adrenergen Rezeptoren kodieren. In Übereinstimmung mit diesen genetischen Faktoren haben Studien mit transgenen Mausmodellen für AD gezeigt, dass mittels systemischer Immunstimulation, Beeinträchtigung von NA Transmission, und Reduktion von Reelin Expression der Phänotyp dieser AD-transgenen Mäuse stark verschlimmert werden kann.

Darüber hinaus hat unser Labor kürzlich gezeigt, dass Wildtypmäuse bei zweifacher, prä- und postnataler Behandlung ("double hit" Mausmodell) mit dem viralen Imitator polyriboinosinic-polyribocytidilic acid (PolyI:C), welcher eine starke Entzündungsreaktion verursacht, im Alter einen AD-ähnlichen Phänotyp entwickeln. Diese Ergebnisse unterstützen das Konzept, dass chronische Entzündungen eine Schlüsselrolle in der AD Pathogenese spielen. Eine einmalige pränatale Immunstimulation führte schon zu anhaltender, peripherer und zentraler Erhöhung von

proinflammatorischen Zytokinen, erhöhter Produktion des Amyloidvorläuferproteins (APP, Englisch: amyloid precursor protein, dessen Spaltprodukte die Hauptbestandteile der Amyloid-Plaques sind) und erhöhter Phosphorylierung von Tau (dem Hauptbestandteil von neurofibrillären Bündeln). Zudem führte diese, zu Störungen des Kurzzeitgedächtnisses in den gealterten Nachkommen. Die zweite Immunstimulation während des Erwachsenenalters verschlimmerte den histopathologischen Phänotyp noch weiter. Neben der Aktivierung von Mikroglia und Astrozyten konnte eine weitere Zunahme von APP festgestellt werden, begleitet von der Entstehung von APP-positiven Plaques und einer pathologischen Ansammlung von phosphoryliertem Tau-Protein in neuronalen Zellkörpern und Dendriten.

In der *ersten Studie* haben wir die Charakterisierung der altersbedingten Reelin positiven Ablagerungen, welche im Hippocampus von Nagern sowie nicht-humanen Primaten gefunden wurden, auf menschliches hippocampales Gewebe erweitert. Insbesondere interessierte uns die Frage, ob ähnliche Strukturen im menschlichen Gewebe vorhanden sind und ob diese in AD-Patienten vermehrt vorkommen. Unsere Resultate zeigten, dass die Reelin Immunoreaktivität, entgegen der Beobachtung in Tieren, in Corpora Amylacea (CAm) zu finden ist. CAm sind altersbedingte Ablagerungen, die in bestimmten Hirnregionen, einschliesslich faserreicher Gebiete, vorkommen. Sie bestehen hauptsächlich aus Glukosepolymeren und Proteinen. Über ihre genaue Funktion und Entstehungsweise ist bis heute wenig bekannt. Der hohe Anteil an Polysacchariden deutet jedoch daraufhin, dass CAm wahrscheinlich etwas mit gestörtem Glukosehaushalt zu tun haben. Zudem sprechen die dendritischen und axonalen Proteine, die in CAm nachgewiesen wurden, und die Tatsache, dass keine Glia-Markern gefunden werden konnten, für eine neuronale Herkunft. Die Präsenz von Aβ Peptiden und das erhöhte Vorkommen von CAm in faserreichen Hirnarealen deutet daraufhin, dass CAm durch Störungen der axonalen Funktion und Transport entstehen könnten – ein Mechanismus, der kürzlich für die Bildung von senilen Plaques und fibrillären Bündel vorgeschlagen wurde. Dies würde zudem mit den leicht erhöhten CAm levels in der ersten Schicht des Subikulums von AD Patienten im Vergleich zu nicht-dementen Kontrollen übereinstimmen.

Die *zweite Studie* wurde entworfen, um die Auswirkung der Kombination von PolyI:C-ausgelösten Änderungen mit NA Ablation zu prüfen. Unser Ziel war es, zu testen, ob gestörte NA Signalwege die neuropathologischen Veränderungen, die durch Entzündungsreaktionen ausgelöst werden, verstärken und damit eine treibende Kraft in der Pathogenese des sporadischen AD darstellen können. Zusätzlich wollten wir testen, ob die pränatale Immunstimulation eine Langzeitfolge auf die Regenerationsfähigkeit der NA Axonen hat. Dafür wurden C57Bl6/JOla

Wildtypmäuse pränatal und postnatal immunstimuliert und zusätzlich mit dem NA Neurotoxin N-(2-chloroethyl)-N-ethyl-2-bromobenzylamine (DSP-4) einfach oder mehrfach behandelt, um eine Langzeitablation von NA Axonen im Locus Coeruleus (LC) hervorzurufen. Es stellte sich heraus, dass eine pränatale Immunsystemaktivierung während der späten Embryonalentwicklung die Regenerationskapazität der NA Axone beeinträchtigt. Zudem konnten wir bestätigen, dass pränatale PolyI:C Behandlung einen Langzeiteffekt auf das angeborene Immunsystem hat. Jedoch konnte keine Korrelation zwischen diesen beiden Langzeitveränderungen im Gehirn gefunden werden. Dies deutet darauf hin, dass diese unabhängig voneinander entstehen.

Überraschenderweise löste die doppelte Immunstimulation dieser Studie nicht die erwartete, vorherig beschriebene, starke und langanhaltende Immunantwort in gealterten Mäusen aus. Daher fanden wir auch in keiner der unterschiedlich behandelten Tiergruppen AD-assoziierten Veränderungen. Es konnten zudem keine Veränderungen in der Dichte der gemessenen, regenerierten NA Axone nach multiplen DSP-4 Behandlungen nachgewiesen werden. Dies weist darauf hin, dass die Regenerationskapazität gealterter Mäuse mit multipler DSP-4 Behandlung nicht durch die PolyI:C-Stimulation beeinflusst wurde. Zudem hatte die Kombination von PolyI:C und multiplen DSP-4 oder NaCl Behandlungen weder einen Effekt auf das Kurzzeitgedächtnis noch auf den Glukosehaushalt im Gehirn, den wir mittels Positron Emissions Tomographie (PET) untersuchten. Eine *a priori* Analyse, in der wir nur die NaCl-Kontrollgruppe mit der pränatal-PolyI:C-ausgesetzten Gruppe (gefolgt von mehreren NaCl Injektionen) verglichen, zeigte jedoch, dass die pränatal-immunstimulierten Tiere ein mildes aber signifikantes Defizit im Kurzzeitgedächtnis aufwiesen, vergleichbar mit früheren Studien.

Um zu verstehen, woher diese Diskrepanz zwischen unseren und früheren Befunden stammt, haben wir zusätzlich eine *dritte Studie* durchgeführt. In dieser Studie testeten wir, welche Effekte verschiedene PolyI:C Chargen und der genetische Hintergrund zweier Mausstämme, die sich in der An-/Abwesenheit von α-Synuclein unterscheiden, auf die akute systemische Antwort gegenüber einer Immunstimulation haben. Es wurden keine Unterschiede in der Antwort von proinflammatorischen Zytokinen gegenüber PolyI:C Injektion zwischen den verschiedenen Chargen oder Stämmen gefunden. Dies deutet darauf hin, dass die Mäuse in der *zweiten Studie* die zu erwartende PolyI:C-induzierte Immunantwort aufwiesen. Es gibt jedoch eine Menge anderer möglicher Ursachen – wie zum Beispiel eine eventuelle Desensibilisierung ausgelöst durch Stress –, die zu dieser Diskrepanz zwischen der jetzigen und der früheren Studie geführt haben könnten.

Da wir keine wesentlichen Veränderungen nach doppelter Immunstimulation in dieser Studie feststellen konnten, ermöglichen unsere Resultate keine Schlussfolgerung bezüglich der potenziellen Rolle des gestörten NA Systems in der Pathogenese von AD-ähnlichen Veränderungen in Wildtypmäusen. Dennoch konnten wir eine wichtige Interaktion zwischen pränataler Immunstimulation und der axonalen Regenerationskapazität von LC Neuronen in adulten Mäusen nachweisen.

ABSTRACT

Sporadic Alzheimer's disease (AD) is the most common ageing-associated dementia. AD is characterized by fast progression of cognitive decline and neurodegeneration. Histopathologically, it is defined by the presence of amyloid plaques and neurofibrillary tangles (NFTs), as well as neuroinflammation. At disease onset, alterations in brain glucose metabolism and energy supply as well as in the integrity of central cholinergic and monoaminergic neurons are evident. In contrast to the very rare familial form – caused by a single autosomal dominant mutation – sporadic AD represents a multifactorial disease with multiple mechanisms acting synergistically towards developing AD, or not. Over the past decades, a large number of genetic and environmental risk factors have been associated with increasing the risk to develop and/or promoting disease progression.

The general aim of this study was to focus on three such systems known to be affected by normal ageing and exacerbated during early phases of the disease. They include Reelin signaling, chronic neuroinflammation, and the central noradrenergic (NA) system. All three systems comprise genetic polymorphisms associated with increased risk to develop AD. These polymorphisms are notably found in genes encoding components of the innate immune system, Reelin, DBH (dopamine β-hydroxylase – the crucial enzyme in NA synthesis) and β_2-adrenergic receptors. In line with these genetic findings, studies in transgenic animal models of AD have shown that acute systemic inflammatory insult, impaired NA transmission, and the reduction of Reelin expression strongly exacerbate the phenotype in AD-transgenic mice.

Furthermore, in support for a key role of chronic neuroinflammation in the progression of sporadic AD, our lab has recently reported the development of AD-like pathological features in aged wild type mice subjected to a double (prenatal and postnatal) immune challenge, induced by the viral mimic polyriboinosinic-polyribocytidilic acid (PolyI:C) ("double hit" mouse model). The prenatal immune challenge resulted in sustained peripheral and central increase in pro-inflammatory cytokine levels, increased levels of amyloid precursor protein (APP) (its cleavage products are the most abundant component of senile plaques) and increased levels of phosphorylated Tau (pTau) (the main component of NFTs). In addition, prenatal immune activation impaired short-term memory performance in old offspring. The second immune challenge during late adulthood exacerbated the histopathological phenotype, resulting in micro- and astrogliosis, further increase of APP levels and the formation of APP-positive plaques, as well as increased levels of paired helical filaments (PHFs) and a somatodendritic shift of pTau.

In the *first study,* we further characterized the age-dependent formation of Reelin-positive deposits, detected in the hippocampus of rodents and non-human primates, by focusing on Reelin aggregates in human hippocampal tissue. In particular, we aimed to determine whether similar structures are present in the human hippocampal formation and whether they are more abundant in AD patients compared to age-matched non-demented controls. The results revealed that, unlike in rodents and non-human primates, Reelin immunoreactivity was associated with corpora amylacea (CAm) – an ageing-associated structure located in particular brain regions, including fiber-rich domains, mainly consisting of polysaccharides and proteins. Their exact role and/or origin are not yet defined. However, the high content of polysaccharides points towards mechanisms that might involve impaired glucose metabolism. Further, detection of dendritic and axonal proteins, along with the lack of glial cell markers, strongly supports a neuronal origin. The presence of Aβ peptides and the high abundance of CAm in fiber-rich regions further suggest that CAm evolve through impairment of axonal function and transport, as suggested for senile plaque and NFT formation by our lab. In accordance with this hypothesis, we detected a subtle but significant increase in CAm numbers in layer I of the subiculum of AD patients compared to non-demented controls.

The *second study* was designed to explore the significance of combining PolyI:C-induced alterations with NA depletion. Thereby, we sought to determine whether altered NA signaling might be a driving force for neuropathological changes in animals subjected to pre- and/or postnatal immune challenges. In addition, we aimed to investigate whether a prenatal immune challenge could alter the regeneration capacity of NA axons. Wild type C57Bl6/JOla mice were subjected to a prenatal and a postnatal immune challenge, combined with injections of the NA neurotoxin N-(2-chloroethyl)-N-ethyl-2-bromobenzylamine (DSP-4) during ageing to cause enduring depletion of NA axons from the locus coeruleus (LC). We observed that prenatal immune activation during late gestation alters the regeneration capacity of NA axons in adult offspring. Further, we confirmed that prenatal PolyI:C exposure induces long-term alterations on the innate immune system, as reflected, for example, by the increased microglia located in the CA1 region of the hippocampus. However, there was no correlation between the severity of these effects on innate immune system and NA axonal regeneration, suggesting that they occur independently of each other.

Surprisingly, double immune challenges combined with DSP-4 or NaCl injections in this study did not induce the expected strong and sustained immune response in aged mice, as previously described. Thus, we did not observe changes in AD-related proteins between the different

treatment groups. No changes in NA axon densities were detected, indicating that the regeneration capacity after multiple DSP-4 treatments was not affected by PolyI:C exposure (single or double). In addition, combined PolyI:C exposure and DSP-4/NaCl treatment had no effect on short-term memory performance or glucose metabolism measured by PET imaging. *A priori* analysis, however – comparing NaCl control to prenatal PolyI:C exposed followed by NaCl treatments – revealed a mild but significant impairment of non-spatial short-term memory performance, as reported previously.

In search for possible causes for this discrepancy we performed an additional *third study*, where we assessed putative effects of different PolyI:C batches and genetic background of two mouse strains, differing by the presence/absence of α-synuclein, on the acute response toward immune stimulation. We observed no difference in the pro-inflammatory cytokine responses towards PolyI:C between two different batches or strains, indicating that the mice used in this study responded as expected. Several other pitfalls, however, – including desensitization due to stress – could account for these discrepancies between the current and previous study.

Large parts of our results remain inconclusive because of the absence of the required basis to study the role of NA signaling depletion in double immune-challenged mice. Nevertheless, we uncovered important interactions between the effects of a prenatal immune challenge and the regenerative capacity of LC neurons in the adult brain.

I. GENERAL INTRODUCTION

Dementia, Alzheimer's Disease and the Worldwide Burden

Dementia is considered to be the number one disabling disease in age. In 2013, the number of people suffering from dementia was estimated to exceed 44 million worldwide (Alzheimer's disease International, http://www.alz.co.uk/research/statistics). The most common form of ageing-associated dementia is late-onset or sporadic AD with an estimate of almost 36 million patients worldwide (2014, http://www.alzheimers.net/resources/alzheimers-statistics/). AD represents a chronic, progressive disease affecting cognitive functions. In initial stages, patients can still manage to pursue their daily routine. However, with time they become unable to manage normal life and depend on external help (family members or professional care givers). Advanced stages of the disease are characterized by complete loss of self-awareness and independency, requiring around-the-clock professional care.

The incidence of AD doubles every 5 years after the age of 65. The chance to be diagnosed with AD at the age of 85 is, therefore, one in three. With the increasing life expectancy, the worldwide burden of AD will grow tremendously, with an estimate of approximately 100 million people who will suffer from AD by 2050. Thus, it is a major priority to understand the pathological mechanisms underlying this devastating disease and to devise novel treatment strategies allowing at least the prolongation of the phase of independence and relieving the burden upon public health care systems.

Alzheimer's Disease

The psychiatrist and neuropathologist Alois Alzheimer was one of the first scientists who systematically evaluated and correlated neuropathological with neuropsychological changes. More than a century ago, he presented his first case of Auguste D. whom he declared to suffer from a pre-senile form of dementia with the concomitant appearance of two neuropathological characteristics, amyloid plaques and NFTs. Despite intensive research, the pathological mechanisms underlying this form of dementia still remain unresolved. Only 5 drugs are approved today, which mildly improve some cognitive symptoms in early stages of AD patients (Cummings et al., 2014)(Alzheimer's Society, http://www.alzheimers.org.uk).

Next to the progressive and severe loss of cognitive functions, AD is characterized by extensive neurodegeneration, leading to severe brain tissue atrophy of both grey and white matter. Further, early characteristics of the disease include increased oxidative stress, neuroinflammation, as well as impairment in brain glucose uptake and metabolism.

Two types of AD are distinguished. The familial, or early-onset (EOAD) form associated with fast and severe progression and – as indicated by the name – affecting people below the age of 60. EOAD is caused by dominant inheritance of a single mutation located in one of the three genes *PSEN1*, *PSEN2* and *APP*. The second type is the sporadic or late-onset (LOAD) form, which accounts for more than 99% of all AD cases (Iqbal and Grundke-Iqbal, 2010). In this form, ageing is considered the highest risk factor affecting people older than 65. During my PhD thesis, I focused on the latter type.

Two Histopathological Hallmarks

Senile Plaques – Extracellular Amyloid

AD-associated senile plaques consist of many peptides with amyloid-β (Aβ) being the principal biochemical components (Ueda et al., 1993). Aβ comprise different species and arise through proteolytic processing of the APP, a type I transmembrane glycoprotein. The physiological function of APP remains largely elusive. It has, however, been associated to be involved in cognitive performances (Luo et al., 1992, Huber et al., 1993) as well as to participate in the immune response towards injury or other insults (Ciallella et al., 2002, Itoh et al., 2009, Song et al., 2013). APP can be cleaved by 3 enzymes, α-, β-, and γ-secretase. Dependent on the sequence of cleavage, Aβ species (Aβ $_{1\text{-}37,\ -38,\ -40,\ -41,\ \text{or}\ -42}$) are produced (amyloidogenic β-secretase followed by γ-secretase cleavage) or not (non-amyloidogenic α-secretase followed by γ-secretase) (Benilova et al., 2012).

Aβ peptides (in particular Aβ $_{1\text{-}42}$) gained increasing interest by the fact that monomers are prone to self-assemble into oligomers (2-6 peptides) followed by further aggregation into intermediate assemblies (several oligomers), which can grow into fibrils and then assemble into insoluble fibers (fibrillary plaques) (Rambaldi et al., 2009). Oligomers of $A\beta_{1\text{-}42}$ have been shown to have neurotoxic features (Chromy et al., 2003, Ono et al., 2009), notably *in vitro* and/or at high doses. However, the nature and significance of this neurotoxicity for AD pathophysiology remains unresolved (Benilova et al., 2012). Next to putative harmful effects, others have assigned neurotrophic properties to shorter forms of Aβ (Whitson et al., 1989, Yankner et al., 1990).

Amyloidogenic cleavage results further in the production of soluble N-terminal fragment sAPPβ and the APP intracellular domain (AICD), which was suggested to have a nuclear signaling function (von Rotz et al., 2004). In contrast, non-amyloidogenic cleavage produces soluble APPα (sAPPα), which was associated with beneficial effects being involved in synaptic signaling (Furukawa et al., 1996), neuritic outgrowth (Mattson, 1994), synaptogenesis (Roch et al., 1994), synaptic plasticity (Luo et al., 1992, Huber et al., 1993), and cell survival and protection of neurons against excitotoxic, oxidative and metabolic insults (Mattson et al., 1993a, Mattson et al., 1993b); and the intracellular AICD and P3 fragment (Haass et al., 2012). Currently, it is considered that during AD pathogenesis a shift from non- to amyloidogenic processing of APP occurs, resulting in increased production of aggregation prone species. How and where these species are secreted into the extracellular space and where senile plaques are formed is still under debate. In the paragraph – "Inflammation Hypothesis" and Axonopathy in Sporadic AD – I present one possible scenario recently put forward by our lab, suggesting a sequence of events that could lead to the formation of senile plaques in AD.

Neurofibrillary Tangles – Intracellular Amyloid

NFTs – in contrast to plaques – are intracellular accumulations of amyloids following a remarkable pattern in their appearance during the disease progression. In contrast to senile plaques, their appearance and distribution pattern can be positively correlated with the cognitive impairments and thereby are applied as a useful tool in post-mortem staging of AD patients (Braak and Braak, 1991, Arriagada et al., 1992a, Arriagada et al., 1992b). The major component of NFTs is the microtubule (MT) stabilizing protein, Tau, which is concentrated in distal segments of axons. Under normal physiological conditions, Tau is continuously being phosphorylated and dephosphorylated (Iqbal and Grundke-Iqbal, 2010). Phosphorylation of Tau results in its detachment from MTs altering their stability (Ballatore et al., 2007). Excessive or aberrant phosphorylation, including N-terminus and C-terminus of Tau, causes pTau to redistribute from axonal to somatodendritic compartments (Ittner et al., 2010), self-assemble, and interact with other MT stabilizing proteins (MAP1 and MAP2). As a result, MTs are destabilized affecting the stability of axons and impairing transport mechanisms and synaptic function (Grundke-Iqbal et al., 1986, Iqbal and Grundke-Iqbal, 2010) (figure 3, box 1). Self-assembly of pTau leads to the formation of intracellular paired helical filaments (PHFs), which finally form NFTs and neuropil threads that can induce cell death (Ballatore et al., 2007, Iqbal and Grundke-Iqbal, 2010).

Acetylcholine Hypothesis

The earliest hypothesis formulated for the pathophysiology in AD is the "acetylcholine (ACh) hypothesis". It arose during the late 60s to mid-70s, when systematic screenings of postmortem histopathological and biochemical alterations were performed and correlated with the mental state of patients. Several independent reports revealed an early deficit in the neocortical and hippocampal cholinergic system. These reports revealed decreased levels in presynaptic markers of cholinergic transmission, including decreased activity of choline acetyltransferase (ChAT) (Bowen et al., 1976, Davies and Maloney, 1976, Perry et al., 1977), reduced choline uptake (Rylett et al., 1983) and ACh release (Nilsson et al., 1986), reduced levels of nicotinic and muscarinic M2 receptors (Whitehouse et al., 1988, Nordberg et al., 1992) at presynaptic terminals, as well as atrophy of ACh producing cells in the basal forebrain and medial septum (Whitehouse et al., 1982, Francis et al., 1999), whereas levels of postsynaptic muscarinic receptors seemed to be less affected (Whitehouse et al., 1988, Nordberg et al., 1992). In the brain, ACh exerts a neuromodulatory and recently identified deterministic function on neurons affecting learning and memory (Picciotto et al., 2012, Sarter et al., 2014). Further, *in vitro* studies have demonstrated that stimulation of M1 muscarinic receptors resulted in decreased Tau phosphorylation (Sadot et al., 1996). Accordingly, a study performed in mice indirectly showed that muscarinic M1 affects the level of activated GSK-3β a major Tau kinase (see Paragraph "Reelin") (Medeiros et al., 2011). Additional inhibition of GSK-3β activation was revealed to be mediated through α7-nicotinic receptors (Krafft et al., 2012).

Supporting a major role of ACh in AD pathogenesis is the fact that 4 out of the 5 currently approved drugs for the treatment of AD are reversible inhibitors of ACh esterase. Albeit not effective in all patients, these drugs temporarily promote cognitive improvements (Francis et al., 1999, Cummings et al., 2014). However, the inconsistencies in therapeutic success and lack of long lasting effects of these drugs provided strong arguments to question the validity and relevance of the "ACh hypothesis", even though the early and profound loss of cholinergic neurons in AD patients is indisputable. Therefore, the hypothesis has been revised to point out the major role of ACh as a co-factor in sporadic AD (Craig et al., 2011).

APP, *PSEN1* and *PSEN2* – "Amyloid Cascade Hypothesis"

So far, more than 200 autosomal dominant mutations have been identified that cause familial AD. All of them have been identified confined to only 3 different genetic loci, including *APP* itself and the γ-secretase active core proteins presenilin-1 (*PSEN1*) and presenilin-2 (*PSEN2*) (Tanzi and Bertram, 2005, Bird, 2008, Bertram et al., 2010), and are associated with alterations in APP processing. Accordingly, altered ratios in Aβ peptide composition – showing an increase in $A\beta_{1\text{-}42/40}$ ratio – have been reported in the cerebral spinal fluid (CSF) of AD patients. These discoveries led to the formulation of the "amyloid-cascade hypothesis", which postulates that AD is induced by an increased production of neurotoxic Aβ peptides and positions Aβ upstream of all other pathological changes detected in AD (Hardy and Higgins, 1992, Hardy and Selkoe, 2002).

While this hypothesis accounts for many aspects of familial AD, accumulating evidence over the past years indicates that the sporadic form presumably depends on different distinct mechanisms independent of Aβ. This evidence includes genome-wide association studies (GWAS) identifying several susceptibility genes associated with increasing the risk for AD (Bertram et al., 2007, Harold et al., 2009, Hollingworth et al., 2011), none of which identifying *APP* or *PSEN*s as risk genes. Further *in vitro* studies testing a subset of these susceptibility genes revealed that – unlike mutations in familial form – they had no effect on $A\beta_{1\text{-}42/40}$ ratio (Bali et al., 2012). Further various drug trials using active or passive immunization against Aβ were – to date – unsuccessful (Becker et al., 2014, Cummings et al., 2014, Schneider et al., 2014).

ApoE4 - the Strongest Genetic Risk Factor in Sporadic AD

The strongest susceptibility gene identified was *APOE*, encoding the apolipoprotein E (ApoE) (Corder et al., 1993). ApoE belongs to the family of lipoprotein transporters involved in the regulation of lipid plasma levels and uptake into cells. ApoE is enriched in high density-like (HDL) lipoprotein particles, and in the brain, is the most prevalent lipoprotein mainly produced by astrocytes (Pitas et al., 1987a, Grehan et al., 2001). It is involved in cholesterol transport and neuronal uptake via apolipoprotein receptors (Pitas et al., 1987b), which was suggested to play a role in synaptogenesis and maintenance of synaptic connections (Pfrieger, 2003). However, its exact role in cholesterol homeostasis is not yet fully understood (Holtzman et al., 2012). In humans, 3 common apoE isoforms have been identified, apoE2, apoE3, and apoE4 encoded by their corresponding alleles *APOE ε2*, *ε3* and *ε4* with *APOE ε4* being the allele strongest

associated to increase the risk and decrease the age of onset of sporadic AD. Carriers of one allele have an approximate 2-3 fold increased risk, whereas in carriers of two alleles the risk increases to approximately 12-fold (Corder et al., 1993, Gomez-Isla et al., 1996b, Roses, 1996, Bertram et al., 2007, Bertram and Tanzi, 2009). The mechanisms on how apoE4 contributes to the induction and progression of sporadic AD remain unclear; several studies expressing different isoforms in mice suggested an isoform-specific alteration in basal apoE concentration (with apoE2>E3>E4) (Kim et al., 2009). Further apoE4 was shown to deposit in neuritic plaques as well as NFTs (Hartig et al., 1997, Burns et al., 2003) and *APOE ε4* allele carriers were associated with increased levels of Aβ deposits (Barthel et al., 2011). *APOE ε4* carriers display accelerated ageing-associated alterations, including volumetric changes in the hippocampus and the cerebral cortex correlating with cognitive performance (Reiman et al., 1998) and decreased levels of cerebral glucose levels – an early sign associated with AD (Shaw et al., 2007).

ApoE undergoes proteolytic processing resulting in neurotoxic C-terminal truncated fragments detected in transgenic animals (Harris et al., 2003). In contrast to apoE3, apoE4 is more prone to proteolysis likely due to its decreased levels of lipidation (Koldamova et al., 2005, Boehm-Cagan and Michaelson, 2014) and was shown to affect cytoskeletal structures by increasing Tau phosphorylation resulting in the formation of tangle-like inclusions (Huang et al., 2001, Brecht et al., 2004). In addition, isoform specific alterations in the corresponding receptors have been detected (Holtzman et al., 2012). For example, hippocampal CA1 and CA3 pyramidal cells have decreased levels of the apolipoprotein receptor 2 (ApoER2) upon apoE4 compared to apoE3 expression, further impairing lipid transport into neurons and decreasing protective signaling pathways mediated through ApoER2, such as Reelin (see paragraph "Reelin") (Holtzman et al., 2012, Gilat-Frenkel et al., 2014).

Despite the strong evidence for apoE4 involvement in major AD-associated processes, by far not all *APOE ε4* carriers develop AD. As for ACh, apoE4 therefore represents yet another co-factor that promotes the development and progression of AD.

As put forward by (McDonald, 2002), sporadic AD therefore reflects a multifactorial disease with a multitude of mechanisms synergistically setting the path of developing AD, or not. Hence, AD represents a disease with high inter-patient variability in the presentation of pathological symptoms including cognition, appearance of pathological hallmarks, progression and responsiveness to drug treatment. Therefore, it is crucial to investigate ageing-associated changes, which are exacerbated in very early stages of the disease, and thereby classify patients

into different AD subtypes (Iqbal and Grundke-Iqbal, 2010). This approach might then allow us to design AD-subtype targeted drug treatments.

Focusing on the role of chronic inflammation and the contribution of abnormal neurodevelopmental processes to age-related central nervous system (CNS) pathologies, our lab has recently developed a model of sporadic AD in wild type mice. The analysis of this model suggested that AD involves axonopathy of long-projecting neurons primarily induced by ageing-associated changes with chronic neuroinflammation as one of the strongest driver in the disease pathogenesis (Krstic and Knuesel, 2013).

Here, I will briefly introduce this hypothesis and further expand it by considering three additional systems that are affected by normal aging and worsened in early stages of the disease. Thereby, I will present a scenario on how AD onset and progression is determined by these systems, which interact synergistically to shift from healthy to pathological ageing. This scenario formed the starting point of my PhD thesis.

The "Inflammation Hypothesis" and Axonopathy in Sporadic AD

The association of increased brain inflammation with the strongest risk factor *APOE ε4* in sporadic AD (Egensperger et al., 1998) and a multitude of additional data have prompted our lab to develop the "inflammation hypothesis" with axonopathy. Here, I will very briefly delineate the main concepts (reviewed in (Krstic and Knuesel, 2013)).

Next to the two histopathological hallmarks, amyloid plaques and NFTs, a prominent characteristic of AD is neuroinflammation detected by increased levels of pro-inflammatory cytokines, microglia activation and astrogliosis (Castellani et al., 2010). For several decades, neuroinflammation has been considered a consequence of potential toxic protein aggregations and neurodegeneration rather than a cause actively contributing to the onset of disease and its progression. However, the importance of inflammatory processes as a causative factor in neurodegenerative diseases has increasingly gained interest (Frank-Cannon et al., 2009, Pizza et al., 2011b, a). Several susceptibility genes identified in recent GWAS are related to the innate immune system (Harold et al., 2009, Lambert et al., 2009), and positron emission tomography (PET) imaging studies could positively correlate cognitive deficits of patients with the level of microglia markers but not with senile plaques (Edison et al., 2008, Yokokura et al., 2011). A determining role for inflammatory processes have further been shown by studies demonstrating

that inflammatory mediators, such as pro-inflammatory cytokines and chemokines, directly affect APP levels and processing (Goldgaber et al., 1989, Rogers et al., 1999, Ciallella et al., 2002, Itoh et al., 2009, Song et al., 2013) as well as Tau phosphorylation (Li et al., 2003, Bhaskar et al., 2010) (figure 3, box 2).

In vitro and *in vivo* studies have revealed a close link between Aβ and Tau showing that Aβ-induced changes are dependent on the presence of Tau (Rapoport et al., 2002, Roberson et al., 2007). However, the sequence of events leading to the appearance of amyloid plaques and NFTs in specific brain regions during disease progression is still unknown. Albeit several have suggested Aβ plaque formation to occur in the extracellular space by aggregation of secreted Aβ species, electron microscopy studies have identified mitochondria and other organelles in plaque cores, suggesting that initial core formation occurs intracellular (Malamud N and Hirano A, 1974, McGeer et al., 1992). Detection of APP and Aβ species located to axonal swellings (Xiao et al., 2011) – described to appear prior to AD-related pathology in transgenic mice (Stokin et al., 2005, Wirths et al., 2006), monkeys (Martin et al., 1994, Fiala et al., 2007) and AD patients (Yu et al., 2005) – indicates that the origin of amyloid plaques lay in these axonal swellings (Xiao et al., 2011). Intrigued by these and our own findings in regard to ageing-associated, intracellular Reelin accumulation (see Paragraph "Reelin") Krstic and Knuesel propose that these intracellular aggregates evolve through impairment in the axonal transport machinery. Such transport deficits are suggested to be induced by cytoskeleton abnormalities found in AD patients (Iqbal et al., 1986). Our lab has therefore suggested phosphorylation of Tau to be the major link between axonal transport deficits (i.e. microtubule destabilization) and neuroinflammation, as increased tau phosphorylation is induced by inflammatory stimulations. By that we suggest the following scenario to occur:

Ageing is associated with increased neuroinflammation, e.g. due to ageing-associated impairments in mitochondrial function leading to the production of reactive oxygen species, as well as a gradual imbalance in protein metabolism and clearance. Ageing-associated increase in aberrant phosphorylation of Tau – presumably induced by neuroinflammation and oxidative stress – results in its detachment, translocation and aggregation in somatodendritic compartments leading to the destabilization of microtubule networks affecting axonal stability and transport. Consequently, impaired axonal transport is likely to cause intra-axonal accumulation of transported proteins along axons, such as APP and its cleaved fragments, which again further impair the transport machinery (figure 3, box 1). Healthy neurons will clear such accumulations by extrusion of these protein aggregates, which will be then cleared from the extracellular space

by microglia through phagocytosis. Ageing is associated with decreased phagocytic properties of microglia, thereby resulting in the accumulation of extracellular budd-offs, reflected in granular Reelin deposits (Knuesel et al., 2009). In contrast to healthy neurons, old and stressed neurons are likely to accumulate these intracellular aggregates instead of extruding them, likely hindering or fully blocking axonal transport. This will affect presynaptic terminals as they lack supply of newly synthetized proteins, resulting in loss of synaptic function and eventually synapse retraction. The loss of synaptic inputs could alter postsynaptic target cells. Ultimately, the protein clot will grow to a point where axons burst and leak, forming senile plaques and inducing strong, local immune responses. This again affects cells in target areas – both neurons and in particular microglia – which will be further stimulated, generating a vicious cycle promoting disease progression. Finally, axons will degenerate leaving dystrophic neurites and plaques along the projection and target areas and NFTs where the somas of the cells were located.

This hypothesis provides a plausible chain of events occurring in AD, explaining early atrophy detected in areas harboring long-projection neurons (noradrenergic (NA) cells of the LC (see Paragraph "NA system"); ACh expressing cells of nucleus basalis of Meynert and medial septum (see Paragraph "ACh hypothesis"); and entorhinal cortex (EC) layer II pyramidal cells (see Paragraph "Reelin")), as well as the first appearance of NFTs in these areas. It further explains loss in synapses and axonal impairments at early stages of AD (Bozoki et al., 2012, Cross et al., 2013). Finally, it offers a reasonable explanation why the two histopathological hallmarks of AD do not appear in the same brain areas at the same time and why tangles follow a stereotyped regional pattern during disease progression, whereas plaques appear rather diffusely throughout the cerebral cortex (Duyckaerts et al., 1986, Braak and Braak, 1991, Duyckaerts et al., 1997, Krstic et al., 2013).

Reelin

Decreased levels of the extracellular matrix protein Reelin have been associated with early cases of sporadic AD (Chin et al., 2007, Herring et al., 2012). In line polymorphisms spanning the *RELN* locus identified by GWAS have been positively correlated with Tau pathology in healthy aged individuals (Kramer et al., 2011) or directly associated with AD (Seripa et al., 2008).

Reelin is a large glycoprotein, which is expressed and secreted by Cajal Retzius cells located in the marginal zone during development. Serving as stop signal for both migrating neurons and growing fibers, it plays a crucial role in cortical lamination and lamina-specific axonal

innervation (Frotscher, 1998, Derer et al., 2001, Bock et al., 2003, Frotscher et al., 2003, Frotscher, 2010). In the adult brain, Reelin is mainly expressed by remaining Cajal Retzius cells, cortical γ-aminobutyric acid (GABA)ergic interneurons, and layer II pyramidal cells of the EC (Alcantara et al., 1998, Pesold et al., 1998, Martinez-Cerdeno and Clasca, 2002, Martinez-Cerdeno et al., 2002, Abraham and Meyer, 2003). The latter are particularly vulnerable to neurodegeneration (Gomez-Isla et al., 1996a) and are among the first to contain NFTs at the onset of AD (Braak and Braak, 1991).

Functional Reelin dimer binds to two receptors, the very low density lipoprotein receptor (VLDLR) and the ApoER2, both located in the plasma membrane (Trommsdorff et al., 1999). Upon binding of Reelin, receptor dimerization induces the phosphorylation of Dab1, which subsequently activates different cytosolic kinase cascades (Hiesberger et al., 1999, Strasser et al., 2004, Kuo et al., 2005). Reelin signaling in the adult brain was demonstrated to modulate synaptic plasticity through direct alteration of AMPA and NMDA receptor composition (Sinagra et al., 2005, Qiu et al., 2006b) and NMDA receptor phosphorylation at the postsynaptic membrane (Weeber et al., 2002, Beffert et al., 2005). Accordingly, ageing-associated cognitive impairments in rats were correlated with decreased levels of Reelin in the EC (Stranahan et al., 2011). Besides modulating synaptic plasticity, Reelin controls both actin and microtubule cytoskeleton dynamics affecting synaptogenesis (i.e. altering size, shape and density of spines in the dendritic compartments, as well as axonal and dendritic branching and growth) (Del Rio et al., 1997, Borrell et al., 1999, Liu et al., 2001, Jossin and Goffinet, 2007, MacLaurin et al., 2007, Qiu and Weeber, 2007, Niu et al., 2008). Reelin signaling was shown to inhibit the activity of two major Tau kinases – GSK-3β (Beffert et al., 2002, Bock and Herz, 2003, Huang et al., 2005) and CDK5 (figure 3, box 3) (Beffert et al., 2004) – both of which are associated with aberrant hyperphosphorylation of Tau detected in AD (Ballatore et al., 2007, Iqbal and Grundke-Iqbal, 2010). Thus, Reelin deficiency was associated with increased levels of pTau (Hiesberger et al., 1999, Beffert et al., 2002, Ohkubo et al., 2003). *In vitro* studies further revealed Reelin signaling to favor non-amyloidogenic processing of APP associated with increased production and beneficial effects of sAPPα (see Paragraph "Senile Plaques – Extracellular Amyloid") and decreased production of Aβ peptides (Trommsdorff et al., 1998, Hoe et al., 2006). In line with this, reduced Reelin expression in transgenic mice overexpressing two mutations of familial AD resulted in earlier and persistent Aβ plaque formation and the appearance of Tau pathology (Kocherhans et al., 2010).

Reelin is catalytically processed at two sites by the metalloproteinase ADAMTS-4 and 5 as well as the serine protease plasminogen activator (tPA) (Krstic et al., 2012b), resulting in the production of 5 different fragments. The physiological roles of these fragments are currently not understood. Various studies did, however, assign specific roles to the different Reelin domains. Thus, the N-terminal fragment is required for Reelin homo-dimerization – necessary to bind and activate receptors – and signaling (Kubo et al., 2002, Kohno et al., 2009). The receptor binding motif was identified on the central fragment (Jossin et al., 2004, Jossin et al., 2007). The C-terminus is involved in protein folding (de Bergeyck et al., 1997) and is crucial for full activation of signaling pathways (Nakano et al., 2007, Kohno et al., 2009). *In vitro* studies have further shown that N-terminal cleavage occurs after endocytosis of Reelin/receptor complex and secreted into the extracellular space via recycling endosomes (Hibi and Hattori, 2009). In addition, N-terminal fragments are likely to aggregate (Utsunomiya-Tate et al., 2000), whereas Reelin fragments lacking the N-terminus interact with each other forming complexes that exceed the size of functional dimers (Kubo et al., 2002). The role and putative toxicity of these aggregates are unknown.

Reelin expression and processing are affected in normal ageing, resulting in decreased levels of Reelin in interneurons as well as a concomitant accumulation of amyloid-like Reelin deposits in distinct areas of the hippocampus of aged mice (Knuesel et al., 2009). 3D reconstruction electron microscopy analyses, performed in our lab, revealed that these deposits were in part associated with neurites and contain intracellular organelles. Therefore, we suggested them to arise from extrusion processes as a consequence of impaired axonal transport, as described in the paragraph "The "Inflammation Hypothesis" and Axonopathy in Sporadic AD" (Doehner et al., 2012a). In line with axonal deficits induced by increased inflammatory processes, our lab could demonstrate that a prenatal immune challenge significantly accelerates the ageing-associated loss of Reelin in interneurons and appearance of Reelin deposits in the hippocampus (Knuesel et al., 2009). Reduced Reelin expression is likely accompanied by a decrease in beneficial Reelin signaling and thereby affecting basic neuronal mechanisms, including synaptic plasticity and the axonal transport machinery. Therefore, it is conceivable that decreased Reelin signaling might exacerbate inflammation-induced alterations, promoting the shift from healthy to pathological ageing. In accordance with this hypothesis, Reelin expressing cells in the adult brain are found along the olfactory-limbic pathway comprising areas known to be affected at early stages of AD (Bozoki et al., 2012, Cross et al., 2013, Krstic et al., 2013)

Prenatal Exposure to Inflammatory Insults and Its Long-Term Effect on Basal Brain Functions

In recent years, it has become evident that maternal infections during pregnancy can have long-term effects on neurodevelopmental processes, and represent a risk factor for neuropsychiatric and neurodegenerative diseases (Knuesel et al., 2014, Meyer, 2014). The fetal phase is a sensitive period during which external influences on pregnant mothers can induce major changes in the fetal environment and thereby interfere with developmental processes, including the CNS. Accordingly, experimental evidence shows that offspring exposed to prenatal maternal infections can exhibit major alterations in basal brain functions. Long-term modifications of neurotransmitter systems, including GABAergic (Richetto et al., 2014), glutamatergic (Meyer et al., 2008c) and the mesocorticolimbic dopaminergic (Vuillermot et al., 2010, Vuillermot et al., 2012) systems, as well as altered basal state of microglia have been reported (Borrell et al., 2002, Krstic et al., 2012a). These alterations were consistently shown to have long-term effects on behavioral performances in tests of social interaction, anxiety, and cognition. Epidemiological studies, as well as various animal models of prenatal infection, report a clear association between prenatal exposure to inflammatory insults and the development of schizophrenia and autism. Additional evidence links prenatal immune challenges to other neurological diseases, including epilepsy, cerebral palsy, and albeit to a lesser extent to ageing-associated neurodegenerative diseases (Knuesel et al., 2014).

In animal models, prenatal exposure to immune activation can be induced in various ways. Most common is the use of agents that mimic bacterial or viral infections and cause a strong rise in inflammatory cytokine and chemokine levels (Meyer, 2014). The synthetic double-stranded RNA PolyI:C is commonly used to mimic a viral infection. PolyI:C is a potent activator of the innate immune system and induces a robust, but time-limited, acute phase response that is typically seen after virus infections (Cunningham et al., 2007).

PolyI:C is recognized by the transmembrane pattern recognition receptor the toll-like receptor 3 (TLR3) localized on intracellular endosomes. TLR3 receptors are mainly expressed by peripheral dendritic and natural killer cells, which are most responsive towards retroviruses (Muzio et al., 2000). Receptor activation induces intracellular signaling pathways, activating NFκB (Alexopoulou et al., 2001), which triggers the expression of a whole set of immune genes, including inflammatory cytokines, and via the interferon regulatory factor (IRF) induces type I interferon (IFN) expression (figure 1) (Mallard, 2012). Systemic PolyI:C injection acutely upregulates peripheral as well as central cytokines, including increased expression of

cyclooxygenase 2 (COX2) and the pro-inflammatory cytokines interleukin (IL)-1β, IL-6, tumor necrosis factor (TNF)-α, as well as the anti-inflammatory cytokines IL-4 and IL-10 (Cunningham et al., 2007, Mallard, 2012).

In the CNS, TLR3 receptor expression has been identified in microglia (Olson and Miller, 2004, Town et al., 2006) and astrocytes (Farina et al., 2005). Intra-parenchymal injection of PolyI:C into the brain induces local inflammatory responses likely through glial TLR3 signaling (Melton et al., 2003, Town et al., 2006). However, PolyI:C cannot cross the blood brain barrier (BBB) (Mallard, 2012). It was therefore suggested that central immune responses, towards systemic PolyI:C application, reflect an indirect rather than a direct effect of PolyI:C on microglia. Another route through which PolyI:C can affect the CNS through the activation of blood vessel endothelial cells. Accordingly, endothelial cells respond to PolyI:C in a TLR3-dependent manner, including increased production of IFN (Garfinkel et al., 1992, Conaldi et al., 1997, Imaizumi et al., 2004, Ishikawa et al., 2004, Kraus et al., 2004, Imaizumi et al., 2005, Tissari et al., 2005).

Acute elevation of serum cytokine levels in pregnant dams post-PolyI:C treatment has been shown to recover within hours; and yet they are potent enough to persistently alter neurodevelopmental processes (Meyer et al., 2006b, Meyer et al., 2008a). As for maternal serum cytokine levels, acute elevation of cytokines is detectable in the fetal brain (Meyer et al., 2006b, Abazyan et al., 2010). Similar to systemic PolyI:C-induced central changes, alterations in fetal environment represent mostly an indirect PolyI:C effect. There are three putative ways on how PolyI:C administration to pregnant dams can increase fetal cytokine levels: maternal inflammatory cytokines, which, in contrast to PolyI:C, cross the placental barrier (Zaretsky et al., 2004, Dahlgren et al., 2006); cytokines that are produced in uterine and placental cells (Schaefer et al., 2005, Ashdown et al., 2006); and fetal cytokine production, which was shown to be dependent on the fetal developmental stage (Meyer et al., 2006b) (figure 1). Concomitant increases in the levels of IL-10 and TNF-α mRNA and protein in the fetal brain after prenatal immune challenge was only observed when PolyI:C stimulation occurred during late gestation (Meyer et al., 2006b). Therefore, prenatal immune challenges can induce autonomous activation of the fetal immune system, which can outlive acute maternal immune reactions and could therefore affect fetal development during longer time periods.

The time-point of immune activation during gestation is further determinant for the nature of neurodevelopmental alterations caused by prenatal exposure to PolyI:C (Meyer et al., 2006b).

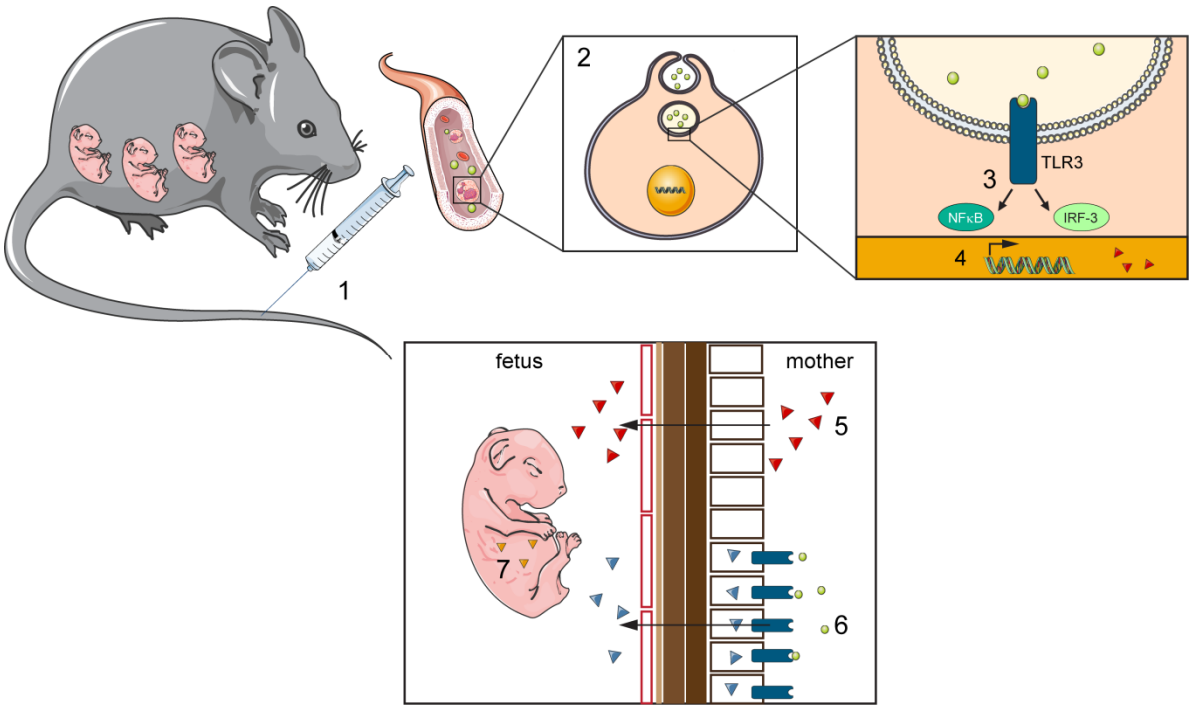

Figure1: Indirect action of PolyI:C to increase fetal cytokine levels and affect the developing embryo. I.v. injected PolyI:C into pregnant dams (1) is endocytosed through leukocytes in the bloodstream (2). TLR3 receptors located in the membrane of endosomes recognize the synthetic double-stranded RNA and activate TLR-specific signaling pathways (3). These include the activation and translocation of NFκB and IRF-3 to the nucleus where they activate a variety of genes resulting in increased production of inflammatory cytokines (red triangles) (4). These maternally produced cytokines enter the bloodstream, some of which can cross the blood-placental barrier (5). Alternatively, PolyI:C may increase fetal cytokine levels through placental-induced cytokine expression (6, blue triangle) or by fetal cytokine production (7, yellow triangle). Images were adapted from www.servier.com.

Stimulation during early and mid-gestation results in multiple structural and functional brain abnormalities used to model schizophrenia and autism-related disorders. Stimulation during late gestation, on the other hand, is associated with subtle and more limited structural and functional alterations still potently disrupting behavioral performances (Meyer et al., 2006b, Meyer et al., 2007, Meyer et al., 2008c). Further, manipulations during late gestation were shown to accelerate ageing-associated processes, including sustained increase in both peripheral and central pro-inflammatory cytokine levels (Krstic et al., 2012a) as well as alterations in Reelin expression and aggregation discussed above (see Paragraph “Reelin”) (Knuesel et al., 2009).

"Double Hit" Model – Wild Type Mouse Model for Sporadic AD

Based on this property of accelerating ageing-associated alterations, our lab sought to use this prenatal manipulation paradigm to study ageing-related changes relevant for sporadic AD. Upon receiving a second immune challenge during adulthood, wild type mice prenatally exposed to PolyI:C at GD17 developed a phenotype closely associated with sporadic AD (Krstic et al., 2012a) (figure 2). PolyI:C administration to pregnant dams caused persistent increases in the levels of both peripheral and central cytokine in offspring up to the age of 15 months. Further, it caused an age-dependent increase in APP levels and alterations in Tau phosphorylation. The second immune challenge at the age of 12 months ("double hit") exacerbated central inflammatory responses, as evidenced by microgliosis and astrogliosis, and caused further elevation of APP levels, appearance of APP-positive plaques, as well as increased levels of PHFs and a distinct relocalization of pTau to somatodendritic compartments.

These findings are in accordance with studies demonstrating a direct link between inflammatory processes and increased expression of APP and Tau phosphorylation. However, most of these studies were performed *in vitro* (Goldgaber et al., 1989, Rogers et al., 1999) or through harsher approaches such as head traumas (Ciallella et al., 2002, Itoh et al., 2009) and intra-parenchymal application of cytokines (Song et al., 2013). A direct link between chronic increases in central cytokine levels and AD-associated changes was further demonstrated by injecting transgenic AD mice with PolyI:C at the age of 9 months, which strongly exacerbated plaque formation and glia activation (Krstic et al., 2012a).

Ever since the identification of familial AD-inducing mutations, a large variety of transgenic mouse models overexpressing one to several of these mutations were produced and used to study both familial and sporadic AD. The combination of prenatal and postnatal PolyI:C exposure in wild type mice, therefore, enabled to develop a more physiological model to study ageing-associated, AD-related pathological changes.

These findings lend strong support to the hypothesis that early inflammatory events are key players in AD pathogenesis. And further suggests that maternal infections during late pregnancy can prime peripheral and central innate immune systems making them more vulnerable to following insults later during life.

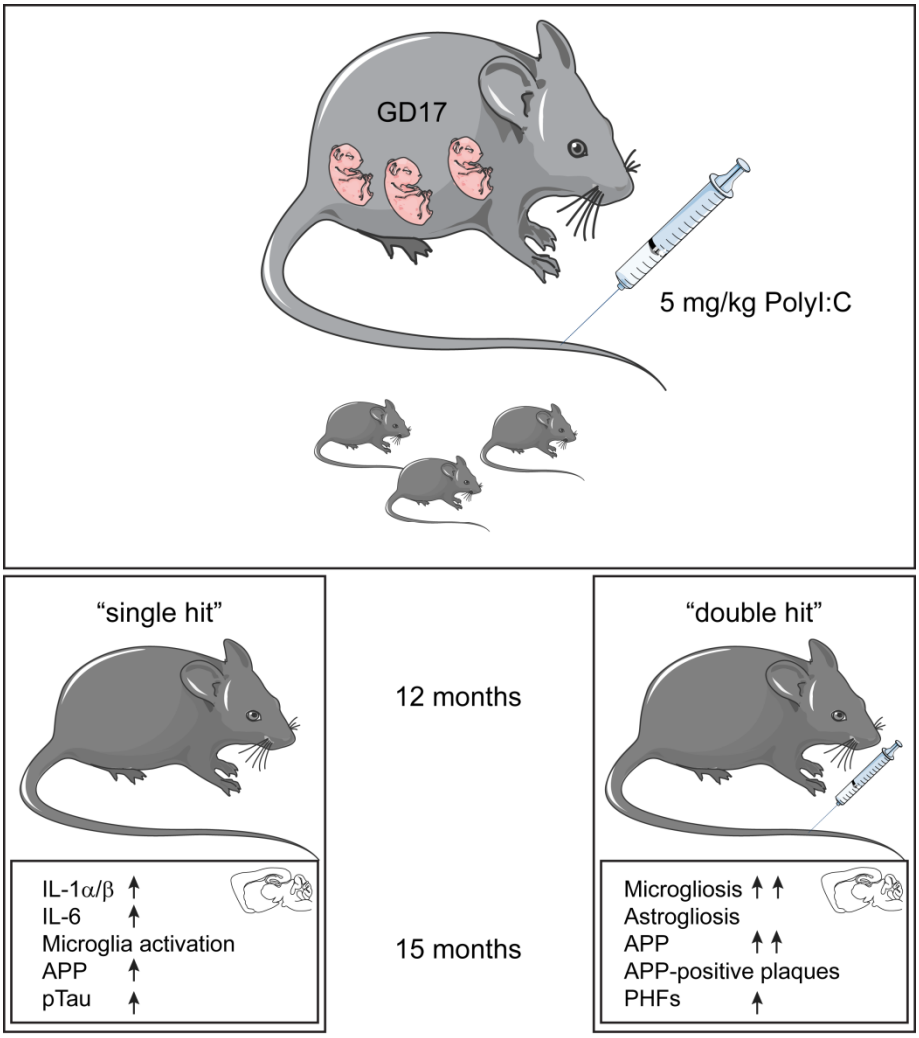

Figure 2: "Double-hit" mouse model for sporadic AD – the central changes. Pregnant dams (GD17) are subjected to 5 mg/kg of PolyI:C (i.v.) injection. 15 months-old offspring that were exposed to only prenatal PolyI:C ("single hit") develop ageing-dependent, AD-related changes, including central increased levels of pro-inflammatory cytokines (IL-1α and -1β and IL-6), activation of microglia and increased levels of APP and pTau. A second PolyI:C (5 mg/kg) exposure at the age of 12 months exacerbates this phenotype detected at the age of 15 months ("double hit"), resulting in more pronounced microglia activation and astrogliosis, further APP elevation and formation of APP-positive plaques as well as increased formation of PHFs and a somatodendritic shift of pTau. Images were adapted from www.servier.com.

The Noradrenergic System in AD

The observation that the appearance of NFTs follows a specific regional pattern during disease progression stimulated research to understand where, how and when the disease starts. And even more so, whether the disease has a focal starting point, as suggested by the "ACh hypothesis" for the nucleus basalis of Meynert. A study systematically analyzing brain tissue from individuals aged between 0-100 reported a striking and highly reproducible ageing-dependent accumulation of hyperphosphorylated Tau in neurons of the LC (Braak et al., 2011). The LC consists of long projecting, noradrenaline (NA) secreting neurons that innervate the entire neuraxis. Intriguingly, the LC has been shown by several early studies to be severely affected in AD patients (Tomlinson et al., 1981, Iversen et al., 1983, Bondareff et al., 1987, Chan-Palay and Asan, 1989, German et al., 1992), in particular at disease onset (Grudzien et al., 2007). Therefore, it has been proposed that the LC could represent a seeding point for the formation of NFT, rather than the previously assumed EC (Braak and Del Tredici, 2012). The reason for its vulnerability to ageing-associated diseases is currently not well understood. However, LC neurons have among the longest axons in the CNS and were shown to exhibit increased mitochondrial oxidative stress during aging (Sanchez-Padilla et al., 2014). In line with the proposed "inflammation hypothesis" and axonopathy for AD, it is conceivable that early changes in Tau hyperphosphorylation and aggregation are induced by increased inflammatory processes resulting from oxidative stress. In addition, oxidative stress has been shown to directly induce Tau assembly (Schweers et al., 1995), further potentiating the formation of PHFs and early NFT-induced neurodegeneration (Grudzien et al., 2007).

NA binds to and exerts its function through G-protein coupled adrenergic receptors (α_1, α_2, β_1, β_2) expressed in the CNS by neurons, astrocytes and microglia. NA is a major neurotransmitter in the sympathetic nervous system, whereas in the brain, it exerts a neuromodulatory function on attention, sleep, arousal, and cognitive processing (Berridge and Waterhouse, 2003). Selective attention modulation was shown in various animal models; stimulation and lesion studies performed in rats revealed that LC-mediated NA release increases attentional shift (Devauges and Sara, 1990, Yu and Dayan, 2005). Tonic LC firing has been further associated with explorative behavior coordinating sensory input, processing, motor output and feedback mechanisms (Usher et al., 1999). Phasic LC firing was shown to be induced by strong task-relevant sensory stimuli associated with behavioral performance. Electrophysiological recordings in non-human primates revealed that LC phasic firing occurs immediately before behavioral output in a forced task-related test paradigm. This led to the suggestion that phasic LC firing is

associated with task-related performance rather than sensory input and processing (Clayton et al., 2004). In general, both tonic and phasic LC firing contribute to subtle modulations that affect accurate and effective decision making.

The NA system was further associated with regulation of sleep pattern. Tonic LC activity decreases during sleep, leading to increased levels of TNF-α and IL1-β, which are both known to induce non-REM sleep (Aston-Jones and Bloom, 1981, Opp, 2005). Intriguingly, an early symptom of AD is disturbance of sleep, which might impair sleep-dependent consolidation processes linked to cognitive performance (Hahn et al., 2014, Ownby et al., 2014, Peter-Derex et al., 2015). However, sleep deficits in AD patients mainly affect total REM sleep duration, which was attributed to modulation of ACh signaling (Platt and Riedel, 2011, Peter-Derex et al., 2015). To what extent decreased NA-mediated signaling accounts for disturbed sleep patterns in ageing and AD remains to be determined.

NA signaling through both α_2, and β_1 receptors expressed on astrocytes was demonstrated to regulate normal brain glucose metabolism by modulating glycogenesis as well as glycogenolysis, and was, therefore suggested to regulate the bioenergetic homeostasis in neurons (Hertz et al., 2007). Intriguingly, *in vitro* studies in cultivated astrocytes revealed that glycogenolysis and glycogenesis are both mediated via the same β-adrenergic signaling pathway involving intracellular cyclic AMP (cAMP) production, but in a time-dependent manner (Sorg and Magistretti, 1992). NA therefore could function as a homeostatic regulator to keep glucose levels in balance and ready to be shuttled to neurons.

NA was further associated with brain energy homeostasis by the fact that NA is a potent modulator of cerebral blood flow. Expression of adrenergic receptors was detected in vascular endothelial cells and smooth muscle cells (Nathanson and Glaser, 1979, Wroblewska et al., 1984, Bacic et al., 1992). LC stimulation was shown to both increase brain perfusion by increasing local cerebral blood flow (Toussay et al., 2013), as well as decreasing it, likely dependent on the frequency of stimulation (Goadsby and Duckworth, 1989). Further NA signaling was linked to increased permeability and thereby facilitating transport via BBB (Raichle et al., 1975, Borges et al., 1994, Sarmento et al., 1994). Light- and electron microscopy studies revealed close associations of LC terminals with astrocytic processes in close proximity of brain microvessel. It was therefore suggested that NA is exerting its modulatory function on brain vasculature via neuron-glia-vasculature interactions (Cohen et al., 1997). The study performed in rats by Toussay et al. showed that activity-dependent increase in brain perfusion is modulated by LC

activity (Toussay et al., 2013). They further supported the neuron-glia-vasculature interaction by the fact that increased blood flow was induced by vasoactive compounds produced and secreted by activated neurons and astrocytes rather than directly by LC innervation.

The immune system is the third system closely related to AD, which is modulated by NA signaling. NA has been identified as a potent permissive modulator of central immune responses by directly affecting microglia cells mainly via β_2-adrenergic receptors. The major role of microglia during normal conditions is to survey brain parenchyma. In response to injury, microglial cells proliferate, migrate to the area of insult, induce phagocytosis of injured brain tissue or pathogens, and express and secrete inflammatory cytokines and chemokine to attract more immune cells, as well as to induce their controlled inflammatory reactions. Upon binding to β_2-adrenergic receptor on microglia, NA decreases the production of pro-inflammatory cytokines (Hetier et al., 1991, Feinstein et al., 2002, Heneka et al., 2010), thereby protecting the brain from avert effects of overproduction and hyper-activation of inflammatory processes (Griffin et al., 1998, Campbell, 2004, Griffin, 2006). While microglia process extension was shown to be dependent on purinergic signaling, soma migration was attributed to NA signaling. This was evidenced in both *in vitro* and *in vivo* studies, showing that NA depletion results in the suppression of microglia migration (Heneka et al., 2010). In line, stimulation of β-adrenergic receptors in cultured microglia promoted migration (Kettenmann et al., 2011). Activation of β_2-adrenergic receptors was shown to promote Aβ phagocytosis and degradation in microglia culture systems (Kong et al., 2010) and was confirmed by depletion studies, resulting in significantly decreased phagocytosis of Aβ (Heneka et al., 2010).

In accordance with these findings, NA lesion studies in transgenic AD animal models revealed sustained exacerbation of AD related phenotypes including strong and early upregulation of neuroinflammatory processes and increased plaque formation, as well as increased cognitive deficits (Heneka et al., 2006, Kalinin et al., 2007, Pugh et al., 2007, Jardanhazi-Kurutz et al., 2010, Rey et al., 2012, Hammerschmidt et al., 2013). Finally, in line with LC atrophy in AD patients, degeneration of LC neurons has been reported in an AD-transgenic mouse model (German et al., 2005).

Taken together, it is conceivable that early loss of protective NA signaling together with increased inflammation during ageing synergistically promote the shift from healthy to pathological ageing (figure 3, box 4).

Impaired Glucose Metabolism, Bioenergetic Insufficiency

High blood pressure, vascular diseases, and insulin resistance (diabetes type II) have early on been associated with increasing the risk of AD. As these diseases are all related to alterations in blood vessel function and thereby thought to affect brain energy supply, bioenergetic deficiency has been proposed to play a fundamental role in the pathological mechanisms involved in AD. The brain - albeit representing only 2% of the body weight is a highly oxygen (app. 20% of total body O_2) and energy (approximately 25% of total body glucose) consuming organ. And the major energy substrate for the brain is blood glucose. Thereby, altering blood supply or blood-brain metabolite exchange can have major effects on brain function.

Hypometabolism has been confirmed by several neuroimaging PET studies showing region-specific reductions in glucose uptake in AD patients (Mosconi et al., 2005). The accuracy of these studies is such that they allow distinguishing between healthy controls and AD patients (Herholz et al., 2002). It was debated, however, whether decreased glucose uptake solely reflected decrease in the demand due to brain atrophy or whether glucose deficiency is apparent before major synapse and neuronal degeneration. Recent studies have demonstrated that impaired glucose uptake is detectable in early prodromal cases, lacking evident brain atrophy (Mosconi, 2005, Mosconi et al., 2008a, Mosconi et al., 2008b). The reasons for these early changes are yet unknown and need further clarification. However, several labs favor the view that systemic alterations – including insulin resistance – induced by western diet play a major role in altering brain glucose uptake mechanisms.

Impairment in brain glucose uptake will eventually lead to energy deficiency, which can have devastating effects on proper neuronal signaling, function – including axonal transport machinery – and thereby cell survival. In addition, combining glucose uptake deficits with alterations in local storage and release upon glycogen turnover – through deficient NA signaling and its modification on brain perfusion and BBB permeability (figure 3, box 4) – could further amplify the deficit in energy supply. In line with this, apoE4 has been associated with increased susceptibility of the BBB to injury (Bell et al., 2012) and decreased glucose metabolism has been detected in young healthy *APOE e4* carriers (Shaw et al., 2007).

Intriguingly, several studies using prenatal immune challenges have detected alterations in metabolic processes, including increase in food intake and fat deposits, glucose tolerance and insulin resistance (Dahlgren et al., 2001, Nilsson et al., 2001, Niklasson et al., 2006, Meyer et al., 2009, Pacheco-Lopez et al., 2013, Meyer, 2014).

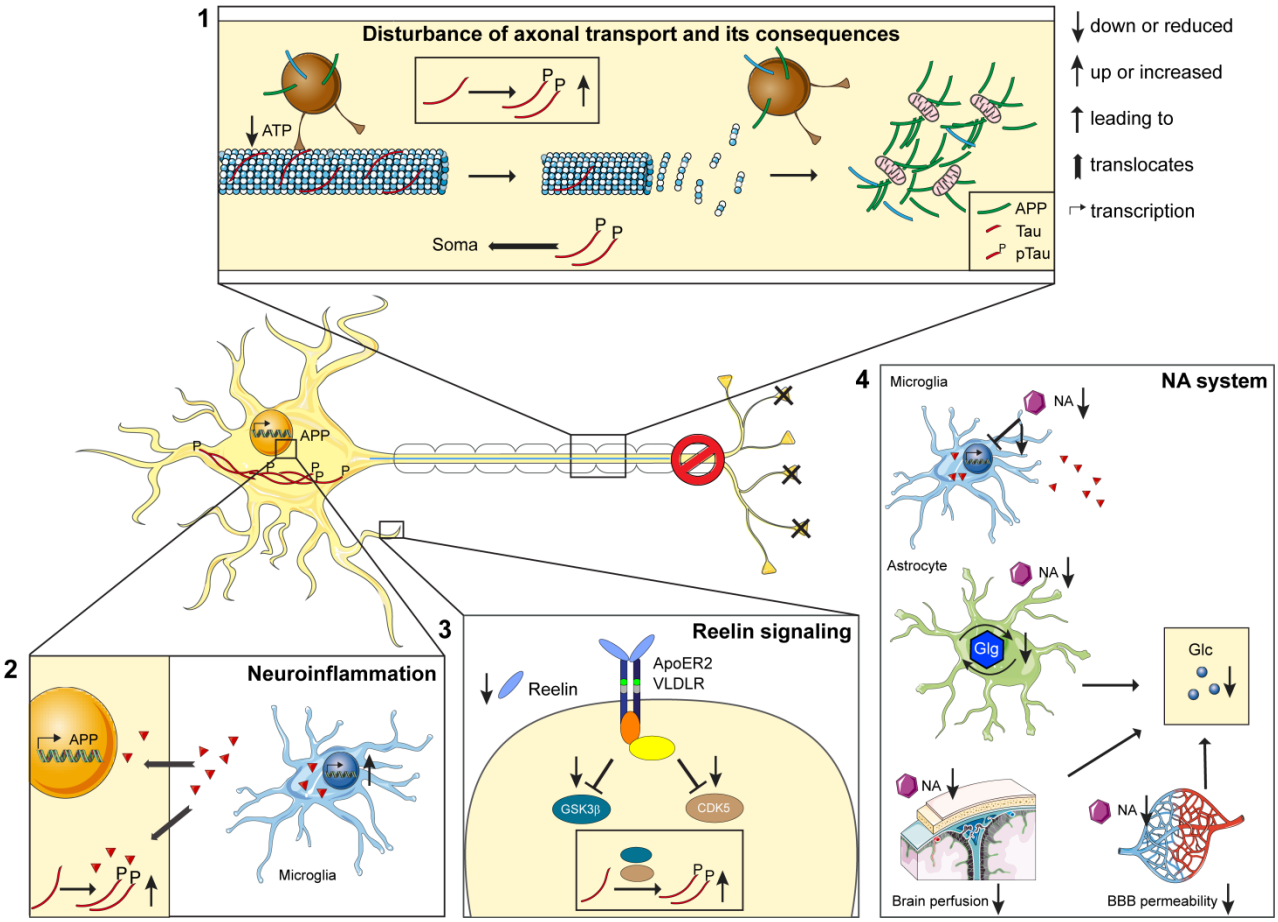

Figure 3: Risk factors in AD and how they affect cytoskeletal integrity and axonal transport promoting the formation of senile plaques and NFTs. Schematic overview of the main neuronal changes (i.e. increased phosphorylation of tau and increased expression of APP) proposed to result in the formation of senile plaques and NFTs (Krstic and Knuesel). Box1: Disturbance of axonal transport and its consequences: Motor proteins kinesin (anterograde transport) and dynein (retrograde transport) are essential to transport cargo from the soma to synapses and vice versa. They are dependent on ATP (the "fuel" for cells) and microtubule (MT) stability, which is assured through microtubule stabilizing proteins such as Tau. Tau is continuously phosphorylated (pTau) and dephosphorylated. Upon phosphorylation it detaches from microtubules. In pathological condition (AD) this equilibrium between pTau and Tau is disturbed resulting in aberrant hyperphosphorylation of Tau, which detaches from MT and translocates to somato-dendritic compartments. This results in destabilization and depolymerization of MT, impairment in transport and to axonal accumulations of cargo proteins (including APP) and other cellular components (such as mitochondria). In addition impaired transport leads to lack of crucial synaptic proteins (e.g. neurotransmitters) resulting in impaired synaptic transmission (overview of neuron). Box2: Neuroinflammation: Ageing is associated with increased inflammation resulting in increased cytokine levels. In the brain of AD patients this activation is increased, resulting in elevated production and secretion of pro-inflammatory cytokines – predominantly produced by activated microglia – that can promote APP transcription and stimulate phosphorylation of Tau in neurons. Box3: Reelin signaling: One of the major targets of Reelin signaling pathways are the two Tau kinases (GSK-3β and CDK5) resulting in their inhibition. MCI and AD patients display decreased levels of Reelin in the brain, and could therefore account for decreased inhibition of GSK-3β and CDK5 leading to increased phosphorylation of Tau and thereby instability of MT network. NA system: decreased NA detected in AD patients could result in: increased levels of pro-inflammatory cytokines due to decreased NA-mediated inhibition of cytokine expression in microglia. Further it might contribute to the glucose and energy (ATP) deficiency detected early in the disease progression by impaired glycogen turnover in astrocytes, decreased brain perfusion and BBB permeability. This bioenergetic deficiency can have major effects on basic cellular processes including axonal transport. Images were adapted from www.servier.com.

In line with this, PET imaging studies could correlate hypometabolism with increased microglia markers in immune-challenged rats (Yokokura et al., 2011). These findings suggest that long-term changes induced by prenatal immune challenges prime – next to players of the innate immune systems – mechanisms involved in systemic metabolism, rendering it more vulnerable to ageing-associated changes and resulting in impaired brain glucose uptake; thereby decreasing brain energy supply as detected in AD.

Taken together, the findings summarized here show how multiple, functionally interconnected systems, can drive normal into pathological ageing, in particular upon conditions of chronic activation of the immune system. During aging, certain environmental and or genetic predispositions might reach a threshold beyond which these systems will synergistically harm each other, resulting in the switch from healthy to self-propagating pathological ageing.

Of all mechanisms discussed above, I have investigated three systems in more detail during my PhD (see overview figure 3). First, I focused on the role of ageing-associated Reelin aggregation detected in animals and expanded these studies to the analysis of Reelin aggregates in the human hippocampal formation. In particular, I wanted to test whether Reelin deposits could be involved in AD pathogenesis, as seen for altered Reelin signaling pathway. Second, I have investigated the role of NA depletion in the "double hit" mouse model of sporadic AD to evaluate whether concomitant alterations of the immune and NA systems are sufficient to potentiate the AD-like phenotype seen in wild type mice, allowing to further study specific changes detected in sporadic AD.

II. AIM OF THE THESIS

The overall objective of this thesis was to evaluate the potential contribution of the three particular systems Reelin, neuroinflammation and the NA system in sporadic AD, using human brain tissue and a modified "double hit" model of pre and postnatal immune challenges in wild type mice.

Study I **Reelin Immunoreactivity in Neuritic Varicosities in the Human Hippocampal Formation of Non-Demented Subjects and Alzheimer's Disease Patients**

In this study we aimed to further characterize ageing-associated changes in Reelin, detected in rodents and non-human primates, by focusing on Reelin deposits in human cortical tissue. we hereby aimed to answer the following questions:

- Does Reelin in the human hippocampal formation accumulate in aggregates similar to those described in other mammals?
- Do these aggregates have a distribution pattern similar to that detected in animals?
- What other components are detected in association with Reelin deposits and what could be their origin?
- Does the amount of Reelin deposits correlate with the occurrence of AD?

To address these questions, we performed immunohistochemistry (IHC) with antibodies against Reelin in paraffin-embedded sections containing the hippocampal formation of AD patients and age-matched, non-demented individuals combined with unbiased stereological analyses. To determine the composition of Reelin aggregates and thereby their putative origin, we performed immunoperoxidase staining supplemented by double immunofluorescence staining using various antibodies against axonal, synaptic, and glial markers. In parallel to this analysis, we performed immunoblotting of cerebrospinal fluid (CSF) of AD patients and age-matched, non-demented controls to examine putative alterations in Reelin levels and proteolytic processing.

Study II **Effects of Acute and Chronic Noradrenergic Axon Depletion in a Wild Type Mouse Model of Sporadic Alzheimer's Disease**

Here, we aimed to understand the significance of combining PolyI:C-induced alterations with NA depletion, in order to determine whether altered NA signaling, known to occur early in AD, might be a driving force for neuropathological changes in animals subjected to pre- and/or postnatal immune challenges. we hereby aimed to answer the following questions:

- Can prenatally evoked long-term changes induced by PolyI:C exposure affect the regeneration capacity of NA axons upon axonal depletion by DSP-4?
- Does chronic NA depletion aggravate AD-like neuropathology in PolyI:C-exposed wild type mice during aging?

To address these questions, we performed IHC and immunoblotting experiments. Due to the large number of mice required for this study, we developed a new technique allowing the preparation of extracts for immunoblotting from one hemisphere and sections for IHC from the other hemisphere, without compromising the quality and sensitivity of either technique. This approach allowed me to study both biochemical and histochemical changes within the brain of the same mouse, minimizing the number of mice. The technique involves perfusion of anesthetized mice with oxygenated artificial CSF (aCSF) to keep brain tissue alive, followed by immediate immersion fixation with paraformaldehyde for histology, and homogenization for biochemistry (see Appendix, Notter et al., 2014 *EJN*). This approach enables direct comparison of protein distribution within brain sections and semi-quantitative analyses of protein levels measured in immunoblotting experiments.

Two cohorts of mice were prepared to address each of these questions. The first cohort was exposed prenatally to PolyI:C and postnatally treated with a single injection of the NA neurotoxin DSP-4 to deplete axons from the LC. Regeneration of these axons and putative activation of microglia and astrocytes, APP expression/processing and Tau phosphorylation and distribution were assessed 3 months later. The second cohort was likewise exposed prenatally to PolyI:C, followed by repeated DSP-4 injections every 3 months during 9 months, and a second exposure to PolyI:C at 12 months of age. At the age of 15 months, cognitive performance was tested behaviorally, brain glucose uptake measured by PET imaging, and histology/biochemistry performed to assess the status of the NA system, activation of microglia and astrocytes, and alterations in APP expression/processing and Tau phosphorylation and distribution.

III. RESULTS

STUDY I: REELIN IMMUNOREACTIVITY IN NEURITIC VARICOSITIES IN THE HUMAN HIPPOCAMPAL FORMATION OF NON-DEMENTED SUBJECTS AND ALZHEIMER'S DISEASE PATIENTS

Tina Notter[1] and Irene Knuesel[1]

[1] Institute of Pharmacology and Toxicology, University of Zurich, Switzerland

Published in Acta Neuropathologica Communications 2013; 1:27

Authors' contributions

All the experimental procedures were carried out by TN. TN and IK wrote the manuscript. Both authors read and approved the final version of the manuscript.

Abstract

Background: Reelin and its downstream signaling members are important modulators of actin and microtubule cytoskeleton dynamics, a fundamental prerequisite for proper neurodevelopment and adult neuronal functions. Reductions in Reelin levels have been suggested to contribute to AD pathophysiology. We have previously reported an age-related reduction in Reelin levels and its accumulation in neuritic varicosities along the olfactory-limbic tracts, which correlated with cognitive impairments in aged mice. Here, we aimed to investigate whether a similar Reelin-associated neuropathology is observed in the aged human hippocampus and whether it correlated with dementia status.

Results: Our immunohistochemical stainings revealed the presence of N- and C-terminus-containing Reelin fragments in CAm, aging-associated spherical deposits. The density of these deposits was increased in the molecular layer of the subiculum of AD compared to non-demented individuals. Despite the limitation of a small sample size, our evaluation of several neuronal and glial markers indicates that the presence of Reelin in CAm might be related to aging-associated impairments in neuronal transport leading to accumulation of organelles and protein metabolites in neuritic varicosities, as previously suggested by the findings and discussions in rodents and primates.

Conclusion: Our results indicate that aging- and disease-associated changes in Reelin levels and proteolytic processing might play a role in the formation of CAm by altering cytoskeletal dynamics. However, its presence may also be an indicator of a degenerative state of neuritic compartments.

Introduction

The increase in human life expectancy has entailed a pronounced rise in age-associated neurodegenerative diseases with the most prominent form being AD, affecting over 26 million people worldwide (Brookmeyer et al., 2007). Despite extensive research performed during the past, no efficient therapies for this progressive brain disease are currently available. Most of the scientific approaches were based on the "amyloid cascade hypothesis" that placed the β- and γ-secretase-generated Aβ peptides as causal factors of the pathophysiology (Hardy and Higgins, 1992, Hardy and Selkoe, 2002). While this may hold true for the familial form of AD with its dominant mutations in either the amyloid precursor protein (*APP*, (Van Broeckhoven et al., 1990, Goate et al., 1991)) or presenilin 1 and 2 (*PSEN*; (St George-Hyslop et al., 1992, Sherrington et al., 1995)) genes, the initiating trigger of the aging-associated, sporadic form of AD is still unknown. Based on recent experimental evidence demonstrating that multiple exposures to viral-like immune challenges are sufficient to induce AD-like neuropathology in aged wild type mice (Krstic et al., 2012a), we were able to identify a crucial trigger and to reconstruct the temporal-spatial sequence of pathophysiological changes that characterize the earliest disease stages. The integration of experimental data of the last three decades enabled us to substantiate and expand our findings to propose a cellular mechanism of the neuropathological changes and its progression across interconnected brain areas that characterize sporadic AD (Krstic and Knuesel, 2013, Krstic et al., 2013). The new hypothesis highlights the detrimental effect of chronic inflammatory conditions on basic cellular functions in long-projection neurons of the olfactory-limbic system during aging. The selective vulnerability of these neurons includes inflammation-induced impairments in the Reelin-mediated signaling pathway across these fundamental neuronal networks (Krstic et al., 2013). By binding to the ApoER2 and the VLDLR (Hiesberger et al., 1999, Strasser et al., 2004), the extracellular matrix protein Reelin regulates cytoskeletal dynamics essential for migrating neurons (D'Arcangelo et al., 1995, Borrell et al., 1999), developing neurites (Leemhuis et al., 2010, Meseke et al., 2013) and adult spines (Pujadas et al., 2010, Freiman et al., 2011). The signaling pathway involves cytosolic cascades that ultimately inhibit the major tau kinases, Glycogen Synthase Kinase 3β (GSK-3β) and Cyclin-Dependent Kinase 5 (CDK5) (Beffert et al., 2002, Bock et al., 2003, Huang et al., 2005), as well as activates the LIM1 kinase and increases n-cofilin phosphorylation (Chai et al., 2009) to modulate both the microtubule and actin cytoskeleton, respectively. Engaging the same signaling pathway, Reelin also exerts a crucial role at adult synaptic sites by modulating NMDA receptor

functions (Weeber et al., 2002, Qiu et al., 2006a, Qiu et al., 2006b, Qiu and Weeber, 2007, Chen et al., 2010). Recent experimental evidence further highlighted that Reelin maintains synaptic plasticity by competing with ApoE4 to prevent the latter from sequestering NMDA, AMPA, and ApoER2 receptors in intracellular compartments (Chen et al., 2010). In line with the well described aging-associated synaptic impairments, Reelin expression has been shown to decline in aging rodents, correlating with hippocampus-dependent learning and memory performance (Knuesel et al., 2009, Stranahan et al., 2011). Furthermore, Reelin accumulates within neuritic varicosities in both rodents and non-human primates (Knuesel et al., 2009, Doehner et al., 2012b), possibly related to the aging associated decrease in Reelin signaling and its protective modulation of cytoskeleton dynamics (Krstic et al., 2013). In agreement with these experimental data, recent GWAS performed in elderly, non-demented individuals identified three single nucleotide polymorphisms (SNPs) in the Reelin gene that significantly correlated with increased Tau phosphorylation and concomitant appearance of NFTs (Kramer et al., 2011). Moreover, immunohistochemical investigations involving human brains revealed significantly decreased levels of Reelin in patients with mild cognitive impairments (MCI) and AD compared to non-demented subjects (Chin et al., 2007, Herring et al., 2012). Further evidence of altered Reelin-mediated signaling in AD was provided by genetic (Seripa et al., 2008) and biochemical studies (Saez-Valero et al., 2003, Botella-Lopez et al., 2010) suggesting that decreased Reelin production may contribute to the initiation and progression of AD by impairing synaptic functions, cytoskeleton stability and proper axonal transport. Interestingly, alterations in Reelin glycosylation, its proteolytic cleavage and degradation, as well as changes in its mRNA stability were shown to be changed in brain homogenates of AD patients (Saez-Valero et al., 2003, Botella-Lopez et al., 2010), further highlighting the importance of proper Reelin signaling during aging.

Here, we investigated the localization and levels of Reelin in the postmortem human brain by selectively assessing its putative accumulation in neuritic varicosities in non-demented elderly and patients with AD by IHC and unbiased stereological analyses. Complementary immunoblotting of corresponding CSF samples was performed to examine potential alterations in Reelin proteolytic processing.

Materials and Methods

Human Tissue

Formalin fixed paraffin-embedded hippocampal brain tissue blocks of eight AD patients and eight age-matched non-demented individuals were obtained from the Netherland Brain Bank, Amsterdam, Netherlands (table 1). Blocks were de- and re-paraffinized with fresh paraffin. Serial sections (5 μm) were cut on a sliding microtome with an inter-section interval of 100 μm. CSF (obtained postmortem from the lateral ventricles with an 18GA 3.50 inch spinal needle) of each subject was thawed and centrifuged at 20'000 rpm for 15 minutes at 4 °C, the supernatant aliquoted and stored at −80°C until further use. Quality assessments revealed no blood contaminations in the CSF samples. Additional test tissue for qualitative investigations included paraffin-embedded sections (cut at 10 μm) from the hippocampus of 6 non-demented and 6 age-matched AD patients (kindly provided by Professor Manuela Neumann, German Center for Neurodegenerative Diseases (DZNE) Tübingen and Institute of Pathology and Neuropathology).

Antibodies

The following antibodies were used: mouse monoclonal anti-Reelin recognizing the N-terminus (clone G10, MAB 5364, Milipore 1:200 and clone 142, MAB 5366, Milipore 1:200); mouse monoclonal anti-Reelin antibodies (C-terminal subrepeats 8A and 8B, 1:200 each, kindly provided by Professor André Goffinet, University of Louvain Medical School, Brussels, Belgium); rabbit polyclonal anti-amyloid β (1-40/42), (AB5076; Millipore, 1:200); mouse monoclonal anti APP-A4, clone 22C11 (MAB348 Millipore, 1:500), mouse monoclonal anti-PHF Tau (clone AT100, MN1060; Thermo Scientific, 1:1000); polyclonal rabbit anti-Tau pS422 (44-764G, Invitrogen,1:1000); rabbit polyclonal anti-GFAP (Z0334, DAKO, 1:2500); mouse monoclonal anti-GFAP (MAB 360, Millipore, 1:10'000); rabbit polyclonal anti-Iba1 (019–19741, Wako Pure Chemical, 1:2000); polyclonal rabbit anti-MAP2(26*) (microtubule-associated protein 2) (AB5622, Chemicon, 1:2000); polyclonal rabbit anti-Synapsin-1 (A-6442, Molecular Probes, 1:1000); polyclonal rabbit anti-Synaptophysin (A010, DAKO, 1:500); rabbit polyclonal anti-α-Synuclein (ab52168, Abcam, 1:250); mouse monoclonal anti-CD 45 (M0701, 1:100, kindly provided by Prof. Karl Frei, Department of Neurosurgery, University Hospital Zürich, Switzerland).

Table 1 Details of human postmortem brain tissue included in the analyses.

NBB-Code	Sex	Age (years)	PMD (h.min)	Brain weight (g)	Braak stages*	Apoe genotype	Clinicopathological data	pH (csf)	[Protein] mg/ml
Controls									
07-082§	M	81	7.55	1194	2 0	3/3	Renal insufficiency and decompensatio cordis	6.23	4.6
00-142	F	82	5.30	1260	1 A	3/2	Myocardial infarct	6.60	3.14
03-061	F	83	5.30	1274	1 B	3/2	Squamous cell carcinoma of the left maxilla	6.48	3.62
05-083	F	85	5.00	1217	1 B	3/3	Multi organ failure after a ruptured abdominal aneurysm	6.72	4.46
98-157§	M	85	5.13	1383	2 A	3/2	Cardiac tamponade	6.23	2.92
04-061	F	88	6.15	1121	? B	3/3	Old age	6.98	2.79
96-105§	M	88	5.40	1120	4	4/3	Cardiac arrest	6.65	1.4
96-044§	F	90	5.50	1046	2 A	3/3	unknown	7.00	2.79
AD									
06-013§	M	81	4.50	1193	4 C	4/4	Dehydration, sepsis?	6.42	3.02
09-105	F	82	5.25	999	5 C	n/a	Heart failure	6.08	3.63
00-138§	F	84	5.15	1098	5 C	3/3	Pneumonia with dehydration	6.65	2.2
97-093	M	86	5.35	1250	5 C	4/3	CVA/Myocardial infarction	6.39	1.93
06-044	F	86	5.55	930	4 B	4/3	Cachexia	6.85	1.8
04-064	F	88	6.25	1079	5 C	3/3	Organ failure due to dehydration	6.60	2.88
97-003§	M	88	5.10	984	5 B	4/3	Pneumonia	6.45	2.38
96-049	F	90	3.50	925	5	4/3	Dehydration	7.02	2.81

*According to (Braak and Braak, 1991, 1995). PMD = postmortem delay

§ Tissue blocks containing hippocampus and EC.

Immunohistochemistry

Immunoperoxidase Staining

Sections were deparaffinized in xylol (3 times for 3 minutes), rehydrated in decreasing ethanol concentrations (twice 100%, 96%, 70% and twice dH2O for 3 minutes each) and washed in 50 mM Tris-saline, pH 7.4 (1xTris). The following antigen retrieval techniques were applied: two 5-minute citrate buffer microwave irradiations at 800 W (to visualize Reelin-producing cells with anti-Reelin 142 antibody, see additional file 1: figure S1), 10-minute citrate buffer microwave irradiation at 80°C, either followed by a 10-minute pepsin treatment (Doehner et al., 2010) or not, and a 5-minute 95% formic acid (FA) treatment (to visualize Aβ plaques). Furthermore, a 10-minute 3% H2O2/methanol treatment was used to block endogenous peroxidase reactivity. Sections were then incubated for 30 min in blocking solution (1xTris containing 5% normal horse serum, 5% normal goat serum, 4% of bovine serum albumin (BSA)), transferred to the primary antibody solution (diluted in 1xTris, containing 2.5% normal horse serum, 2.5% normal goat serum, 2% BSA) for overnight incubation at 4°C. Sections were washed in 1xTris and incubated for 30 minutes with biotinylated secondary antibodies (1:200 in same solution as used for primary antibodies). After 3 washes in 1xTris, sections were processed for the 3,3-diaminobenzidine (DAB; Sigma–Aldrich Inc.) immunoperoxidase using the Avidin-Peroxidase-Complex (ABC, Vectastain Elite kit) staining techniques as described previously (Hsu et al., 1981; Loup et al., 1998; Loup et al., 2000). To visualize cell nuclei and CAm, sections were counterstained with Harry's Hematoxylin (HHS-128, Sigma-Aldrich; very weak staining of CAm) or Ehrlich's Hematoxylin (100 ml dH2O, 100 ml 96% ethanol, 100 ml glycerol, 10 ml glacial acetic acid, 2 g hematoxylin, 3g kalialaun, 0.4g sodium jodate; strongly reacts with CAm (MacKenzie, 1993), kindly provided by Charlotte Burger, University of Zurich, Institute for Anatomy). In brief, sections were incubated for 2 minutes in the Hematoxylin solution, rinsed in tap water, differentiated in acetic alcohol and blued in running tap water for 10 minutes, dehydrated and coverslipped with Eukitt (Erne Chemie). Toloidinblue staining was performed according to standard protocols.

Immunofluorescence Staining

The protocol was identical to the described immunoperoxidase staining with the following changes: All washing steps and antibody dilutions were done in phosphate-buffered saline (PBS) at pH 7.4. Sections were blocked for 1 hour and incubated for 45 min with the secondary antibodies (coupled to either Alexa Fluor488 or Cy3 (dilution 1:1000 and 1:500, respectively; Molecular Probes, Invitrogen). To reduce lipofuscin-associated auto-fluorescence in aged cells,

sections were incubated in 0.1% Sudan Black (Carl Roth GmbH) dissolved in 70% methanol for 2 minutes, briefly washed with PBS and air-dried (Schnell et al., 1999). Sections were then coverslipped with Dako-DAPI solution (Dako) or ProLong Gold Antifade reagent (Invitrogen) to visualize cell nuclei.

Microscopy and Image Acquisition

Immunoperoxidase-stained sections were scanned and visualized with an automated upright slide-scanning microscope (Zeiss) in brightfield mode and the Pannoramic Viewer 1.8.3.0 (3D Histotech Ltd), respectively. High magnification images were acquired with a brightfield light microscope (Axioscop 2, Zeiss) connected to a digital camera (AxioCam, Zeiss) and captured with AxioVision software (Version 4.5., Zeiss), or with a confocal microscope (LSM 710, Zeiss) and processed with Imaris 7.1.1 software (Bitplane Inc.) and Adobe Photoshop CS5 (Adobe) software.

Quantitative and Statistical Analyses

Stereological estimations of Reelin-positive CAm area and density were performed using the Stereo Investigator 10.50 software (Microbrightfield Bioscience). Two sections with an intersection distance of 200 μm were used for quantification. The following regions were included for the analyses based on the density of the deposits (figure 1): fornix, stratum lacunosum moleculare (SLM), layer I of subiculum, layer I of pre/parasubiculum and layer I of EC (West and Gundersen, 1990; West and Slomianka, 1998). Other areas of the hippocampal formation were not included to minimize measurement errors. The Cavalieri estimator with a grid spacing of 100 μm was used to estimate the area of the region of interest. For fractionator sampling, an unbiased counting frame sized between 80 and 200 μm (depending on the deposit density) was applied to estimate the Reelin-positive CAm profile density. Concomitantly, the individual CAm areas were estimated using the nucleator with 4 rays. The area fraction (AF) was calculated using the following equation: AF = NCA x ACA/Atot, where NCA is the estimated profile number of Reelin-positive CAm within the measured area, ACA is the mean area of CAm within the measured area, and Atot is the total area measured. Statistical analysis of the area and density of Reelin-positive CAm was performed using StatView software. For each brain region, a factorial ANOVA was performed with Group (2 levels: ND and AD) and Deposit type (2 levels: filled vs hollow) as independent variables, and AF (area fraction), ACA (mean CAm size), NCA (estimated number of Reelin-positive CAm) as dependent variables. Pearson's product moment correlations were performed between Reelin-positive CAm (AF, filled and

hollow combined) and Western blot data (full-length Reelin, NR2, NR6 and 60 kDa fragments). Statistical significance was set at $p < 0.05$.

Western Blot Analysis

Protein concentrations of the CSF samples were measured using NanoDrop (table 1). Equal volumes of CSF were analyzed. The sample preparation was performed as previously described (Krstic et al., 2012b). Western blotting was done as described (Krstic et al., 2012b) with the following adaptations: 3–8% Tris-Acetate Midi Gels were used (NuPAGE Novex Tris-Acetate Midi Gel). The electrophoresis was performed using the Xcell4 SureLock Midi-Cell system (Cat.No. WR0100, Invitrogen). Proteins were blotted onto PVDF membranes using the Novex Semi-Dry Blotter (Cat.No. SD1000, Invitrogen). Films were scanned and analyzed using ImageJ Launcher software; intensities of bands were measured (area under the curve (AUC)) and quantified. Reelin immunoreactivity was statistically compared between ND and AD subjects using the non-parametrical Mann–Whitney U test using StatView software. Statistical significance was set at $p < 0.05$. Scanned films were processed with Adobe Photoshop CS5 for visual display (Adobe software).

Results

Reelin Immunoreactivity in the Human Hippocampal Formation

To analyze the localization and levels of Reelin in the human hippocampal formation we performed an immunoperoxidase staining using Reelin antibodies recognizing the N- (G10 and 142) and C-terminal domains of Reelin (R12/14), to identify putative enrichments in proteolytic fragments of Reelin. Paraffin-embedded sections of ND and AD (n = 8, table 1) were employed. We detected spherical Reelin-positive structures varying in their size from approximately 60 up to 250 μm^2 predominantly located in fiber-rich structures (figure 1 and additional file 1: figure S1) in both groups of subjects. They were most abundant in the fornix, enriched in myelinated axons of afferent and efferent projection neurons. A high density of these immunoreactive deposits was also evident in the neuropil of layer I of the pre-/parasubiculum and subiculum. Fewer deposits were detected in layer I of the EC and the SLM of the hippocampus (see figure 1A for overview). In some cases, Reelin deposits were located in the hilus and rarely also in the pyramidal layer of CA3 and CA1. The immunoreactive signals were specific for Reelin, since control stainings with isotypic immunoglobulins (IgGs) (mouse anti-human CD45) or the omission of primary antibodies did not yield any specific labeling (figure 1D-E). The control staining using the well-characterized anti-CD45 antibody also indicated that the Reelin-immunoreactivity was not linked to putative invading lymphocytes. Based on their distinct morphology and enrichment in fiber-rich structures, however, we reasoned that they might be related to CAm, the age-related spherical bodies suggested to contain a collection of neuronal breakdown products including aggregated proteins and abnormal glycogen bodies (Cavanagh, 1999, Meng et al., 2009). Indeed, hematoxylin (according to Ehrlich) and toloidinblue counterstaining identified the Reelin-positive structures as CAm. While all antigen retrieval techniques applied here diminished the Hematoxylin or Toloidinblue stainings, the immunoreactive anti-Reelin signal associated with CAm was never affected (see methods and additional data).

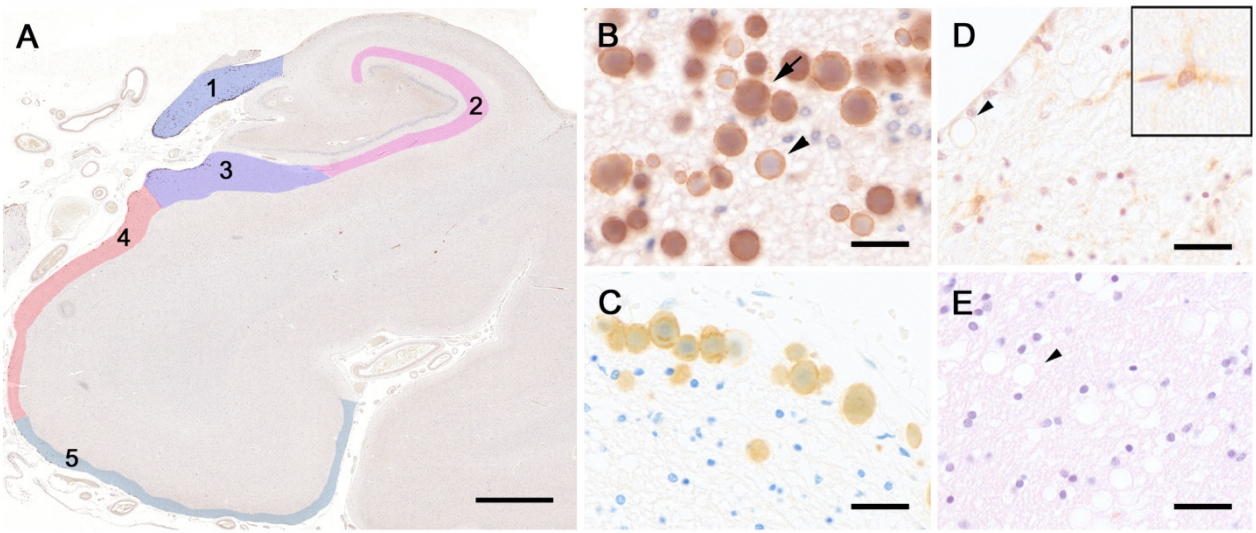

Figure 1 Reelin immunoreactivity in the aged human hippocampal formation. A. Reelin (G10 antibody) immunoperoxidase labeling in combination with hematoxylin (Ehrlich) counterstaining. The tissue section was obtained from an 88 year-old ND individual. The color-coding represents the areas included in the stereological analysis: 1 = fornix, 2 = stratum lacunosum moleculare (SLM), 3 = molecular layer of subiculum, 4 = molecular layer of pre/parasubiculum, 5 = molecular layer of entorhinal cortex (EC). **B.** Higher magnification view of Reelin-positive deposits in the fornix. Arrow points to a filled deposit, arrowhead indicates a hollow deposit. **C.** Reelin (G10) immunoperoxidase labeling combined with toloidinblue counterstaining in the fornix border area. Tissue section was obtained from an 80 year-old AD patient. **D.** Control staining using isogenic IgGs (mouse anti-human CD45 antibody) following antigen retrieval (microwave irradiation in citrate buffer plus pepsin pretreatment) and Hematoxylin (Harrys) counterstaining. Brain section was obtained from a 79 year-old ND individual. Arrowhead points to a CD45-negative deposit, insert represents a CD45-positive lymphocyte associated with a brain capillary. **E)** Control staining without primary antibody following antigen retrieval and Hematoxylin/Eosin counterstaining. Brain section was obtained from an 81 year-old ND individual. Arrowhead points to an immune-negative deposit. Scale bars: A = 2 mm, B - D = 30 µm.

Reelin-Positive Deposits in AD versus Non-Demented Subjects

With our staining protocol, we were able to identify two different types of Reelin-positive CAm: 1) A filled type; with the entire area of CAm being Reelin immunoreactive (figure 1B arrow), and 2) a hollow type; with Reelin immunoreactivity being located around the acidic core of CAm (figure 1B arrowhead). Here, we were interested to determine whether their density differed between ND and AD subjects. We performed a stereological analysis within selected areas of the hippocampal formation (figure 1). The statistical evaluation of AF using a one-way ANOVA revealed a significant increase in the area covered by the deposits in AD patients compared to ND controls in the molecular layer of the subiculum ($F_{(1,28)} = 4.31$, $p = 0.047$). A similar elevation in deposit area in AD versus NA subjects was seen in the pre/parasubiculum, however, the ANOVA only yielded a statistical trend ($F_{(1,26)} = 3.21$, $p = 0.085$; figure 2C). No statistical group difference regarding the density of Reelin/CAm was evident in the other brain areas (all F

< 0.93, all $p > 0.36$). The statistical analysis, however, revealed a significantly higher density of the filled compared to the hollow type in all areas investigated (fornix: $F_{(1,26)} = 11.47$, $p = 0.002$; SLM: $F_{(1,28)} = 14.34$, $p = 0.001$; subiculum: $F_{(1,28)} = 15.52$, $p = 0.001$; pre/parasubiculum: $F_{(1,26)} = 13.52$, $p = 0.001$; EC: $F_{(1,10)} = 20.95$, $p = 0.001$), that was independent of the dementia status (figure 2). Despite this dominance of filled deposits, the significant increase in total amount of deposits in the subiculum molecular layer in AD was not solely attributed to filled deposits (ANOVA: group x type interaction: $F_{(1,28)} = 2.00$, $p = 0.168$) but related to a concomitant increase in both types of deposits.

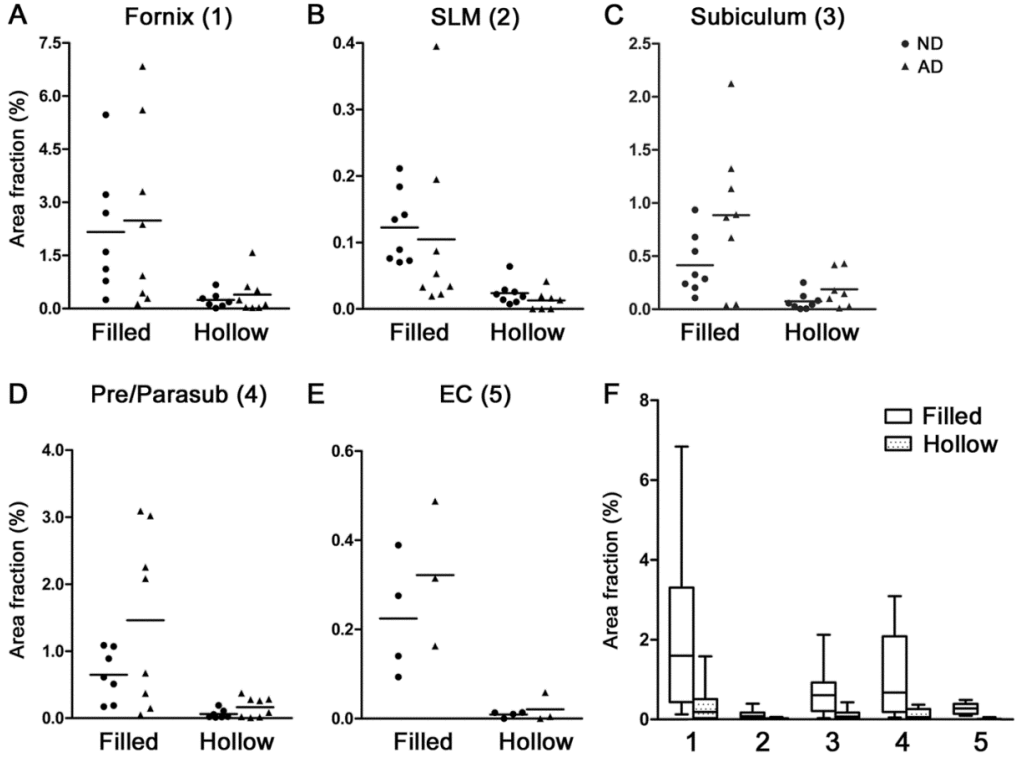

Figure 2 Summary of stereological analyses of Reelin-positive deposits in ND versus AD individuals. A-E. Scatter plots of the estimated density of filled and hollow deposits in different areas in the human hippocampus representing the % area covered by Reelin deposits in relation to the total region of interest (AF, area fraction). Horizontal lines represent group average. Statistical analysis yielded a significant group effect for the subiculum ($F_{(1.28)} = 4.312$, $p = 0.047$), and showed a similar trend for the pre/parasubiculum ($F_{(1,26)} = 3.21$, $p = 0.085$). Note that 4 out of 8 ND and 5 out of 8 AD hippocampi blocks were dissected at a level where no EC was present. **F.** Overview of estimated filled and hollow deposit densities across the five brain areas analyzed. Values are displayed in box plot graphs, with the box dimension indicating the 75th (top) and 25th percentile (bottom) and the mean line. The upper and lower error bars indicate the minimum and maximum, respectively. One way ANOVA analysis revealed a significant main effect of deposit type in all areas analyzed that was independent of the dementia status: 1) fornix: $F_{(1,26)} = 11.45$, $p = 0.002$; 2) SLM: $F_{(1,28)} = 14.34$, $p = 0.001$; 3) subiculum: $F_{(1,28)} = 15.52$, $p = 0.001$; 4) pre/parasubiculum: $F_{(1,26)} = 13.52$, $p = 0.001$; 5) entorhinal cortex: $F_{(1,10)} = 20.95$, $p = 0.001$, statistical significance was set at $p < 0.05$.

Reelin Levels in the Human Cerebral Spinal Fluid

To assess whether the immunohistochemical findings correlate with the levels of Reelin and its physiologically produced proteolytic fragments in the CSF, previously investigated in AD and ND subjects but yielding conflicting results (Botella-Lopez et al., 2006; Ignatova et al., 2004; Saez-Valero et al., 2003), we performed a biochemical analysis of the CSF samples collected for each individual of our study. Besides the well-described immunoreactive bands representing full-length Reelin, the NR6 (310 kDa) and NR2 (180 kDa) fragments, we detected an additional band running at around 60 kDa. This recently described novel N-terminal Reelin fragment (Krstic et al., 2012b) likely represents the ADAMTS-5-mediated degradation product of Reelin (figure 3A) that is enriched in aged brain tissue homogenates (Krstic et al., 2012b) and detected upon internalization (TN, unpublished findings). Semi-quantitative analysis of two repeated experiments revealed high between-subjects variability and no significant differences regarding the levels of Reelin and the three proteolytic fragments emerged between AD and ND subjects (figure 3B).

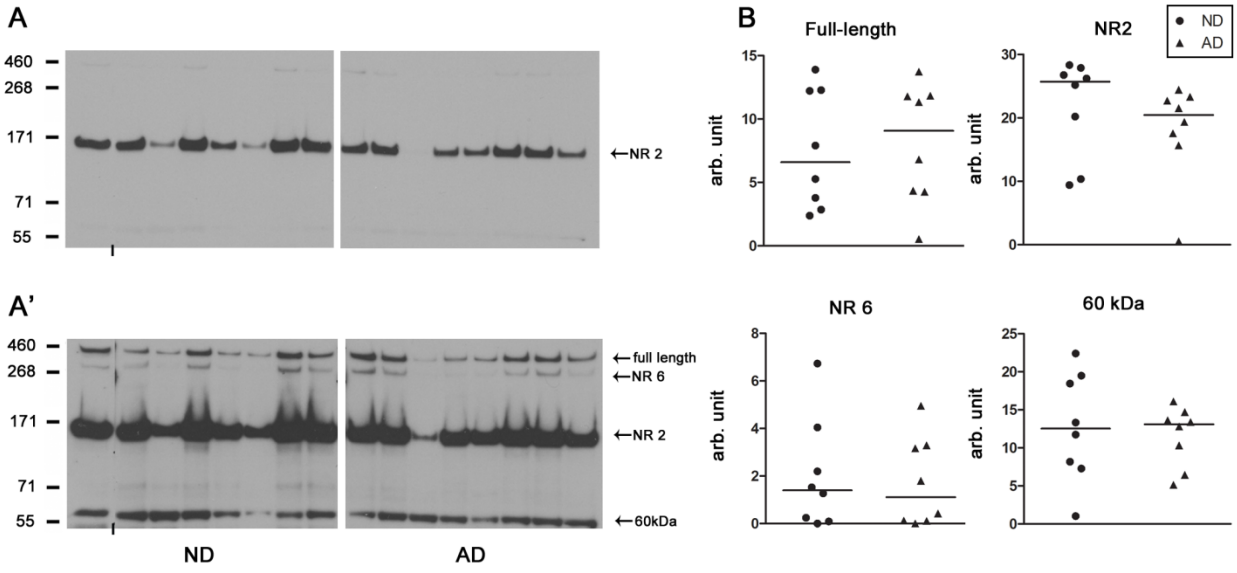

Figure 3 Reelin levels in the CSF. A. Anti-Reelin 142 immunoreactive signals on Western blots at low exposure time (40 seconds) to visualize the NR2 fragment. A') Higher exposure time (18 minutes) of the same blot as A to visualize full-length (~460 kDa), NR6 (~ 310 kDa) and the additional band at ~ 60 kD. Images of immunoblots were cut in half to separate ND from AD for visual display. The short vertical lines at the bottom of the blot indicate joined bands for visual presentation. The HiMark Pre-Stained Standard was used as ladder. **B.** Semi-quantitative analysis of the levels of full-length Reelin and its proteolytic fragments in the CNS. Scatter plots representing relative optical densities expressed in arbitrary units (arb. unit) of CSF samples obtained from ND and AD individuals. Lines represent the group median. Mann–Whitney U-test revealed no significant differences between groups.

However, despite the unknown causal link and the limitations of our sample size, a correlation analyses highlighted a significant relationship between the levels of the 60kDa fragment and the overall CAm density in subiculum and pre/parasubiculum in ND subjects (subiculum: r = 0.857, $p = 0.004$; pre/parasubiculum: r = 0.845, $p = 0.006$) that was lost in AD patient (subiculum: r = 0.098, $p = 0.826$: pre/parasubiculum: r = 0.275, $p = 0.529$), pointing to putative alterations in Reelin proteolytic degradation in AD. None of the other parameters (subfields, Reelin fragments) yielded any significant relationships and no confounding effect of the postmortem interval, pH, brain size or ApoE genotype contributed to this effect.

Levels of AD-Relevant Proteins in Reelin-Positive CAm

Based on the Reelin-dependent modulation of several AD-relevant pathways, including APP proteolytic processing (Kocherhans et al., 2010; Rice et al., 2013) and Tau phosphorylation (Kocherhans et al., 2010; Krstic et al., 2012a), we were interested in determining whether these and other disease-associated proteins were present in the aging-associated Reelin-CAm deposits. Double-immunofluorescence stainings using antibodies raised against the N-terminal domain of APP and β−amyloid sequence 1-40/42 ($A\beta_{1–40/42}$) or anti-$A\beta_{1–40/42}$ in combination with anti-Reelin antibodies revealed their co-localization in most CAm in all areas independent of disease state (figure 4A). However, the intensity varied depending on the antigen retrieval technique used, in line with previous reports using paraffin-embedded postmortem human brain samples (Lucassen et al., 1993; Shi et al., 1991). For both, N-terminal APP and $A\beta_{1–40/42}$ antibodies the antigen retrieval methods applied here either strongly decreased the staining intensity (citrate irradiation and pepsin treatment) or completely diminished it (95% FA; additional figure 2) in comparison to non-pretreated sections, suggesting the presence of soluble APP and/or APP fragments rather than Aβ aggregates. Double immunofluorescence stainings using anti-Tau, pTau or PHF in combination with anti-Reelin antibodies revealed the presence of Tau, however, no enrichment in pTau species in Reelin-positive CAm (figure 4, Additional file 2: figure S2). To confirm and further investigate their origin, we performed double-immunofluorescence staining using additional antibodies recognizing synaptic, axonal and dendritic proteins. In accordance with previous findings α-Synuclein (Wilhelmus et al., 2011), our double-immunofluorescence staining confirmed the presence of α-Synuclein in Reelin-positive CAm. As with the $A\beta_{1–40/42}$ antibodies, the signal intensity dropped upon antigen retrieval technique (additional figure 2).

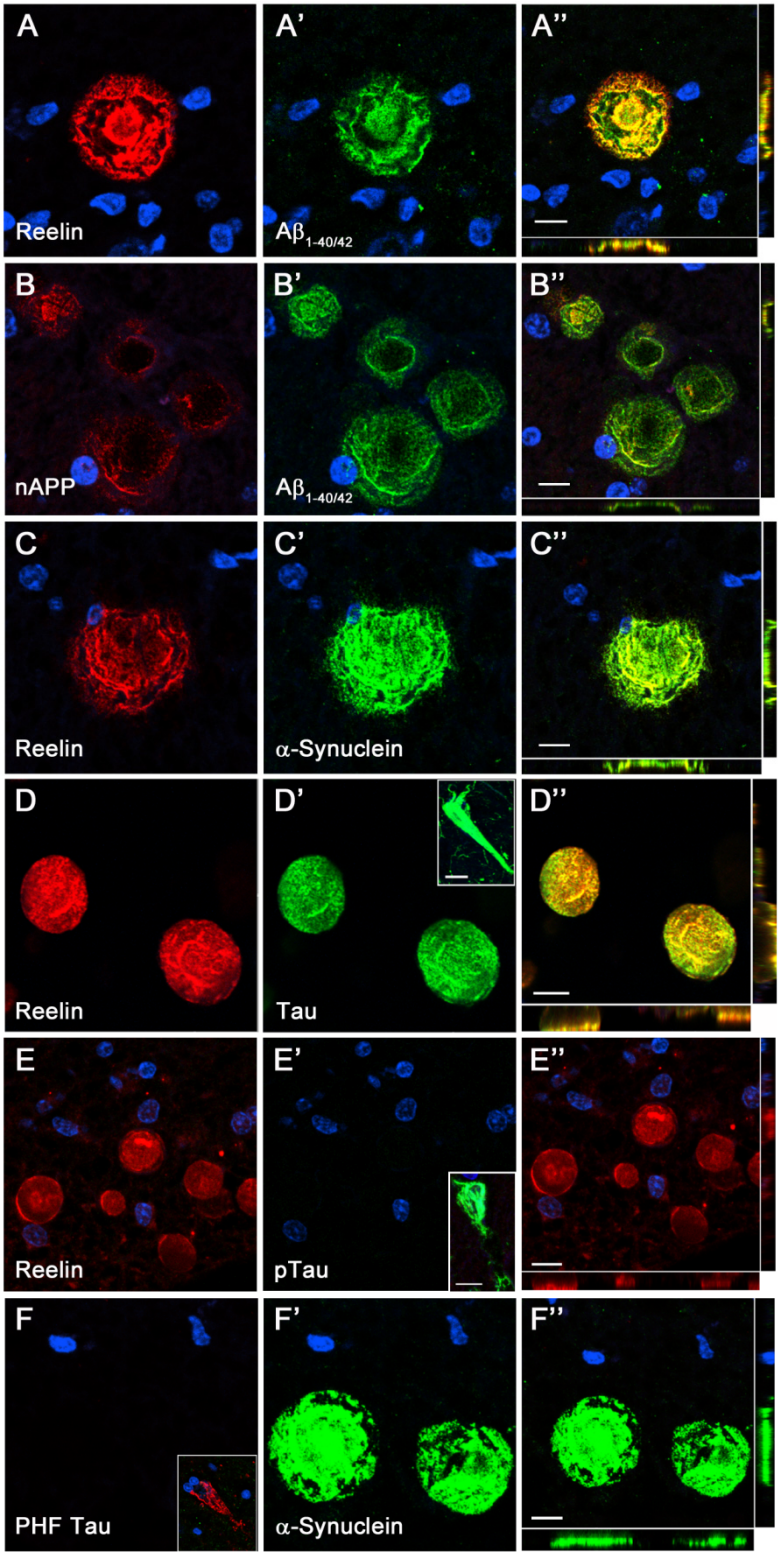

Figure 4 AD-relevant proteins are present in CAm. Representative images of double immunofluorescence labeling involving brain sections obtained from an 82 year-old ND individual counterstained with the nuclear dye DAPI (blue). Red channels show the anti-Reelin (antibody 142; **A, C, D, E**), anti-N-APP **(B)**, and anti-PHF Tau (paired helical filament, **F)** stainings. Green channels depict the anti-$A\beta_{1-40/42}$ (A'-B'), anti-α-Synuclein **(C', F')**, anti Tau **(D')** and anti-pTau **(E')** signals. Merged channels are shown in A"-F". Inserts in E' and F highlight NFT in CA1 region stained with anti-pTau and anti-PHF Tau antibodies, respectively. Scale bars = 10 µm.

However, anti-Synapsin-1 and anti-Synaptophysin stainings did not show a positive signal of these two abundant synaptic proteins within CAm (figure 5). On the other hand, the dendritic marker, MAP2, was detected in CAm using immunoperoxidase staining (figure 5), confirming a neuronal origin and indicating that CAm may originate from both dendritic and axonal compartments. Based on previous findings reporting an association of CAm with astroglia (Cavanagh, 1999), we were interested in determining whether Reelin-positive CAm show a similar relationship to glial cells. To this end we performed an immunhistochemical analysis using antibodies against glial fibrillary acidic proteins (GFAP) to stain astrocytes as well as an anti-Iba1 antibody to label microglia.

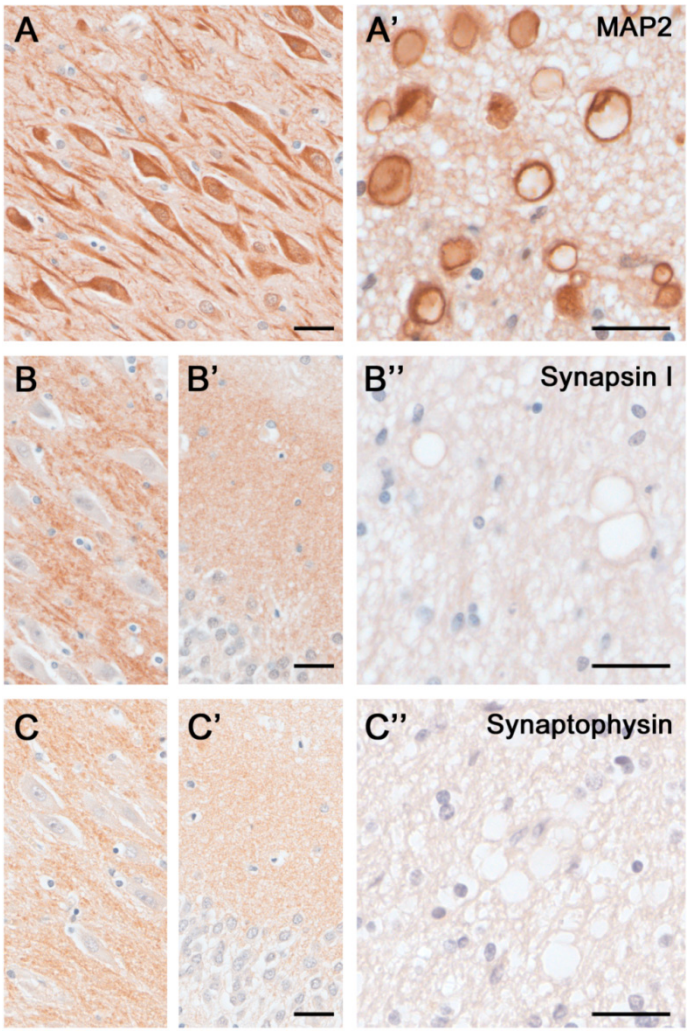

Figure 5 Dendritic and synaptic proteins in the aged human hippocampus: Differential association with CAm. Immunoperoxidase-hematoxylin staining of brain sections obtained from an 85 year-old ND individual. **A.** Representative images of the CA2 subfield and fornix (A') labeled with the dendritic cytoskeletal marker anti-MAP2. Note the strong immunoreactivity in pyramidal cell bodies and dendrites, as well as CAm (A'). **B-C.** Immunoperoxidase staining using anti-Synapsin-1 (B) and anti-Synaptophysin antibodies (C) depicting the CA2 pyramidal cell layer (B, C), the dentate gyrus molecular layer (B', C') and the fornix (B'', C''). While a characteristic synaptic immunoreactivity of both markers was evident in the hippocampus proper and dentate gyrus, no accumulation of these synaptic proteins was seen in CAm. Scale bars: A-C = 30 µm, A'-C' = 30 µm.

As reported, the GFAP immunoreactivity was highest in all fiber-rich structures, as well as prominent in glial endfeet enclosing the cerebral vasculature vessels and ventricle walls (figure 6). In areas with high labeling, GFAP immunoreactivity was found in association with CAm. However, the glial marker was found to be restricted to the border of deposits, but was not associated with any of the other markers that were enriched in CAm, such as APP, Aβ or α-Synuclein. No co-association of Iba1 with CAm was obtained by either immunoperoxidase or -fluorescence stainings. Rather, the staining intensity was homogenous across all areas, indicating that these aging-associated neuronal structures are inert and do not provoke a microglia activation.

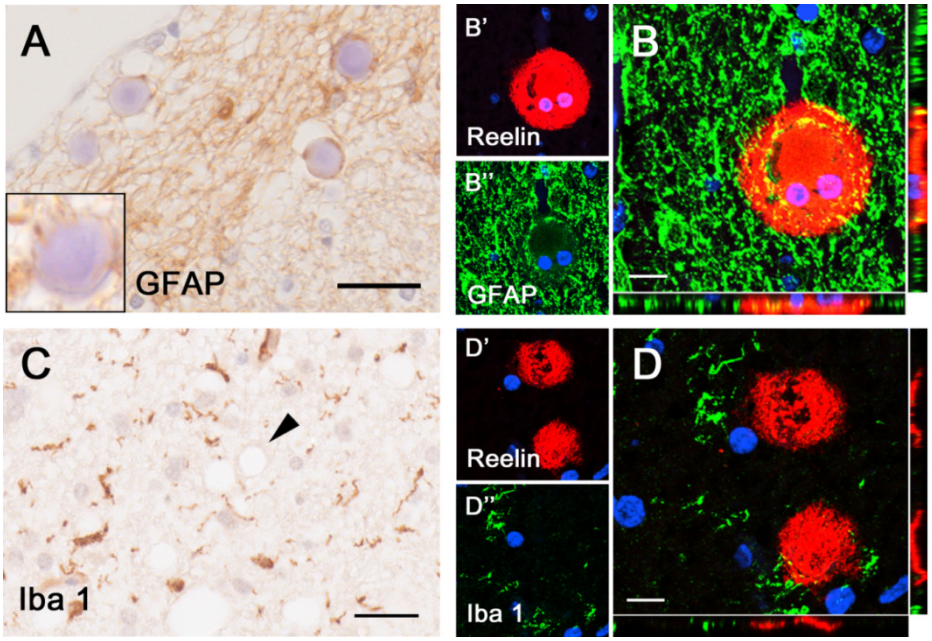

Figure 6 Association of astrocytes but not microglia with Reelin/CAm deposits. Immunohistochemical analyses involving brain sections obtained from an 82 year-old ND individual. **A.** Representative image of the fornix labeled with anti-GFAP antibodies and hematoxylin (Ehrlich) staining. Note the GFAP immunoreactivity enclosing the CAm in the dense glial network. Insert represents a Reelin/CAm deposit in an area with low GFAP intensity. **B.** Double immunofluorescence staining with anti-Reelin antibody (142, red, B') and anti-GFAP antibody (green, B''). Nuclei are visualized with DAPI-enriched mounting medium. **C.** Immunoperoxidase staining using anti-Iba1 antibody and hematoxylin (Ehrlich) counterstaining. The pretreatment of the tissue sections with 10 minute citrate irradiation completely diminishes the CAm labeling (arrowhead). **D.** Double immunofluorescence staining using anti-Reelin antibody (142, red, D') and anti-Iba1 antibody (green, D''). Scale bars: A, C = 30 µm; B, D = 10 µm.

Discussion

Here we describe for the first time the presence of the extracellular matrix protein Reelin within spherical depositions in the human hippocampal formation. Our immunohistochemical stainings revealed the presence of considerable amounts of N- and C-terminus-containing Reelin fragments in these deposits. Stereological analyses indicated that their density in the hippocampal formation is largely independent of the dementia status; however, it revealed a trend towards higher levels in patients with AD and a putative link to alterations in Reelin proteolytic processing. Based on hematoxylin and toluidinblue labeling and their distinct morphology, it is highly conceivable that Reelin and its fragments constitute a major component of CAm, a prominent structure of the aging human brain whose origin and biological significance in the CNS is poorly understood. In the following, we summarize the current status of the CAm literature and discuss the presence and putative role of Reelin in their formation in the human hippocampal formation.

Aging-Associated CAm in the Human Hippocampal Formation

Despite the numerous studies, the role of CAm during aging and neurological diseases has remained obscure. They are commonly seen in the glial feltwork of subpial, subependymal, and perivascular regions, but can also be detected in fiber-rich areas in the CNS, most prominently within the hippocampal formation (Cavanagh, 1999). The major components of CAm are glucose polymers, presumably linked to aging associated glucose metabolism defects, peptides and proteins (approximately 4%), many of which have been linked to cellular stress responses (Cisse et al., 1991; Selmaj et al., 2008; Wilhelmus et al., 2011). Several studies indicated that they evolve from neurons, astrocytes or oligodendrocytes due to the presence of cell-specific proteins (Buervenich et al., 2001; Cavanagh, 1999; Meng et al., 2009; Singhrao et al., 1994). However, it is currently unclear whether their glial association is the result of phagocytosis of remnants of degenerated neurons/neurites and vascular metabolites (Meng et al., 2009; Singhrao et al., 1995) or an indicator of glia pathophysiology/degeneration (Suzuki et al., 2012). In line with these data, neurological and neurodegenerative diseases such as temporal lobe epilepsy, multiple sclerosis, and AD are characterized by elevated levels CAm (Singhrao et al., 1995; Van Paesschen et al., 1997), and these spherical bodies were shown to correlate with neuronal loss associated with hippocampal sclerosis (Van Paesschen et al., 1997). The frequent detection of CAm within axons and terminal neurites in the aging ocular system (Rejdak et al., 2011), as well

as the prominent accumulation of axonal proteins including Tau (Loeffler et al., 1993; Wilhelmus et al., 2011), APP (Tate-Ostroff et al., 1989), and α-Synuclein (Wilhelmus et al., 2011), indicate that they may form in response to cellular stress and/or aging-related impairments in cytoskeletal stability and axonal transport that ultimately lead to axonal swellings, a mechanism recently proposed for amyloid plaque formation in AD (Krstic and Knuesel, 2013).

Reelin Accumulates in Two Types of CAm – Link to Its Expression Pattern?

Intriguingly, many of the areas enriched in CAm overlap with the localization of Reelin. This relates to the well characterized cell types in the murine brain that are part of the entorhino-hippocampal, lateral olfactory and retino-collicular tract as well as the parallel fiber system of the cerebellum (Alcantara et al., 1998; Martinez-Cerdeno and Clasca, 2002; Martinez-Cerdeno et al., 2003; Pesold et al., 1998; Ramos-Moreno et al., 2006). Furthermore, *in vitro* studies reported the expression of Reelin in progenitor cells of oligodendrocytes as well as mature oligodendrocytes (Siebert and Osterhout, 2011), highlighting the possibility that the Reelin immunoreactivity associated with CAm in fiber-rich areas like the fornix may stem from its production and secretion by progenitors of oligodendrocytes and oligodendrocytes (Siebert and Osterhout, 2011). Studies in primates identified additional areas with Reelin-positive cells showing a wider distribution of Reelin throughout cortical areas than in any other species, indicating that Reelin influences most cerebral circuits in higher mammals (Martinez-Cerdeno et al., 2002). Findings in macaque monkeys showed strong Reelin immunoreactive soma of Cajal-Retzius cells located in layer I, pyramidal neurons in EC layer II, and interneurons of the subicular complex molecular layer (subiculum, pre/parasubiculum), areas which harbor considerable amounts of Reelin-positive CAm. It is conceivable that these cells, shown to degenerate during preclinical stages of AD (Baloyannis, 2005; Kordower et al., 2001; Price et al., 2001) are a major source of Reelin that is detected within CAm. In line with the findings that Reelin is transported along axons and secreted to act on postsynaptic cells (Martinez-Cerdeno et al., 2003; Pesold et al., 1998; Ramos-Moreno et al., 2006), the deposits located in the SLM, the projection zone of the layer II pyramidal cells, are most likely distal axonal accumulations of Reelin. It is conceivable that aging-associated impairments of axonal stability and hence axonal transport increase the likelihood of accumulations of transported proteins and organelles. This may aggravate during phases of cellular stress that is frequently accompanied by increased levels in damaged and misfolded proteins, which show a much higher propensity to aggregate (for recent review, see (Krstic and Knuesel, 2013)). It is therefore plausible, that the decrease in Reelin levels during aging (Chin et al., 2007; Herring et al., 2012; Knuesel et al., 2009) with its

concomitant in- and decrease in Tau (Hiesberger et al., 1999; Kocherhans et al., 2010) and n-cofilin phosphorylation (Chai et al., 2009), respectively, may reduce axonal and dendritic cytoskeletal stabilities and strongly impair transport from and to synaptic sites. In agreement with this hypothesis, our data showed that highly abundant and cellular stress-induced/associated axonal proteins such as APP and α-Synuclein co-accumulate with Reelin in CAm. Our findings that the FA pretreatment (used to detect Aβ peptides in amyloid plaques) abolished the anti-$A\beta_{1-40/42}$ immunoreactivity in CAm indicates that soluble APP and/or APP fragments, rather than Aβ peptide aggregates, accumulate in CAm, which is in line with previous reports (Tate-Ostroff et al., 1989). The presence of MAP2 in CAm may be indicative of dendritic varicosities or related to missorting of this dendritic cytoskeletal protein into axonal compartments. In support of a putative protein mistargeting, we did not find evidence of pTau species in Reelin-positive CAm, a result that is also in agreement with previous studies (Loeffler et al., 1993; Wilhelmus et al., 2011). This phenomenon may also be linked to potential dephosphorylation of Tau in the putative acidic (Krstic et al., 2012a) and/or protein cross-linking and polymerization environment (Wilhelmus et al., 2011), a potential scenario that would also explain the lack of Synapsin-1 and Synaptophysin immunoreactivity in CAm. It is further conceivable that the change in glucose metabolism – potentially linked to aging-related alterations in glial support – promote the formation of abnormal polysaccharide chains that further block axonal transport. The presence of Reelin in the filled type of CAm could be indicative of such an axonal pathophysiology as previously suggested by the findings and discussions in rodents and primates (Doehner et al., 2012; Fiala et al., 2007; Krstic and Knuesel, 2013). However, the detection of Reelin in the hollow type shows that the core of CAm can be formed independently of Reelin and could indicate that this rare type of spheroid might be linked to the accumulation of Reelin in astrocytic endfeet (Doehner et al., 2010). This is in agreement with the findings shown here and by others that GFAP-positive astrocytes are associated with but not found in the core of CAm (Singhrao et al., 1994). This hypothesis is also in line with our previous findings, demonstrating with 3D-electron microscopy that Reelin-positive varicosities can be extruded from neurites and detected in astrocytic endfeet, potentially related to phagocytosis (Doehner et al., 2012). The lack of CAm-associated microglia activation reported here is also indicative that these spherical bodies are inert, despite the presence of putative toxic peptides, proteins and cellular metabolites (Singhrao et al., 1995). The distinct association of Reelin at the boarder of CAm – particularly prominent in the hollow type - may be linked to its extracellular secretion and accumulation around CAm that precludes a microglia response. Altogether, this may explain why CAm – despite their close association with aging-associated neurodegenerative processes linked to

impairments in glucose metabolism, protein synthesis, transport and degradation – have no major effects on the physiology of neighboring neurons. It would be highly relevant to assess the levels of Reelin associated with CAm localized outside the hippocampal formation (i.e. hypothalamic nuclei), which have been reported to display pronounced cytoskeletal alterations during the course of aging and AD (Swaab et al., 1993).

Reelin Levels and Deposits in AD Compared to ND Individuals

Previous reports indicated that several neurological and neurodegenerative conditions are accompanied by an increase in CAm, potentially linked to higher levels of cellular stress. However, quantitative data are largely missing. Here, we intended to assess the density of Reelin-positive CAm with an unbiased stereological approach involving five distinct areas of the hippocampal formation, complemented with immunoblot analyses to measure the Reelin levels in CSF samples of the same ND and AD individuals. Our stereological analysis revealed that the total amount of Reelin-positive CAm – independent of the type of deposit - was found to be increased in the subicular complex of AD compared to ND individuals. However, due to the small cohort and the high between subject-variability, only the density in the subiculum molecular layer yielded a significant group effect. Despite the limitation due to the small sample size, our data indicate the increase in CAm density may reflect the aggravation the aging-related impairments in cellular functions that result in increased intracellular accumulation of missorted, misfolded or poorly degraded proteins which is known to be increased in AD (Krstic and Knuesel, 2013). It is very likely that putative differences in other areas measured were covered by an aging effect, as there is a clear age-dependent increase in the number of CAm (Cavanagh, 1999). Currently, it is unknown how these histopathological changes relate to the level of Reelin protein and its proteolytic products in the CSF. While our assessment of full-length Reelin and its proteolytic fragments in the CSF revealed no statistical differences between groups, a correlation analyses highlighted a significant relationship between the levels of the 60kDa fragment and the overall CAm density in the susubiculum and pre/parasubiculum in ND subjects but not AD patients. While a higher sample size is absolutely required to substantiate this finding, the preliminary data indicate that the accumulation of Reelin in CAm might be related to its proteolytic degradation, a phenomenon that appears to be altered in AD versus ND subjects. It will also be highly relevant to assess Reelin levels in CSF and brain tissue homogenates in younger cohorts of ND subjects, as well as MCI and early stages of AD, which is expected to show larger differences to age-matched ND individuals. Differences in the age range of the subjects included in previous studies may have also accounted for the conflicting results

regarding the levels of Reelin and its fragments in the CSF published earlier (Botella-Lopez et al., 2006; Ignatova et al., 2004; Saez-Valero et al., 2003). It would be therefore highly relevant to investigate the levels of Reelin and all its proteolytic fragments (including the 60 kDa product) and its putative enrichment in neuritic varicosities in a substantially larger cohort of human subjects across aging and AD.

Conclusion

Altogether, our results indicate that aging- and disease-associated changes in Reelin levels and proteolytic processing might play a role in the formation of CAm by altering cytoskeletal dynamics. Its presence may also be an indicator of a degenerative state of neuritic compartments. However, this remains to be experimentally determined using preclinical models of aging and AD.

Additional Files

Additional Text

We detected the Reelin-positive deposits using various antibodies raised against different Reelin epitopes (Additional file 1: figure S1A-C). Reelin deposits were stained with all antibodies used, independently of the antigen retrieval technique. To visualize CAm with hematoxylin or toloidinblue, antigen retrieval was omitted in order to maintain the coloration. figure 1E illustrates the high morphological variations in Reelin/CAm deposits. Besides the prominent staining of Reelin within deposits, we also detected intracellular Reelin immunoreactivity in pyramidal cells of the cornu ammonis, particularly in CA3 and to lesser extent CA1 pyramidal cells, using N-terminal but not C-terminal targeting antibodies (Additional file 1: figure S1F), in line with a previous report (Kramer et al., 2011). These immunoreactive signals were, however, only seen using an antigen retrieval approach involving microwave irradiation in citrate buffer followed by pepsin pretreatment (see material and methods). Chromatin filters and high magnification microscopy revealed Reelin to be present within cytosolic vesicles (insert, Additional file 1: figure S1F). To visualize Reelin-expressing cells, which were sparse in our cohort of aged non-demented individuals and shown to further decrease in AD patients (Chin et al., 2007; Deguchi et al., 2003), repeated microwave irradiation in citrate buffer had to be applied (Additional file 1: figure S1C, insert).

Additional 1: Figure S1 Immunoperoxidase stainings of paraffin-embedded hippocampal brain sections. **A.** Anti-Reelin immunoreactivity (G10 antibody) in tissue section obtained from a 63 year-old ND individual following antigen retrieval with microwave irradiation in citrate buffer and pepsin pretreatment. **B.** Brain sections of an 89 year-old AD patient, processed for antigen retrieval (citrate and pepsin pretreatment), stained with anti-Reelin (142) antibodies. **C.** Anti-Reelin (142 antibody) immunoperoxidase and hematoxylin staining of tissue section obtained from an 88 year-old ND individual following repeated microwave irradiation in citrate buffer. Insert shows a Reelin-expressing cell located in SLM. **D.** Reelin immunoreactivity (R12/14 antibodies) in tissue section of a ND individual (63 years old) pretreated with citrate and pepsin. **E.** Morphological variations of Reelin-positive deposits located in five brain regions included in the stereological analysis. Representative pictures of immunoperoxidase staining using anti-Reelin antibody (G10) combined with microwave irradiation in citrate buffer and pepsin pretreatments. **F.** Reelin immunoreactivity in pyramidal cells of AD patient (80 years old) visualized with anti-Reelin antibody (G10) following citrate/pepsin pretreatments. **G.** Reelin immunoreactivity (R12/14 antibodies) in tissue section of an AD individual (78 years old) pretreated with citrate and pepsin. Arrowheads point to cytosolic vesicles with immunopositive Reelin labeling. Scale bars: A-D, F =30 μm; E = 25 μm.

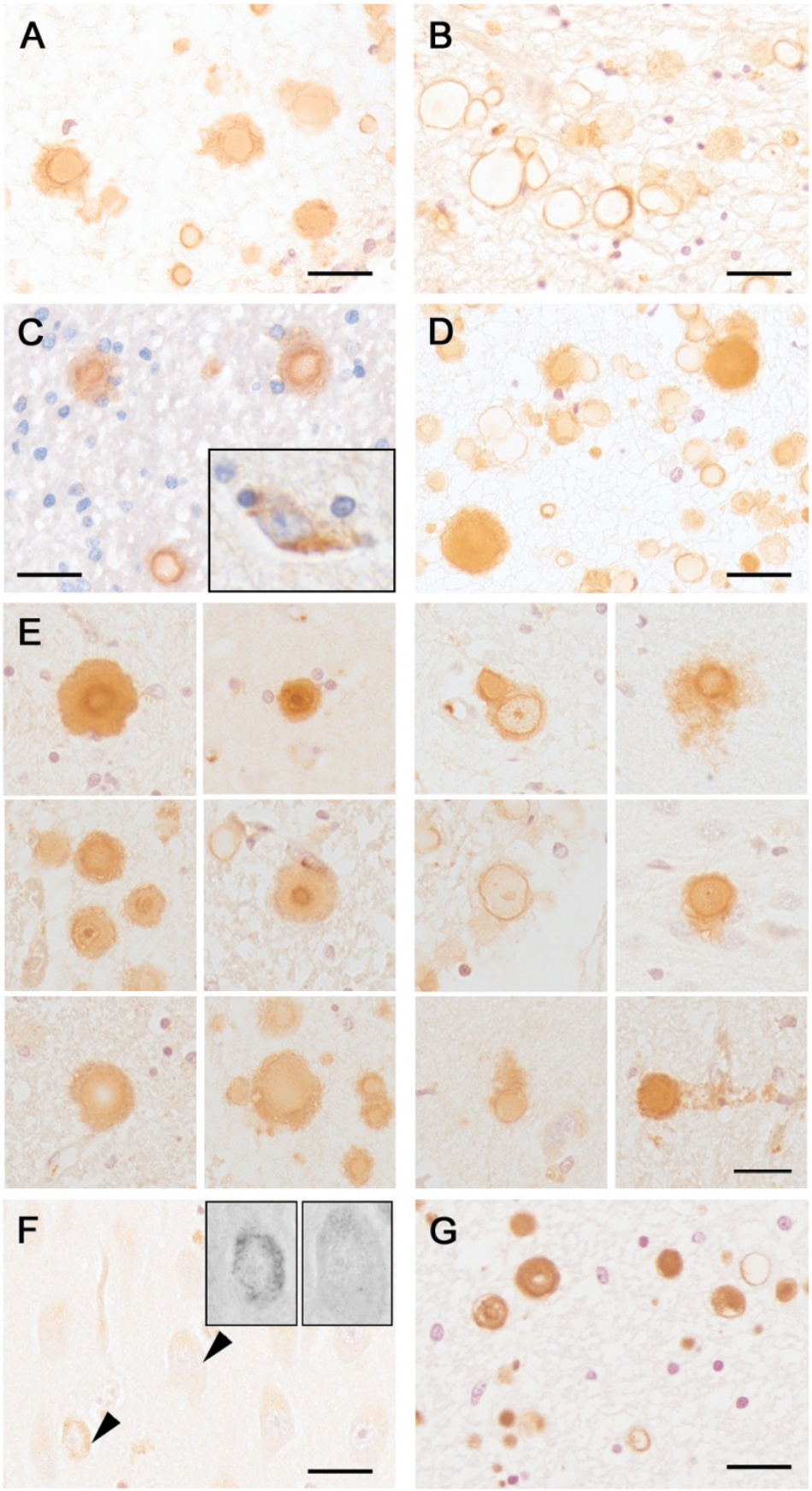
A
B
C
D
E
F
G

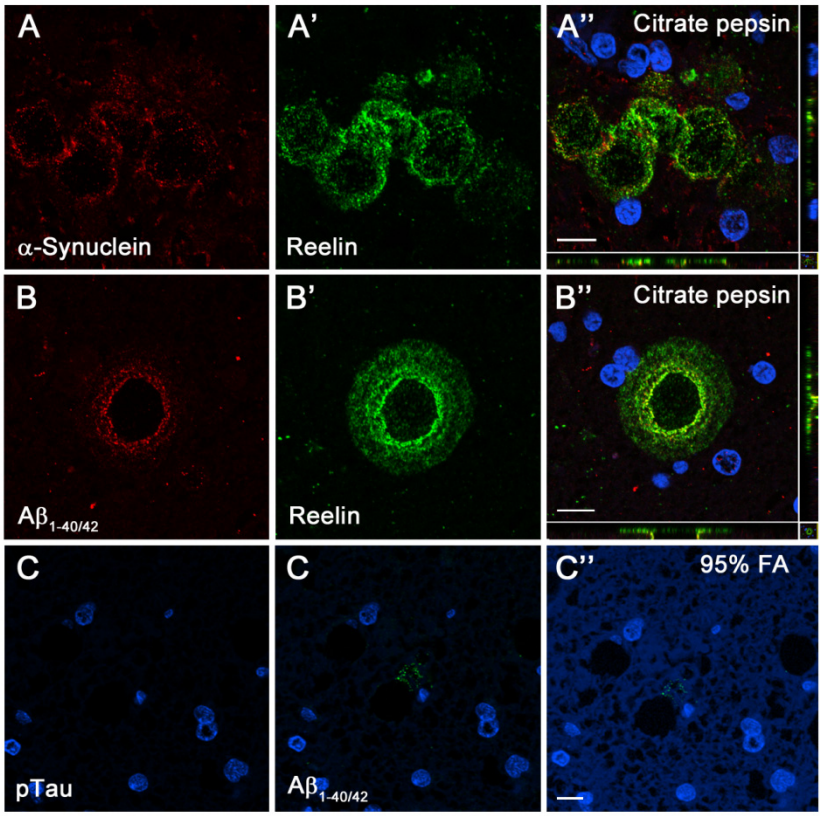

Additional 2: Figure S2 Antigen retrieval and its effect on staining intensities of AD-relevant proteins in CAm. Representative images of immunofluorescence staining involving brain sections obtained from a ND individual (82 years old) counterstained with the nuclear dye DAPI (blue). Antigen retrieval involved either microwave irradiation in citrate buffer followed by pepsin incubation (A-B) or a 95% formic acid (FA) pretreatment (C). **A.** Double labeling using anti-α-Synuclein (red, A) and anti-Reelin (G10, green, A') antibodies, merged in A". **B.** Anti-$A\beta_{1–40/42}$ antibody (red, B) combined with anti-Reelin antibodies (G10, green, B') show a large degree of overlap (B", merged). **C.** Double immunofluorescence staining using anti-pTau (red, C) and anti-$A\beta_{1–40/42}$ antibodies (green, C'). Note that the FA treatment destroys the anti-$A\beta_{1–40/42}$ signal in the CAm but not in amyloid deposits (arrowhead). The pixel brightness is increased in the merged channels to visualize the presence of the immunonegative deposits (C"). Scale bars = 10 µm.

Acknowledgements

This study was supported by the Swiss National Science Foundation grant number 310030–132629, Center for Neuroscience Zurich (ZNZ), University of Zurich Candoc Forschungskredit, and Rahn & Bodmer, Private Banking, Zurich. We thank the Netherland Brain Bank and Professor Manuela Neumann, University of Tubingen, for providing the post-mortem human tissue and CSF samples, as well as Dr Lutz Slomianka and Ms Charlotte Burger and Iris Miescher, Institute of Anatomie, University of Zurich, for their expert stereology and experimental support, respectively. We are also very grateful to Professor Karl Frei, University Hospital Zurich and Professor André Goffinet, Catholic University of Louvain, for providing the anti-CD45 and anti-Reelin antibodies, respectively, as well as Professor Jean-Marc Fritschy, Dr Dimitrije Krstic and Sandra Pfister, Institute of Pharmacology and Toxicology, for their advice and inputs to this project.

STUDY II: EFFECTS OF ACUTE AND CHRONIC NORADRENERGIC AXON DEPLETION IN A WILD TYPE MOUSE MODEL FOR SPORADIC ALZHEIMER'S DISEASE

Tina Notter[1,2], Matthias Wyss[1,2], Irene Knuesel[1,3], Jean-Marc Fritschy[1,2]

[1]Institute of Pharmacology and Toxicology, University of Zurich, Winterthurerstrasse 190, CH-8057, Zurich, Switzerland

[2]Neuroscience Center Zurich, University of Zurich and ETH Zurich, Winterthurerstrasse 190, CH-8057 Zurich, Switzerland

[3] Present address: Roche Pharmaceutical Research and Early Development, NORD Discovery & Translational Area, Roche Innovation Center Basel, Grenzacherstrasse 124, Basel, Switzerland

In preparation for publication

Author's contribution

All the experimental procedures were carried out by TN. PET imaging studies were performed with MW in the animal imaging center of ETH (PD Dr. Stefanie Kraemer). TN, IK and JMF wrote the manuscript. Authors have no conflict of interest to declare.

.

Abstract

The LC is one of the first structures affected in AD. It consists of long projecting NA neurons innervating the entire neuraxis. Noradrenaline (NA) is known to play a role in inflammatory responses, regulation of neurovascular coupling and energy metabolism, as well as to contribute to attention and cognitive processing. The early impairment of NA signaling could, therefore, be a key player shifting normal to pathological ageing. Recently we have shown that combined prenatal and postnatal systemic immune challenges ("double hit" model) induced with the viral mimic PolyI:C evokes an AD-like pathology in aged wild type mice (Krstic et al., 2012a). Here, we aimed to evaluate the role of NA signaling in pathological mechanisms involved in sporadic AD by combining the PolyI:C model (single or double immune challenges) with DSP-4 treatment, a drug which selectively targets LC axons and causes widespread NA denervation in the CNS and subsequent degeneration of LC neurons. Specifically, we aimed to determine whether a prenatal inflammatory insult during late gestation affected the regeneration capacity of LC neurons at both young and advanced age. Further, we evaluated whether the AD-related phenotype detected in the double hit PolyI:C model was exacerbated by the loss of NA innervation, using histological, biochemical, behavioral and PET imaging approaches.

Prenatal PolyI:C-exposed mice were treated with DSP-4 at the age of 3 months and analyzed 3 months later. They exhibited a significant decrease in NA axon density in the primary visual cortex (V1) and CA1 area of the hippocampus, indicative of impaired regeneration, but no change in LC neuron survival. The combined treatments did not exacerbate inflammatory responses induced by the prenatal immune challenge and, therefore, did not result in detectable microgliosis or astrogliosis. A second cohort of mice prenatally exposed to PolyI:C was repeatedly treated with DSP-4 until 12 months of age and received a second PolyI:C exposure (i.v.). They were tested behaviorally at 16 months, subjected to PET imaging to assess cerebral glucose uptake, followed by postmortem histological and biochemical analyses. Unexpectedly, double PolyI:C exposure did not evoke a strong inflammatory response as reported previously using a similar protocol (Krstic et al., 2012a). In accordance, we did not observe AD-like changes in these double immune-challenged mice, which served as a "control" towards the "double hit" model previously described. Chronic NA axonal depletion had no additional effects on APP expression and proteolytic processing, Tau phosphorylation, expression of inflammatory markers in microglia, and glucose uptake. However, prenatal immune-challenged mice exhibited

at 16 months of age a mild deficit in non-spatial short-term memory, a well characterized phenotype in this model.

These results indicate that prenatal PolyI:C exposure induces a persistent deficit in the regenerating capacity of NA axons in young adult mice. However, NA depletion does not accelerate AD-related changes in aged mice in which the prenatal immune challenge failed to induce a chronic pro-inflammatory state.

Introduction

AD is characterized by severe, progressive loss of cognitive functions, extensive neurodegeneration, neuroinflammation, and the appearance of amyloid plaques and NFTs. Ageing is considered to be the main risk factor of sporadic AD. The pathophysiological mechanisms underlying this form of the disease, in particular the early changes that shift normal to pathological ageing are yet poorly understood.

One of the first brain structures to be affected in AD is the LC, a brainstem nucleus that harbors long-projecting NA neurons innervating the entire neuraxis (Grudzien et al., 2007, Braak et al., 2011, Braak and Del Tredici, 2012). A general decrease in NA levels in the brain of AD patients is detected, as a consequence of early neurodegeneration of the LC (Tomlinson et al., 1981, Iversen et al., 1983, Bondareff et al., 1987, Chan-Palay and Asan, 1989, German et al., 1992) and likely due to increased NA metabolism in its remaining cells (Hoogendijk et al., 1999).

The NA system regulates numerous neuronal processes that might contribute to the ethiopathology of AD, including attention, arousal, and cognitive processing (Berridge and Waterhouse, 2003, Rinaman, 2011). Adrenergic receptor activation was shown to potentiate glutamate buffering and potassium clearance, both assuring proper synaptic signaling during phases of high neuronal firing (Pesce et al., 2003, Hayes et al., 2004). NA was further associated with a regulatory function in brain energy supply by its modulatory effect on different levels, including brain perfusion (Toussay et al., 2013), BBB permeability (Raichle et al., 1975, Borges et al., 1994, Sarmento et al., 1994) and astrocytic glycogenesis and glycogenolysis (Sorg and Magistretti, 1992). NA signaling also regulates inflammatory processes, as evidenced by reduced production of pro-inflammatory cytokines by microglia as well as stimulation of their migration and phagocytosis (Heneka et al., 2010, O'Donnell et al., 2012). The alkylating agent DSP-4 is an experimental tool to deplete NA innervation in the CNS, and thereby study its function (Jonsson et al., 1981). A single intraperitoneal injection (i.p.) of 50 mg/kg DSP4 induces profound axonal degeneration, followed by partial regeneration, selectively of LC neurons (Fritschy and Grzanna, 1992). Several studies performed in transgenic AD mice have reported that DSP-4 treatment potentiates AD-like neuropathology, including increased neuroinflammation, Aβ plaque formation, synaptic loss, impaired glucose uptake, as well as cognitive impairments (Heneka et al., 2006, Kalinin et al., 2007, Pugh et al., 2007, Jardanhazi-Kurutz et al., 2010, Rey et al., 2012, Hammerschmidt et al., 2013).

Our group has recently shown that major signs of AD-like pathology, including age-dependent increase in APP expression and Tau phosphorylation, occur in wild type mice subjected to a prenatal immune challenge during late gestation – induced by treating pregnant dams with the viral mimic PolyI:C. A 2nd PolyI:C injection at the age of 12 months (so-called "double hit" model) leads to further increases in APP levels and results in APP-positive plaques, increase in PHFs and somatodendritic shift of pTau, and activation of both microglia and astrocytes (Krstic et al., 2012a). Prenatal PolyI:C exposure at GD17 also causes selective cognitive deficits in non-spatial short-term memory (Krstic et al., 2012a), which might be linked to increased levels of APP, known to impair cognitive performance in transgenic mice (Simon et al., 2009). These features suggested that the "double hit" model might be useful to investigate the mechanisms of sporadic AD (Krstic and Knuesel, 2013).

In the present study, we combined the "double hit" model with DSP-4 treatment to address the following specific aims: 1) Do inflammatory mechanisms, triggered PolyI:C-induced immune challenge, affect the regeneration capacity of NA axons? 2) Does chronic NA depletion aggravate AD-like neuropathology in PolyI:C-exposed wild type mice during aging, thereby providing potential clues for the significance of alterations in the central NA system detected in AD patients?

Materials and Methods

Animals

All animal experiments were carried out in accordance with Swiss law on animal experimentation and approved by the cantonal veterinary office of Zurich.

Experiments were performed with time-pregnant C57Bl6/JOla mice purchased from Harlan Laboratories (Horst, the Netherlands). Pregnant dams were shipped on gestational day (GD) 14 and injected with PolyI:C at GD17. Offspring (for the complete list see table 1) were housed in an optimized in-house hygiene area (Institute of Pharmacology and Toxicology, University of Zurich, Switzerland) under a 12 hour light/dark cycle, with access to food and water *ad libitum* until 3, 5, 6 or 16 months of age.

At the age of 12 months, immediately after DSP-4 injections, mice were ear-marked using a sterile ear-marking tool.

Polyriboinosinic-Polyribocytidilic Acid (PolyI:C) Injections

Pregnant mouse dams of the C57Bl/6JOla strain were given a single intravenous injection (i.v.) of 5 mg/kg PolyI:C potassium salt (P9582, 50 mg; Sigma-Aldrich Chemie GmbH, Buchs, Switzerland) dissolved in 0.9% sterile, pyrogen-free NaCl. Calculation of dose was based on the pure form. The injection volume was 5 mL/kg body weight or an equivalent volume of saline at GD17. The animals were mildly restrained during the injection procedure using an acrylic mouse restrainer (PlasLabs, Inc. #561-RC). After the injection, dams were immediately returned to their home cage and left undisturbed until the first cage change 1 week after delivery. A group of offspring (see table 1) was injected with PolyI:C or NaCl at the age of 12 months as described in (Krstic et al., 2012a).

N-(2-chloroethyl)-N-Ethyl-2-Bromobenzylamine (DSP-4) Injections

Starting at the age of 3 months, mice were i.p. injected with 50 mg/kg DSP-4 dissolved in 0.9% sterile, pyrogen-free NaCl or an equivalent volume of NaCl. Due to light sensitivity and instability, DSP-4 was freshly dissolved after every other mouse. Mice of the 1st cohort were treated only once; for the 2nd cohort (figure 1A) this procedure was repeated 3 times every 3 months

Table 1 Animals used in this study.

Age (months)	Prenatal treatment (i.v.)	Postnatal treatments (i.p.)	Postnatal treatment (i.v.)	Group abbreviation	Number of mice/group
3	NaCl	DSP-4	-	ND	10
	PolyI:C	DSP-4	-	PD	10
5	NaCl	-	-		8
	PolyI:C	-	-		8
6	NaCl	DSP-4	-	ND	10
	PolyI:C	DSP-4	-	PD	10
16	NaCl	NaCl	NaCl	NNN	12
	PolyI:C	NaCl	NaCl	PNN	8
	PolyI:C	NaCl	PolyI:C	PNP	11
	PolyI:C	DSP-4	NaCl	PDN	10
	PolyI:C	DSP-4	PolyI:C	PDP	11*
	NaCl	DSP-4	PolyI:C	NDP	12

*one mouse with hydrocephalus, was excluded for IHC and PET analyses

Behavioral Testing

To assess whether NA depletion worsens the cognitive deficits reported previously in aged prenatally immune-challenged mice (Krstic et al., 2012a), animals of the 2nd cohort (table 1 and figure 1A) were subjected to two different tests using the elevated Y-maze. The first task assessed spatial short-term memory performance using the sample/choice paradigm (described below). The second task tested non-spatial short-term memory performance (spontaneous alternation).

Apparatus

The Y-maze apparatus consisted of 3 identical arms (500 mm long × 90 mm wide) surrounded by transparent (in sample/choice task) or opaque (covered with white paper for the spontaneous alternation test) plexiglas walls 100 mm in height. The 3 arms radiated from a central equilateral triangle. The floor of the maze was either covered with sawdust bedding, which was changed between each test run (for sample/choice task) or kept uncovered and cleaned with water between each test run (spontaneous alternation task). The maze was placed onto a desk which

was encircled by black curtains (to separate the maze from the rest of the room, approximately 1.5 x 1.5 m) to assure optimal conditions such as light intensity and spare the mouse from putative distractions other than visual cues placed on the wall and curtains, if needed). A digital camera was mounted above the Y-maze apparatus. All experiments were videotaped and simultaneously analyzed using EthoVisionPro tracking system (Version 2.2.14, Noldus Information Technology,)

Procedure for Sample/Choice Task

Before starting the test, the mouse was transferred to an empty cage. Sample phase: one arm of the maze was blocked using a plexiglas blocker (between mice and groups the blocked arm was alternated to avoid bias). The mouse was placed in the start arm - this was kept constant between the two phases but was alternated between mice and groups to avoid bias - and allowed to explore the two arms. After 5 min the mouse was taken out of the maze and returned to the empty cage. The bedding was changed and the blocker removed. After a delay of approximately 2 min the mouse was put back into the start arm and allowed to explore the maze for another 5 min. The percent of time spent in the novel and familiar arms was calculated after 2 min of testing. Chance level is defined as 33.3%, indicating that the mouse has no preference towards the novel arm and therefore was not able to distinguish between familiar and novel arms. Total distance moved was recorded and analyzed to assess general activity during the choice phase.

Procedure for Spontaneous Alternations

Before starting the test, the mouse was transferred to an empty cage. The mouse was then placed into one arm of the Y-maze (kept constant for all animals). An observer located in the same room – separated by the curtains – monitored the mouse through the video camera, and recorded the number and sequence of arm entries (defined as entry of the whole body into an arm) during a period of 5 min. Alternation was defined as entry into the 3 arms in any non-repeating order (for example, ABC, BAC, CBA). The percentage of alternation was calculated as the total number of alternations divided by the possible number of alternations given by the number of arm entries (total number of arm entries -2). Chance level is defined as 50% alternation. In addition to the analysis of percentage alternation, the total number of arm entries was recorded and analyzed to assess general activity during the 5-min test period.

[^{18}F]-Fluorodeoxyglucose (FDG) Positron Emission Tomography (PET) Measurement

FDG PET Acquisition

1 week before PET acquisitions, animals were transferred to the animal imaging center at the ETH Zurich. Animals were housed under approved conditions and had free access to food and water before the experiments. Animals of all 6 groups (NNN n = 8; PNN = 7; PNP = 9; PDN = 10; PDP = 8; NDP = 9) were weighed immediately prior to PET imaging (27.7 g to 59.7 g). Mice were anesthetized with isoflurane (5 % for induction, 2.5 to 3.5% for maintenance during image acquisition) in a mixture of air and oxygen (70/30%). After induction, animals were placed in the scanner and a tail vein catheter (PE10 tube) was placed for [^{18}F]-FDG injection. Immediately before PET acquisitions, a blood sample was collected for the measurement of the glucose level (ranging from 4.1 to 9.5 mM).

[^{18}F]-FDG (5.18 to 15.52 MBq in 112 µL saline) freshly obtained from the University hospital Zurich (routinely produced for clinical use) was injected over a period of 3 min with a syringe pump (Harvard Apparatus). The mouse was centered in a scanner with a 4.8 mm axial field of view (VISTA eXplore [GE Healthcare]). First a computed tomography scout image was acquired and bed position was adjusted, if necessary, in such a way that the head and the thoracic region were acquired simultaneously. PET coincidence events were acquired in list mode over a 45 min scan period. PET acquisitions and tracer injections were started at the same time. During imaging, the respiratory rate was monitored (1025L; SA Instruments) and maintained at 90 bpm by adjusting isoflurane concentration if required. In addition, mouse body temperature was kept at 37°C by a fan controlled by a rectal temperature probe.

Once a day, the PET scanner was calibrated to kBq/cm^3 by means of a 5-mL syringe filled with a [^{18}F]-FDG solution of known radioactivity concentration (~1 MBq/mL). With the same settings as for the PET mouse scans a static scan of 5 min was acquired.

Image Analysis

PET images were reconstructed to a nominal voxel size of 0.3875 x 0.3875 x 0.775 mm (actual resolution of 0.9 mm in full width at half maximum in the center of the field of view (FOV) with a 3-dimensional FORE/2-dimensional OSEM algorithm). Scatter correction was applied. Data were not corrected for attenuation. List mode data were rebinned (30 x 10 sec, 20 x 15 sec, 5 x 60 sec, 6 x 300 sec). Finally, the last 15 min of acquisition were averaged and taken for further analysis. The software package PMOD 3.5 (PMOD Technologies Ltd, Zürich, Switzerland) was then used for PET data analysis. For each mouse brain, volumes of interest (VOIs) were drawn

for the following regions guided by a mouse magnetic resonance template (Mirrione et al., 2007), which was co-registered to our PET data: Cerebral cortex, left and right hippocampus, thalamus, olfactory bulb (OB) and cerebellum.

Tracer uptake was expressed in kBq/cm^3 using the syringe calibration. Dividing the tissue tracer uptake by the injected activity per gram of body weight yielded the standardized uptake value (SUV).

Tissue Preparation for Immunohistochemistry and Biochemistry

Tissue preparation was performed as previously described (Notter et al., 2014). In brief, mice were deeply anesthetized with sodium pentobarbital (Nembutal; 50 mg/kg; i.p.) and perfused intracardially with 15–20 mL ice-cold, oxygenated aCSF [containing (mM) NaCl 125, KCl 2.5, $CaCl_2$, 3.7, $MgCl_2$ 2, $NaHCO_3$ 26, NaH_2PO_4 1.25, glucose 25], pH 7.4, at a flow rate of 10–15 mL/min. Animals were decapitated, the brain immediately extracted from the skull and divided into 3 blocks: cerebellum/brainstem and each of the 2 hemispheres. The right hemisphere and the cerebellum/brainstem were immediately immersion-fixed for 3 hours in ice-cold, freshly prepared fixative [4% paraformaldehyde dissolved in 0.15 M sodium phosphate buffer containing 15% saturated picric acid], pH 7.4, before it was rinsed with PBS (pH = 7.4) and cryoprotected overnight in 30% sucrose in PBS at 4°C.

The fixed tissue was then frozen and cut with a sliding microtome at a thickness of 40 μm into serial sagittal (hemisphere) or coronal (brainstem/cerebellum) sections collected in ice-cold PBS. The sections were stored at -20°C in cryoprotectant solution (50 mM sodium phosphate buffer, pH 7.4, containing 15% glucose and 30% ethylene glycol; Sigma-Aldrich) until used for IHC.

The left hemisphere was used for Western blotting. It was dissected on ice to separate the hippocampus, cortex, entorhinal/piriform cortex, and OB. Tissue was immediately frozen with dry ice in safe-lock Eppendorf tubes and stored at -80°C until lysis.

Immunohistochemistry

All staining were performed in either 1:18 (all analyses of sagittal sections) or 1:2 (stereological counting of LC neurons) series.

After rinsing the sections in Tris-buffer (pH 7.4), they were incubated overnight at 4°C under constant agitation in primary antibody solution (0.2% Triton X-100, 2% normal serum and the antibody of choice (table 2)).

Table 2 List of primary antibodies used in this study.

Target	Distributor	Description, Ca. no.	Dilution	Application
cAPP	Immunogens	Rabbit poyclonal, custom made, S511_112	1:100'000 1:200'000	IHC (DAB) WB
nAPP	Millipore, Billerica, MA, USA	Mouse monoclonal, (A4), N-terminal, clone 22 C 11, MAB348	1:5000	WB
CD11b	eBioscience Inc.	Monoclonal rat, 14-0112	1:2000	IHC (DAB)
CD68	AbD Serotec Ltd, Oxford, UK	Rat monoclonal, clone FA11, MCA1957GA	1:3000	IHC (DAB)
COX2	Abcam	Rabbit polyclonal, ab15191	1:4000	IHC (DAB)
GFAP	Dako Schweiz AG, Baar, Switzerland	Rabbit polyclonal, Z 334	1:15'000	IHC (DAB)
Iba1	Wako	Rabbit polyclonal, 019-19741	1:3000	IHC (DAB)
Noradrenaline transporter (NAT)	Mab Technologies, Inc.	Mouse monoclonal, NET05-2	1:5000	IHC (DI)
Tau	Thermo Fisher Scientific, Waltham	Mouse monoclonal, total Tau, clone Tau-5	1:48'000	WB
pTauT205	Abcam	Rabbit polyclonal, Ab4841	1:20'000	WB
Tyrosine hydroxylase (TH)	Thermo Fisher Scientific, Waltham	Rabbit polyclonal, AB152	1:3000 1:5000	IHC (DAB) IHC (DI)

Immunoperoxidase staining: Sections were washed 3 x 10 min in Tris buffer and incubated for 30 min at room temperature in biotinylated secondary antibodies (Jackson ImmunoResearch Laboratories Inc., West Grove, PA, USA) diluted 1:300 in Tris buffer containing 2% normal serum, followed by 3 washes in Tris-buffer. Sections were then incubated for 30 min in ABC solution (Vectastain Elite kit; Vector Laboratories, Burlingham, CA, USA), washed again and processed for immunoperoxidase staining using 3,3-diaminobenzidine (DAB; Sigma–Aldrich Inc.) as a substrate and hydrogen peroxide following the manufacturer's instructions. After 3 thorough washes in PBS, the sections were mounted onto gelatinized glass slides and air-dried overnight, dehydrated through ethanol, cleared in xylene and coverslipped with resinous

(Eukitt™™; Sigma-Aldrich) mounting medium or DPX mountant for histology (06522; Sigma-life science) for dark-field microscopy.

Immunofluorescence staining: sections were washed 3 x 10 min in Tris buffer, incubated for 30 min at room temperature with secondary antibodies coupled to Alexa488 (diluted 1:1000; Molecular Probes, Eugene, OR, USA), Cy3 (diluted 1:500; Jackson Immunoresearch). After incubation - shielded from light - sections were washed thoroughly, mounted onto gelatinized glass slides, coverslipped with Dako fluorescence mounting medium and stored in the dark at 4°C.

Nissl Staining

To determine the number of LC cells, brainstem sections were stained with Cresyl violet. Every other coronal section containing cerebellum and brainstem was rinsed in PBS, mounted onto gelatinized glass slides and air dried overnight. The slides were dipped successively in the following solutions: 5 min in dH_2O, 5 min in filtered Cresyl violet solution ($C_{18}H_{15}N_3O_3$, M 321.34, Fluka BioChemika, Cat. no. 10510-54-0), 30 sec in dH_2O and cleared in 96% ethanol containing 0.5% acetic acid until the desired coloration was obtained, 5 min in isopropanol, 5 min in isopropanol:Xylene (1:2) and 4 times in xylene for 2 min. They were then coverslipped with Eukitt.

Image Acquisition

Images were acquired in 4 ways:

For display, images were acquired with a color digital camera using either bright- or dark-field illumination (Zeiss Axioskop, Jena, Germany). Digital images were taken with a 10x (air, numerical aperture (NA) 0.75) objective.

1st cohort, CD68 IHC: sections were scanned with an automated upright slide scanning microscope (Zeiss) in the bright-field mode; specific scanning settings were programmed with the Mirax Viewer 1.8.3.0 (Zeiss) software. Image acquisition was performed by a digital camera (Axiocam monochrome CCD, 1288 x 1040 pixels with a pixel size of 0.23 μm, Zeiss) using a 20x objective (air, NA 0.8). Areas of interest were exported as TIFF files for densitometry analysis using either ImageJ or the Mirax Viewer (3D Histech Lid., Germany).

2nd cohort, TH and CD68 IHC: images were acquired with a black and white digital camera using either bright- or dark-field illumination (Zeiss Apotome, ImagerZ1, Jena, Germany).

Digital images were acquired with a 10x (air, NA 0.3) objective for TH staining or 20x (air, NA 0.8) objective for CD68 staining.

Double fluorescence staining: Sections were visualized by confocal laser scanning microscopy (LSM-700; Zeiss, Jena, Germany) using a 40× (oil, NA 1.4) objective and sequential acquisition of separate channels. Z-stacks of consecutive optical sections (20-23; 1024 × 1024 pixels, spaced 0.6 µm in *z*) were merged and projected using the maximal intensity mode using the image analysis software Imaris (Bitplane, Zurich, Switzerland) for display.

Cropping of images, adjustments of brightness and contrast were performed using Adobe Photoshop and were identical for each staining. A sharpening filter was applied to images of TH staining.

Immunohistochemistry Analysis

TH Staining

The density of TH immunopositive axons was determined using an intensity threshold algorithm (ImageJ software) and calculated as percentage surface in the area of interest. The average density per mouse was calculated from 2-3 serial sections spaced 720 µm.

CD68 Profile Count Analysis

The density of microglial cells was determined using threshold segmentation and the particle count tool of ImageJ. Average profile density per mouse was calculated in 2-3 serial sections spaced 720 µm.

Iba1 Profile Count Analysis

To confirm the results of the CD68 immunostaining, microglial cells were counted stereologically in sections stained for Iba1 (2-3 serial sections spaced 720 µm) using the Mercator software (Mercator Pro rev. 7.8.2, Explora Nova, La Rochelle, France). The sections were viewed using an Axioplan 2 bright-field microscope (Zeiss, Feldbach, Switzerland) with 20x (air, NA 0.75) objective. The following counting parameters were used: a counting frame 100 x 100 µm and a space between frames of 80 µm. The cell number was calculated by optical fractionator with the following parameters: section thickness 40 µm and optical fractionator sampling fraction (ssf): 1/18. The volume was calculated based on: $V = \sum A \times t_{nom} \times 1/ssf$; with V representing analyzed volume, A representing analyzed areas, and t_{nom} representing nominal section thickness (40 µm). The number of cells was depicted as number of cells/volume analyzed.

Densitometry Analysis

Densitometry analyses of immunoperoxidase staining intensity were performed using the MCID software of Imaging research Inc.. Images were digitized using a precision illuminator and photo-camera. Grey values were calibrated using the Kodak step tablet no. 310ST607. The intensity values in the different areas of interest were normalized to the intensity of the whole section to correct for variations in background staining – observed, in particular, in ND mice with antibodies against inflammatory markers.

Stereological Analysis of LC Cell Number

The number of LC cells was determined stereologically in Nissl-stained sections. A 1:2 series of serial sections was viewed using an Axioplan 2 bright-field microscope (Zeiss, Feldbach, Switzerland) with 40x (oil, NA 1.3) objective. The number of cells were counted and estimated with Mercator software (Mercator Pro rev. 7.8.2, Explora Nova, La Rochelle, France). The following counting parameters were used: counting frame 50 x 50 µm and a space between frames of 30 µm. Only cells with nucleoli in focus were counted. Cell number was calculated by optical fractionator with the following parameters: section thickness 40 µm and ssf: 1/2.

Western Blotting

Brain lysis and sample preparation were performed as previously described (Krstic et al., 2012a), with the following adaptations: Tissue was sonicated in 300 µL (hippocampus) or 200 µL (cortex, EC and OB) ice-cold RIPA buffer and centrifuged at 40,000 g at 4°C for 20 min. Total protein concentration in the supernatant was measured with a spectrophotometer (NanoDrop; Thermo Fisher Scientific Inc., Rockford, IL, USA).

Protein separation and immunoblotting were performed as described (Krstic et al., 2012a), using samples of 80 (cortex), 60 (hippocampus and EC) and 40 (OB) µg protein (1st cohort) or 40 µg protein (2nd cohort) loaded onto 8-12% Bis-Tris Midi Gels (NuPAGE Novex Bis-Tris Midi Gel, 26 wells). The electrophoresis was performed using the Xcell4 SureLock Midi-Cell system (Cat.No. WR0100, Invitrogen). Proteins were separated during 40 (cAPP) or 45 (all other markers) min at 200V. Proteins were blotted for 30 min at 20V using the Novex Semi-Dry Blotter (Cat.No. SD1000, Invitrogen).

Proteins were visualized using the primary antibodies listed in table 2. Signals were visualized either with a chemiluminescence system with antibodies coupled to horseradish peroxidase (classical X-ray film exposure to detect C-terminal cleaved fragments of APP, or for stronger

signals the Fujifilm system and ImageReader LAS-1000 software, using Adobe Photoshop to visualize bands) or with fluorescence with secondary antibodies coupled to a fluorochrome (Odyssey infrared imaging system).

Signal Quantification

Each Western blot was performed at least 3 times and the figures show representative blots and their corresponding quantifications.

Chemiluminescence signals were analyzed using ImageJ Launcher software. The intensity of the bands of interest (AUC) was determined and normalized to the actin band in the same lane. Fluorescence signals were analyzed using the (Odyssey ImageStudio 3.1.4 software).

In the 2nd cohort, the 64 samples were analyzed in 2 different ways: The 64 samples were evenly distributed among 3 midigels (chemiluminescence). This did not allow pooling of data (making the number of samples to be compared very small). To be able to pool the data, 4 midigels were loaded as follows: for each gel samples from the same 8 NNN controls (serving as internal control) were taken and the remaining lanes were filled up with different samples from the remaining groups (figure 7 and supplementary figure S4). Each signal was first normalized to the corresponding actin signal and then normalized to the mean of the internal controls.

Statistical Analyses

Data are presented as mean ± SEM. Values were tested for Gaussian distribution using the Kolmogorov-Smirnov test (Prism software, GraphPad version6). Outliers were determined and excluded using the Gubb's test – also called ESD (extreme studentized deviate) – in online Quick Calcs provided by GraphPad Software. Statistical analyses in the 1st cohort were made using unpaired *t* test, two-tailed (Prism software, GraphPad version6). Statistical analyses in the 2nd cohort were made using one-way ANOVA followed where appropriate by Bonferroni - test (Prism software, GraphPad version6) or Fisher's least significant difference (LSD) *post-hoc* test (StatView software).

Results

Effect of DSP-4 on Prenatally PolyI:C-Exposed Mice

The 2 cohorts of mice and their treatment paradigms used for this study are depicted in figure 1A and summarized in table 1. The first cohort consisted of 10 prenatally-exposed PolyI:C (P) mice and 10 NaCl (N) controls were subjected to a single postnatal DSP-4 (D) injection at 3 months of age and subsequently examined histologically at 6 months (group abbreviations for PolyI:C-exposed mice are PD and ND for NaCl controls, respectively). The purpose of these experiments was to determine whether the regeneration capacity of LC axons in young adult mice is influenced by the effects of PolyI:C exposure. In addition, we aimed to evaluate whether combined PolyI:C and DSP-4 treatment influences innate immunity and induces changes in AD-associated proteins levels at this stage. These results will be presented in figures 2 to 4. *Post-hoc*, this cohort was completed by a group of prenatally-exposed PolyI:C mice that were not treated with DSP-4 to evaluate the effect of PolyI:C alone on innate immunity.

The 2nd cohort consisted of 64 mice that were also exposed prenatally to PolyI:C (or NaCl) and received DSP-4 injections every 3 months starting at 3 months of age (NaCl injections served as control). At 12 months – 7 days after the last DSP-4 injection – mice were either treated with PolyI:C or NaCl i.v. (as in the "double hit" model (Krstic et al., 2012a)) and aged for additional 3 months before undergoing behavioral tests. Finally, prior to tissue collection [^{18}F]-FDG PET imaging was performed to evaluate cerebral glucose uptake in the different treatment groups. This cohort consisted of the following 6 groups (nomenclature: the 1st letter stands for prenatal PolyI:C or NaCl treatment; the 2nd for multiple postnatal DSP-4 or NaCl treatments; and the 3rd for postnatal PolyI:C or NaCl treatment (figure 1A and table 1)), NNN animals served as basal controls. PNN and PNP represented the single and double immune challenged groups. PDN allowed validating NA depletion after prenatal PolyI:C exposure and the PDP NA depletion in mice pre- and postnatally exposed to PolyI:C, respectively. NDP served as a control towards PDP to validate the importance of the prenatal PolyI:C exposure. This group was necessary, since we have previously shown that postnatal PolyI:C alone had no effect on AD-like changes in aged animals (Krstic et al., 2012a). We were, therefore, interested in seeing whether postnatal PolyI:C in a NA depleted background was sufficient to induce changes. Two control groups were omitted: NNP, for the reason mentioned above, that postnatal PolyI:C has no effect on AD-like changes in aged wild type animals.

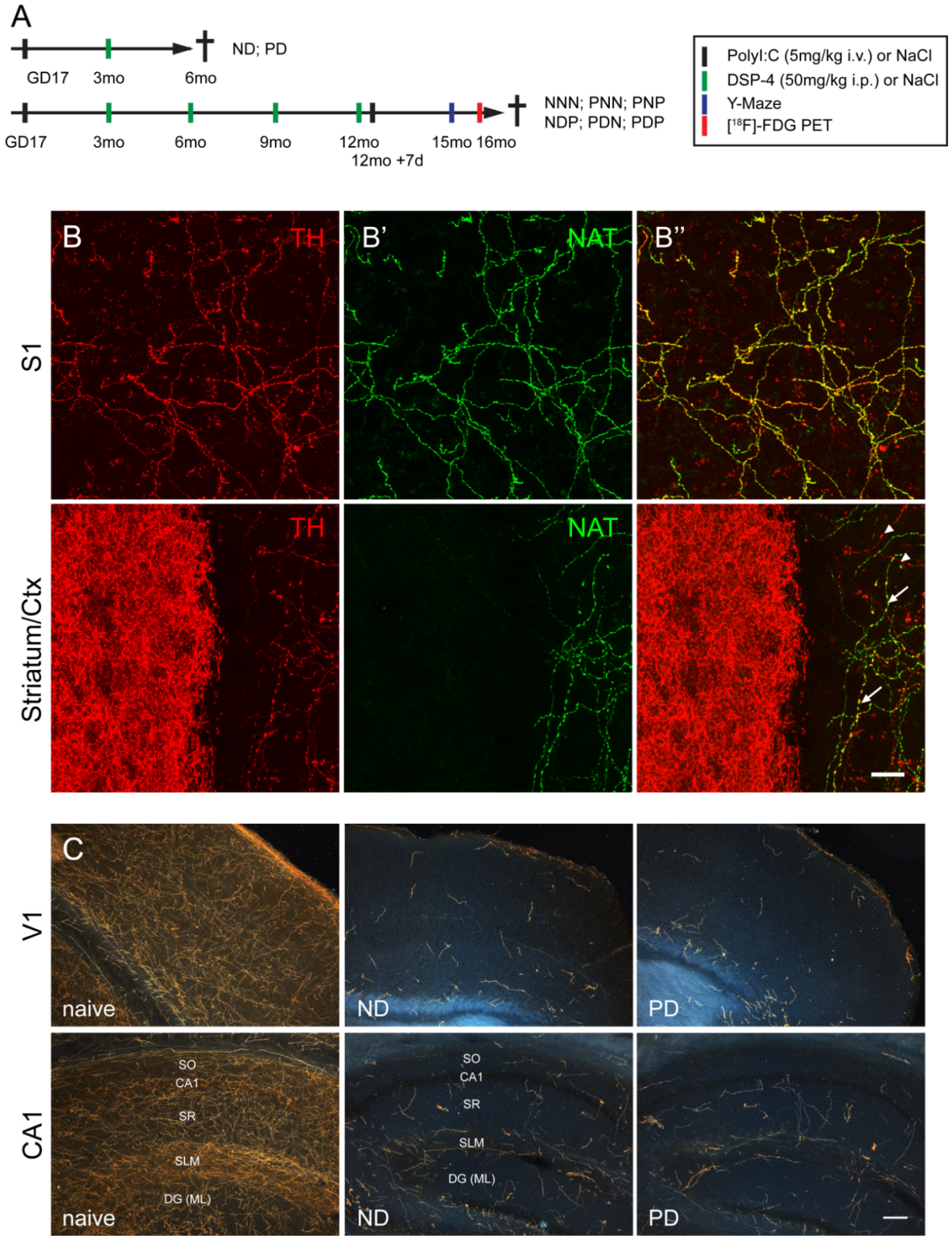
A
ND; PD
GD17
3mo
6mo
GD17
3mo
6mo
9mo
12mo
12mo +7d
15mo 16mo
NNN; PNN; PNP
NDP; PDN; PDP
PolyI:C (5mg/kg i.v.) or NaCl
DSP-4 (50mg/kg i.p.) or NaCl
Y-Maze
[18F]-FDG PET
B
TH
B'
NAT
B''
S1
Striatum/Ctx
TH
NAT
C
V1
naive
ND
PD
CA1
SO
CA1
SR
SLM
DG (ML)
naive
SO
CA1
SR
SLM
DG (ML)
ND
PD

And the NDN group, because pilot experiments revealed that a single DSP-4 treatment in aged mice did not affect AD-related proteins or inflammatory responses (data not shown). In line, previous studies observed no AD-like changes after multiple DSP-4 treatments in C57BL/6J mice (Heneka et al., 2006).

Preliminary IHC experiments in tissue from 16 to 20 month-old mice showed that mouse monoclonal antibodies could not be used due to high levels of non-specific binding of secondary antibodies (against mouse IgG) occurring in tissue of old mice. Therefore, we selected antibodies from non-rodent species for all IHC experiments. Nevertheless we verified in young mice that TH antibodies can be used to visualize LC axons by double labelling with a polyclonal rabbit antibody against tyrosine hydroxylase (TH) and a mouse monoclonal against the NA transporter (NAT). As expected, TH and NA immunofluorescence is co-localized in brain areas innervated by NA axons, e.g., the primary somatosensory (S1) (figure 1B) and visual (V1) cortex, as well as the CA1 area of the hippocampus, and the thalamus (basolateral nucleus) (not shown). The striatum, which is mainly innervated by dopaminergic neurons and contains only a few, isolated LC axons, was almost completely devoid of NAT immunofluorescence (figure 1B). Some TH-positive axons, lacking NAT-staining, were seen, as expected, in the frontal cortex.

Figure 1: Effect of DSP-4 in prenatal PolyI:C-exposed animals. A. Treatment paradigm of the two cohorts used for this study. Black bar represents intravenous (i.v.) PolyI:C (5 mg/kg) or NaCl injections (prenatal exposure at GD17 and postnatally at 12 months). Green bars represent intraperitoneal (i.p.) DSP-4 (50 mg/kg) injection for the 1st cohort, or DSP-4 (50 mg/kg) or NaCl injection for the 2nd cohort. Blue bar represents behavioral experiments (Y-maze spontaneous alternation and sample/choice test). Red bars represent (^{18}F)-FDG PET imaging study. Tissue was collected after completion of PET imaging studies at 16 months of age. Abbreviations: gestational day (GD), months (mo), days (d). **B.** Double immunofluorescence staining for tyrosine hydroxylase (TH) (B; red) and NA transporter (NAT) (B'; green) in primary somatosensory cortex (S1) and striatum/frontal cortex of 5 month-old control mice, imaged by confocal laser scanning microscopy. Images represent stacks of 20-23 pictures spaced 0.6 μm. Merged images (B") illustrate the paucity of dopaminergic axons (TH^+/NAT^-; arrowheads) in cerebral cortex, as well as the absence of NA axons (TH^+/NA^+) in the striatum. Scale bar: 20 μm. **C.** Demonstration of DSP-4 toxicity in prenatally PolyI:C immune-challenged mice. Dark-field microscopy images of sections stained by immunoperoxidase against TH in the primary visual cortex (V1) and CA1 from naïve or prenatal NaCl (ND) and prenatal PolyI:C (PD) mice 7 days after DSP-4 treatment. NA axon depletion is clearly evident by the drastic reduction of TH-positive axons, and it did not differ between the 2 treatment groups. Abbreviation: stratum oriens (SO), stratum pyramidale (SP), stratum radiatum (SR), stratum lacunosum moleculare (SLM) and molecular layer of dentate gyrus (DG (ML)), scale bar: 200 μm.

To evaluate whether exposure to PolyI:C could have an effect on DSP-4 toxicity, we injected adult prenatally-exposed PolyI:C/NaCl mice with DSP-4 and examined them 7 days later, when LC axon degeneration was expected to be maximal in rodents (Jonsson et al., 1981, Fritschy et al., 1990, Fornai et al., 1996). DSP-4 treatment caused an almost complete loss of TH-positive LC axons (figure 1C). Based on visual examination, no difference in axon densities between the 2 groups was evident in any of the regions examined (frontal cortex, S1, V1, CA1, thalamus, striatum), indicating that prenatal immune challenge had no detectable effect on DSP-4 acute toxicity.

Prenatal Immune Challenge: LC Axonal Regeneration Capacity

An extensive LC axonal regeneration study performed in rats revealed that there is a region-specific difference in the temporal pattern of axonal regeneration after a single DSP-4 treatment (Fritschy and Grzanna, 1992). They observed the fastest reinnervation in thalamus, followed by the cerebral cortex (in a rostro-caudal manner) and the hippocampus. Interestingly, hindbrain areas such as tectum and cerebellum remained devoid of axons 1 year after DSP-4 treatment. This study confirmed the remarkable regeneration capacity of LC axons in the absence of any other perturbation in the adult CNS. The mechanisms governing the specific pattern of regrowing axons, however, are still unknown.

To evaluate whether prenatal PolyI:C exposure could have an effect on the regeneration capacity of LC axons, we performed IHC staining against TH in sagittal brain sections of 6 month-old mice (cohort 1; injection paradigm see figure 1A). Densitometry analysis of TH-positive axons was performed in cortical areas (frontal, S1 and V1) and the hippocampus (CA1 - including stratum oriens (SO), stratum pyramidale (SP) and stratum radiatum (SR) - and the molecular layer of dentate gyrus (DG (ML)). The cortical area furthest away from the LC, V1 and the CA1 area, displayed a significantly lower axon density in animals that were prenatally challenged with PolyI:C compared to NaCl controls (unpaired *t* test, two-tailed: CA1: $t_{18} = 2.97$, $p = 0.008$; V1: $t_{17} = 2.38$, $p = 0.029$; frontal: $t_{18} = 1.63$; S1: $t_{18} = 2.05$; DG (ML): $t_{17} = 1.64$) (figure 2A and B). DSP-4 treatment is known to induce subsequent partial neurodegeneration of LC neurons. To test whether PolyI:C exposure had an effect on LC cell survival, a stereological counting of LC neurons in Nissl-stained coronal brainstem sections was performed. The analysis revealed no significant difference in the number of LC neurons between the 2 groups (unpaired *t* test, two-tailed: $t_{16} = 0.96$). The number of LC neurons was reduced by 17% (ND) and 14% (PD) compared to 6 month-old naïve mice (figure 2C). This result indicates that prenatal immune

activation affects axonal regeneration mechanisms in the adult brain without worsening neurodegeneration.

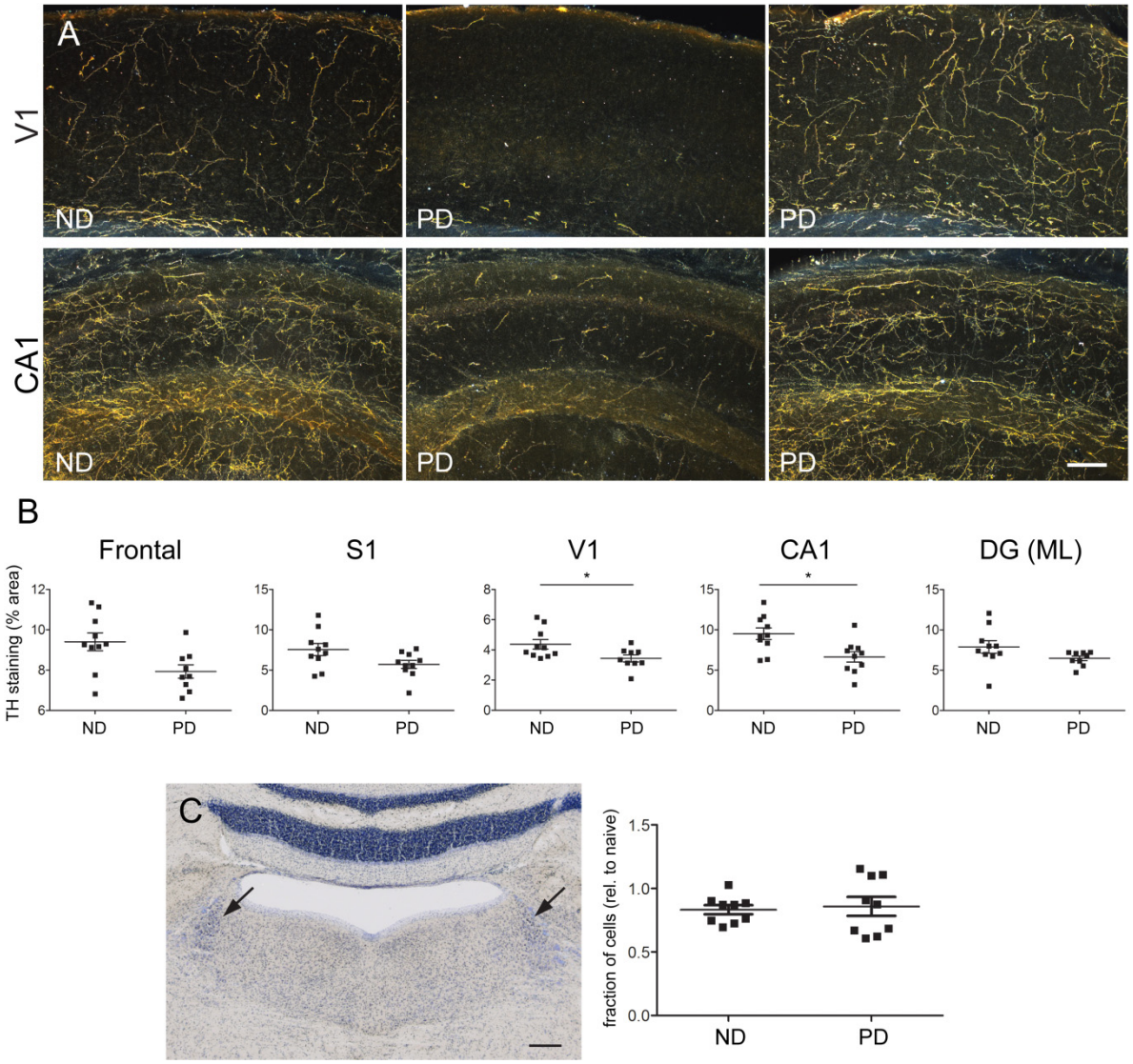

Figure 2: Effect of prenatal PolyI:C on the regeneration capacity of NA axons 3 months after DSP-4 treatment. A. Representative dark-field microscopy image of DAB stained sections against tyrosine hydroxylase (TH) from ND (left) and 2 different PD (middle and right) mice. Representative images of immunoperoxidase staining against TH in sections from ND (left) and 2 PD (middle and right) mice. Axonal regeneration in the primary visual (V1) cortex and CA1 region (including SO, SP, SR, SLM, DG (ML)) is evidenced by the partial recovery of TH staining (compared to naïve mice shown in figure 1C); scale bar: 200 µm. **B.** Quantifications of density (area fraction) of TH-positive axons in frontal cortex, S1, V1, CA1 region and the molecular layer (ML) of the DG (mean ± SEM). Significant decrease of axon density is detected in V1 and CA1. **C.** Representative Nissl-stained coronal section of the brainstem containing the LC (arrows), scale bar: 200 µm. Unbiased quantification of neuron density is presented relative to naïve mice (Mean ± SEM). Statistical test: unpaired *t* test, two-tailed; **p* < 0.05.

Combined Prenatal PolyI:C and DSP-4: Microglia and Astrocytes

We have previously shown that prenatal PolyI:C exposure leads to a sustained increase in pro-inflammatory cytokine levels (Krstic et al., 2012a). However, evident IHC changes in microglia and astrocyte reactivity were only detected in 15 month-old animals that received a 2nd PolyI:C treatment at 12 months of age.

To evaluate whether the temporary loss of LC axons could have had an effect on immune cell activation in mice primed with PolyI:C, we performed IHC staining against the following immune cell markers: CD68 – a lysosome-associated membrane glycoprotein known to be increased in activated microglia cells; Iba1 – a cytoplasmic calcium binding adaptor molecule; CD11b – a part of the complement receptor 3 complex; COX2 – known to be increased in inflammation; and GFAP – an intermediate filament which is selectively expressed by astrocytes. All markers were quantitatively analyzed by profile counting and/or densitometry analysis in the same areas as those in which TH-axon densities were measured. The results are provided in figure 3 and S1.

For CD68 staining, profile counting revealed that prenatally PolyI:C-exposed mice (PD) exhibit an increase of approximately 13% in the number of microglial cells in CA1 compared to ND mice (unpaired *t* test, two-tailed: CA1: $t_{17} = 3.27$, $p = 0.005$; V1: $t_{18} = 0.47$) (figure 3A). This result was confirmed by stereological analyses of the CA1 region in sections stained against Iba1 (unpaired *t* test, two-tailed: CA1: $t_{17} = 2.74$, $p = 0.014$) (figure 3C). All other areas analyzed showed no difference in terms of profile counts (unpaired *t* test, two-tailed: frontal: $t_{18} = 1.63$; S1: $t_{18} = 1.23$; DG (ML): $t_{16} = 1.75$, thalamus: $t_{15} = 0.23$) (figure 3B).

To evaluate to what extent the increase in CD68 positive microglia is dependent on NA depletion, we performed the same analysis in sections obtained from a separate group of 5 month-old mice prenatally subjected to PolyI:C or NaCl (see table 1). Profile count analysis revealed a significant increase of approximately 18% in PolyI:C compared to NaCl exposed mice (unpaired *t* test, two-tailed: CA1: $t_{14} = 2.29$, $p = 0.038$) (figure 3D). As in the 1st cohort, numbers of microglia cells were unchanged in cortical regions (unpaired *t* test, two-tailed: S1: $t_{12} = 1.5$), indicating that DSP-4 treatment does not influence the increase in CD68-positive cells occurring after prenatal PolyI:C.

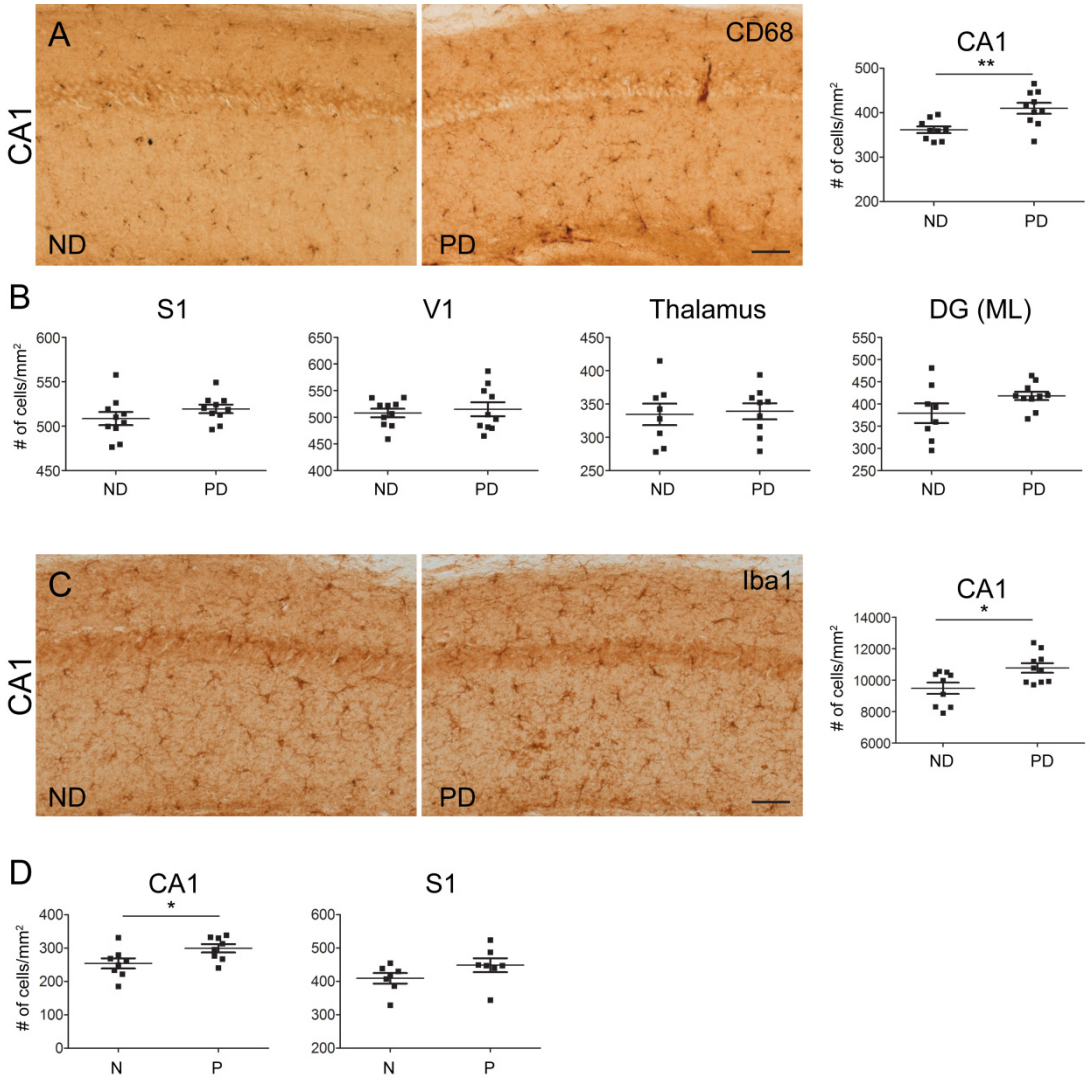

Figure 3: Effect of PolyI:C on microglia activation in 1st cohort. A. Representative bright-field microscopy images of the CA1 region from both treatment groups, depicting CD68 immunoperoxidase staining; scale bar: 200 µm. Corresponding quantification of CD68-positive profile count analysis in CA1 (mean ± SEM) are depicted on the right side, showing increased microglia in PD compared to ND. **B.** Quantification of CD68-positive profile count analyses in the primary somatosensory cortex (S1), primary visual cortex (V1), thalamus (basolateral nucleus) and the molecular layer of the dentate gyrus (DG (ML)) (mean ± SEM); revealed no significant difference in any of these regions. **C.** Representative bright-field microscopy images of Iba1 immunoperoxidase staining in the CA1 area of both treatment groups; scale bar: 200 µm. Corresponding unbiased quantification of Iba1-positive cells in the CA1 area are depicted on the right side confirming the increase in the PD group compared to ND (mean ± SEM). **D.** *Post-hoc* quantification of CD68-positive profile count analysis in CA1 (mean ± SEM) in sections from prenatal NaCl or PolyI:C-exposed 5 month-old mice are depicted on the right side, showing increased microglia in PD compared to ND. Statistical test: unpaired *t* test, two-tailed; $^{**}p < 0.01$, $^{*}p < 0.05$.

Densitometry analyses in sections stained against GFAP (unpaired *t* test, two-tailed: CA1: t_{18} = 3.86, p = 0.001) and CD11b (unpaired *t* test, two-tailed: CA1: t_{18} = 2.67, p = 0.016), but not against COX2 (unpaired *t* test, two-tailed: CA1: t_{18} = 1.70) and CD68 (unpaired *t* test, two-tailed: CA1: t_{18} = 1.70), further confirmed that CA1 display higher levels of inflammatory markers in PD mice compared to ND. In addition to CA1, the same changes were detected in DG (ML) (unpaired *t* test, two-tailed: GFAP: t_{18} = 3.54, p = 0.002; CD11b: t_{18} = 2.30, p = 0.034) (figure S1). Since CA1 was among the regions with the lowest reinnervation, we checked whether axon density correlated with the number of microglia. For both markers, no correlation between number of microglia cells and axon densities were detected. Further analyses revealed no significant correlation between any of the inflammatory marker analyzed and axon densities (relative staining intensities of GFAP and CD11b (CA1) and COX2 (V1) with axon densities). Therefore, it is unlikely that microglia proliferate more in PD mice due to decreased levels of NA and vice versa. The densitometry analyses in the remaining areas are represented in figure S1 and statistical analyses summarized in table 3. No significant changes were observed. These results suggest that the hippocampal formation is particularly prone to changes in inflammatory markers induced by PolyI:C.

Combined Prenatal PolyI:C and DSP-4: AD-Related Proteins

We have shown before that mice exposed prenatally to PolyI:C exhibit an age-dependent increase in levels of AD-related proteins, such as APP (full length and its cleavage products), as well as age-dependent differences in phosphorylation of Tau. Therefore, we hypothesized that the inflammatory changes detected in PD mice could accelerate these changes and result in earlier or stronger increase of APP levels and Tau phosphorylation.

We performed Western blot analyses using brain lysates from the contralateral hemisphere of the mice used in the IHC experiments. The following brain structures were analyzed: whole hippocampus, EC, frontal cortex (motor area) and the OB. All Western blots were performed at least 3 times using the chemiluminescence detection method, and the results illustrated were replicated at least once. In figure 4, 1 representative Western blot for each antibody used is depicted (hippocampus lysates).

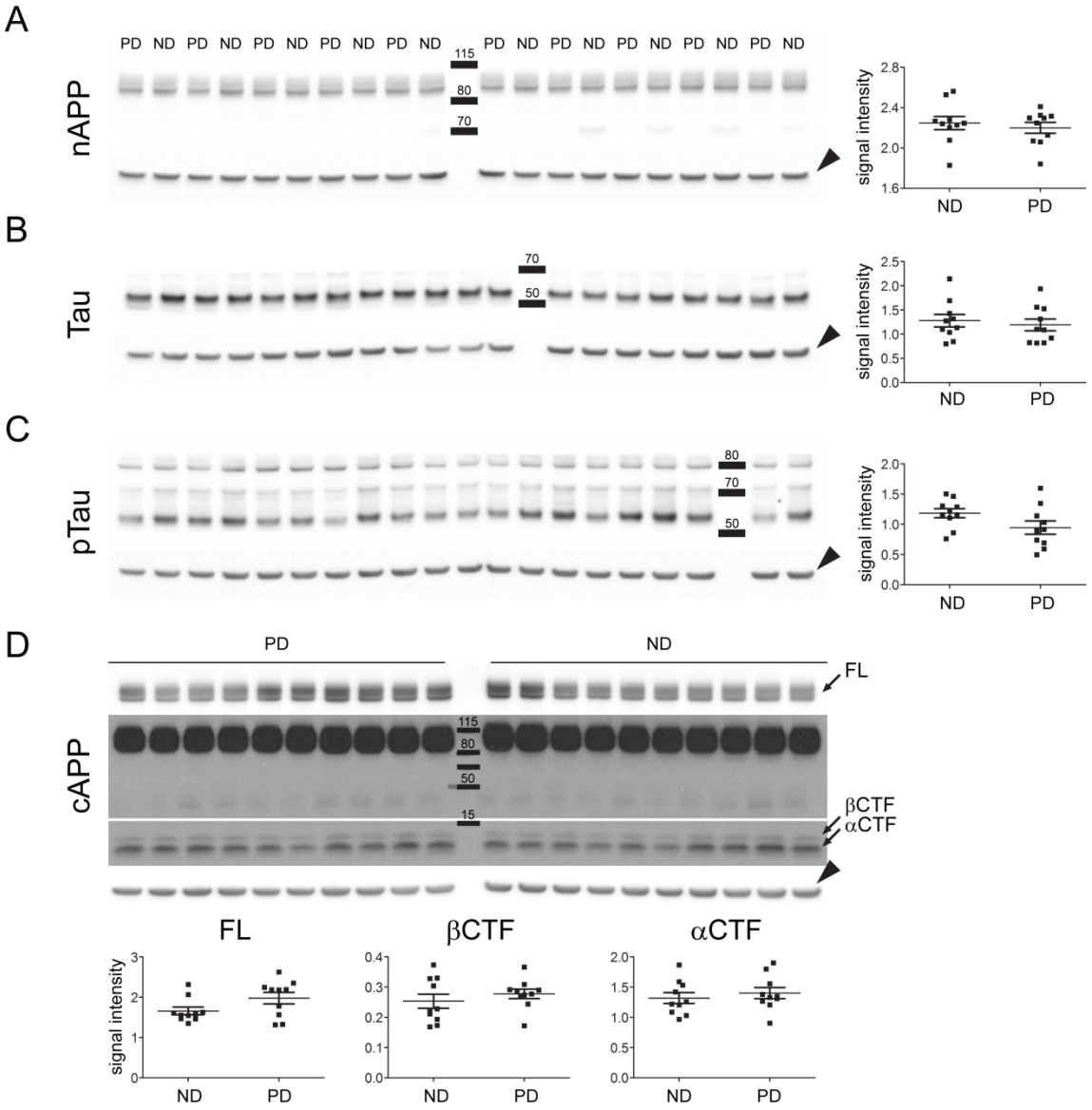

Figure 4: Western blot analyses of AD-related protein expression in the hippocampus of mice from 1st cohort. A representative Western blot for each marker is presented along with the densitometry analysis of the corresponding protein bands (line indicates group mean ± SEM). Molecular weights in kDa are indicated. Samples were loaded either by alternating between lysates from PD and ND lysates (A-C) or PD lysates were loaded in the 1st 10 lanes followed by ND (D). 60 µg of each sample was loaded and the respective loading control (actin band) is shown below each blot. **A.** Full length APP detected with an N-terminal antibody (apparent molecular weight, 100 kDa). No changes were observed between the 2 groups. **B.** Tau, detected with a phosphorylation-independent antibody (apparent molecular weight between 50-60 kDa). **C.** PTau, expected to run at a molecular weight slightly larger than Tau. Non-specific bands at 75 and 80 kDa were ignored. Again, no difference was observed between groups, even upon normalization of p-Tau over total Tau. **D.** Full-length APP and C-terminal fragments (CTFs) detected with a C-terminal antibody. 2 different exposures are shown for full length APP (apparent molecular weight, 100 kDa). CTFs dependent on α- or β-secretase cleavage are distinguished as indicated with arrows. Densitometry revealed no changes between groups.

The two to three bands (depending on the running buffer used during electrophoresis) migrating at around 100 kDa in APP Western blots against the N- (figure 4A) or C-terminus (figure 4D) represent full length APP. The bands could either reflect APP isoforms (Loffler and Huber, 1992) or are the product of posttranslational modifications such as glycosylation, sulfation and phosphorylation (Walter and Haass, 2000). Intensities were measured using the ImageJ analysis software and normalized to actin. No differences in full length APP or the C-terminal cleavage product levels were detected between lysates of ND and PD mice (unpaired *t* test, two-tailed: $nAPP_{FL}$: $t_{18} = 0.56$; $cAPP_{FL}$: $t_{18} = 1.87$; βCTF: $t_{18} = 0.87$; αCTF: $t_{18} = 0.64$).

Tau has an apparent molecular weight of 50-60 kDa and is slightly shifted upwards upon phosphorylation. $pTau^{T205}$ antibody used here only detects Tau that is phosphorylated at threonine 205. Similarly to APP, no changes were detected in total Tau (unpaired *t* test, two-tailed: $t_{18} = 0.50$) (figure 4B) or pTau (unpaired *t* test, two-tailed: $t_{18} = 1.81$) (figure 4C). Normalization of pTau to total Tau levels also revealed no differences between ND and PD mice (unpaired *t* test, two-tailed: $t_{18} = 0.89$). Similar results were obtained with Western blots performed with the other brain regions (figure S2).

These findings suggest that the inflammatory changes induced by combined PolyI:C and DSP-4 treatment were not sufficient to affect expression and/or processing of APP and phosphorylation of Tau at this age.

Combined PolyI:C and Multiple DSP-4: LC Axonal Regeneration Capacity

As we have shown in the 1st cohort, prenatal PolyI:C exposure affects both LC axonal regeneration and the immune response 3 months after DSP-4 treatment. However, this cohort did not show AD-like changes as reported to occur in 12 month-old mice prenatally challenged with PolyI:C (Krstic et al., 2012a).

Figure 5: Effect of multiple DSP-4 injections in PolyI:C-exposed mice of 2nd cohort on the regeneration of NA axons. A. Overview of the experimental design, listing the 6 treatment groups analyzed. **B**. Dark-field microscopy images from sections stained by immunoperoxidase against tyrosine hydroxylase TH. For each group, one representative image of the primary visual cortex (V1) and the CA1 area are shown; scale bar: 200 μm. **C**. Quantification of TH-positive axons in 6 selected regions (primary somatosensory (S1), primary visual (V1), CA1, molecular layer of the dentate gyrus (DG (ML)) and the thalamus (basolateral nucleus)), reporting the % of surface area covered by TH staining in the area of interest (mean ± SEM). In all regions except the thalamus (basolateral nucleus), DSP-4 treatment caused a decreased density of TH-positive axons, whereas pre- and/or postnatal PolyI:C exposure had no effect. Compared with figure 1, a partial regeneration is evident in all areas, leading to full recovery in the thalamus (basolateral nucleus). Statistical test: one-way ANOVA and Bonferroni *post-hoc*; ***$p < 0.001$, **$p < 0.01$* $p < 0.05$.

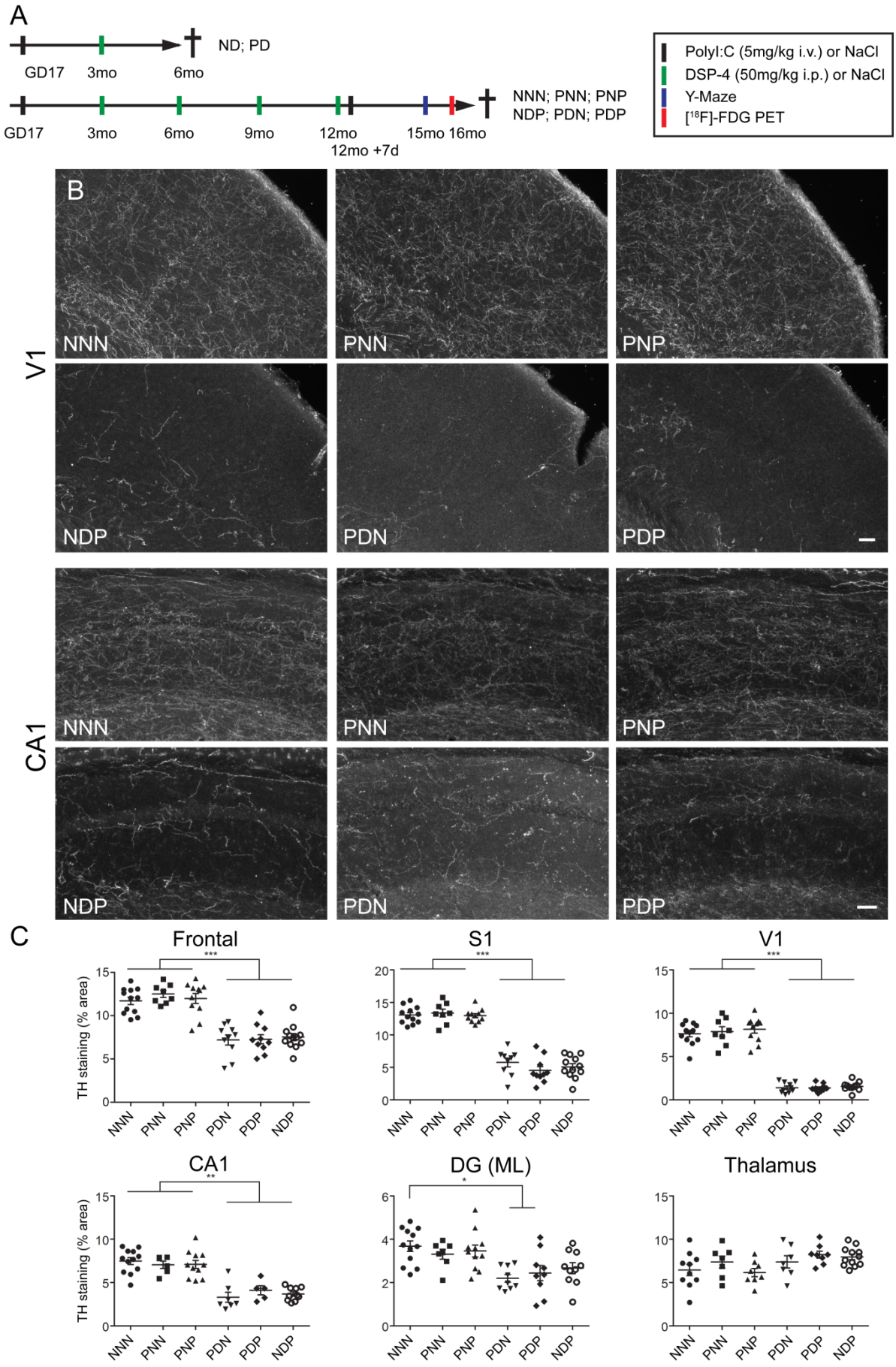
A
ND; PD
GD17
3mo
6mo
GD17
3mo
6mo
9mo
12mo
12mo +7d
15mo 16mo
NNN; PNN; PNP
NDP; PDN; PDP
Polyl:C (5mg/kg i.v.) or NaCl
DSP-4 (50mg/kg i.p.) or NaCl
Y-Maze
[18F]-FDG PET
B
V1
CA1
NNN
PNN
PNP
NDP
PDN
PDP
C
Frontal
S1
V1
CA1
DG (ML)
Thalamus
TH staining (% area)
NNN
PNN
PNP
PDN
PDP
NDP

Therefore, we extended our analysis to aged mice and refined the model by applying multiple DSP-4 injections (every 3 months) to achieve a long-lasting depletion of LC axons, followed by a 2nd PolyI:C exposure at 12 months of age. Tissue was collected 4 months after the 2nd hit of PolyI:C (see overview figure 5A). Control mice were treated with vehicle (NaCl) instead of DSP-4 or PolyI:C. To assess the effect of multiple DSP-4 treatments on LC axonal density within the same regions as analyzed in the 1st cohort, we again performed IHC staining and quantifications against TH.

To our surprise, repeated LC axonal depletion did not prevent axons from regenerating between 12 and 16 months of age. The frontal cortex, as well as the CA1 region of the hippocampus, recovered more than half of the density compared to NaCl controls 4 months after the last DSP-4 treatment (figure 5B and C). As expected, axon densities decreased in a rostro-caudal manner in cortical areas (from approximately 60% recovery (frontal) to 18% in V1), precisely reflecting the regeneration pattern seen after a single DSP-4 treatment. Differences between DSP-4 and NaCl treatment were less pronounced in DG (ML) although the group effect was highly significant (one-way ANOVA, DG (ML): $F_{(5,57)} = 5.44$; $p = 0.0004$). No significant group effect was detected in the thalamus (one-way ANOVA, thalamus: $F_{(5,51)} = 2.45$; $p = 0.050$) in line with the fact that this region is reinnervated fastest in rats post-DSP-4 treatment (Fritschy et al., 1992). Although a significant DSP-4 effect was detected (one-way ANOVA; frontal: $F_{(5,62)} = 26.87$, $p < 0.0001$; S1: $F_{(5,61)} = 75.60$, $p < 0.0001$; V1: $F_{(5,61)} = 113.70$, $p < 0.0001$; CA1: $F_{(5,50)} = 19.92$, $p < 0.0001$) the regeneration deficit seen in 6 month-old mice prenatally exposed to PolyI:C was not evident in this cohort. All 3 groups of DSP-4-treated mice exhibited the same density of TH axons, irrespective of pre- or postnatal PolyI:C exposure (figure 5C). Indicating that prenatal or postnatal PolyI:C-induced changes had no long-term effect on fiber regeneration capacity.

Combined PolyI:C and Multiple DSP-4: Microglia and Astrocytes

As we have previously shown, prenatal PolyI:C exposure can lead to a chronic subthreshold inflammatory response reflected in sustained increased levels of pro-inflammatory cytokines measured in blood and brain tissue lysates. To induce central astro- and microgliosis, however, a 2nd PolyI:C treatment in aged mice was needed.

The 2nd cohort was designed to determine whether long-lasting LC axon depletion worsens the effects of a 2nd PolyI:C exposure (PDP vs. PNP mice or might even mimic a 2nd PolyI:C treatment (PDN) mice). The PNN and PNP groups served as controls to confirm the effects of the "double hit" model. Based on the results from the 1st cohort, showing increased number of microglial cells and increased GFAP immunoreactivity in CA1 in mice exposed to prenatal PolyI:C and DSP-4, we anticipated an aggravation of inflammatory responses in PDN and PDP mice.

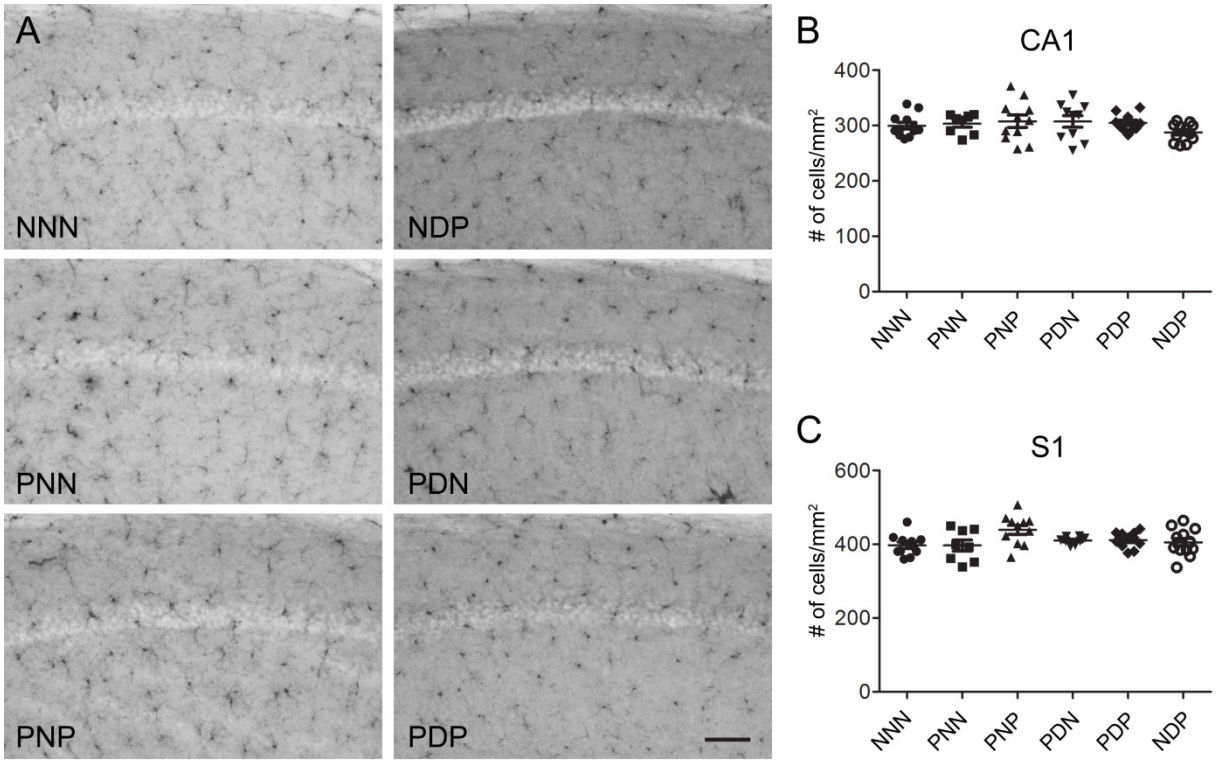

Figure 6: Effect of multiple DSP-4 injections in PolyI:C-exposed mice of 2nd cohort on microglia activation. A. Bright-field microscopy acquisitions from sections stained by immunoperoxidase against CD68. For each group, 1 representative image taken from the CA1 area is depicted; scale bar: 200 µm. **B.** Quantification of CD68-positive profile count analyses in CA1 area (mean ± SEM); no significant difference was observed in any of these regions. **C.** Quantification of CD68-positive profile count analyses in S1 (mean ± SEM) – serving as control area to exclude region specific differences; no significant main treatment effect was observed.

Unexpectedly, however, we could not detect any changes in the number of CD68-positive microglial cells in any of the treatment groups in the CA1 region compared to NNN control mice (one-way ANOVA, $F_{(5,62)} = 1.05$). No change was detected in S1 either, which we analyzed here to exclude the possibility of region-specific effects seen in the 1st cohort (one-way ANOVA, $F_{(5,59)} = 2.38$) (figure 6).

To further evaluate putative changes in inflammatory processes, the following markers were investigated: CD68, GFAP and COX2. All staining patterns were of good quality, excluding technical issues in this tissue from 16 month-old mice. CD68 staining was mainly restricted to microglial cell bodies evenly distributed throughout the cortical areas (figure 6, figure S3). Inferring from their size and shape, microglial cells were not activated in any of the treatment groups. As for GFAP, no obvious astrogliosis was detected. COX2 staining was, as anticipated, selectively restricted to microglial cells and to CA3 and to a lesser extend to CA1pyramidal cells and granule cells of DG, in line with the expression pattern seen with in situ hybridization studies (Allen brain atlas, http://mouse.brain-map.org/).

To determine whether the expression pattern of these markers – as seen in the "double hit" model (Krstic et al., 2012a) – rather than the number of cells was changed, we performed densitometry analyses in the same areas where the TH axon densities were measured. All values were normalized to the staining intensity of the whole section. No changes in any of the areas analyzed were detected for the 3 markers between the 6 treatment groups (figure S3 A-C). Altogether, these results indicate that brain innate immune cells were not altered in our cohort, and chronic LC axon depletion had no effect on astrocytes and microglia at the age of 16 months.

Combined PolyI:C and Multiple DSP-4: AD-Related Proteins

Despite these negative results on inflammatory markers, we tested the mice of the 2nd cohort for changes in AD-related proteins. Since our previous study showed that APP expression levels were strongly affected by either prenatal or pre- and postnatal PolyI:C exposures, we performed IHC staining, using an antibody raised against the C-terminus of APP. Densitometry analyses of CA1 (figure 7A) and all hippocampus subregions – CA1 SO, SP, SR, SLM, CA3 SP and stratum lucidum (SL), DG (ML) and granule layer (GL) –revealed no differences in staining intensity or laminar expression pattern (data not shown). In line with this result and the fact that brain immune cells were not activated in any of the treatment groups, densitometry analysis in all regions investigated in cohort 1 revealed no differences among the 6 groups (data not shown).

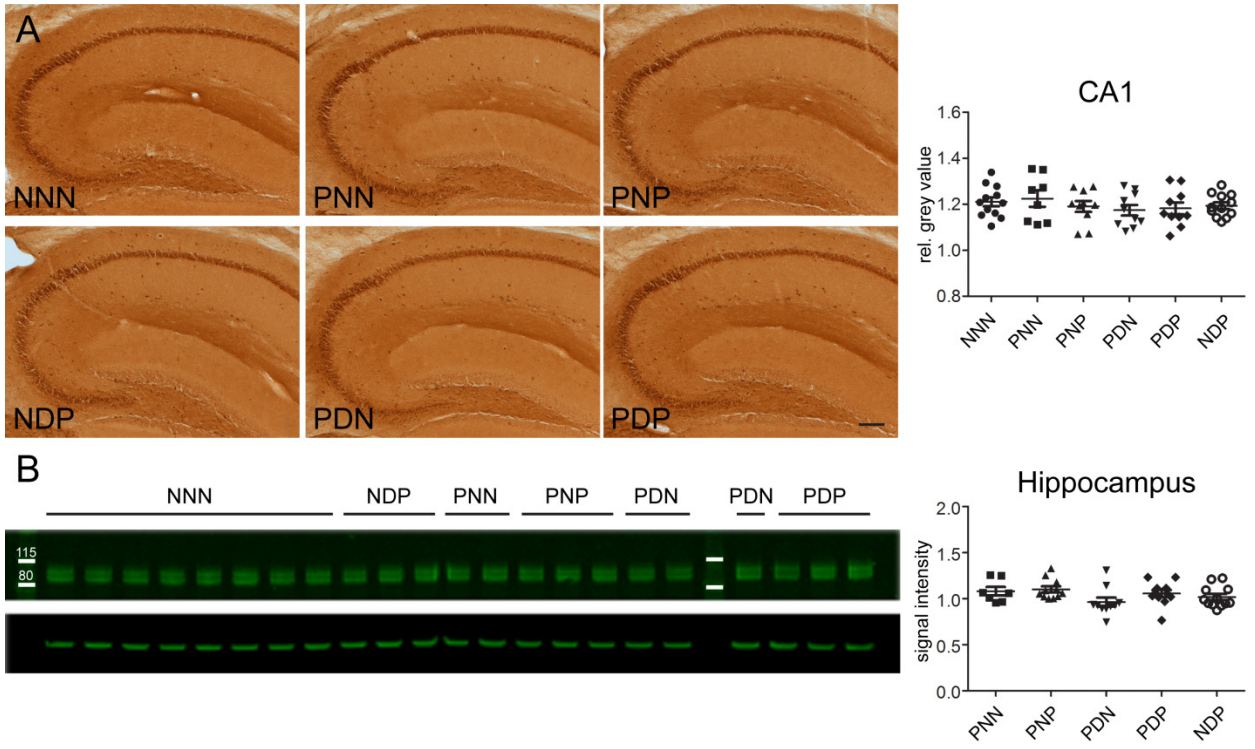

Figure 7: IHC and Western blot analyses of cAPP expression in the hippocampus of mice from 2nd cohort. A. Bright-field microscopy images from sections stained by immunoperoxidase against cAPP. For each group, 1 representative image taken from the CA1 area is depicted; scale bar: 200 µm. Densitometry analyses revealed no significant main effect between treatment groups. **B.** A representative Western blot against cAPP is presented, along with the densitometry analysis of the corresponding protein bands from all 4 Western blots (line indicates group mean ± SEM). Molecular weights in kDa are indicated. Samples were loaded as indicated. 40 µg of each sample was loaded and the respective loading control (actin band) is shown below the blot. Full length APP is detected (apparent molecular weight 100 kDa). Along with IHC results, treatment groups showed no difference.

To further support this finding, we performed semi-quantitative Western blot analyses using hippocampus lysates from the contralateral hemisphere of the mice used in the IHC experiments. Each experiment was performed 3 times, twice using chemiluminescence and once using fluorescence signal detection systems. In this assay all experimental groups were normalized to NNN precluding statistical analyses given the small sample size. A representative Western blot against cAPP using fluorescence detection is shown in figure 7B. The corresponding quantification supported the IHC findings showing no evident difference among treatment groups in the measured intensity of bands corresponding to full-length APP (figure 7B). This result was further replicated using an antibody against the N-terminus of APP (figure S4). No differences were further obvious in Western blot analyses with antibodies against Tau or pTau (figure S4). Based on these negative results, no other brain region was analyzed biochemically.

Combined PolyI:C and Multiple DSP-4: Short-Term Memory Performance

We have previously shown that prenatal PolyI:C exposure leads to age-dependent deficits in non-spatial short-term memory in 20 month-old offspring (Krstic et al., 2012a). As central NA signaling has been shown to have cognitive effects (Rinaman, 2011), we therefore hypothesized that NA depletion would exacerbate cognitive impairments in mice that were subjected to a single (prenatal) or combined (prenatal and postnatal) PolyI:C challenge. To assess this, we measured short-term spatial recognition memory using a sample-choice Y-maze paradigm. This test is based on the natural tendency of rodents to explore novel over familiar spatial environments (Dellu et al., 1992). In addition, we tested the animals' cognitive performance using a spontaneous alternation test in the Y-maze, which measures non-spatial short-term memory (Lalonde, 2002) and was applied in our previous study (Krstic et al., 2012a). In addition to this, both tests have previously been used to identify cognitive impairments in PolyI:C-exposed offspring (Bitanihirwe et al., 2010, Connor et al., 2012, Richetto et al., 2013).

In the sample-choice Y-maze test, the critical measure of spatial recognition memory is the relative time spent in the novel (previously unexplored) arm during the choice phase of this test (figure 8A). As depicted in figure 8A', NNN control animals failed to display a clear preference towards the novel arm versus the previously explored arms, and so did the animals from all other treatment groups. Hence, animals from all treatment groups mostly performed at chance levels (33% of time spent in the novel arm), and no group differences were detectable in regard to this measure of short-term spatial recognition memory (one-way ANOVA: $F_{(5.58)} = 0.70$). There were also no group differences in the total distance moved (one-way ANOVA: $F_{(5,58)} = 0.75$), suggesting that basal locomotor activity were not affected by the different treatments (figure 8A''). In the spontaneous alternation test of non-spatial short-term memory, the alternation scores ranged from 61.6±2.9% in the NNN group (highest score) to 46.3±5.2% in the PNN group (lowest score) (figure 8B'). ANOVA analyses, however, did not reveal a significant main effect of treatment (one-way ANOVA: $F_{(5,56)} = 1.12$) indicating no behavioral deficit among the treatment groups both in spatial and non-spatial short-term memory.

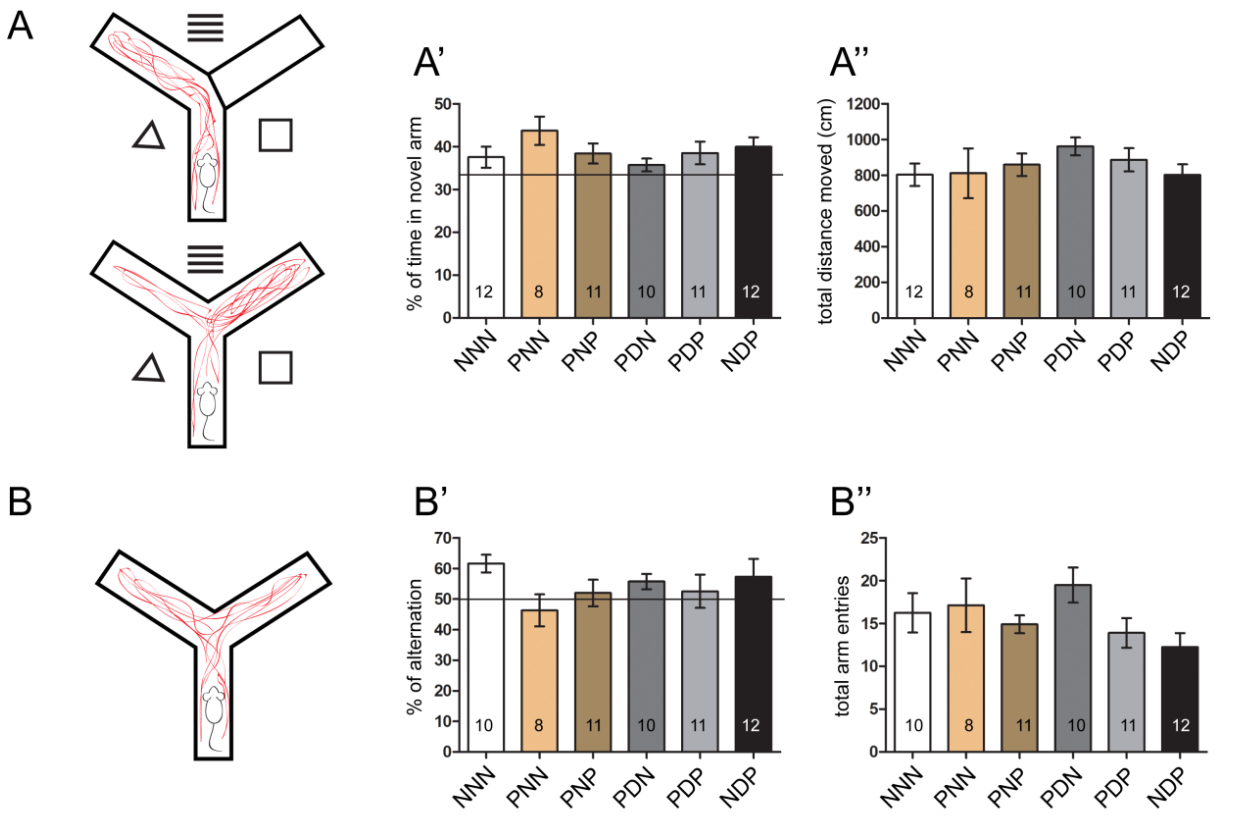

Figure 8: Behavioral Y-maze test for short-term spatial and non-spatial memory performed in the 2nd cohort. **A.** Scheme of Y-maze sample/choice test designed to study spatial short-term memory performance. The Y-maze is transparent and spatial cues are given (indicated by the triangle, square and lines). Sample phase (upper maze): the mouse is allowed to explore 2 arms of the maze. Choice phase (lower maze): the mouse is able to explore all 3 arms. Spatial memory is evaluated by the time spent in novel arm. Chance level is set at 33% of time spent in the novel arm (line in bar plot (A')). A'. % of time spent in novel arm is presented (mean ± SEM); number in bar represents sample size. No significant main effect was detected among treatment groups. A''. Represents mean total distance moved ± SEM; No significant difference in movement was detected among treatment groups. **B.** Scheme of the Y-maze spontaneous alternation test designed to study non-spatial short-term memory performance. The Y-maze is opaque and mice are allowed to freely explore all 3 arms. B'. % of alternation between arms of all treatment groups is depicted as mean ± SEM; Chance level is 50% alternation and indicated by dotted line. Comparison between treatment groups revealed no significant difference in main effect. B''. Represents mean arm entries ± SEM; no difference in number of arm entries – as a measure of movement – was detected.

Combined PolyI:C and Multiple DSP-4: Glucose Metabolism

Functional changes in the brain such as glucose metabolism can be used as diagnostic tool for AD. [^{18}F]-FDG PET imaging was shown to be able to distinguish healthy aged individuals from AD cases with high accuracy (Herholz et al., 2002). In addition to human applications, a previous study performed in a transgenic animal model for AD showed that NA depletion resulted in small reductions of cortical glucose uptake measured by micro-PET (Heneka et al., 2006).

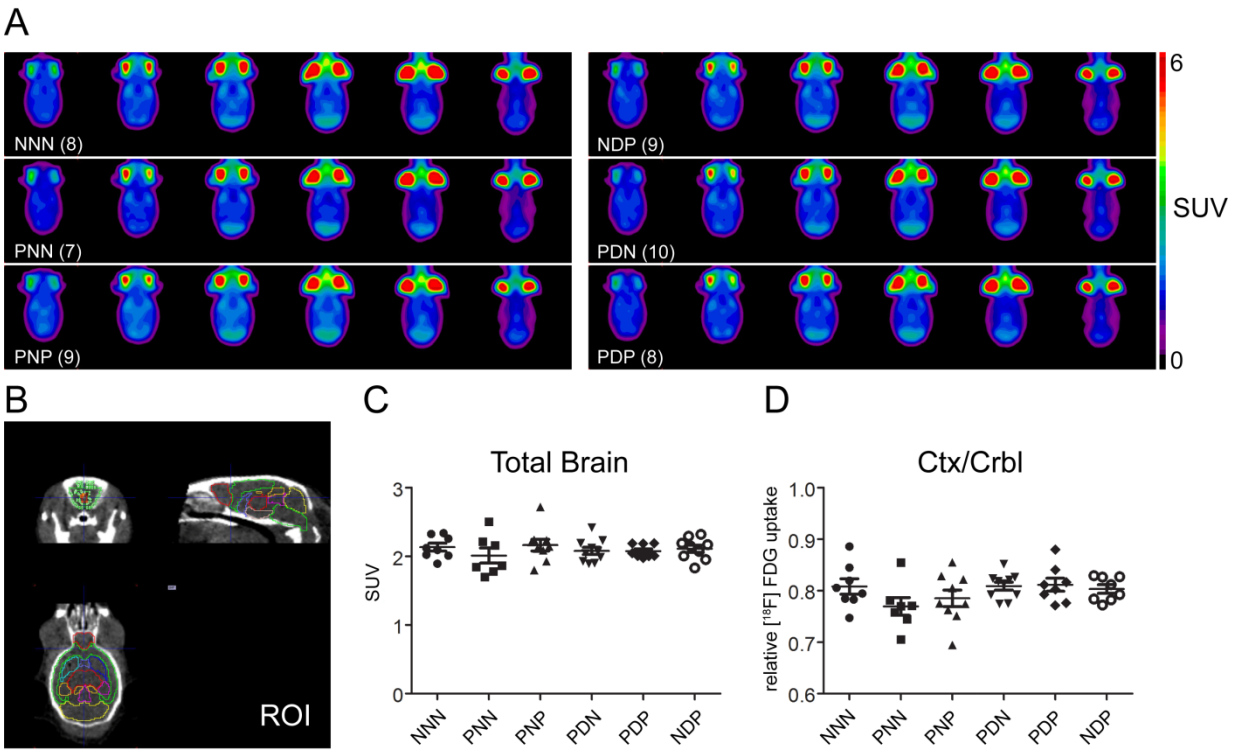

Figure 9: [^{18}F]-FDG PET imaging study measuring glucose uptake in the 2nd cohort. A. Averaged standardized uptake values (SUV) per treatment group are presented in false color images. Values within brackets in the inscription represent the number of animals analyzed per group. Corresponding SUVs to false color coding is represented on the right side of the pictures. **B.** High resolution computed tomography image with region of interest (ROI) analyzed. ROIs analyzed: green = cortex; pink = right hippocampus, orange = left hippocampus; red = thalamus; yellow = cerebellum; red = OB. **C.** Mean SUVs from total brain, including all ROIs (± SEM). No difference among treatment groups was detected. **D.** Mean cortical uptake values relative to the cerebellum (± SEM). No significant difference was detected.

Intrigued by these findings, we subjected the 16 month-old mice of the 2nd cohort to [^{18}F]-FDG PET imaging to investigate whether NA depletion in the double immune challenged mice has a similar effect on regional glucose metabolism. Averaged SUVs for each treatment group were calculated (figure 9A). Regions of interest (ROI) were defined with the help of co-registered images of the mouse head taken by high resolution computer tomography (figure 9B). Semi-quantitative analysis revealed no significant main treatment effect in SUV in any ROI analyzed. The SUVs of total brain [^{18}F]-FDG uptake of the 6 examined groups are represented in figure 9C (one-way ANOVA $F_{(5,50)} = 0.58$) whereas figure 9D represents the [^{18}F]-FDG uptake normalized to the cerebellum (one-way ANOVA $F_{(5,49)} = 1.55$), indicating that DSP-4 depletion independent on immune challenges had no effect on Glucose uptake into the brain.

Prenatal PolyI:C Effects

To evaluate whether the lack of immune activation-induced phenotype and thereby differences between treatment groups was due to inefficacy of PolyI:C treatment we performed *a priori* comparison between NNN and PNN. We chose PNN since prenatal PolyI:C-exposed (GD17) offspring have been previously shown by us and others to develop a robust phenotype in regard to memory performance (Bitanihirwe et al., 2010, Connor et al., 2012, Krstic et al., 2012a, Richetto et al., 2013).

As expected, TH fiber densities did not differ between NNN and PNN indicating that prenatal PolyI:C exposure has no long-term effect on basal NA axon densities. *A priori* comparison of the number of CD68-positive cells did not reveal significant increases in both CA1 and S1 in PNN compared to NNN nor did the intensity of the three inflammatory markers CD68, GFAP and COX2 increase. Significant increased intensity in COX2 was however detected in V1 (unpaired *t* test two-tailed: $t_{18} = 2.998$; $p = 0.008$). In contrast significant decreased CD68 staining intensities in PNN compared to NNN were detected in CA1 (unpaired *t* test two-tailed: $t_{18} = 2.478$; $p = 0.023$), DG (ML) (unpaired *t* test two-tailed: $t_{18} = 2.535$; $p = 0.021$), striatum (unpaired *t* test two-tailed: $t_{18} = 2.198$; $p = 0.041$) and thalamus (unpaired *t* test two-tailed: $t_{18} = 2.108$; $p = 0.049$). In line with the lack of increased inflammation in the hippocampus, densitometry analysis of cAPP levels measured in CA1 revealed no difference. Further glucose uptake measured with [^{18}F]-FDG-PET imaging analysis revealed no significant difference between NNN and PNN.

In line with previous findings (Connor et al., 2012, Krstic et al., 2012a), however, *a priori* comparison revealed that PNN animals displayed a significantly lower alternation score compared with NNN animals in the Y-maze spontaneous alternation task (unpaired *t* test, two-tailed: $t_{16} = 2.69$; $p = 0.016$). By comparing the alternation scores of NNN animals to the inherent chance level score of 50%, we further found that the NNN group significantly performed above chance level (one-sample unpaired *t* test, two-tailed: $t_9 = 3.99$; $p = 0.003$). The *a priori* comparisons between NNN and PNN animals, therefore, suggest that we could at least partially replicate previous findings of deficient spontaneous alternation in aged offspring exposed to prenatal PolyI:C treatment.

Discussion

The present study shows that prenatal PolyI:C exposure induces persisting changes in the brain and/or immune system, which affect the regeneration capacity of NA axons, at least in young adult mice. Further, we show that this prenatal immune challenge leads to an increased density of microglia within the CA1 area of the hippocampus, which is not influenced by NA depletion. Unexpectedly, subjecting mice of the second cohort to a prenatal and postnatal immune challenge and DSP-4 or NaCl treatments did not evoke the same response as previously detected in the "double hit" model of sporadic AD. Thus, the repeated PolyI:C exposure did not evoke neuroinflammation and subsequent changes in AD-related proteins in the aged cohort analyzed here, in contrast to what was reported in (Krstic et al., 2012a). Also, chronic NA depletion in mice exposed to PolyI:C either prenatally, or twice, did not enhance expression or processing of AD-related proteins, nor influence glucose uptake and metabolism at the age of 16 months. However, a well-characterized effect of prenatal PolyI:C on neurodevelopmental processes was reproduced, as evidenced by the mild deficit in non-spatial short-term memory observed in PNN compared to NNN mice. Among possible reasons, it is conceivable that the effects of prenatal and postnatal PolyI:C exposure differ between mouse strains or the handling stress caused by the repeated i.p. injections of DSP-4 or NaCl. Therefore, the lack of the AD-like phenotype in mice from cohort 2 precludes conclusions about the putative role of NA signaling in the pathological mechanism underlying sporadic AD. Nevertheless, our results show that an acute or chronic NA depletion of LC axons using DSP-4 has little, if any, effect on brain immune cells, whereas activation of peripheral immunity by prenatal PolyI:C reduces the regeneration capacity (or possibly TH expression) of LC axons in young adult mice.

Prenatal PolyI:C Affects the Regeneration Capacity of NA Axons

The TH-positive axon density measurements revealed a significant decrease in V1 and CA1 in PD compared to ND mice of the 1st cohort. Previous studies have shown that substantial regrowth and sprouting of NA axons into target areas occurs within weeks after depletion, independently of the toxin used (Bjorklund et al., 1975, Bjorklund and Lindvall, 1979, Fritschy and Grzanna, 1992). The pattern and speed of reinnervation varies between areas, from rapid and extensive reinnervation (thalamus, cortical areas and hippocampus) to very little recovery even 1 year post injection (tectum and cerebellum) (Fritschy and Grzanna, 1992). Our findings show that mechanisms involved in axonal growth, as well as axonal guidance, are unaffected by

PolyI:C exposure. Decreased LC axon density in V1 – being the area measured furthest away from LC – points to an involvement of prenatal PolyI:C in the rate of regeneration. This conclusion is supported by deficits detected in the CA1 area – known to show fast reinnervation post-DSP-4 treatment (Fritschy and Grzanna, 1992) – as the path from the LC to the hippocampus is even longer than to V1.

Studies conducted to investigate time-dependent LC neurodegeneration showed that rats displayed a 19% decrease of cells 2 weeks post injection of DSP-4 (50 mg/kg). This degeneration further increased to 36% after 6 months and finally resulted in a 57% loss of cells after 1 year (Fritschy and Grzanna, 1992). In the current study, we detected a depletion of approximately 15% after 3 months, which is less than expected but possibly due to the high variability in the number of cells loss upon a single DSP-4 injection (Fritschy and Grzanna, 1991). No difference in terms of LC cell numbers were detected between ND and PD, indicating that prenatal PolyI:C exposure does not sensitize LC neurons to the effects of DSP-4. This was confirmed by previous studies showing that neurodegeneration is unaffected by toxic insults such as overexpression of AD mutations (Heneka et al., 2006, Jardanhazi-Kurutz et al., 2010). In the study from 2006, however, they reported a 50-60% decrease in LC cell numbers 6 months post treatment in both transgenic and wild type controls. Possible reasons for this discrepancy in neurodegeneration between our cohort and their mice are likely due to time of investigation post-injection, injection paradigm, and mouse strain (C57Bl/6J).

NA Depletion Does Not Increase Brain Immune Responses in Mice Prenatally Exposed to PolyI:C

Previous studies have shown that NA depletion exacerbates immune responses towards toxic insults (Heneka et al., 2002). In line with this observation, our results at first suggested that the combined treatment of PolyI:C and DSP-4 can have an effect on immune responses. Microglial cell counts revealed an increase of approximately 13% in the CA1 area of the hippocampus of PD compared to ND mice. Further, we detected increases in staining intensity of CD11b (part of the complement system labeling microglia and dendritic cells) and GFAP (intermediate filament highly expressed by astrocytes) in areas of the hippocampus in PD compared to ND mice (figure S1). *Post-hoc* verification using a 2nd series of 5 month-old prenatal PolyI:C or NaCl challenged mice without NA depletion, however, revealed an increase of about 18% in CD68-positive microglial cell density in the CA1 area (figure 3D). This finding is in line with our previous observations that prenatal PolyI:C exposure affecting the brain's innate immune system (Krstic

et al., 2012a). Hence, we can conclude that the prenatal PolyI:C-induced effects on innate immune responses are not exacerbated by NA depletion.

As the CA1 area belongs to the 2 areas with impaired regeneration of NA axons (figure 2), we tested whether there is a relationship between the changes in immune cells and the regeneration capacity. The lack of correlation between the number of microglia cells and axon densities indicates that regeneration deficits – observed in the 1st cohort – are independent of the density of CD68-positive microglia. This conclusion is also supported by the fact that V1, albeit showing decreased LC axon density, had equal numbers of microglia in PD and ND mice. In addition, we found no correlation between LC axon density and relative intensities of GFAP and CD11b (CA1 area) and COX2 (V1) immunoreactivity. Therefore, we conclude that NA axon depletion does not impinge on the inflammatory changes induced by PolyI:C.

NA Depletion After Prenatal PolyI:C Exposure Does Not Evoke AD-Related Changes in Young Adult Mice

There is increasing evidence for inflammatory processes to be a major, early driving force in sporadic AD (for review see (Krstic and Knuesel, 2013)). Chronic inflammation increases APP levels (Goldgaber et al., 1989, Rogers et al., 1999, Ciallella et al., 2002, Itoh et al., 2009, Song et al., 2013) and causes hyperphosphorylation of Tau (Li et al., 2003, Bhaskar et al., 2010). In line with the lack of evident neuroinflammation – including microglia activation and astrogliosis – no difference in any of the AD-associated markers tested was detected in mice of the 1st cohort. Per se, this finding was not surprising, as we have shown previously that ageing is a crucial factor in the development of AD-related changes. However, it was conceivable that NA depletion following prenatal PolyI:C exposure would accelerate the appearance in AD-like changes, as they have been reported in models of familial AD. These studies, however, applied DSP-4 to transgenic mouse models for familial AD, which overexpress one to several human mutations in APP and presenilins, resulting in Aβ–plaque formation, micro- and astrogliosis, increase in oxidative stress and inflammatory cytokines (Irizarry et al., 1997, Frautschy et al., 1998, Pappolla et al., 1998, Smith et al., 1998, Benzing et al., 1999, Dodart and May, 2005). Recent studies have further shown that overexpression of APP alone – even without mutation – has major effects on phosphorylation of Tau, neurochemical composition of proteins involved in synaptic signaling, cell survival, and behavioral performance (Neve and Robakis, 1998, Simon et al., 2009). Transgenic overexpression of mutated APP thereby alters basic neuronal mechanisms making them more vulnerable to manipulations with DSP-4. Furthermore, NA depletion was

shown to impair microglia phagocytic function in transgenic animals resulting in decreased clearance of Aβ explaining increased plaque formation seen in all NA depletion studies (Heneka et al., 2010). In line with this, NA depletion resulted in increased inflammatory response upon intracranial Aβ injections resulting in increased inflammation (Heneka et al., 2002). Thereby, it is conceivable that DSP-4 treatment in transgenic animals shows this remarkable potentiation of phenotype due to basic impaired conditions in contrast to the subtle changes induced by prenatal PolyI:C exposure detected here.

The Regeneration Capacity of LC Axons Is Retained Upon Multiple DSP-4 Treatments

The expected degeneration and regeneration pattern of NA axons was still evident after multiple DSP-4 treatments (figure 5). Intriguingly, the pattern and density of TH-positive axons seen at 16 months in mice from cohort 2 were comparable to those seen in a pilot experiment, in which aged mice (19 months) were analyzed 3 months after a single DSP-4 injection (data not shown). The toxic action of DSP-4 is dependent on uptake via the NA transporter (Ross, 1976). The exact mechanism of action however is still unknown (Jaim-Etcheverry and Zieher, 1980, Fritschy and Grzanna, 1989, Grzanna et al., 1989, Lyons et al., 1989). It is conceivable that multiple injections induce less degeneration if NAT expression were reduced during the maturation of regenerating axons, but there is no experimental data supporting this idea. Rather, a recent study using monthly DSP-4 injections applied throughout ageing detected no difference in regenerating axons in the cortex 1 ½ months after the last DSP-4 injection, independently of how many times it was applied (Jardanhazi-Kurutz et al., 2010). Therefore, our findings confirm the robust capacity of NA axons to regrow even after repeated insults.

However, the prenatal PolyI:C effect on NA axonal regeneration – detected in the 1st cohort – was lost upon multiple DSP-4 treatments. When designing the study, we selected not to include the NDN group, because we had seen in a pilot experiment that postnatal PolyI:C treatment in 16 month-old animals has no effect on regenerating LC axons 3 months post DSP-4 (data not shown). Since the effect seen in the "double hit" model were not reproduced in 2nd cohort, we cannot determine whether multiple central NA depletions would overcome the prenatal PolyI:C effects. This would be conceivable, though, since a recent study reported that central NA depletion results in decreased cytokine levels in the spleen, indicating that central NA signaling indeed affects the peripheral immune system (Engler et al., 2010). However, because we saw no correlation in 1st cohort between regeneration impairment and activation of microglia, we

consider it unlikely that suppression of peripheral immune system through multiple DSP-4 treatments overcame the regeneration deficit induced by PolyI:C in 1st cohort.

Mild Prenatal PolyI:C Effect on Performance in Spontaneous Alternation Task

Even though our study did not replicate the previous findings of increased central inflammation and subsequent AD-related changes in PolyI:C-exposed offspring (Krstic et al., 2012a), we nevertheless observed that the prenatal manipulation alone was sufficient to mildly impair short-term non-spatial memory. Indeed, our *a priori* analysis between PNN and NNN offspring revealed that the former displayed a mild but significant decrease in spontaneous alternation relative to the latter group. This result, however, needs to be interpreted with caution because of the rather week – albeit significantly above chance level – performance in the NNN group. Consistent with this finding, numerous previous studies have reported that prenatal PolyI:C exposure can lead to long-term behavioral and cognitive impairments even in the absence of persistent changes in systemic or hippocampal inflammation (Willi et al., 2013, Arsenault et al., 2014, Mattei et al., 2014). This dissociation suggests that at least some of the behavioral and cognitive disturbances induced by prenatal immune activation are likely to be caused by neurodevelopmental changes rather than by persistent effects on inflammatory processes. The neuronal substrates of prenatal infection-induced deficits in behavioral and cognitive functions likely involve abnormalities in various neurotransmitter systems and/or brain areas (Meyer and Feldon, 2009), including the prefrontal GABAergic system (Richetto et al., 2014) and the mesocorticolimbic dopamine system (Vuillermot et al., 2010, Vuillermot et al., 2012) as well as glutamatergic system (Meyer et al., 2008c).

In addition to such neurodevelopmental changes, overexpression of wild type APP has previously been shown to lead to spatial and non-spatial learning deficits in the Morris water maze and the novel object recognition task, respectively (Simon et al., 2009). These findings suggest that the presence of increased APP levels can negatively affect cognitive functions. In contrast to this, our findings indicate that (mild) cognitive impairments following prenatal immune activation can occur in the absence of such AD-related pathology. It thus appears that the negative impact of APP on cognitive functions cannot be generalized from one model (or pathological condition) to another.

Even though we did not further compare the cognitive performances between NNN offspring and offspring with multiple treatments using *a priori* comparisons, it appeared that the latter groups did not display any signs of impaired spontaneous alternation as we have observed it in the PNN

group. At present, we have no satisfactory explanation for this unexpected finding. However, the differential performance between animals subjected to prenatal immune activation alone (PNN) and animals receiving multiple treatments suggests that the postnatal manipulations exerted, if anything, a beneficial effect on non-spatial short-term memory deficits typically seen in animals exposed to prenatal immune activation alone. The mechanisms underlying these effects remain unclear and need to be further investigated.

Possible Explanations for the Lack of Phenotype by Prenatal and Postnatal Immune Challenges in the 2nd Cohort

So far there is little evidence that prenatal PolyI:C exposure induces sustained, increased levels of pro-inflammatory cytokines or microgliosis later in the brain. Most studies that addressed this issue were performed at early stages of development (GD9-12.5) – a stage where the embryonic immune system is still immature – and most effects of PolyI:C are therefore mediated through the activation of maternal immune system (Meyer et al., 2006b, Garay et al., 2013). Arsenault et al., comparing the effects of immune stimulation between the bacterial lipopolysaccharide (LPS) with PolyI:C at GD17, reported no sustained elevation of pro-inflammatory cytokines and CD68 in the brain of offspring at postnatal day 10 (Arsenault et al., 2014). This stands in contrast to the study from our lab, which detected increased IL-1/IL-6 levels and microgliosis in the hippocampus of 15 months old progeny (Krstic et al., 2012a). However, no information is available on the central pro-inflammatory cytokine profile during adulthood (3-12 months). Therefore, it is possible that PolyI:C had the expected effect in this experiment, but that the deterioration seen by Krstic et al. did not occur due to desensitization caused by the repeated i.p. injections of DSP-4/NaCl.

There are other possible pitfalls that need to be considered to explain the partial or total absence of phenotype. These include the strain of mice, their preparation (timed-matings, transport), the injection procedure, the effects of repeated stress through handling, litter effects, and the housing of the offspring.

Differences between our previous and present work concern the strain and preparation of mice for PolyI:C injections. Here, we opted for ordering time-pregnant C57Bl/6JOla mice from Harlan laboratories, shipped on GD14, and injected with PolyI:C on GD17. As far as we are aware, housing conditions were similar between both studies. However, a major difference lies in the handling of mice repeatedly subjected to NaCl (i.p.) injections.

Mouse strain

The C57Bl/6JOla strain - unlike the C57Bl/6JRcc strain used previously (Krstic et al., 2012a) - carries a spontaneous mutation, leading to the suppression of α-synuclein expression. α-synuclein is considered to be mainly expressed in the brain, located in presynaptic terminals. The exact function of α-synuclein is not yet understood, however, it was shown to be involved in SNARE complex assembly (Burre et al., 2010). Further, α-synuclein is considered one of the most important players of Parkinson's disease (PD) (Stefanis, 2012). However, α-synuclein is also expressed in peripheral erythrocytes and in mononuclear cells. Interestingly, its expression is increased in peripheral blood mononuclear cells of PD patients and associated with increased glucocorticoid-induced apoptosis (Kim et al., 2004). This finding indicated for the first time a putative role of α-synuclein in the peripheral immune system. What exactly this role is, still needs to be clarified. Assuming α-synuclein does affect the peripheral immune system, we need to consider that its absence might have had a major impact on the immune response towards PolyI:C.

Transport prior to PolyI:C injection

In the previous study (Krstic et al., 2012a), PolyI:C injections were administered to in-house time pregnant mice, whereas in the current study, pregnant dams were shipped at GD14 and had only 3 days to recover from this stress. It is well established that stress reactions increase glucocorticoid levels in rodents. Early studies that measured corticosterone levels in mice that have been transported by plane or ship revealed that levels of corticosterone rise and remain elevated 48 hours after arrival (Landi et al., 1982). Others have suggested, however, that even 4 days of acclimatization post-transport are insufficient despite normalization of corticosterone levels measured after 1 day upon arrival (Tuli et al., 1995). It is, therefore, plausible that 3 days of acclimatization for the pregnant mice of this study was not enough to return stress hormones to baseline and thereby putatively dampened the response towards an immune challenge.

Litter effect

As mice are multiparous species, a potential litter effect cannot be excluded for both the present and the previous study. Pups from the same mother are highly interdependent on many levels, including genetics, epigenetics, and environmental influences through the dam. This dependency can induce strong and persistent litter effects that could lead to false positive or false negative results (Zorrilla, 1997, Meyer et al., 2009). Such litter effects might as well account for the discrepancy towards prenatal and postnatal PolyI:C challenge in the previous and current study.

Effect of repeated stress induced by handling during i.p. injections

In our previous study mice were subjected to one single postnatal i.v. injection at the age of 12 months. The time before and after this single intervention they were left undisturbed in their home cages with the only disturbances being cage changes performed by animal caretakers. In the present study mice were subjected 4 additional times to single i.p. injections during aging. The effect of multiple injections of NaCl during ageing on behavioral performance, stress hormone levels and in particular on immune response has never been tested and represents a distinct difference between this and the previous study. It therefore remains unknown whether these 4 very mild stresses every three months desensitized offspring towards the second PolyI:C exposure resulting in the lack of increased inflammation in this study compared to the previous. Based on the results from Giovanoli et al, who showed that stress during a critical phase of development induced microglia activation in mice prenatally exposed to PolyI:C at GD9 (Giovanoli et al., 2013), we expected that the stress related to DSP-4 or NaCl treatments might also activate microglia. The lack of effect seen after PolyI:C injections could be therefore conceived as evidence that repeated mild stress rather desensitizes the immune system, as suggested by (Lewitus and Schwartz, 2009).

CONCLUSION

While large parts of our results remain inconclusive because of the absence of chronic neuroinflammation induced by combined pre- and postnatal PolyI:C exposure, we nevertheless uncovered important interactions between the effects of a prenatal immune challenge and the regenerative capacity of LC neurons in the adult brain. Further in line with previous reports, we show that multiple DSP-4 treatments have no effects on AD-related proteins. Hence, we suggest that DSP-4-induced exacerbation of inflammatory responses require a certain level of peripheral and central inflammation.

Supplementary Results

Table 3 Results from Student's *t* test two-tailed for densitometry analyses in first cohort.

Area	CD68	COX2	GFAP	CD11b
Frontal	$t_{17} = 0.72$	$t_{18} = 1.64$	$t_{18} = 1.70$	$t_{18} = 1.46$
S1	$t_{18} = 2.00$	$t_{18} = 0.07$	$t_{18} = 0.53$	$t_{18} = 0.97$
V1	$t_{17} = 1.28$	$t_{18} = 2.93$ *	$t_{18} = 0.24$	$t_{17} = 1.11$
CA1	$t_{17} = 1.21$	$t_{18} = 1.70$	$t_{18} = 3.86$ *	$t_{18} = 2.67$ *
DG (ML)	$t_{18} = 0.17$	$t_{18} = 0.91$	$t_{18} = 3.54$ *	$t_{18} = 2.30$ *
Thalamus	$t_{17} = 0.69$	$t_{17} = 0.09$	$t_{18} = 0.23$	$t_{17} = 1.67$
Striatum	$t_{18} = 0.35$	$t_{17} = 0.94$	$t_{18} = 0.35$	$t_{18} = 0.20$

*$p < 0.05$

Supplementary Figure 1: Densitometry analyses of various immunoperoxidase staining against inflammatory markers in the 1st cohort. Bright-field microscopy images of immunoperoxidase-stained sections against the 4 markers analyzed are represented. For each marker, 1 representative image taken from the CA1 area is depicted; scale bar: 200 μm. Corresponding densitometry analyses are presented. **A.** CD68 staining and corresponding analyses in the frontal cortex, primary somatosensory cortex (S1), primary visual cortex (V1), CA1 area, molecular layer of the dentate gyrus (DG (ML)), thalamus (basolateral nucleus) and striatum revealed no significant differences between treatment groups (mean ± SEM). **B.** Staining pattern and corresponding densitometry analysis revealed significant increase of the inflammatory marker COX2 (mean ± SEM). **C.** Staining pattern and corresponding densitometry analysis revealed significant increase of GFAP in CA1 and DG (ML). Remaining areas showed no difference (mean ± SEM). **D.** Staining pattern and corresponding densitometry analysis revealed significant increase of CD11b in CA1 and DG (ML) but no changes in remaining areas analyzed (mean ± SEM). Statistical test: unpaired *t* test, two-tailed; $*p < 0.05$. Results of statistical analyses are depicted in table 3.

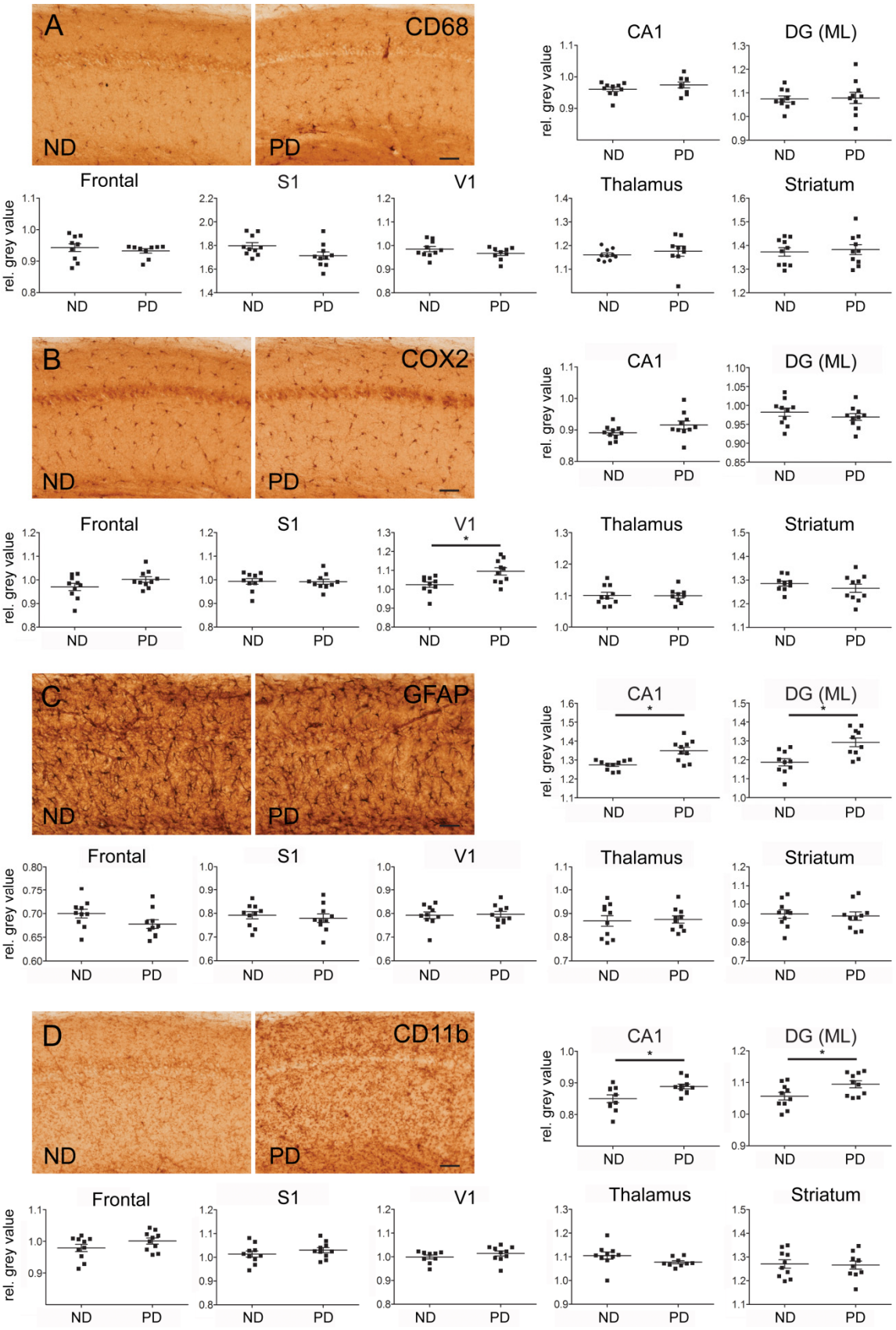
A
CD68
ND
PD
CA1
DG (ML)
Frontal
S1
V1
Thalamus
Striatum
rel. grey value
B
COX2
C
GFAP
D
CD11b
*

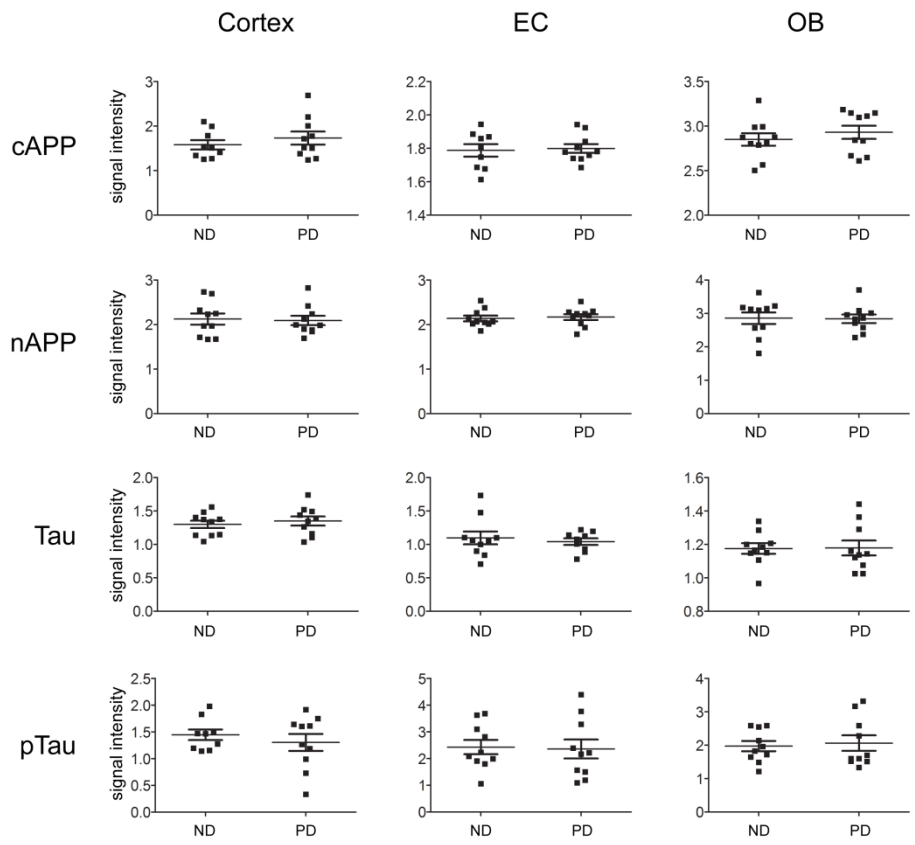

Supplementary Figure 2: Western blot analyses of AD-related protein expressions in the cortex, entorhinal cortex (EC) and olfactory bulb (OB) of mice from 1st cohort. Densitometry analyses of the corresponding protein bands (mean ± SEM) of the 4 AD markers performed within the different brain areas (cortex, EC and OB) are presented. No significant group difference was detected in any of the AD-relevant markers tested for.

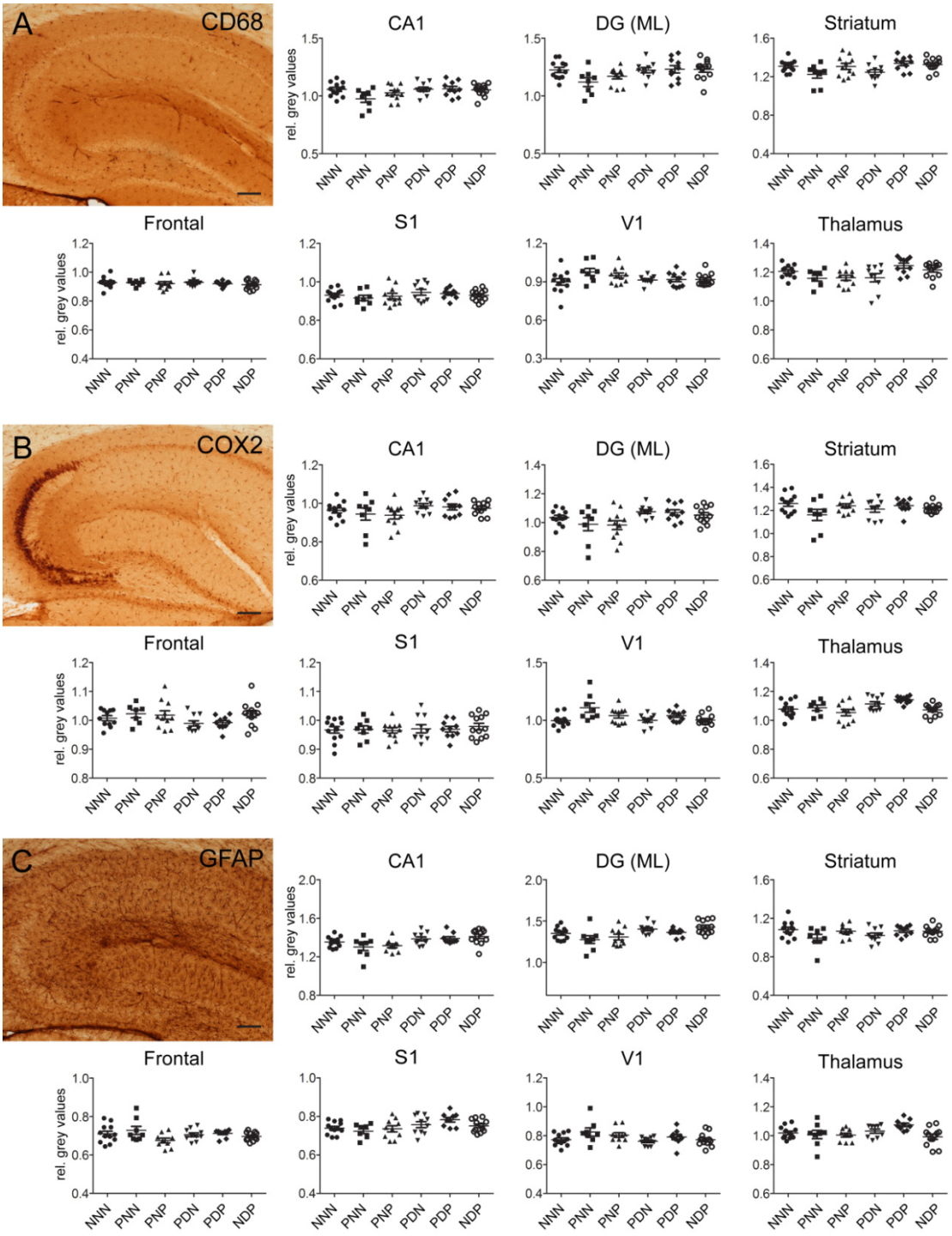

Supplementary Figure 3: Densitometry analyses of various inflammatory markers in the 2nd cohort. Bright-field microscopy images of immunoperoxidase-stained sections against the 3 markers analyzed are represented. For each marker, 1 representative image taken from the hippocampus is shown; scale bar: 400 µm. Corresponding densitometry analyses are depicted. As in supplementary figure 1, **A.** CD68 staining and corresponding analyses in the frontal cortex, primary somatosensory cortex (S1), primary visual cortex (V1), CA1 area, molecular layer of the dentate gyrus (DG (ML)), thalamus (basolateral nucleus) and striatum revealed no significant differences between treatment groups. **B.** Staining pattern of COX2 and corresponding densitometry analyses revealed no significant main effect between treatment groups. **C.** Staining pattern of GFAP and corresponding densitometry analyses revealed no significant main effect between treatment groups in all areas analyzed.

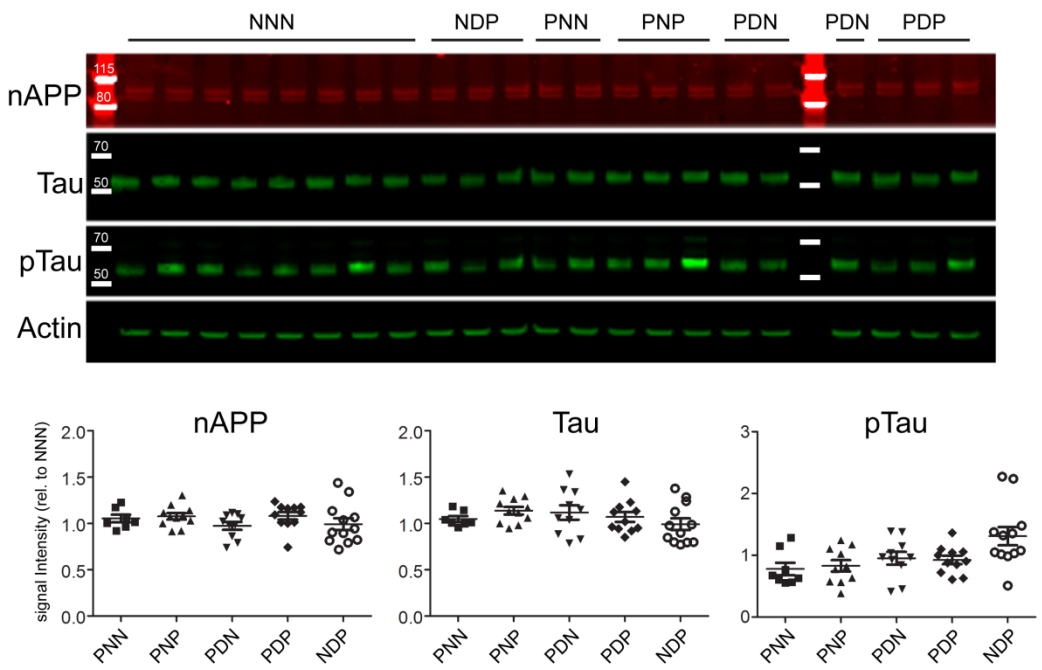

Supplementary Figure 4: Western blot analyses of AD-relevant proteins in hippocampus lysates from the 2nd cohort. Representative Western blots (same as depicted in figure 7) for each marker is presented along with the densitometry analysis of the corresponding protein bands (line indicates group mean ± SEM). Relative signal intensities to the mean intensity of the NNN group (n = 8) are presented. Molecular weights in kDa are indicated. Samples were loaded as indicated above the blot. 40 µg of each sample was loaded and the respective loading control (actin band) is shown below each blot. Blots were stripped once for $pTauT^{205}$ and again for Tau. Full length APP detected with an N-terminal antibody (apparent molecular weight, 100 kDa). Tau, detected with a phosphorylation-independent antibody (apparent molecular weight between 50-60 kDa). PTau with an antibody against $pTauT^{205}$, expected to run at a molecular weight slightly larger than Tau. Non-specific bands at 75 and 80 kDa were ignored. No changes were observed between the treatment groups in any of the markers analyzed.

Acknowledgements

This study was supported by the Swiss National Science Foundation grant number 310030–132629.We thank PD Dr. Stefanie Kraemer and Claudia Keller, Animal Imaging Center ETH Zurich, for their experimental support and enabling us to perform the PET imaging studies in their facility.

STUDY III: ACUTE PERIPHERAL IMMUNE RESPONSE IN PRO-INFLAMMATORY CYTOKINE LEVELS UPON SYSTEMIC POLYI:C INJECTIONS DO NOT DIFFER BETWEEN C57BL/6JOLA AND C57BL/6N MICE

Tina Notter[1,2], Tilo Gschwind[1,2], Stephanie Vuillermot[3], Jean-Marc Fritschy[1,2]

[1]Institute of Pharmacology and Toxicology, University of Zurich, Winterthurerstrasse 190, CH-8057, Zurich, Switzerland

[2]Neuroscience Center Zurich, University of Zurich and ETH Zurich, Winterthurerstrasse 190, CH-8057 Zurich, Switzerland

[3]Department of Health Sciences and Technology, ETH Zurich, Schorenstrasse 16, Schwerzenbach CH-8603, Switzerland

In preparation for publication

Author's contribution

PolyI:C injections were performed by TN and TG, blood collection and plasma extractions were carried out by TN and TG. Cytokine measurements were carried out by SV. TN and JMF wrote the manuscript. All authors read and approved the final version of the manuscript. Authors have no conflict of interest to declare.

Abstract

In recent years it has become evident that exposure to prenatal inflammation can increase the risk to developing neuropsychiatric as well as neurodegenerative diseases in offspring. Our lab has recently developed a mouse model for sporadic AD by subjecting wild type animals to prenatal and postnatal immune-challenged induced by the viral mimic PolyI:C. In a second study, where mice of a different strain (C57Bl6/JOla) were subjected to both immune challenges and to repeated i.p. NaCl or DSP-4 injections during adulthood, the expected PolyI:C effect on immune activation and AD-like neuropathology could not be observed. C57Bl6/JOla mice lack α-synuclein, a protein expressed on peripheral blood cells. Therefore, this strain difference might be responsible for the discrepancy between the two studies. Another confounding factor might be the quality of PolyI:C. Here, we tested these two factors by assessing the acute inflammatory response to systemic PolyI:C injection in adult mice. First, we tested two batches of PolyI:C in female C57Bl6/N mice. Second, we compared C57Bl6/JOla and C57Bl6/N mice. Trunk blood was collected at different time points after i.v. PolyI:C or NaCl injection, and serum levels of three prototypic pro-inflammatory cytokines IL-1β, IL-6 and TNF-α were measured by multiplex electrochemiluminescent immunoassay. We observed no differences in cytokine levels 3 hours post-administration of the two PolyI:C batches. Likewise, no genotype difference was detected in the cytokine profile post-PolyI:C injections, indicating that acute response towards immune stimulus is independent of α-synuclein in adult female mice.

Introduction

Inflammation-mediated neurodevelopmental animal models have gained increasing attention in preclinical studies of psychiatric and neurodegenerative diseases. These models typically involve subjecting pregnant animals to immune-activating agents with the aim to induce fetal inflammatory responses and subsequent neurodevelopmental defects in the offspring (Meyer, 2014). One of the most widely used experimental approach is based on prenatal treatment with the viral mimetic PolyI:C, a synthetic analog of double-stranded RNA that induces a cytokine-associated viral-like acute phase response (Meyer and Feldon, 2012). Since its initial establishment and application to preclinical schizophrenia research (Shi et al., 2003, Zuckerman et al., 2003, Meyer et al., 2005), the PolyI:C model has made a great impact in the field of neurodevelopmental and neuroimmunological bases of complex human brain disorders, such as schizophrenia and autism. As a consequence, the model now enjoys wide recognition in the international scientific community. More recently, prenatal PolyI:C exposure and other developmental immune activation models in rodents have also been applied to experimental investigations of brain disorders that are characterized by progressive neurodegeneration, including AD and PD (Harvey and Boksa, 2012a, Knuesel et al., 2014).

We have previously shown that prenatal PolyI:C-induced maternal immune activation during late gestation (GD17) in mice persistently increased peripheral (IL-1β) and central (IL-1α, IL-1β and IL6) levels of pro-inflammatory cytokines in the offspring (Krstic et al., 2012a). Subjecting these offspring to a second immune challenge during adulthood further exacerbated the central inflammatory phenotype resulting in increased hippocampal levels of CD68 and GFAP, which reflected microglia activation and astrocyte reactivity, respectively (Krstic et al., 2012a). These studies were conducted in wild type mice of the C57Bl/6J strain. Based on these findings, we concluded that prenatal immune activation during late gestation leads to a priming of both peripheral and central immune cells, so that exposure to a second immune challenge in postnatal life leads a more vigorous inflammatory response in primed *versus* non-primed mice.

We have recently performed a second study using the same protocol (PolyI:C exposure at GD17 and PolyI:C injection at 12 months of age), and in addition, 4 i.p. injections of DSP-4 or NaCl between the age of 3 and 12 months. This study was performed using a different wild type strain (C57Bl/6JOla) purchased from Harlan Laboratories (The Netherlands). This strain lacks α-synuclein due to a spontaneous mutation in the *Snca* gene (Specht and Schoepfer, 2001). Contrary to the "double hit" model (Krstic et al., 2012a), we failed to detect changes in central

inflammatory markers after pre- and postnatal PolyI:C exposure combined with DSP-4/NaCl. The lack of α-synuclein, known to be expressed in peripheral immune cells (Kim et al., 2004) suggests, that they might develop a blunted response towards PolyI:C, and therefore, lack persistent inflammatory changes in the offspring following maternal stimulation. Another immediate possibility for the results of the second study may be that different batches of PolyI:C, even if provided by the same supplier, could have a differential potency to induce cytokine-associated immune responses. Such batch effects have indeed been documented in a recent study in mice (Harvey and Boksa, 2012a).

Results and Discussion

Here, we examined these two potential confounding factors by evaluating the influence of the genetic background and different PolyI:C batches on acute cytokine responses elicited in adult mice upon i.v. injection. In a first set of experiments, we used C57Bl6/N female mice (10 weeks old; Harlan Laboratories, The Netherlands) to compare the plasma levels of prototypical pro-inflammatory cytokines (IL-1β, IL-6, and TNF-α) in response to two different batches of Poly(I:C) (lot#1 and lot#2; both provided by Sigma-Aldrich, Switzerland). C57Bl6/N female mice have been widely used in models of prenatal PolyI:C-induced immune activation (e.g., (Richetto et al., 2015)). Lot#1 of PolyI:C was previously used by our own group (Krstic et al., 2012a) and (Notter et al., *second study*), whereas lot #2 was used by another research group (Richetto et al., 2015). C57Bl6/N female mice (n = 6 per group) were injected i.v. with 5 mg/kg of PolyI:C (lot #1 or #2) or vehicle (pyrogen-free 0.9% NaCl) as described before (Krstic et al., 2012a) and were decapitated 3 hours (hrs) post-injection for trunk blood collection. The sampling time was selected based on studies reporting robust increases in plasma cytokine levels following PolyI:C treatment in mice (Meyer et al., 2006b, Harvey and Boksa, 2012a). Plasma samples were prepared as described (Giovanoli et al., 2013) and stored at -20° C until cytokine measurements were performed using an established multiplex electrochemiluminescent immunoassay (Mesoscale Discovery [MSD], Rockville, USA) for pro-inflammatory cytokines (Bastarache et al., 2014). The assay procedures were closely following the protocols provided by the supplier (Mesoscale Discovery [MSD], Rockville, USA). We found that both batches of PolyI:C induced a significant elevation plasma cytokines compared to vehicle treatment (figure 1). Importantly, there were no differences between the two PolyI:C batches, as seen with the similar up-regulation of IL-1β (main effect by one-way ANOVA: $F_{2,15} = 13.01$), IL-6 (main effect by one-way ANOVA: $F_{2,15} = 12.04$, $p < 0.001$), and TNF-α (main effect by one-way ANOVA: $F_{2,15} = 17.47$, $p < 0.001$). Subsequent Fisher's LSD *post-hoc* test comparisons confirmed the significant differences in the levels of the 3 cytokines (IL-1β, IL-6, TNF-α) between vehicle and lot #1 or lot #2 (all p's < 0.001), but not between lot #1 and lot#2 (all p's > 0.5). The lack of differences between lot #1 or lot #2 is contrary to the findings reported by (Harvey and Boksa, 2012a), who found noticeable differences between individual PolyI:C batches in terms of their potency to induce plasma IL-6 responses in mice. Even though our results do not generally exclude the possibility of such batch differences, they clearly demonstrate the absence of sucheffects in the two batches of PolyI:C used in this study, which

included the batch previously used by our own research group (Notter et al., *second study*) and by others (e.g., (Richetto et al., 2015)).

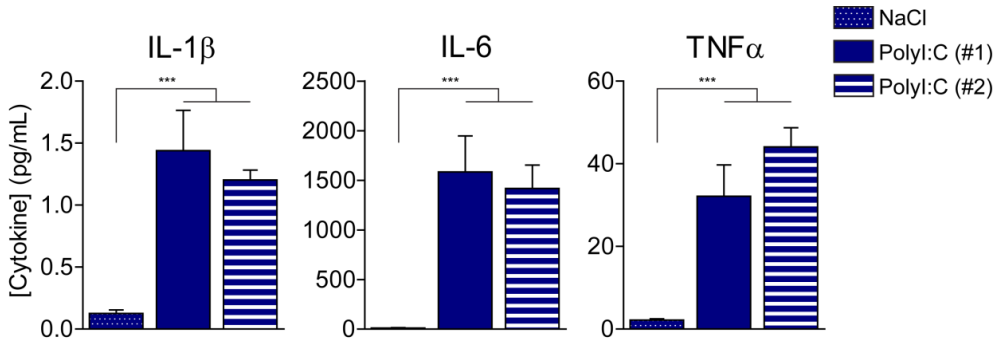

Figure 1: Acute peripheral pro-inflammatory cytokine responses 3 hrs post-PolyI:C injection into C57Bl6/N mice, using two different batches. Mean cytokine concentrations (± SEM) after vehicle, PolyI:C #1 and PolyI:C#2 treatments are represented in bar plots. A significant elevation of prototypical pro-inflammatory cytokines (IL-1β, IL-6 and TNF-α) was detected 3 hrs post-PolyI:C injection. No difference between the two PolyI:C batches was evident. Statistical test: one-way ANOVA followed by Fisher's LSD *post-hoc* test; ***$p < 0.001$.

In a next series of experiments, we assessed the possible influence of the genetic background on the PolyI:C-induced cytokine response. We measured plasma cytokine levels of IL-1β, IL-6, and TNF-α following vehicle (NaCl, n = 4 per genotype) treatment at 1 h post-injection to determine baseline cytokine levels in handled mice and compared these baseline levels with the cytokine levels induced by PolyI:C (n = 6 per genotype) 1 h post injection in female C57Bl6/JOla and C57Bl6/N mice (9 weeks old; both strains were supplied by Harlan Laboratories, The Netherlands) (figure 2A). In addition, we compared the same cytokine levels at 1, 3, and 6 hrs after PolyI:C exposure between the two mouse strains (n = 6 per genotype and time point post-treatment) (figure 2B).

PolyI:C (5 mg/kg, i.v) and vehicle (pyrogen-free 0.9% NaCl, i.v.) preparation and injection, as well as blood collection and plasma cytokine levels measurements were performed as described above. We found that PolyI:C treatment led to a pronounced elevation of IL-6 and TNF-α plasma levels, which peaked at 1 h post-treatment and subsided afterwards (figure 2B). Even though to a lesser extent, PolyI:C treatment also increased plasma IL-1β levels, and this effect reached maximal levels at 3 hrs post-treatment (figure 2B). The initial 2 x 2 (treatment x genotype ANOVA at the 1 h condition revealed a highly significant main effect of treatment (IL-1β: $F_{1,16} = 11.19$, $p < 0.001$; IL-6: $F_{1,16} = 106.18$, $p < 0.001$; TNF-α: $F_{1,16} = 83.86$, $p < 0.001$), but not of genotype for all three cytokines (F's$_{1,16} \leq 1.26$, p's ≥ 0.28). Hence, the cytokine profiles were

highly comparable between C57Bl6/JOla and C57Bl6/N mice, both under basal conditions and following PolyI:C treatment (figure 2A).

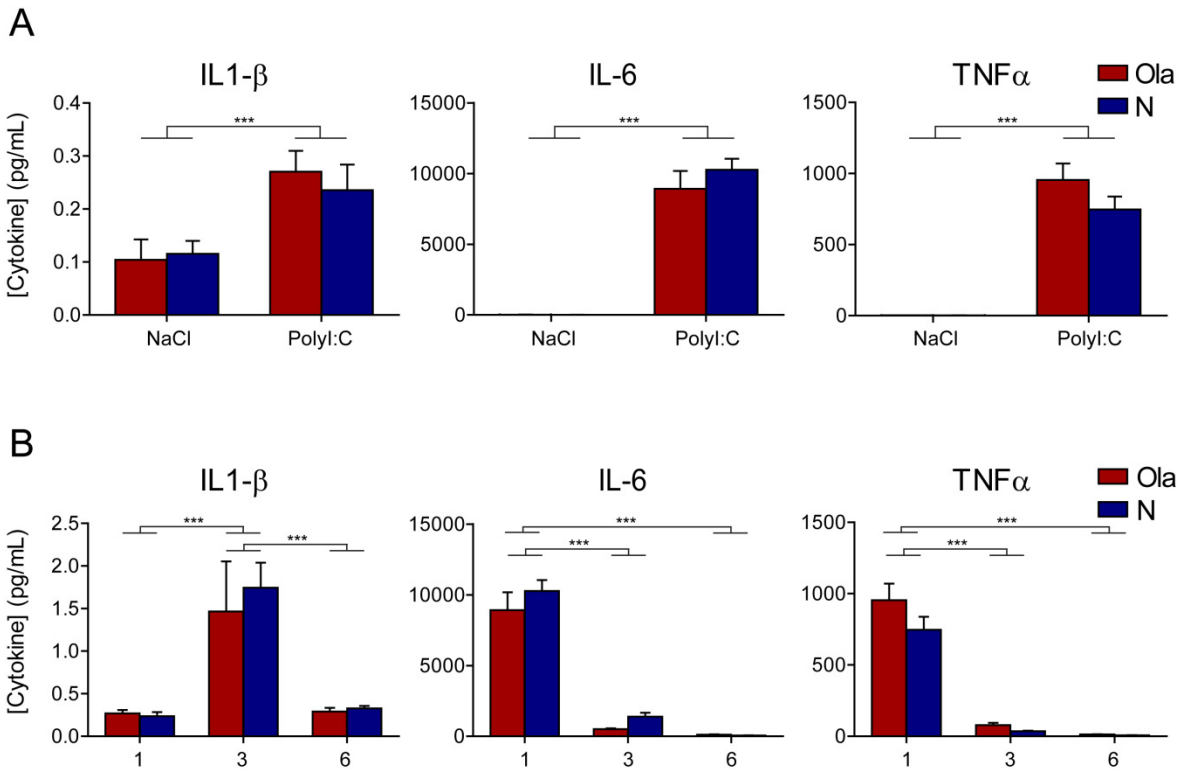

Figure 2: Acute peripheral pro-inflammatory cytokine responses in two strains of mice (C57Bl6/JOla vs C57Bl6/N) under basal conditions (= 1 h following vehicle or PolyI:C treatment (A)) and after different time-points (1, 3 or 6 hrs) post-PolyI:C injection (B). Mean cytokine concentrations (± SEM) after NaCl (n = 4 per genotype) or PolyI:C treatment (n = 6 per genotype) at different time points post-injection are depicted in bar plots (red = C57Bl6/JOla, blue = C57Bl6/N). **A.** Statistical analysis of the cytokine levels 1 h post-injection revealed a significant treatment effect but no genotype difference under basal conditions or after PolyI:C treatment in all three cytokines measured. **B.** A significant main effect of time-point was detected in all three cytokine levels measured post-PolyI:C injections. Peak levels of IL-6 and TNF-α were identified 1h post injection and 3hrs post injection for IL-1β. No differences in cytokine response profile were detected between genotypes. Statistical tests: 2x2 ANOVA (treatment x genotype) and 2x3 ANOVA (genotype x time points) followed by Fisher's LSD *post-hoc* test; ***p < 0.001.

An additional 2 x 3 (genotype x time point) ANOVA was then conducted to evaluate the temporal cytokine profile following PolyI:C treatment. For all three cytokines, this analysis revealed highly significant main effect of time (IL-1β: $F_{2,30} = 15.92$, $p < 0.001$; IL-6: $F_{2,30} = 144.43$, $p < 0.001$; TNF-α: $F_{2,30} = 120.49$, $p < 0.001$) (figure 2B). The main effect of genotype (for all cytokines F's$_{1,30} \leq 2.95$, p's ≥ 0.10) or interaction between genotype and time (for all cytokines F's$_{2,30} \leq 1.56$, p's ≥ 0.23) failed to reach statistical significance. Subsequent Fisher's LSD *post-hoc* comparisons confirmed significant differences for IL-1β levels between 1 h and 3

hrs, and between 3 hrs and 6 hrs (p's < 0.001), but not between 1 h and 6 hrs (p > 0.83). IL-6 and TNF-α levels significantly differed between 1h and 3hrs as well as between 1h and 6hrs (all p's < 0.001), however, not between 3hrs and 6hrs (IL-6: p > 0.18; TNF-α: p > 0.44). These findings suggest that C57Bl6/JOla and C57Bl6/N mice display comparable acute PolyI:C-induced cytokine responses, at least for the prototypical pro-inflammatory cytokines such as IL-1β, IL-6, and TNF-α.

Based on these results, we conclude that the differences between our initial study (Krstic et al., 2012a) and subsequent investigations (Notter et al., *second study*) cannot be explained by a relative incapacity of C57Bl6/JOla mice to mount prototypical pro-inflammatory cytokine responses to PolyI:C treatment. Thus, we consider that the lack of central inflammation-related changes in C57Bl6/JOla offspring subjected to a single (prenatal) or combined (prenatal and postnatal) PolyI:C exposures is unlikely to be attributable to differences in the genetic background. Moreover, since the two batches of PolyI:C induced highly comparable cytokine responses, the maternal PolyI:C treatments in our second study have most likely been effective in inducing the desired immune reactions. This conclusion is further supported by our findings that prenatal PolyI:C exposure per se, i.e., in the absence of any other postnatal immune challenge, caused a mild impairment of non-spatial short-term memory in the aged offspring (Notter et al., *second study*) without being associated with signs of central inflammation. The lack of persistent inflammatory changes as seen in our second study would in fact be consistent with other studies conducted in various mouse strains, including C57Bl6/J (Pacheco-Lopez et al., 2013, Pineda et al., 2013, Willi et al., 2013) and Meyer, *personal communication*) and FVB (Meyer et al., 2008b) strains. However, comparisons with previous studies are limited by differences in the pregnancy stage at the time of treatment, which might have an impact on the long-term alterations of immune system function. Further investigations are required to provide a satisfactory explanation as to why persistent inflammatory changes were noticeable after single (prenatal) or combined (prenatal and postnatal) PolyI:C exposure in our initial (Krstic et al., 2012a) but not in the subsequent (Notter et al., *second study*) study. Such future investigations should test, for example, the role of the housing conditions, stress during transport of pregnant females, as well as stress induced by repeated handling and i.p. injections, which all might impact on the responsiveness of the immune system.

Materials and Methods

Animals

All animal experiments were carried out in accordance with Swiss law on animal experimentation and approved by the cantonal veterinary office of Zurich.
10 week-old female mice of the strains C57Bl6/JOla and C57Bl6/N were purchased from Harlan Laboratories (Horst, the Netherlands) and were accustomed for 1 week prior to immune stimulation. They were housed in groups in a temperature- and humidity-controlled (21 ± 1 °C, 55 ± 5%) holding facility under a reversed light–dark cycle (lights off: 8:00 A.M. to 8:00 P.M.) with access to food and water *ad libitum.*

PolyI:C Injections

Mice were subjected to a single i.v. of 5 mg/kg PolyI:C potassium salt (P9582, 50 mg; Sigma-Aldrich Chemie GmbH, Buchs, Switzerland) dissolved in 0.9% sterile, pyrogen-free NaCl. Calculation of dose was based on the pure form. The injection volume was 5 mL/kg body weight or an equivalent volume of vehicle. During the injection procedure, mice were mildly restrained using an acrylic mouse restrainer (PlasLabs, Inc. #561-RC). After the injection, they were immediately returned to their home cage and left undisturbed until decapitated.

Plasma Cytokine Measurements

Mice were decapitated and trunk blood was collected in EDTA coated tubes. Plasma was directly isolated by 10 min centrifugation at 10'000 rpm at 4°C and stored at -20°C until used. Plasma cytokine protein concentrations were determined by multiplex electrochemiluminescent immunoassay (Mesoscale Discovery [MSD], Rockville, USA) for pro-inflammatory cytokines (Bastarache et al., 2014). The assay procedures were performed according to the manufacturer's protocols (Mesoscale Discovery [MSD], Rockville, USA).

Statistical Analysis

Data are presented as mean ± SEM. Values were tested for Gaussian distribution using the Kolmogorov-Smirnov test (Prism software, GraphPad version6). Statistical analysis in the first experiment, comparing PolyI:C batches to vehicle control, was performed by one-way ANOVA followed by Fisher's LSD *post-hoc* test. In the second experiment, the putative effects of genotype on cytokine levels were explored by 2x2 (treatment [NaCl or PolyI:C] x genotype

[C57Bl6/JOla or C57Bl6/N]) ANOVA at 1 h condition and a 2x3 (genotype [C57Bl6/JOla or C57Bl6/N] x time point [1 h, 3 hrs, or 6 hrs post-treatment) ANOVA followed by Fisher's LSD *post-hoc* tests. Statistical significance was set at $p < 0.05$. All statistical analyses were conducted in the statistical software StatView (version 5.0).

Acknowledgements

We thank Prof. Dr. Urs Meyer from the Institute for Veterinary Pharmacology and Toxicology UZH, for providing us a platform to perform the cytokine measurement studies at the Department of Health Sciences and Technology, ETH Zurich, Schwerzenbach.

IV. GENERAL DISCUSSION

The overall objective of this study was to evaluate three particular systems and their potential role as a co-factor in the pathological mechanism underlying sporadic AD. We have chosen to focus on Reelin, neuroinflammation, and NA signaling due to their vulnerability towards ageing and to the exacerbation of these ageing-associated changes observed at early stages of AD. As noted in the introduction, GWAS have identified several polymorphisms positively correlated with increased risk to develop AD on genes related to the innate immune system (Harold et al., 2009, Lambert et al., 2009, Yu et al., 2009), or encoding Reelin (Seripa et al., 2008, Kramer et al., 2011), DBH (dopamine β-hydroxylase – the crucial enzyme in NA synthesis) (Combarros et al., 2010), and β_2-adrenergic receptors (Yu et al., 2008) .

The evaluation of ageing-associated Reelin aggregates in the human hippocampal formation of non-demented individuals in the *first study* revealed the strong association of Reelin immunoreactivity with CAm – an ageing-associated structure located in particular brain regions, including fiber-rich structures (figure 1, *study I*). In the human tissue that we analyzed, Reelin did not appear as granular deposits, as seen in aged mice, rats, and non-human primates. Despite this morphological discrepancy, we suggest CAm to represent, at least in part, neuritic accumulations of glucose polymers and intracellular proteins, based on the presence of axonal and synaptic proteins (figure 4 and 5*, study I*). It is not established whether they are formed exclusively by neurons or whether they involve other cell types – e.g., astrocytes due to the high glucose content. However, the high abundance of axonal proteins that we could detect by IHC can be taken as evidence that they might evolve through similar mechanisms as suggested for senile plaques (Krstic and Knuesel, 2013). The slight elevation of Reelin-associated CAm detected in the subiculum of AD patients compared to non-demented controls (figure 2, *study I*) is in line with a previous study (Singhrao et al., 1993) and indicates that CAm potentially result from impaired glucose metabolism and axonal transport deficits, which are both known to be exacerbated in AD patients compared to non-demented controls.

Our second study revealed that prenatal immune activation during late gestation can alter the regeneration capacity of NA axons in adult offspring (figure 2, *study II*). The mechanisms underlying this effect need yet to be identified. Prenatal PolyI:C exposure further induced a long-term effect on the innate immune system, as reflected by the increased microglia located in the CA1 region of the hippocampus, as well as concomitant increase in relative levels of GFAP and CD11b immunoreactivity, measured by densitometry analyses (figure S1, *study II*). However,

these long-term effects on innate immune system and NA axonal regeneration induced by prenatal PolyI:C were independent of each other. For unknown reasons, we were unable to induce the chronic, age-related inflammatory state required to investigate the role of impaired NA signaling in double immune-challenged mice in the cohort used for the *second study* (figure 6 and figure S3, *study II*).

Corpora Amylacea - Ageing Associated Disturbances of Basic Cell Functioning?

CAm are present in normal aged CNS tissue of different species, albeit showing a different regional distribution and seemingly different composition (Cavanagh, 1999, Sinadinos et al., 2014). They are detected along the walls of ventricles, the medial surface of the temporal lobe over the hippocampal formation, as well as in glial networks of subpial, subependymal and perivascular regions and in fiber-rich structures of the hippocampal formation (Chung and Horoupian, 1996, Cavanagh, 1999, Notter and Knuesel, 2013, Sinadinos et al., 2014). CAm are ill-characterized structures and, due to their apparent inert composition, have been widely neglected by neuroscientists. CAm mainly consist of polysaccharides. Purification studies revealed that CAm comprise of approximately 4% proteins (Steyaert et al., 1990) and approximately 2% phosphate and are devoid of both DNA and RNA despite their acidic nature (Sakai et al., 1969). Studies performed to resolve their origin so far remained inconclusive.

Glycogen production in the CNS was long thought to occur exclusively in astrocytes. A recent study, however, has shown that neurons produce very small but detectable amounts of glycogen (Saez et al., 2014). In line with this finding, the co-association of axonal and dendritic proteins, including Reelin, APP, MAP2, α-synuclein, and Tau detected in the *first study*, points towards a neuronal origin of CAm. This is in accordance with previous studies detecting CAm in terminal neurites and within axons in cortex (Anzil et al., 1974), striatum (Averback, 1981), ventral posterolateral nucleus of the thalamus (Mizutani et al., 1987), as well as the spinal cord (Takahashi et al., 1975), primarily in neurons associated to motor function but were never associated with neuronal perikarya (Cavanagh, 1999). The presence of Reelin in the core of CAm has led us to propose them to evolve through a similar mechanism as amyloid plaques, namely through aberrant accumulation of proteins transported along axons and dendrites due to ageing-associated deficiency in transport machinery. The detection of stress-related proteins such as heat shock proteins and ubiquitin in CAm further supports this possibility (Cisse et al., 1991, Cisse et al., 1993). In accordance, neuronal loss in amyotrophic lateral sclerosis patients was

correlated with a decrease in CAm number detected in the grey matter of the anterior horn of the spinal cord, strongly favoring a neuronal dependent development of CAm (Cavanagh, 1998).

Intriguingly, a recent study investigating polyglucosan bodies – equivalent to CAm – in aged mouse hippocampus detected granular depositions highly resembling the granular Reelin deposits accumulating with age (Knuesel et al., 2009). In line with the *first study*, these deposits positively stained for stress-related proteins and α-synuclein (Sinadinos et al., 2014). These authors further showed that inhibition of glycogen synthesis completely abolished the formation of these deposits, including the accumulation of proteins. They, therefore, concluded that the formation of these granular deposits is purely dependent on intraneuronal glycogen synthesis (Sinadinos et al., 2014). Whether some Reelin deposits detected in our previous studies might represent polyglucosan bodies still remains to be determined. Their ageing-associated appearance and localization – including the detection of polyglucosan bodies in parvalbumin positive interneurons (Sinadinos et al., 2014) – would favor the idea that Reelin deposits could, in part, represent polyglucosan bodies similar to CAm found in humans. However, Sindadinos did not detect a co-association of polyglucosan bodies with Aβ, whereas Reelin granular deposits clearly co-localize with Aβ containing fragments (Doehner et al., 2010). Additional studies are required to determine and characterize ageing-associated murine Reelin deposits.

Despite the strong evidence for the formation of neuronal CAm, correlation between neuronal loss and CAm abundance was shown to be dependent on their location (Cavanagh, 1998). These findings suggest the existence of different subtypes of CAm, which could be formed by different cell types.

The high abundance of glucose polymers (96%) and their appearance in glial cells and perivascular regions suggests them to evolve within astrocytes. Astrocytes have a key role in local storage of glucose in the form of glycogen in order to provide additional glucose to neurons at times of high neuronal activity (Obel et al., 2012). Therefore, it is conceivable that ageing-associated alterations in astrocyte function can cause aberrant glycogen polymerization. 3D reconstruction of brain CAm in frontal, temporal, parietal and occipital lobe tissue revealed that they form complex interconnected structures rather than single spherical accumulation of glucose polymers and proteins. This observation further supports the notion of CAm predominantly representing a dysfunction in glucose polymerization and, therefore, aberrant glycogen elongations resulting in interconnected elongated inclusions (Pirici et al., 2014). Intriguingly, in accordance with the *first study* presented here, these interconnected CAm were not co-localized

with but rather enwrapped by astrocytes, suggesting them to evolve in other cell types (figure 6, *study I*). Others, however, have claimed them to be detected within astrocytic processes (Ramsey, 1965, Anzil et al., 1974, Palmucci et al., 1982). To date, it remains unclear whether and how aberrant glycogenesis in astrocytes contributes to the formation of CAm.

The role of CAm in neurological diseases remains obscure. In line with our findings, increased levels of CAm have been reported in AD (Singhrao et al., 1993), multiple sclerosis (Singhrao et al., 1995), and PD (Mizutani et al., 1987). These increases were subtle and, therefore, likely to reflect ageing- and disease-associated impairments rather than actively contributing to disease progression or onset. In line with this conclusion, CAm were detected in spinal cord and retina tissue from children of the age of 10 and below 10, respectively (Cavanagh, 1999). Although present very early, CAm did not correlate with any form of disease, further showing their inertness. In contrast, recent *in vitro* and *in vivo* studies in mice and Drosophila revealed that aberrant intraneuronal glycogen production and accumulation can induce neurodegeneration (Vilchez et al., 2007, Duran et al., 2012). This observation suggests that – at least in part – CAm might indeed contribute to neuronal loss detected in some neurodegenerative diseases including AD.

Considering the recent findings in mice (Sinadinos et al., 2014), supporting our previous proposition on how CAm are formed, we conclude that CAm development in the human hippocampal formation results from both ageing-associated aberrant glycogen metabolism as well as impaired axonal protein transport in aged neurons (Krstic and Knuesel, 2013). These aberrant accumulations of glycogen polymers and proteins in neuronal processes could then subsequently lead to neurodegeneration. Increased cellular stress during ageing and/or pathological conditions may potentiate their formation, as well as neurodegeneration, as indicated by the subtle but significant increase in CAm in the subiculum of AD patients compared to non-demented controls in the *first study*. To what extent CAm formation correlates with progression of the disease and how they are linked to severe neurodegeneration detected in AD remains to be further examined.

Albeit additional studies are required to substantiate and clarify the impact and origin of CAm, a critical role for both aberrant glucose metabolism and neuronal transport is evident. It is therefore conceivable that putative ageing-associated impairment in NA signaling could alter astrocytic regulation of glycogenesis and glycogenolysis, favoring the formation of polyglucosan inclusions and affecting proper axonal transport.

PolyI:C Effect on the Regeneration Capacity of Noradrenergic Axons

Monoaminergic systems – such as the NA system – are known to retain a high level of function even after severe lesions (Bjorklund and Lindvall, 1979, Zigmond et al., 1990). There are two main mechanisms by which they can assure this compensation; adaptations in neurochemical components, (e.g., increased production of neurotransmitter or increased expression of receptors) and/or axonal regeneration of monoaminergic neurons both evidenced in AD patients (Hoogendijk et al., 1999, Szot et al., 2006, 2007). These compensatory mechanisms to regain NA signaling as fast as possible are detectable in lesion studies performed in rodents. 7 days post-DSP-4 treatment levels of adrenergic receptors (α- and β) are increased in the rat brain. One year post-single DSP-4 treatment, this compensation returned to baseline levels, except for β-adrenergic receptors (Wolfman et al., 1994). In parallel, independently on whether depletion was induced through DSP-4 or other toxins, intense regrowth and sprouting of NA axons into target areas starts within weeks post-lesion (Bjorklund et al., 1975, Bjorklund and Lindvall, 1979, Fritschy and Grzanna, 1992). The pattern and speed of reinnervation varies between areas, from fast and high reinnervation (thalamus, cortical areas and hippocampus) to almost complete absence of axons, even one 1 year post-injection (tectum and cerebellum)(Fritschy and Grzanna, 1992). Despite the substantiated knowledge on the time-dependent induction of these compensatory mechanisms in rodents, we lack the identity of the particular factors involved in this remarkable and fast reacting system.

Ever since the studies performed up to the early 90s, little new insights were gained on NA regeneration properties in the CNS. Regenerative sprouting is only observed in NA axons of LC and no other areas after LC depletion (Fritschy and Grzanna, 1992). This indicates that NA neurons require a trigger – here in the form of DSP-4 induced axon degeneration – to induce regeneration and sprouting of axons.

Next to factors inducing extensive sprouting and regrowth of NA axons, the signals that guide NA axons to their target areas during regeneration also remain to be further determined. Interestingly, LC deletion studies revealed a different regeneration pattern when applied in neonates compared to older rats. As such, cerebellum and brainstem are mainly devoid of regeneration post-LC depletion in adult rats but - in contrast - are hyperinnervated when LC depletion occurred in neonates (Sachs et al., 1974, Kostrzewa and Garey, 1976, Bendeich et al., 1978, Konkol et al., 1978, Schmidt and Bhatnagar, 1979, Levitt and Moore, 1980, Jonsson and

Hallman, 1982, Jonsson et al., 1982). This phenomenon of hyperinnervation of cerebellum and brainstem disappear with time and are lost when NA axon lesions are induced in rats of 5-7 days of age (Schmidt et al., 1980). Since the basal regeneration capacity of NA axons is not disturbed but only the target area of innervation changed, a shift in the expression pattern of certain trophic factors in target areas might be responsible for specific patterning of regeneration (Fritschy and Grzanna, 1992). Albeit this was proposed more than 20 years ago, to my knowledge, these trophic factors have never been identified. Therefore, it remains unknown whether prenatal PolyI:C treatment could have a long-term effect on the composition and/or concentration of such trophic factors.

Intriguingly, increased electrical stimulation in the initial phase of peripheral motor axon regeneration of the femoral nerve revealed significantly faster and more precise regeneration, which is dependent on cell body signaling through BDNF and trkB pathways (Al-Majed et al., 2000a, Al-Majed et al., 2000b). These authors have therefore suggested that an initial boost of regenerating neurons through electrical stimulation can activate trophic factor expression that induces long-term effects on regeneration mechanisms. These studies were performed in peripheral nerve fibers; thus, it still needs to be confirmed whether a similar stimulation mechanism could hold true for central axonal regeneration. If confirmed, one could speculate whether PolyI:C-induced changes could alter the velocity of regenerating NA axons by affecting levels of neurotrophic factors and activity patterns of LC neurons. In the following paragraphs, I will discuss this idea further and address different aspects that could – if tested and confirmed – explain how long-term effects induced by prenatal PolyI:C exposure during late gestation could alter regeneration velocity.

Prenatal PolyI:C exposure during late gestation has long-term effects on the GABAergic system in the prefrontal cortex (Richetto et al., 2014) and dorsal hippocampus (Richetto et al., 2013). In the first, both presynaptic ($GAD_{65}/_{67}$, VGAT) and postsynaptic ($GABA_A$ receptor subunits as well as KCC2 levels) GABAergic markers are decreased in adult offspring. Similar changes are found in the dorsal hippocampus evident by decreased mRNA levels of $GAD_{65/67}$ in prenatally PolyI:C-exposed adult offspring (Richetto et al., 2013). Furthermore, parvalbumin- and Reelin-positive interneurons are decreased in prefrontal cortex and hippocampus of adult offspring exposed to PolyI:C (Meyer et al., 2006b, Meyer et al., 2008c, Knuesel et al., 2009). In general, these observations suggest that PolyI:C has a long-term effect on inhibitory signaling pathways.

In the adult brain, GABA and glycine are the main inhibitory neurotransmitters. $GABA_A$ receptors are ionotrophic receptors selectively permeable for Cl^- and HCO_3^-. Their function lies

in controlling neuronal activity of excitatory transmission through hyperpolarization (inward current of Cl^- due to higher extracellular Cl^- ($[Cl]_e$) compared to intracellular ($[Cl]_i$) concentrations) of the postsynaptic target cells. Immature neurons, however, have higher intracellular concentrations of Cl^- due to the high expression of NKCC1 (inward Cl^- transport, high $[Cl]_i$) and low expression of KCC2 (outward Cl^- transport, low $[Cl]_e$) co-transporter levels (Hubner and Holthoff, 2013). Therefore, $GABA_AR$ activation depolarizes the target cells during developmental periods. Depolarization is accompanied by an increase of intracellular Ca^{2+}, which was proposed to putatively serve as second messenger altering intracellular pathways involved in neuronal maturation. Indeed, disrupting high intracellular Cl^- levels in newborn neurons resulted in decreased proliferation and acute truncated dendritic arborizations, which recovered to some extent resulting in newborn mature neurons with subtle but significant decreased dendritic complexity without affecting dendritic lengths (Young et al., 2012). Therefore, depending on the Cl^- transporter composition, GABAR activation can result in de- or hyperpolarization of the target cells.

Intriguingly, peripheral axonal regeneration studies performed in hypoglossal nerves revealed that post-nerve suturation, regeneration is associated with alterations in the GABAergic system including a transient decreased expression of KCC2 of large regenerating motoneurons (Tatetsu et al., 2012).These findings raise the question whether this temporal decreased expression of KCC2 in regenerating motor neurons could result in increased intracellular Cl^- to an extent that GABAergic signaling would lead to depolarization of cells and therefore induce similar signaling pathways as seen after electrical stimulation of regenerating nerve fibers (Al-Majed et al., 2000b). Thus, during initial phases of axonal regenerative processes GABAergic signaling would transiently switch to depolarization of target cells and thereby improve depolarization-dependent axonal regeneration.

To support this highly speculative hypothesis, three important factors would need to be tested: i) chemical stimulation of hypoglossal motor neurons with GABA agonists in the initial phase of regeneration increases the velocity and precision of axonal regeneration into the target area; ii) LC neurons undergo a similar transient change in expression pattern as seen in regenerating axons of motor neurons of the hypoglossal nerve – indicating that they are responsive to GABAergic signaling in the initial phase; and iii) prenatal PolyI:C exposure results in long-term reduction of GABAergic signaling in the LC. If these three points would hold true, one could speculate that the PolyI:C-induced decrease in the GABAergic system impairs temporal LC depolarization – through GABAergic signaling – during the initial phase of regeneration, which

would thereby result in the subtle effect on the regeneration capacity of NA axons detected in the *first cohort* of the *second study* (figure 2, *study II*).

Another way of how prenatal PolyI:C could affect regeneration of NA axons is through its property in accelerating ageing-associated changes (Knuesel et al., 2009). Several findings in our lab have led to the proposal that prenatal PolyI:C could indirectly affect cytoskeleton integrity and thereby axonal transport mechanisms (Doehner et al., 2012a, Krstic and Knuesel, 2013). Although, we still lack direct evidence that PolyI:C-induced changes alter microtubule integrity and axonal transport, it is conceivable that altered axonal transport could play a major role in axonal regeneration capacity.

Although we currently do not understand how prenatal immune activation results in the changes observed in NA axonal regeneration, these findings suggest that prenatal PolyI:C injections did induce changes, which persisted throughout ageing.

Genetic Background and α-Synuclein – Reason for the Lack of PolyI:C-Induced Phenotype?

To address the reasons for the lack of inflammatory response in the second experiment upon single or double immune challenge combined with repeated DSP-4 or NaCl injections, we performed the additional third study. We investigated the acute cytokine response towards PolyI:C in two substrains of C57Bl/6J mice, distinguished mainly by the presence or absence of α-synuclein (see *study III*). *In vitro* studies have revealed that application of exogenous α-synuclein can induce the expression of TLR3 receptors in primary microglia cultures (Beraud et al., 2011). However, the effect of increased mRNA expression on the functional outcome on TLR3-mediated responses towards an immune challenge was not determined in this study. Our pilot experiment revealed that the acute effect of PolyI:C administration on 3 prototypical peripheral pro-inflammatory cytokine levels did not differ between C57Bl6/JOla (lack α-synuclein) and C57Bl6/N (normal α-synuclein) mice (figure 2, *study III*). This observation indicates that the inflammatory response via TLR3 receptor signaling is independent on basal α-synuclein expression. Nevertheless, it is conceivable that during disease condition increased levels of α-synuclein might affect, or perhaps prime, the immune system towards inflammatory insults. In line with our finding, however, a recent *in vitro* study focusing on the α-synuclein priming effect on microglial cells revealed that subsequent stimulation of microglia with PolyI:C post-α-synuclein priming did not exacerbate their response, in contrast to stimulation of other

TLRs with synthetic bacterial lipoprotein Pam3CSK4 (Pam3), and single-stranded ssRNA40/LyoVec (ssRNA)(Roodveldt et al., 2013).

Further, our pilot study revealed that the effects induced by two different batches of PolyI:C (one of which was used in the *second study*) was highly comparable in intensity and time-course for the 3 pro-inflammatory cytokines tested (figure 1, *study III*). This result indicates that the PolyI:C batch used in the *second study* was able to affect the fetuses as expected. Accordingly, both cohorts of the *second study* show some although subtle long-term PolyI:C-induced alterations.

The pattern of acute response towards PolyI:C in this pilot study using young, non-pregnant female mice is comparable to that reported in previous studies in other strains and rats, where peripheral serum cytokine levels were determined after PolyI:C injections in pregnant dams (Meyer et al., 2006a, Meyer et al., 2006b, Connor et al., 2012, Harvey and Boksa, 2012b). Although we cannot completely rule out a potential role of α-synuclein in the immune response during pregnancy, the high similarity between pregnant and non-pregnant mice towards an inflammatory insult induced by PolyI:C suggest a putative pregnancy effect to be rather unlikely.

If acute PolyI:C on pregnant dams is independent of α-synuclein expression, as suggested by our pilot experiment and other findings (see above), we have to consider other confounds that could have masked or prevented the development of the chronic effects. As such, further studies are required to evaluate the effect of central α-synuclein expression on the development of long-term alterations, in particular on the role of α-synuclein in the brain's innate immune system. As shown by *in vitro* studies, α-synuclein can affect microglia expression profile of immune system-related proteins (Beraud et al., 2011). Ageing-associated increased expression of α-synuclein has further been reported in nigral neurons (Chu and Kordower, 2007, Alladi et al., 2010). Whether other brain regions show a similar age-dependent change in α-synuclein remains to be determined. If so, it could be conceivable that α-synuclein affects microglia aging (in terms of activation state) differently depending if they were primed by prenatal PolyI:C exposure or not.

In addition to internal factors, other external influences should be assessed. These include the effect of stress prior to PolyI:C challenge, for example through shipment, as well as putative desensitization effects induced by multiple handling, as discussed in the *second study*.

In conclusion, I suggest that studies conducted to address long-term effects induced by prenatal PolyI:C might require a parallel cohort – exclusively subjected to a single prenatal PolyI:C

challenge – that can be used to regularly monitor the expected age-dependent changes in the status of the immune system. This approach would allow the identification of potential manipulation-induced masking or changing of the expected phenotype.

REFERENCES

Abazyan B, Nomura J, Kannan G, Ishizuka K, Tamashiro KL, Nucifora F, Pogorelov V, Ladenheim B, Yang C, Krasnova IN, et al. (2010) Prenatal interaction of mutant DISC1 and immune activation produces adult psychopathology. Biol Psychiatry 68:1172-1181.

Abraham H, Meyer G (2003) Reelin-expressing neurons in the postnatal and adult human hippocampal formation. Hippocampus 13:715-727.

Al-Majed AA, Brushart TM, Gordon T (2000a) Electrical stimulation accelerates and increases expression of BDNF and trkB mRNA in regenerating rat femoral motoneurons. Eur J Neurosci 12:4381-4390.

Al-Majed AA, Neumann CM, Brushart TM, Gordon T (2000b) Brief electrical stimulation promotes the speed and accuracy of motor axonal regeneration. J Neurosci 20:2602-2608.

Alcantara S, Ruiz M, D'Arcangelo G, Ezan F, de Lecea L, Curran T, Sotelo C, Soriano E (1998) Regional and cellular patterns of reelin mRNA expression in the forebrain of the developing and adult mouse. J Neurosci 18:7779-7799.

Alexopoulou L, Holt AC, Medzhitov R, Flavell RA (2001) Recognition of double-stranded RNA and activation of NF-kappaB by Toll-like receptor 3. Nature 413:732-738.

Alladi PA, Mahadevan A, Vijayalakshmi K, Muthane U, Shankar SK, Raju TR (2010) Ageing enhances alpha-synuclein, ubiquitin and endoplasmic reticular stress protein expression in the nigral neurons of Asian Indians. Neurochem Int 57:530-539.

Anzil AP, Herrlinger H, Blinzinger K, Kronski D (1974) Intraneuritic corpora amylacea. Demonstration in orbital cortex of elderly subjects by means of early postmortem brain sampling and electron microscopy. Virchows Arch A Pathol Anat Histol 364:297-301.

Arriagada PV, Growdon JH, Hedley-Whyte ET, Hyman BT (1992a) Neurofibrillary tangles but not senile plaques parallel duration and severity of Alzheimer's disease. Neurology 42:631-639.

Arriagada PV, Marzloff K, Hyman BT (1992b) Distribution of Alzheimer-type pathologic changes in nondemented elderly individuals matches the pattern in Alzheimer's disease. Neurology 42:1681-1688.

Arsenault D, St-Amour I, Cisbani G, Rousseau LS, Cicchetti F (2014) The different effects of LPS and poly I:C prenatal immune challenges on the behavior, development and inflammatory responses in pregnant mice and their offspring. Brain Behav Immun 38:77-90.

Ashdown H, Dumont Y, Ng M, Poole S, Boksa P, Luheshi GN (2006) The role of cytokines in mediating effects of prenatal infection on the fetus: implications for schizophrenia. Mol Psychiatry 11:47-55.

Aston-Jones G, Bloom FE (1981) Activity of norepinephrine-containing locus coeruleus neurons in behaving rats anticipates fluctuations in the sleep-waking cycle. J Neurosci 1:876-886.

Averback P (1981) Parasynaptic corpora amylacea in the striatum. Arch Pathol Lab Med 105:334-335.

Bacic F, McCarron RM, Uematsu S, Spatz M (1992) Adrenergic receptors coupled to adenylate cyclase in human cerebromicrovascular endothelium. Metab Brain Dis 7:125-137.

Bali J, Gheinani AH, Zurbriggen S, Rajendran L (2012) Role of genes linked to sporadic Alzheimer's disease risk in the production of beta-amyloid peptides. Proc Natl Acad Sci U S A 109:15307-15311.

Ballatore C, Lee VM, Trojanowski JQ (2007) Tau-mediated neurodegeneration in Alzheimer's disease and related disorders. Nat Rev Neurosci 8:663-672.

Barthel H, Gertz HJ, Dresel S, Peters O, Bartenstein P, Buerger K, Hiemeyer F, Wittemer-Rump SM, Seibyl J, Reininger C, et al. (2011) Cerebral amyloid-beta PET with florbetaben (18F) in patients with Alzheimer's disease and healthy controls: a multicentre phase 2 diagnostic study. Lancet Neurol 10:424-435.

Bastarache JA, Koyama T, Wickersham NE, Ware LB (2014) Validation of a multiplex electrochemiluminescent immunoassay platform in human and mouse samples. J Immunol Methods 408:13-23.

Becker RE, Greig NH, Giacobini E, Schneider LS, Ferrucci L (2014) A new roadmap for drug development for Alzheimer's disease. Nat Rev Drug Discov 13:156.

Beffert U, Morfini G, Bock HH, Reyna H, Brady ST, Herz J (2002) Reelin-mediated signaling locally regulates protein kinase B/Akt and glycogen synthase kinase 3beta. J Biol Chem 277:49958-49964.

Beffert U, Weeber EJ, Durudas A, Qiu S, Masiulis I, Sweatt JD, Li WP, Adelmann G, Frotscher M, Hammer RE, et al. (2005) Modulation of synaptic plasticity and memory by Reelin involves differential splicing of the lipoprotein receptor Apoer2. Neuron 47:567-579.

Beffert U, Weeber EJ, Morfini G, Ko J, Brady ST, Tsai LH, Sweatt JD, Herz J (2004) Reelin and cyclin-dependent kinase 5-dependent signals cooperate in regulating neuronal migration and synaptic transmission. J Neurosci 24:1897-1906.

Bell RD, Winkler EA, Singh I, Sagare AP, Deane R, Wu Z, Holtzman DM, Betsholtz C, Armulik A, Sallstrom J, et al. (2012) Apolipoprotein E controls cerebrovascular integrity via cyclophilin A. Nature 485:512-516.

Bendeich E, Konkol RJ, Krigman MR, Breese GR (1978) Morphological evidence for 6-hydroxydopamine-induced sprouting or noradrenergic neurons in the cerebellum. J Neurol Sci 38:47-57.

Benilova I, Karran E, De Strooper B (2012) The toxic Abeta oligomer and Alzheimer's disease: an emperor in need of clothes. Nat Neurosci 15:349-357.

Benzing WC, Wujek JR, Ward EK, Shaffer D, Ashe KH, Younkin SG, Brunden KR (1999) Evidence for glial-mediated inflammation in aged APP(SW) transgenic mice. Neurobiol Aging 20:581-589.

Beraud D, Twomey M, Bloom B, Mittereder A, Ton V, Neitzke K, Chasovskikh S, Mhyre TR, Maguire-Zeiss KA (2011) alpha-Synuclein Alters Toll-Like Receptor Expression. Front Neurosci 5:80.

Berridge CW, Waterhouse BD (2003) The locus coeruleus-noradrenergic system: modulation of behavioral state and state-dependent cognitive processes. Brain Res Brain Res Rev 42:33-84.

Bertram L, Lill CM, Tanzi RE (2010) The genetics of Alzheimer disease: back to the future. Neuron 68:270-281.

Bertram L, McQueen MB, Mullin K, Blacker D, Tanzi RE (2007) Systematic meta-analyses of Alzheimer disease genetic association studies: the AlzGene database. Nat Genet 39:17-23.

Bertram L, Tanzi RE (2009) Genome-wide association studies in Alzheimer's disease. Hum Mol Genet 18:R137-145.

Bhaskar K, Konerth M, Kokiko-Cochran ON, Cardona A, Ransohoff RM, Lamb BT (2010) Regulation of tau pathology by the microglial fractalkine receptor. Neuron 68:19-31.

Bird TD (2008) Genetic aspects of Alzheimer disease. Genet Med 10:231-239.

Bitanihirwe BK, Weber L, Feldon J, Meyer U (2010) Cognitive impairment following prenatal immune challenge in mice correlates with prefrontal cortical AKT1 deficiency. Int J Neuropsychopharmacol 13:981-996.

Bjorklund A, Baumgarten HG, Lachenmayer L, Rosengren E (1975) Recovery of brain noradrenaline after 5,7-dihydroxytryptamine-induced axonal lesions in the rat. Cell Tissue Res 161:145-155.

Bjorklund A, Lindvall O (1979) Regeneration of normal terminal innervation patterns by central noradrenergic neurons after 5,7-dihydroxytryptamine-induced axotomy in the adult rat. Brain Res 171:271-293.

Bock HH, Herz J (2003) Reelin activates SRC family tyrosine kinases in neurons. Curr Biol 13:18-26.

Bock HH, Jossin Y, Liu P, Forster E, May P, Goffinet AM, Herz J (2003) Phosphatidylinositol 3-kinase interacts with the adaptor protein Dab1 in response to Reelin signaling and is required for normal cortical lamination. J Biol Chem 278:38772-38779.

Boehm-Cagan A, Michaelson DM (2014) Reversal of apoE4-driven brain pathology and behavioral deficits by bexarotene. J Neurosci 34:7293-7301.

Bondareff W, Mountjoy CQ, Roth M, Rossor MN, Iversen LL, Reynolds GP, Hauser DL (1987) Neuronal degeneration in locus ceruleus and cortical correlates of Alzheimer disease. Alzheimer Dis Assoc Disord 1:256-262.

Borges N, Shi F, Azevedo I, Audus KL (1994) Changes in brain microvessel endothelial cell monolayer permeability induced by adrenergic drugs. Eur J Pharmacol 269:243-248.

Borrell J, Vela JM, Arevalo-Martin A, Molina-Holgado E, Guaza C (2002) Prenatal immune challenge disrupts sensorimotor gating in adult rats. Implications for the etiopathogenesis of schizophrenia. Neuropsychopharmacology 26:204-215.

Borrell V, Del Rio JA, Alcantara S, Derer M, Martinez A, D'Arcangelo G, Nakajima K, Mikoshiba K, Derer P, Curran T, et al. (1999) Reelin regulates the development and synaptogenesis of the layer-specific entorhino-hippocampal connections. J Neurosci 19:1345-1358.

Botella-Lopez A, Cuchillo-Ibanez I, Cotrufo T, Mok SS, Li QX, Barquero MS, Dierssen M, Soriano E, Saez-Valero J (2010) Beta-amyloid controls altered Reelin expression and processing in Alzheimer's disease. Neurobiol Dis 37:682-691.

Bowen DM, Smith CB, White P, Davison AN (1976) Neurotransmitter-related enzymes and indices of hypoxia in senile dementia and other abiotrophies. Brain 99:459-496.

Bozoki AC, Korolev IO, Davis NC, Hoisington LA, Berger KL (2012) Disruption of limbic white matter pathways in mild cognitive impairment and Alzheimer's disease: a DTI/FDG-PET study. Hum Brain Mapp 33:1792-1802.

Braak H, Braak E (1991) Neuropathological stageing of Alzheimer-related changes. Acta Neuropathol 82:239-259.

Braak H, Del Tredici K (2012) Where, when, and in what form does sporadic Alzheimer's disease begin? Curr Opin Neurol 25:708-714.

Braak H, Thal DR, Ghebremedhin E, Del Tredici K (2011) Stages of the pathologic process in Alzheimer disease: age categories from 1 to 100 years. J Neuropathol Exp Neurol 70:960-969.

Brecht WJ, Harris FM, Chang S, Tesseur I, Yu GQ, Xu Q, Dee Fish J, Wyss-Coray T, Buttini M, Mucke L, et al. (2004) Neuron-specific apolipoprotein e4 proteolysis is associated with increased tau phosphorylation in brains of transgenic mice. J Neurosci 24:2527-2534.

Brookmeyer R, Johnson E, Ziegler-Graham K, Arrighi HM (2007) Forecasting the global burden of Alzheimer's disease. Alzheimers Dement 3:186-191.

Burns MP, Noble WJ, Olm V, Gaynor K, Casey E, LaFrancois J, Wang L, Duff K (2003) Co-localization of cholesterol, apolipoprotein E and fibrillar Abeta in amyloid plaques. Brain Res Mol Brain Res 110:119-125.

Burre J, Sharma M, Tsetsenis T, Buchman V, Etherton MR, Sudhof TC (2010) Alpha-synuclein promotes SNARE-complex assembly in vivo and in vitro. Science 329:1663-1667.

Campbell A (2004) Inflammation, neurodegenerative diseases, and environmental exposures. Ann N Y Acad Sci 1035:117-132.

Castellani RJ, Rolston RK, Smith MA (2010) Alzheimer disease. Dis Mon 56:484-546.

Cavanagh JB (1998) Spinal corpora amylacea and motor neuron disease: a quantitative study. J Neurol Neurosurg Psychiatry 65:488-491.

Cavanagh JB (1999) Corpora-amylacea and the family of polyglucosan diseases. Brain Res Brain Res Rev 29:265-295.

Chai X, Forster E, Zhao S, Bock HH, Frotscher M (2009) Reelin stabilizes the actin cytoskeleton of neuronal processes by inducing n-cofilin phosphorylation at serine3. J Neurosci 29:288-299.

Chan-Palay V, Asan E (1989) Alterations in catecholamine neurons of the locus coeruleus in senile dementia of the Alzheimer type and in Parkinson's disease with and without dementia and depression. J Comp Neurol 287:373-392.

Chen Y, Durakoglugil MS, Xian X, Herz J (2010) ApoE4 reduces glutamate receptor function and synaptic plasticity by selectively impairing ApoE receptor recycling. Proc Natl Acad Sci U S A 107:12011-12016.

Chin J, Massaro CM, Palop JJ, Thwin MT, Yu GQ, Bien-Ly N, Bender A, Mucke L (2007) Reelin depletion in the entorhinal cortex of human amyloid precursor protein transgenic mice and humans with Alzheimer's disease. J Neurosci 27:2727-2733.

Chromy BA, Nowak RJ, Lambert MP, Viola KL, Chang L, Velasco PT, Jones BW, Fernandez SJ, Lacor PN, Horowitz P, et al. (2003) Self-assembly of Abeta(1-42) into globular neurotoxins. Biochemistry 42:12749-12760.

Chu Y, Kordower JH (2007) Age-associated increases of alpha-synuclein in monkeys and humans are associated with nigrostriatal dopamine depletion: Is this the target for Parkinson's disease? Neurobiol Dis 25:134-149.

Chung MH, Horoupian DS (1996) Corpora amylacea: a marker for mesial temporal sclerosis. J Neuropathol Exp Neurol 55:403-408.

Ciallella JR, Ikonomovic MD, Paljug WR, Wilbur YI, Dixon CE, Kochanek PM, Marion DW, DeKosky ST (2002) Changes in expression of amyloid precursor protein and interleukin-1beta after experimental traumatic brain injury in rats. J Neurotrauma 19:1555-1567.

Cisse S, Lacoste-Royal G, Laperriere J, Cabana T, Gauvreau D (1991) Ubiquitin is a component of polypeptides purified from corpora amylacea of aged human brain. Neurochem Res 16:429-433.

Cisse S, Perry G, Lacoste-Royal G, Cabana T, Gauvreau D (1993) Immunochemical identification of ubiquitin and heat-shock proteins in corpora amylacea from normal aged and Alzheimer's disease brains. Acta Neuropathol 85:233-240.

Clayton EC, Rajkowski J, Cohen JD, Aston-Jones G (2004) Phasic activation of monkey locus ceruleus neurons by simple decisions in a forced-choice task. J Neurosci 24:9914-9920.

Cohen Z, Molinatti G, Hamel E (1997) Astroglial and vascular interactions of noradrenaline terminals in the rat cerebral cortex. J Cereb Blood Flow Metab 17:894-904.

Combarros O, Warden DR, Hammond N, Cortina-Borja M, Belbin O, Lehmann MG, Wilcock GK, Brown K, Kehoe PG, Barber R, et al. (2010) The dopamine beta-hydroxylase -1021C/T polymorphism is associated with the risk of Alzheimer's disease in the Epistasis Project. BMC Med Genet 11:162.

Conaldi PG, Serra C, Mossa A, Falcone V, Basolo F, Camussi G, Dolei A, Toniolo A (1997) Persistent infection of human vascular endothelial cells by group B coxsackieviruses. J Infect Dis 175:693-696.

Connor CM, Dincer A, Straubhaar J, Galler JR, Houston IB, Akbarian S (2012) Maternal immune activation alters behavior in adult offspring, with subtle changes in the cortical transcriptome and epigenome. Schizophr Res 140:175-184.

Corder EH, Saunders AM, Strittmatter WJ, Schmechel DE, Gaskell PC, Small GW, Roses AD, Haines JL, Pericak-Vance MA (1993) Gene dose of apolipoprotein E type 4 allele and the risk of Alzheimer's disease in late onset families. Science 261:921-923.

Craig LA, Hong NS, McDonald RJ (2011) Revisiting the cholinergic hypothesis in the development of Alzheimer's disease. Neurosci Biobehav Rev 35:1397-1409.

Cross DJ, Anzai Y, Petrie EC, Martin N, Richards TL, Maravilla KR, Peskind ER, Minoshima S (2013) Loss of olfactory tract integrity affects cortical metabolism in the brain and olfactory regions in aging and mild cognitive impairment. J Nucl Med 54:1278-1284.

Cummings JL, Morstorf T, Zhong K (2014) Alzheimer's disease drug-development pipeline: few candidates, frequent failures. Alzheimers Res Ther 6:37.

Cunningham C, Campion S, Teeling J, Felton L, Perry VH (2007) The sickness behaviour and CNS inflammatory mediator profile induced by systemic challenge of mice with synthetic double-stranded RNA (poly I:C). Brain Behav Immun 21:490-502.

D'Arcangelo G, Miao GG, Chen SC, Soares HD, Morgan JI, Curran T (1995) A protein related to extracellular matrix proteins deleted in the mouse mutant reeler. Nature 374:719-723.

Dahlgren J, Nilsson C, Jennische E, Ho HP, Eriksson E, Niklasson A, Bjorntorp P, Albertsson Wikland K, Holmang A (2001) Prenatal cytokine exposure results in obesity and gender-specific programming. Am J Physiol Endocrinol Metab 281:E326-334.

Dahlgren J, Samuelsson AM, Jansson T, Holmang A (2006) Interleukin-6 in the maternal circulation reaches the rat fetus in mid-gestation. Pediatr Res 60:147-151.

Davies P, Maloney AJ (1976) Selective loss of central cholinergic neurons in Alzheimer's disease. Lancet 2:1403.

de Bergeyck V, Nakajima K, Lambert de Rouvroit C, Naerhuyzen B, Goffinet AM, Miyata T, Ogawa M, Mikoshiba K (1997) A truncated Reelin protein is produced but not secreted in the 'Orleans' reeler mutation (Reln[rl-Orl]). Brain Res Mol Brain Res 50:85-90.

Del Rio JA, Heimrich B, Borrell V, Forster E, Drakew A, Alcantara S, Nakajima K, Miyata T, Ogawa M, Mikoshiba K, et al. (1997) A role for Cajal-Retzius cells and reelin in the development of hippocampal connections. Nature 385:70-74.

Dellu F, Mayo W, Cherkaoui J, Le Moal M, Simon H (1992) A two-trial memory task with automated recording: study in young and aged rats. Brain Res 588:132-139.

Derer P, Derer M, Goffinet A (2001) Axonal secretion of Reelin by Cajal-Retzius cells: evidence from comparison of normal and Reln(Orl) mutant mice. J Comp Neurol 440:136-143.

Devauges V, Sara SJ (1990) Activation of the noradrenergic system facilitates an attentional shift in the rat. Behav Brain Res 39:19-28.

Dodart JC, May P (2005) Overview on rodent models of Alzheimer's disease. Curr Protoc Neurosci Chapter 9:Unit 9 22.

Doehner J, Genoud C, Imhof C, Krstic D, Knuesel I (2012a) Extrusion of misfolded and aggregated proteins--a protective strategy of aging neurons? Eur J Neurosci 35:1938-1950.

Doehner J, Genoud C, Imhof C, Krstic D, Knuesel I (2012b) Extrusion of misfolded and aggregated proteins - a protective strategy of aging neurons? Eur J Neurosci 35:1938-1950.

Doehner J, Madhusudan A, Konietzko U, Fritschy JM, Knuesel I (2010) Co-localization of Reelin and proteolytic AbetaPP fragments in hippocampal plaques in aged wild-type mice. J Alzheimers Dis 19:1339-1357.

Duran J, Tevy MF, Garcia-Rocha M, Calbo J, Milan M, Guinovart JJ (2012) Deleterious effects of neuronal accumulation of glycogen in flies and mice. EMBO Mol Med 4:719-729.

Duyckaerts C, Hauw JJ, Bastenaire F, Piette F, Poulain C, Rainsard V, Javoy-Agid F, Berthaux P (1986) Laminar distribution of neocortical senile plaques in senile dementia of the Alzheimer type. Acta Neuropathol 70:249-256.

Duyckaerts C, Uchihara T, Seilhean D, He Y, Hauw JJ (1997) Dissociation of Alzheimer type pathology in a disconnected piece of cortex. Acta Neuropathol 93:501-507.

Edison P, Archer HA, Gerhard A, Hinz R, Pavese N, Turkheimer FE, Hammers A, Tai YF, Fox N, Kennedy A, et al. (2008) Microglia, amyloid, and cognition in Alzheimer's disease: An [11C](R)PK11195-PET and [11C]PIB-PET study. Neurobiol Dis 32:412-419.

Egensperger R, Kosel S, von Eitzen U, Graeber MB (1998) Microglial activation in Alzheimer disease: Association with APOE genotype. Brain Pathol 8:439-447.

Engler H, Doenlen R, Riether C, Engler A, Besedovsky HO, Del Rey A, Pacheco-Lopez G, Schedlowski M (2010) Chemical destruction of brain noradrenergic neurons affects splenic cytokine production. J Neuroimmunol 219:75-80.

Farina C, Krumbholz M, Giese T, Hartmann G, Aloisi F, Meinl E (2005) Preferential expression and function of Toll-like receptor 3 in human astrocytes. J Neuroimmunol 159:12-19.

Feinstein DL, Heneka MT, Gavrilyuk V, Dello Russo C, Weinberg G, Galea E (2002) Noradrenergic regulation of inflammatory gene expression in brain. Neurochem Int 41:357-365.

Fiala JC, Feinberg M, Peters A, Barbas H (2007) Mitochondrial degeneration in dystrophic neurites of senile plaques may lead to extracellular deposition of fine filaments. Brain Struct Funct 212:195-207.

Fornai F, Bassi L, Torracca MT, Alessandri MG, Scalori V, Corsini GU (1996) Region- and neurotransmitter-dependent species and strain differences in DSP-4-induced monoamine depletion in rodents. Neurodegeneration 5:241-249.

Francis PT, Palmer AM, Snape M, Wilcock GK (1999) The cholinergic hypothesis of Alzheimer's disease: a review of progress. J Neurol Neurosurg Psychiatry 66:137-147.

Frank-Cannon TC, Alto LT, McAlpine FE, Tansey MG (2009) Does neuroinflammation fan the flame in neurodegenerative diseases? Mol Neurodegener 4:47.

Frautschy SA, Yang F, Irrizarry M, Hyman B, Saido TC, Hsiao K, Cole GM (1998) Microglial response to amyloid plaques in APPsw transgenic mice. Am J Pathol 152:307-317.

Freiman TM, Eismann-Schweimler J, Frotscher M (2011) Granule cell dispersion in temporal lobe epilepsy is associated with changes in dendritic orientation and spine distribution. Exp Neurol 229:332-338.

Fritschy JM, Geffard M, Grzanna R (1990) The response of noradrenergic axons to systemically administered DSP-4 in the rat: an immunohistochemical study using antibodies to noradrenaline and dopamine-beta-hydroxylase. J Chem Neuroanat 3:309-321.

Fritschy JM, Grzanna R (1989) Immunohistochemical analysis of the neurotoxic effects of DSP-4 identifies two populations of noradrenergic axon terminals. Neuroscience 30:181-197.

Fritschy JM, Grzanna R (1991) Experimentally-induced neuron loss in the locus coeruleus of adult rats. Exp Neurol 111:123-127.

Fritschy JM, Grzanna R (1992) Restoration of ascending noradrenergic projections by residual locus coeruleus neurons: compensatory response to neurotoxin-induced cell death in the adult rat brain. J Comp Neurol 321:421-441.

Frotscher M (1998) Cajal-Retzius cells, Reelin, and the formation of layers. Curr Opin Neurobiol 8:570-575.

Frotscher M (2010) Role for Reelin in stabilizing cortical architecture. Trends Neurosci 33:407-414.

Frotscher M, Haas CA, Forster E (2003) Reelin controls granule cell migration in the dentate gyrus by acting on the radial glial scaffold. Cereb Cortex 13:634-640.

Furukawa K, Barger SW, Blalock EM, Mattson MP (1996) Activation of K+ channels and suppression of neuronal activity by secreted beta-amyloid-precursor protein. Nature 379:74-78.

Garay PA, Hsiao EY, Patterson PH, McAllister AK (2013) Maternal immune activation causes age- and region-specific changes in brain cytokines in offspring throughout development. Brain Behav Immun 31:54-68.

Garfinkel S, Haines DS, Brown S, Wessendorf J, Gillespie DH, Maciag T (1992) Interleukin-1 alpha mediates an alternative pathway for the antiproliferative action of poly(I.C) on human endothelial cells. J Biol Chem 267:24375-24378.

German DC, Manaye KF, White CL, 3rd, Woodward DJ, McIntire DD, Smith WK, Kalaria RN, Mann DM (1992) Disease-specific patterns of locus coeruleus cell loss. Ann Neurol 32:667-676.

German DC, Nelson O, Liang F, Liang CL, Games D (2005) The PDAPP mouse model of Alzheimer's disease: locus coeruleus neuronal shrinkage. J Comp Neurol 492:469-476.

Gilat-Frenkel M, Boehm-Cagan A, Liraz O, Xian X, Herz J, Michaelson DM (2014) Involvement of the Apoer2 and Lrp1 receptors in mediating the pathological effects of ApoE4 in vivo. Curr Alzheimer Res 11:549-557.

Giovanoli S, Engler H, Engler A, Richetto J, Voget M, Willi R, Winter C, Riva MA, Mortensen PB, Feldon J, et al. (2013) Stress in puberty unmasks latent neuropathological consequences of prenatal immune activation in mice. Science 339:1095-1099.

Goadsby PJ, Duckworth JW (1989) Low frequency stimulation of the locus coeruleus reduces regional cerebral blood flow in the spinalized cat. Brain Res 476:71-77.

Goate A, Chartier-Harlin MC, Mullan M, Brown J, Crawford F, Fidani L, Giuffra L, Haynes A, Irving N, James L, et al. (1991) Segregation of a missense mutation in the amyloid precursor protein gene with familial Alzheimer's disease. Nature 349:704-706.

Goldgaber D, Harris HW, Hla T, Maciag T, Donnelly RJ, Jacobsen JS, Vitek MP, Gajdusek DC (1989) Interleukin 1 regulates synthesis of amyloid beta-protein precursor mRNA in human endothelial cells. Proc Natl Acad Sci U S A 86:7606-7610.

Gomez-Isla T, Price JL, McKeel DW, Jr., Morris JC, Growdon JH, Hyman BT (1996a) Profound loss of layer II entorhinal cortex neurons occurs in very mild Alzheimer's disease. J Neurosci 16:4491-4500.

Gomez-Isla T, West HL, Rebeck GW, Harr SD, Growdon JH, Locascio JJ, Perls TT, Lipsitz LA, Hyman BT (1996b) Clinical and pathological correlates of apolipoprotein E epsilon 4 in Alzheimer's disease. Ann Neurol 39:62-70.

Grehan S, Tse E, Taylor JM (2001) Two distal downstream enhancers direct expression of the human apolipoprotein E gene to astrocytes in the brain. J Neurosci 21:812-822.

Griffin WS (2006) Inflammation and neurodegenerative diseases. Am J Clin Nutr 83:470S-474S.

Griffin WS, Sheng JG, Royston MC, Gentleman SM, McKenzie JE, Graham DI, Roberts GW, Mrak RE (1998) Glial-neuronal interactions in Alzheimer's disease: the potential role of a 'cytokine cycle' in disease progression. Brain Pathol 8:65-72.

Grudzien A, Shaw P, Weintraub S, Bigio E, Mash DC, Mesulam MM (2007) Locus coeruleus neurofibrillary degeneration in aging, mild cognitive impairment and early Alzheimer's disease. Neurobiol Aging 28:327-335.

Grundke-Iqbal I, Iqbal K, Tung YC, Quinlan M, Wisniewski HM, Binder LI (1986) Abnormal phosphorylation of the microtubule-associated protein tau (tau) in Alzheimer cytoskeletal pathology. Proc Natl Acad Sci U S A 83:4913-4917.

Grzanna R, Berger U, Fritschy JM, Geffard M (1989) Acute action of DSP-4 on central norepinephrine axons: biochemical and immunohistochemical evidence for differential effects. J Histochem Cytochem 37:1435-1442.

Haass C, Kaether C, Thinakaran G, Sisodia S (2012) Trafficking and proteolytic processing of APP. Cold Spring Harb Perspect Med 2:a006270.

Hahn EA, Wang HX, Andel R, Fratiglioni L (2014) A change in sleep pattern may predict Alzheimer disease. Am J Geriatr Psychiatry 22:1262-1271.

Hammerschmidt T, Kummer MP, Terwel D, Martinez A, Gorji A, Pape HC, Rommelfanger KS, Schroeder JP, Stoll M, Schultze J, et al. (2013) Selective loss of noradrenaline exacerbates early cognitive dysfunction and synaptic deficits in APP/PS1 mice. Biol Psychiatry 73:454-463.

Hardy J, Selkoe DJ (2002) The amyloid hypothesis of Alzheimer's disease: progress and problems on the road to therapeutics. Science 297:353-356.

Hardy JA, Higgins GA (1992) Alzheimer's disease: the amyloid cascade hypothesis. Science 256:184-185.

Harold D, Abraham R, Hollingworth P, Sims R, Gerrish A, Hamshere ML, Pahwa JS, Moskvina V, Dowzell K, Williams A, et al. (2009) Genome-wide association study identifies variants at CLU and PICALM associated with Alzheimer's disease. Nat Genet 41:1088-1093.

Harris FM, Brecht WJ, Xu Q, Tesseur I, Kekonius L, Wyss-Coray T, Fish JD, Masliah E, Hopkins PC, Scearce-Levie K, et al. (2003) Carboxyl-terminal-truncated apolipoprotein E4 causes Alzheimer's disease-like neurodegeneration and behavioral deficits in transgenic mice. Proc Natl Acad Sci U S A 100:10966-10971.

Hartig W, Bruckner G, Schmidt C, Brauer K, Bodewitz G, Turner JD, Bigl V (1997) Co-localization of beta-amyloid peptides, apolipoprotein E and glial markers in senile plaques in the prefrontal cortex of old rhesus monkeys. Brain Res 751:315-322.

Harvey L, Boksa P (2012a) Prenatal and postnatal animal models of immune activation: relevance to a range of neurodevelopmental disorders. Dev Neurobiol 72:1335-1348.

Harvey L, Boksa P (2012b) A stereological comparison of GAD67 and reelin expression in the hippocampal stratum oriens of offspring from two mouse models of maternal inflammation during pregnancy. Neuropharmacology 62:1767-1776.

Hayes A, Green EK, Pritchard A, Harris JM, Zhang Y, Lambert JC, Chartier-Harlin MC, Pickering-Brown SM, Lendon CL, Mann DM (2004) A polymorphic variation in the interleukin 1A gene increases brain microglial cell activity in Alzheimer's disease. J Neurol Neurosurg Psychiatry 75:1475-1477.

Heneka MT, Galea E, Gavriluyk V, Dumitrescu-Ozimek L, Daeschner J, O'Banion MK, Weinberg G, Klockgether T, Feinstein DL (2002) Noradrenergic depletion potentiates beta -amyloid-induced cortical inflammation: implications for Alzheimer's disease. J Neurosci 22:2434-2442.

Heneka MT, Nadrigny F, Regen T, Martinez-Hernandez A, Dumitrescu-Ozimek L, Terwel D, Jardanhazi-Kurutz D, Walter J, Kirchhoff F, Hanisch UK, et al. (2010) Locus ceruleus controls Alzheimer's disease pathology by modulating microglial functions through norepinephrine. Proc Natl Acad Sci U S A 107:6058-6063.

Heneka MT, Ramanathan M, Jacobs AH, Dumitrescu-Ozimek L, Bilkei-Gorzo A, Debeir T, Sastre M, Galldiks N, Zimmer A, Hoehn M, et al. (2006) Locus ceruleus degeneration promotes Alzheimer pathogenesis in amyloid precursor protein 23 transgenic mice. J Neurosci 26:1343-1354.

Herholz K, Salmon E, Perani D, Baron JC, Holthoff V, Frolich L, Schonknecht P, Ito K, Mielke R, Kalbe E, et al. (2002) Discrimination between Alzheimer dementia and controls by automated analysis of multicenter FDG PET. NeuroImage 17:302-316.

Herring A, Donath A, Steiner KM, Widera MP, Hamzehian S, Kanakis D, Kolble K, ElAli A, Hermann DM, Paulus W, et al. (2012) Reelin depletion is an early phenomenon of Alzheimer's pathology. J Alzheimers Dis 30:963-979.

Hertz L, Peng L, Dienel GA (2007) Energy metabolism in astrocytes: high rate of oxidative metabolism and spatiotemporal dependence on glycolysis/glycogenolysis. J Cereb Blood Flow Metab 27:219-249.

Hetier E, Ayala J, Bousseau A, Prochiantz A (1991) Modulation of interleukin-1 and tumor necrosis factor expression by beta-adrenergic agonists in mouse ameboid microglial cells. Exp Brain Res 86:407-413.

Hibi T, Hattori M (2009) The N-terminal fragment of Reelin is generated after endocytosis and released through the pathway regulated by Rab11. FEBS letters 583:1299-1303.

Hiesberger T, Trommsdorff M, Howell BW, Goffinet A, Mumby MC, Cooper JA, Herz J (1999) Direct binding of Reelin to VLDL receptor and ApoE receptor 2 induces tyrosine phosphorylation of disabled-1 and modulates tau phosphorylation. Neuron 24:481-489.

Hoe HS, Tran TS, Matsuoka Y, Howell BW, Rebeck GW (2006) DAB1 and Reelin effects on amyloid precursor protein and ApoE receptor 2 trafficking and processing. J Biol Chem 281:35176-35185.

Hollingworth P, Harold D, Sims R, Gerrish A, Lambert JC, Carrasquillo MM, Abraham R, Hamshere ML, Pahwa JS, Moskvina V, et al. (2011) Common variants at ABCA7, MS4A6A/MS4A4E, EPHA1, CD33 and CD2AP are associated with Alzheimer's disease. Nat Genet 43:429-435.

Holtzman DM, Herz J, Bu G (2012) Apolipoprotein E and apolipoprotein E receptors: normal biology and roles in Alzheimer disease. Cold Spring Harb Perspect Med 2:a006312.

Hoogendijk WJ, Feenstra MG, Botterblom MH, Gilhuis J, Sommer IE, Kamphorst W, Eikelenboom P, Swaab DF (1999) Increased activity of surviving locus ceruleus neurons in Alzheimer's disease. Ann Neurol 45:82-91.

Huang Y, Liu XQ, Wyss-Coray T, Brecht WJ, Sanan DA, Mahley RW (2001) Apolipoprotein E fragments present in Alzheimer's disease brains induce neurofibrillary tangle-like intracellular inclusions in neurons. Proc Natl Acad Sci U S A 98:8838-8843.

Huang Y, Shah V, Liu T, Keshvara L (2005) Signaling through Disabled 1 requires phosphoinositide binding. Biochem Biophys Res Commun 331:1460-1468.

Huber G, Martin JR, Loffler J, Moreau JL (1993) Involvement of amyloid precursor protein in memory formation in the rat: an indirect antibody approach. Brain Res 603:348-352.

Hubner CA, Holthoff K (2013) Anion transport and GABA signaling. Front Cell Neurosci 7:177.

Imaizumi T, Hatakeyama M, Taima K, Ishikawa A, Yamashita K, Yoshida H, Satoh K (2004) Effect of double-stranded RNA on the expression of epithelial neutrophil activating peptide-78/CXCL-5 in human endothelial cells. Inflammation 28:215-219.

Imaizumi T, Hatakeyama M, Yamashita K, Ishikawa A, Yoshida H, Satoh K, Taima K, Mori F, Wakabayashi K (2005) Double-stranded RNA induces the synthesis of retinoic acid-inducible gene-I in vascular endothelial cells. Endothelium 12:133-137.

Iqbal K, Grundke-Iqbal I (2010) Alzheimer's disease, a multifactorial disorder seeking multitherapies. Alzheimers Dement 6:420-424.

Iqbal K, Grundke-Iqbal I, Zaidi T, Merz PA, Wen GY, Shaikh SS, Wisniewski HM, Alafuzoff I, Winblad B (1986) Defective brain microtubule assembly in Alzheimer's disease. Lancet 2:421-426.

Irizarry MC, McNamara M, Fedorchak K, Hsiao K, Hyman BT (1997) APPSw transgenic mice develop age-related A beta deposits and neuropil abnormalities, but no neuronal loss in CA1. J Neuropathol Exp Neurol 56:965-973.

Ishikawa A, Imaizumi T, Yoshida H, Nishi N, Nakamura T, Hirashima M, Satoh K (2004) Double-stranded RNA enhances the expression of galectin-9 in vascular endothelial cells. Immunol Cell Biol 82:410-414.

Itoh T, Satou T, Nishida S, Tsubaki M, Hashimoto S, Ito H (2009) Expression of amyloid precursor protein after rat traumatic brain injury. Neurol Res 31:103-109.

Ittner LM, Ke YD, Delerue F, Bi M, Gladbach A, van Eersel J, Wolfing H, Chieng BC, Christie MJ, Napier IA, et al. (2010) Dendritic function of tau mediates amyloid-beta toxicity in Alzheimer's disease mouse models. Cell 142:387-397.

Iversen LL, Rossor MN, Reynolds GP, Hills R, Roth M, Mountjoy CQ, Foote SL, Morrison JH, Bloom FE (1983) Loss of pigmented dopamine-beta-hydroxylase positive cells from locus coeruleus in senile dementia of Alzheimer's type. Neurosci Lett 39:95-100.

Jaim-Etcheverry G, Zieher LM (1980) DSP-4: a novel compound with neurotoxic effects on noradrenergic neurons of adult and developing rats. Brain Res 188:513-523.

Jardanhazi-Kurutz D, Kummer MP, Terwel D, Vogel K, Dyrks T, Thiele A, Heneka MT (2010) Induced LC degeneration in APP/PS1 transgenic mice accelerates early cerebral amyloidosis and cognitive deficits. Neurochem Int 57:375-382.

Jonsson G, Hallman H (1982) Response of central monoamine neurons following an early neurotoxic lesion. Bibl Anat 76-92.

Jonsson G, Hallman H, Ponzio F, Ross S (1981) DSP4 (N-(2-chloroethyl)-N-ethyl-2-bromobenzylamine)--a useful denervation tool for central and peripheral noradrenaline neurons. Eur J Pharmacol 72:173-188.

Jonsson G, Hallman H, Sundstrom E (1982) Effects of the noradrenaline neurotoxin DSP4 on the postnatal development of central noradrenaline neurons in the rat. Neuroscience 7:2895-2907.

Jossin Y, Goffinet AM (2007) Reelin signals through phosphatidylinositol 3-kinase and Akt to control cortical development and through mTor to regulate dendritic growth. Mol Cell Biol 27:7113-7124.

Jossin Y, Gui L, Goffinet AM (2007) Processing of Reelin by embryonic neurons is important for function in tissue but not in dissociated cultured neurons. J Neurosci 27:4243-4252.

Jossin Y, Ignatova N, Hiesberger T, Herz J, Lambert de Rouvroit C, Goffinet AM (2004) The central fragment of Reelin, generated by proteolytic processing in vivo, is critical to its function during cortical plate development. J Neurosci 24:514-521.

Kalinin S, Gavrilyuk V, Polak PE, Vasser R, Zhao J, Heneka MT, Feinstein DL (2007) Noradrenaline deficiency in brain increases beta-amyloid plaque burden in an animal model of Alzheimer's disease. Neurobiol Aging 28:1206-1214.

Kettenmann H, Hanisch UK, Noda M, Verkhratsky A (2011) Physiology of microglia. Physiol Rev 91:461-553.

Kim J, Basak JM, Holtzman DM (2009) The role of apolipoprotein E in Alzheimer's disease. Neuron 63:287-303.

Kim S, Jeon BS, Heo C, Im PS, Ahn TB, Seo JH, Kim HS, Park CH, Choi SH, Cho SH, et al. (2004) Alpha-synuclein induces apoptosis by altered expression in human peripheral lymphocyte in Parkinson's disease. FASEB J 18:1615-1617.

Knuesel I, Chicha L, Britschgi M, Schobel SA, Bodmer M, Hellings JA, Toovey S, Prinssen EP (2014) Maternal immune activation and abnormal brain development across CNS disorders. Nat Rev Neurol 10:643-660.

Knuesel I, Nyffeler M, Mormede C, Muhia M, Meyer U, Pietropaolo S, Yee BK, Pryce CR, LaFerla FM, Marighetto A, et al. (2009) Age-related accumulation of Reelin in amyloid-like deposits. Neurobiol Aging 30:697-716.

Kocherhans S, Madhusudan A, Doehner J, Breu KS, Nitsch RM, Fritschy JM, Knuesel I (2010) Reduced Reelin expression accelerates amyloid-beta plaque formation and tau pathology in transgenic Alzheimer's disease mice. J Neurosci 30:9228-9240.

Kohno S, Kohno T, Nakano Y, Suzuki K, Ishii M, Tagami H, Baba A, Hattori M (2009) Mechanism and significance of specific proteolytic cleavage of Reelin. Biochem Biophys Res Commun 380:93-97.

Koldamova R, Staufenbiel M, Lefterov I (2005) Lack of ABCA1 considerably decreases brain ApoE level and increases amyloid deposition in APP23 mice. J Biol Chem 280:43224-43235.

Kong Y, Ruan L, Qian L, Liu X, Le Y (2010) Norepinephrine promotes microglia to uptake and degrade amyloid beta peptide through upregulation of mouse formyl peptide receptor 2 and induction of insulin-degrading enzyme. J Neurosci 30:11848-11857.

Konkol RJ, Bendeich EG, Breese GR (1978) A biochemical and morphological study of the altered growth pattern of central catecholamine neurons following 6-hydroxydopamine. Brain Res 140:125-135.

Kostrzewa RM, Garey RE (1976) Effects of 6-hydroxydopa on noradrenergic neurons in developing rat brain. J Pharmacol Exp Ther 197:105-118.

Krafft PR, Altay O, Rolland WB, Duris K, Lekic T, Tang J, Zhang JH (2012) alpha7 nicotinic acetylcholine receptor agonism confers neuroprotection through GSK-3beta inhibition in a mouse model of intracerebral hemorrhage. Stroke 43:844-850.

Kramer PL, Xu H, Woltjer RL, Westaway SK, Clark D, Erten-Lyons D, Kaye JA, Welsh-Bohmer KA, Troncoso JC, Markesbery WR, et al. (2011) Alzheimer disease pathology in cognitively healthy elderly: a genome-wide study. Neurobiol Aging 32:2113-2122.

Kraus AA, Raftery MJ, Giese T, Ulrich R, Zawatzky R, Hippenstiel S, Suttorp N, Kruger DH, Schonrich G (2004) Differential antiviral response of endothelial cells after infection with pathogenic and nonpathogenic hantaviruses. J Virol 78:6143-6150.

Krstic D, Knuesel I (2013) Deciphering the mechanism underlying late-onset Alzheimer disease. Nat Rev Neurol 9:25-34.

Krstic D, Madhusudan A, Doehner J, Vogel P, Notter T, Imhof C, Manalastas A, Hilfiker M, Pfister S, Schwerdel C, et al. (2012a) Systemic immune challenges trigger and drive Alzheimer-like neuropathology in mice. J Neuroinflammation 9:151.

Krstic D, Pfister S, Notter T, Knuesel I (2013) Decisive role of Reelin signaling during early stages of Alzheimer's disease. Neuroscience 246:108-116.

Krstic D, Rodriguez M, Knuesel I (2012b) Regulated proteolytic processing of Reelin through interplay of tissue plasminogen activator (tPA), ADAMTS-4, ADAMTS-5, and their modulators. PloS one 7:e47793.

Kubo K, Mikoshiba K, Nakajima K (2002) Secreted Reelin molecules form homodimers. Neurosci Res 43:381-388.

Kuo G, Arnaud L, Kronstad-O'Brien P, Cooper JA (2005) Absence of Fyn and Src causes a reeler-like phenotype. J Neurosci 25:8578-8586.

Lalonde R (2002) The neurobiological basis of spontaneous alternation. Neurosci Biobehav Rev 26:91-104.

Lambert JC, Heath S, Even G, Campion D, Sleegers K, Hiltunen M, Combarros O, Zelenika D, Bullido MJ, Tavernier B, et al. (2009) Genome-wide association study identifies variants at CLU and CR1 associated with Alzheimer's disease. Nat Genet 41:1094-1099.

Landi MS, Kreider JW, Lang CM, Bullock LP (1982) Effects of shipping on the immune function in mice. Am J Vet Res 43:1654-1657.

Leemhuis J, Bouche E, Frotscher M, Henle F, Hein L, Herz J, Meyer DK, Pichler M, Roth G, Schwan C, et al. (2010) Reelin signals through apolipoprotein E receptor 2 and Cdc42 to increase growth cone motility and filopodia formation. J Neurosci 30:14759-14772.

Levitt P, Moore RY (1980) Organization of brainstem noradrenaline hyperinnervation following neonatal 6-hydroxydopamine treatment in rat. Anat Embryol (Berl) 158:133-150.

Lewitus GM, Schwartz M (2009) Behavioral immunization: immunity to self-antigens contributes to psychological stress resilience. Mol Psychiatry 14:532-536.

Li Y, Liu L, Barger SW, Griffin WS (2003) Interleukin-1 mediates pathological effects of microglia on tau phosphorylation and on synaptophysin synthesis in cortical neurons through a p38-MAPK pathway. J Neurosci 23:1605-1611.

Liu WS, Pesold C, Rodriguez MA, Carboni G, Auta J, Lacor P, Larson J, Condie BG, Guidotti A, Costa E (2001) Down-regulation of dendritic spine and glutamic acid decarboxylase 67 expressions in the reelin haploinsufficient heterozygous reeler mouse. Proc Natl Acad Sci U S A 98:3477-3482.

Loffler J, Huber G (1992) Beta-amyloid precursor protein isoforms in various rat brain regions and during brain development. J Neurochem 59:1316-1324.

Luo L, Tully T, White K (1992) Human amyloid precursor protein ameliorates behavioral deficit of flies deleted for Appl gene. Neuron 9:595-605.

Lyons WE, Fritschy JM, Grzanna R (1989) The noradrenergic neurotoxin DSP-4 eliminates the coeruleospinal projection but spares projections of the A5 and A7 groups to the ventral horn of the rat spinal cord. J Neurosci 9:1481-1489.

MacLaurin SA, Krucker T, Fish KN (2007) Hippocampal dendritic arbor growth in vitro: regulation by Reelin-Disabled-1 signaling. Brain Res 1172:1-9.

Malamud N, Hirano A (1974) Atlas of Neuropathology. University of California Press 314-327.

Mallard C (2012) Innate immune regulation by toll-like receptors in the brain. ISRN Neurol 2012:701950.

Martin LJ, Pardo CA, Cork LC, Price DL (1994) Synaptic pathology and glial responses to neuronal injury precede the formation of senile plaques and amyloid deposits in the aging cerebral cortex. Am J Pathol 145:1358-1381.

Martinez-Cerdeno V, Clasca F (2002) Reelin immunoreactivity in the adult neocortex: a comparative study in rodents, carnivores, and non-human primates. Brain Res bulletin 57:485-488.

Martinez-Cerdeno V, Galazo MJ, Cavada C, Clasca F (2002) Reelin immunoreactivity in the adult primate brain: intracellular localization in projecting and local circuit neurons of the cerebral cortex, hippocampus and subcortical regions. Cereb Cortex 12:1298-1311.

Mattei D, Djodari-Irani A, Hadar R, Pelz A, de Cossio LF, Goetz T, Matyash M, Kettenmann H, Winter C, Wolf SA (2014) Minocycline rescues decrease in neurogenesis, increase in microglia cytokines and deficits in sensorimotor gating in an animal model of schizophrenia. Brain Behav Immun 38:175-184.

Mattson MP (1994) Secreted forms of beta-amyloid precursor protein modulate dendrite outgrowth and calcium responses to glutamate in cultured embryonic hippocampal neurons. J Neurobiol 25:439-450.

Mattson MP, Cheng B, Culwell AR, Esch FS, Lieberburg I, Rydel RE (1993a) Evidence for excitoprotective and intraneuronal calcium-regulating roles for secreted forms of the beta-amyloid precursor protein. Neuron 10:243-254.

Mattson MP, Lovell MA, Ehmann WD, Markesbery WR (1993b) Comparison of the effects of elevated intracellular aluminum and calcium levels on neuronal survival and tau immunoreactivity. Brain Res 602:21-31.

McDonald RJ (2002) Multiple combinations of co-factors produce variants of age-related cognitive decline: a theory. Can J Exp Psychol 56:221-239.

McGeer PL, Akiyama H, Kawamata T, Yamada T, Walker DG, Ishii T (1992) Immunohistochemical localization of beta-amyloid precursor protein sequences in Alzheimer and normal brain tissue by light and electron microscopy. J Neurosci Res 31:428-442.

Medeiros R, Kitazawa M, Caccamo A, Baglietto-Vargas D, Estrada-Hernandez T, Cribbs DH, Fisher A, LaFerla FM (2011) Loss of muscarinic M1 receptor exacerbates Alzheimer's disease-like pathology and cognitive decline. Am J Pathol 179:980-991.

Melton LM, Keith AB, Davis S, Oakley AE, Edwardson JA, Morris CM (2003) Chronic glial activation, neurodegeneration, and APP immunoreactive deposits following acute administration of double-stranded RNA. Glia 44:1-12.

Meng H, Zhang X, Blaivas M, Wang MM (2009) Localization of blood proteins thrombospondin1 and ADAMTS13 to cerebral corpora amylacea. Neuropathology 29:664-671.

Meseke M, Rosenberger G, Forster E (2013) Reelin and the Cdc42/Rac1 guanine nucleotide exchange factor alphaPIX/Arhgef6 promote dendritic Golgi translocation in hippocampal neurons. Eur J Neurosci.

Meyer U (2014) Prenatal poly(i:C) exposure and other developmental immune activation models in rodent systems. Biol Psychiatry 75:307-315.

Meyer U, Engler A, Weber L, Schedlowski M, Feldon J (2008a) Preliminary evidence for a modulation of fetal dopaminergic development by maternal immune activation during pregnancy. Neuroscience 154:701-709.

Meyer U, Feldon J (2009) Neural basis of psychosis-related behaviour in the infection model of schizophrenia. Behav Brain Res 204:322-334.

Meyer U, Feldon J (2012) To poly(I:C) or not to poly(I:C): advancing preclinical schizophrenia research through the use of prenatal immune activation models. Neuropharmacology 62:1308-1321.

Meyer U, Feldon J, Fatemi SH (2009) In-vivo rodent models for the experimental investigation of prenatal immune activation effects in neurodevelopmental brain disorders. Neurosci Biobehav Rev 33:1061-1079.

Meyer U, Feldon J, Schedlowski M, Yee BK (2005) Towards an immuno-precipitated neurodevelopmental animal model of schizophrenia. Neurosci Biobehav Rev 29:913-947.

Meyer U, Feldon J, Schedlowski M, Yee BK (2006a) Immunological stress at the maternal-foetal interface: a link between neurodevelopment and adult psychopathology. Brain Behav Immun 20:378-388.

Meyer U, Murray PJ, Urwyler A, Yee BK, Schedlowski M, Feldon J (2008b) Adult behavioral and pharmacological dysfunctions following disruption of the fetal brain balance between pro-inflammatory and IL-10-mediated anti-inflammatory signaling. Mol Psychiatry 13:208-221.

Meyer U, Nyffeler M, Engler A, Urwyler A, Schedlowski M, Knuesel I, Yee BK, Feldon J (2006b) The time of prenatal immune challenge determines the specificity of inflammation-mediated brain and behavioral pathology. J Neurosci 26:4752-4762.

Meyer U, Nyffeler M, Yee BK, Knuesel I, Feldon J (2008c) Adult brain and behavioral pathological markers of prenatal immune challenge during early/middle and late fetal development in mice. Brain Behav Immun 22:469-486.

Meyer U, Yee BK, Feldon J (2007) The neurodevelopmental impact of prenatal infections at different times of pregnancy: the earlier the worse? Neuroscientist 13:241-256.

Mirrione MM, Schiffer WK, Fowler JS, Alexoff DL, Dewey SL, Tsirka SE (2007) A novel approach for imaging brain-behavior relationships in mice reveals unexpected metabolic patterns during seizures in the absence of tissue plasminogen activator. NeuroImage 38:34-42.

Mizutani T, Satoh J, Morimatsu Y (1987) Axonal polyglucosan body in the ventral posterolateral nucleus of the human thalamus in relation to ageing. Acta Neuropathol 74:9-12.

Mosconi L (2005) Brain glucose metabolism in the early and specific diagnosis of Alzheimer's disease. FDG-PET studies in MCI and AD. Eur J Nucl Med Mol Imaging 32:486-510.

Mosconi L, De Santi S, Li J, Tsui WH, Li Y, Boppana M, Laska E, Rusinek H, de Leon MJ (2008a) Hippocampal hypometabolism predicts cognitive decline from normal aging. Neurobiol Aging 29:676-692.

Mosconi L, Pupi A, De Leon MJ (2008b) Brain glucose hypometabolism and oxidative stress in preclinical Alzheimer's disease. Ann N Y Acad Sci 1147:180-195.

Mosconi L, Tsui WH, De Santi S, Li J, Rusinek H, Convit A, Li Y, Boppana M, de Leon MJ (2005) Reduced hippocampal metabolism in MCI and AD: automated FDG-PET image analysis. Neurology 64:1860-1867.

Muzio M, Bosisio D, Polentarutti N, D'Amico G, Stoppacciaro A, Mancinelli R, van't Veer C, Penton-Rol G, Ruco LP, Allavena P, et al. (2000) Differential expression and regulation of toll-like receptors (TLR) in human leukocytes: selective expression of TLR3 in dendritic cells. J Immunol 164:5998-6004.

Nakano Y, Kohno T, Hibi T, Kohno S, Baba A, Mikoshiba K, Nakajima K, Hattori M (2007) The extremely conserved C-terminal region of Reelin is not necessary for secretion but is required for efficient activation of downstream signaling. J Biol Chem 282:20544-20552.

Nathanson JA, Glaser GH (1979) Identification of beta-adrenergic-sensitive adenylate cyclase in intracranial blood vessels. Nature 278:567-569.

Neve RL, Robakis NK (1998) Alzheimer's disease: a re-examination of the amyloid hypothesis. Trends Neurosci 21:15-19.

Niklasson B, Samsioe A, Blixt M, Sandler S, Sjoholm A, Lagerquist E, Lernmark A, Klitz W (2006) Prenatal viral exposure followed by adult stress produces glucose intolerance in a mouse model. Diabetologia 49:2192-2199.

Nilsson C, Larsson BM, Jennische E, Eriksson E, Bjorntorp P, York DA, Holmang A (2001) Maternal endotoxemia results in obesity and insulin resistance in adult male offspring. Endocrinology 142:2622-2630.

Nilsson L, Nordberg A, Hardy J, Wester P, Winblad B (1986) Physostigmine restores 3H-acetylcholine efflux from Alzheimer brain slices to normal level. J Neural Transm 67:275-285.

Niu S, Yabut O, D'Arcangelo G (2008) The Reelin signaling pathway promotes dendritic spine development in hippocampal neurons. J Neurosci 28:10339-10348.

Nordberg A, Alafuzoff I, Winblad B (1992) Nicotinic and muscarinic subtypes in the human brain: changes with aging and dementia. J Neurosci Res 31:103-111.

Notter T, Knuesel I (2013) Reelin immunoreactivity in neuritic varicosities in the human hippocampal formation of non-demented subjects and Alzheimer's disease patients. Acta Neuropathol Commun 1:27.

Notter T, Panzanelli P, Pfister S, Mircsof D, Fritschy JM (2014) A protocol for concurrent high-quality immunohistochemical and biochemical analyses in adult mouse central nervous system. Eur J Neurosci 39:165-175.

O'Donnell J, Zeppenfeld D, McConnell E, Pena S, Nedergaard M (2012) Norepinephrine: a neuromodulator that boosts the function of multiple cell types to optimize CNS performance. Neurochem Res 37:2496-2512.

Obel LF, Muller MS, Walls AB, Sickmann HM, Bak LK, Waagepetersen HS, Schousboe A (2012) Brain glycogen-new perspectives on its metabolic function and regulation at the subcellular level. Front Neuroenergetics 4:3.

Ohkubo N, Lee YD, Morishima A, Terashima T, Kikkawa S, Tohyama M, Sakanaka M, Tanaka J, Maeda N, Vitek MP, et al. (2003) Apolipoprotein E and Reelin ligands modulate tau phosphorylation through an apolipoprotein E receptor/disabled-1/glycogen synthase kinase-3beta cascade. FASEB J 17:295-297.

Olson JK, Miller SD (2004) Microglia initiate central nervous system innate and adaptive immune responses through multiple TLRs. J Immunol 173:3916-3924.

Ono K, Condron MM, Teplow DB (2009) Structure-neurotoxicity relationships of amyloid beta-protein oligomers. Proc Natl Acad Sci U S A 106:14745-14750.

Opp MR (2005) Cytokines and sleep. Sleep Med Rev 9:355-364.

Ownby RL, Peruyera G, Acevedo A, Loewenstein D, Sevush S (2014) Subtypes of sleep problems in patients with Alzheimer disease. Am J Geriatr Psychiatry 22:148-156.

Pacheco-Lopez G, Giovanoli S, Langhans W, Meyer U (2013) Priming of metabolic dysfunctions by prenatal immune activation in mice: relevance to schizophrenia. Schizophr Bull 39:319-329.

Palmucci L, Anzil AP, Christomanou H (1982) On the association of excess glycogen granules and polyglucosan bodies (corpora amylacea) in astrocytes of a 17-year-old patient with a neurologic disease of unknown origin: clinical, biochemical, and ultrastructural observations. Clin Neuropathol 1:2-10.

Pappolla MA, Chyan YJ, Omar RA, Hsiao K, Perry G, Smith MA, Bozner P (1998) Evidence of oxidative stress and in vivo neurotoxicity of beta-amyloid in a transgenic mouse model of Alzheimer's disease: a chronic oxidative paradigm for testing antioxidant therapies in vivo. Am J Pathol 152:871-877.

Perry EK, Gibson PH, Blessed G, Perry RH, Tomlinson BE (1977) Neurotransmitter enzyme abnormalities in senile dementia. Choline acetyltransferase and glutamic acid decarboxylase activities in necropsy brain tissue. J Neurol Sci 34:247-265.

Pesce L, Comellas A, Sznajder JI (2003) Beta-adrenergic agonists regulate Na-K-ATPase via p70S6k. Am J Physiol Lung Cell Mol Physiol 285:L802-807.

Pesold C, Impagnatiello F, Pisu MG, Uzunov DP, Costa E, Guidotti A, Caruncho HJ (1998) Reelin is preferentially expressed in neurons synthesizing gamma-aminobutyric acid in cortex and hippocampus of adult rats. Proc Natl Acad Sci U S A 95:3221-3226.

Peter-Derex L, Yammine P, Bastuji H, Croisile B (2015) Sleep and Alzheimer's disease. Sleep Med Rev 19C:29-38.

Pfrieger FW (2003) Role of cholesterol in synapse formation and function. Biochim Biophys Acta 1610:271-280.

Picciotto MR, Higley MJ, Mineur YS (2012) Acetylcholine as a neuromodulator: cholinergic signaling shapes nervous system function and behavior. Neuron 76:116-129.

Pineda E, Shin D, You SJ, Auvin S, Sankar R, Mazarati A (2013) Maternal immune activation promotes hippocampal kindling epileptogenesis in mice. Ann Neurol 74:11-19.

Pirici I, Margaritescu C, Mogoanta L, Petrescu F, Simionescu CE, Popescu ES, Cecoltan S, Pirici D (2014) Corpora amylacea in the brain form highly branched three-dimensional lattices. Rom J Morphol Embryol 55:1071-1077.

Pitas RE, Boyles JK, Lee SH, Foss D, Mahley RW (1987a) Astrocytes synthesize apolipoprotein E and metabolize apolipoprotein E-containing lipoproteins. Biochim Biophys Acta 917:148-161.

Pitas RE, Boyles JK, Lee SH, Hui D, Weisgraber KH (1987b) Lipoproteins and their receptors in the central nervous system. Characterization of the lipoproteins in cerebrospinal fluid and identification of apolipoprotein B,E(LDL) receptors in the brain. J Biol Chem 262:14352-14360.

Pizza V, Agresta A, D'Acunto CW, Festa M, Capasso A (2011a) Neuroinflamm-aging and neurodegenerative diseases: an overview. CNS Neurol Disord Drug Targets 10:621-634.

Pizza V, Agresta A, D'Acunto CW, Festa M, Capasso A (2011b) Neuroinflammation and ageing: current theories and an overview of the data. Rev Recent Clin Trials 6:189-203.

Platt B, Riedel G (2011) The cholinergic system, EEG and sleep. Behav Brain Res 221:499-504.

Pugh PL, Vidgeon-Hart MP, Ashmeade T, Culbert AA, Seymour Z, Perren MJ, Joyce F, Bate ST, Babin A, Virley DJ, et al. (2007) Repeated administration of the noradrenergic neurotoxin N-(2-chloroethyl)-N-ethyl-2-bromobenzylamine (DSP-4) modulates neuroinflammation and amyloid plaque load in mice bearing amyloid precursor protein and presenilin-1 mutant transgenes. J Neuroinflammation 4:8.

Pujadas L, Gruart A, Bosch C, Delgado L, Teixeira CM, Rossi D, de Lecea L, Martinez A, Delgado-Garcia JM, Soriano E (2010) Reelin regulates postnatal neurogenesis and enhances spine hypertrophy and long-term potentiation. J Neurosci 30:4636-4649.

Qiu S, Korwek KM, Pratt-Davis AR, Peters M, Bergman MY, Weeber EJ (2006a) Cognitive disruption and altered hippocampus synaptic function in Reelin haploinsufficient mice. Neurobiol Learn Mem 85:228-242.

Qiu S, Weeber EJ (2007) Reelin signaling facilitates maturation of CA1 glutamatergic synapses. J Neurophysiol 97:2312-2321.

Qiu S, Zhao LF, Korwek KM, Weeber EJ (2006b) Differential reelin-induced enhancement of NMDA and AMPA receptor activity in the adult hippocampus. J Neurosci 26:12943-12955.

Raichle ME, Hartman BK, Eichling JO, Sharpe LG (1975) Central noradrenergic regulation of cerebral blood flow and vascular permeability. Proc Natl Acad Sci U S A 72:3726-3730.

Rambaldi DC, Zattoni A, Reschiglian P, Colombo R, De Lorenzi E (2009) In vitro amyloid Abeta(1-42) peptide aggregation monitoring by asymmetrical flow field-flow fractionation with multi-angle light scattering detection. Anal Bioanal Chem 394:2145-2149.

Ramsey HJ (1965) Ultrastructure of Corpora Amylacea. J Neuropathol Exp Neurol 24:25-39.

Rapoport M, Dawson HN, Binder LI, Vitek MP, Ferreira A (2002) Tau is essential to beta -amyloid-induced neurotoxicity. Proc Natl Acad Sci U S A 99:6364-6369.

Reiman EM, Uecker A, Caselli RJ, Lewis S, Bandy D, de Leon MJ, De Santi S, Convit A, Osborne D, Weaver A, et al. (1998) Hippocampal volumes in cognitively normal persons at genetic risk for Alzheimer's disease. Ann Neurol 44:288-291.

Rey NL, Jardanhazi-Kurutz D, Terwel D, Kummer MP, Jourdan F, Didier A, Heneka MT (2012) Locus coeruleus degeneration exacerbates olfactory deficits in APP/PS1 transgenic mice. Neurobiol Aging 33:426 e421-411.

Richetto J, Calabrese F, Meyer U, Riva MA (2013) Prenatal versus postnatal maternal factors in the development of infection-induced working memory impairments in mice. Brain Behav Immun 33:190-200.

Richetto J, Calabrese F, Riva MA, Meyer U (2014) Prenatal immune activation induces maturation-dependent alterations in the prefrontal GABAergic transcriptome. Schizophr Bull 40:351-361.

Richetto J, Labouesse MA, Poe MM, Cook JM, Grace AA, Riva MA, Meyer U (2015) Behavioral Effects of the Benzodiazepine-Positive Allosteric Modulator SH-053-2'F-S-CH3 in an Immune-Mediated Neurodevelopmental Disruption Model. Int J Neuropsychopharmacol.

Rinaman L (2011) Hindbrain noradrenergic A2 neurons: diverse roles in autonomic, endocrine, cognitive, and behavioral functions. Am J Physiol Regul Integr Comp Physiol 300:R222-235.

Roberson ED, Scearce-Levie K, Palop JJ, Yan F, Cheng IH, Wu T, Gerstein H, Yu GQ, Mucke L (2007) Reducing endogenous tau ameliorates amyloid beta-induced deficits in an Alzheimer's disease mouse model. Science 316:750-754.

Roch JM, Masliah E, Roch-Levecq AC, Sundsmo MP, Otero DA, Veinbergs I, Saitoh T (1994) Increase of synaptic density and memory retention by a peptide representing the trophic domain of the amyloid beta/A4 protein precursor. Proc Natl Acad Sci U S A 91:7450-7454.

Rogers JT, Leiter LM, McPhee J, Cahill CM, Zhan SS, Potter H, Nilsson LN (1999) Translation of the alzheimer amyloid precursor protein mRNA is up-regulated by interleukin-1 through 5'-untranslated region sequences. J Biol Chem 274:6421-6431.

Roodveldt C, Labrador-Garrido A, Gonzalez-Rey E, Lachaud CC, Guilliams T, Fernandez-Montesinos R, Benitez-Rondan A, Robledo G, Hmadcha A, Delgado M, et al. (2013) Preconditioning of microglia by alpha-synuclein strongly affects the response induced by toll-like receptor (TLR) stimulation. PloS one 8:e79160.

Roses AD (1996) Apolipoprotein E alleles as risk factors in Alzheimer's disease. Annu Rev Med 47:387-400.

Ross SB (1976) Long-term effects of N-2-chlorethyl-N-ethyl-2-bromobenzylamine hydrochloride on noradrenergic neurones in the rat brain and heart. British journal of pharmacology 58:521-527.

Rylett RJ, Ball MJ, Colhoun EH (1983) Evidence for high affinity choline transport in synaptosomes prepared from hippocampus and neocortex of patients with Alzheimer's disease. Brain Res 289:169-175.

Sachs C, Pycock C, Jonsson G (1974) Altered development of central noradrenaline neurons during ontogeny by 6-hydroxydopamine. Med Biol 52:55-65.

Sadot E, Gurwitz D, Barg J, Behar L, Ginzburg I, Fisher A (1996) Activation of m1 muscarinic acetylcholine receptor regulates tau phosphorylation in transfected PC12 cells. J Neurochem 66:877-880.

Saez-Valero J, Costell M, Sjogren M, Andreasen N, Blennow K, Luque JM (2003) Altered levels of cerebrospinal fluid reelin in frontotemporal dementia and Alzheimer's disease. J Neurosci Res 72:132-136.

Saez I, Duran J, Sinadinos C, Beltran A, Yanes O, Tevy MF, Martinez-Pons C, Milan M, Guinovart JJ (2014) Neurons have an active glycogen metabolism that contributes to tolerance to hypoxia. J Cereb Blood Flow Metab 34:945-955.

Sakai M, Austin J, Witmer F, Trueb L (1969) Studies of corpora amylacea. I. Isolation and preliminary characterization by chemical and histochemical techniques. Arch Neurol 21:526-544.

Sanchez-Padilla J, Guzman JN, Ilijic E, Kondapalli J, Galtieri DJ, Yang B, Schieber S, Oertel W, Wokosin D, Schumacker PT, et al. (2014) Mitochondrial oxidant stress in locus coeruleus is regulated by activity and nitric oxide synthase. Nat Neurosci 17:832-840.

Sarmento A, Borges N, Lima D (1994) Influence of electrical stimulation of locus coeruleus on the rat blood-brain barrier permeability to sodium fluorescein. Acta Neurochir (Wien) 127:215-219.

Sarter M, Lustig C, Howe WM, Gritton H, Berry AS (2014) Deterministic functions of cortical acetylcholine. Eur J Neurosci 39:1912-1920.

Schaefer TM, Fahey JV, Wright JA, Wira CR (2005) Innate immunity in the human female reproductive tract: antiviral response of uterine epithelial cells to the TLR3 agonist poly(I:C). J Immunol 174:992-1002.

Schmidt RH, Bhatnagar RK (1979) Distribution of hypertrophied locus coeruleus projection to adult cerebellum after neonatal 6-hydroxydopamine. Brain Res 172:23-33.

Schmidt RH, Kasik SA, Bhatnagar RK (1980) Regenerative critical periods for locus coeruleus in postnatal rat pups following intracisternal 6-hydroxydopamine: a model of noradrenergic development. Brain Res 191:173-190.

Schneider LS, Mangialasche F, Andreasen N, Feldman H, Giacobini E, Jones R, Mantua V, Mecocci P, Pani L, Winblad B, et al. (2014) Clinical trials and late-stage drug development for Alzheimer's disease: an appraisal from 1984 to 2014. J Intern Med 275:251-283.

Schweers O, Mandelkow EM, Biernat J, Mandelkow E (1995) Oxidation of cysteine-322 in the repeat domain of microtubule-associated protein tau controls the in vitro assembly of paired helical filaments. Proc Natl Acad Sci U S A 92:8463-8467.

Seripa D, Matera MG, Franceschi M, Daniele A, Bizzarro A, Rinaldi M, Panza F, Fazio VM, Gravina C, D'Onofrio G, et al. (2008) The RELN locus in Alzheimer's disease. J Alzheimers Dis 14:335-344.

Shaw P, Lerch JP, Pruessner JC, Taylor KN, Rose AB, Greenstein D, Clasen L, Evans A, Rapoport JL, Giedd JN (2007) Cortical morphology in children and adolescents with different apolipoprotein E gene polymorphisms: an observational study. Lancet Neurol 6:494-500.

Sherrington R, Rogaev EI, Liang Y, Rogaeva EA, Levesque G, Ikeda M, Chi H, Lin C, Li G, Holman K, et al. (1995) Cloning of a gene bearing missense mutations in early-onset familial Alzheimer's disease. Nature 375:754-760.

Shi L, Fatemi SH, Sidwell RW, Patterson PH (2003) Maternal influenza infection causes marked behavioral and pharmacological changes in the offspring. J Neurosci 23:297-302.

Simon AM, Schiapparelli L, Salazar-Colocho P, Cuadrado-Tejedor M, Escribano L, Lopez de Maturana R, Del Rio J, Perez-Mediavilla A, Frechilla D (2009) Overexpression of wild-type human APP in mice causes cognitive deficits and pathological features unrelated to Abeta levels. Neurobiol Dis 33:369-378.

Sinadinos C, Valles-Ortega J, Boulan L, Solsona E, Tevy MF, Marquez M, Duran J, Lopez-Iglesias C, Calbo J, Blasco E, et al. (2014) Neuronal glycogen synthesis contributes to physiological aging. Aging Cell 13:935-945.

Sinagra M, Verrier D, Frankova D, Korwek KM, Blahos J, Weeber EJ, Manzoni OJ, Chavis P (2005) Reelin, very-low-density lipoprotein receptor, and apolipoprotein E receptor 2 control somatic NMDA receptor composition during hippocampal maturation in vitro. J Neurosci 25:6127-6136.

Singhrao SK, Morgan BP, Neal JW, Newman GR (1995) A functional role for corpora amylacea based on evidence from complement studies. Neurodegeneration 4:335-345.

Singhrao SK, Neal JW, Newman GR (1993) Corpora amylacea could be an indicator of neurodegeneration. Neuropathol Appl Neurobiol 19:269-276.

Smith MA, Hirai K, Hsiao K, Pappolla MA, Harris PL, Siedlak SL, Tabaton M, Perry G (1998) Amyloid-beta deposition in Alzheimer transgenic mice is associated with oxidative stress. J Neurochem 70:2212-2215.

Song C, Zhang Y, Dong Y (2013) Acute and subacute IL-1beta administrations differentially modulate neuroimmune and neurotrophic systems: possible implications for neuroprotection and neurodegeneration. J Neuroinflammation 10:59.

Sorg O, Magistretti PJ (1992) Vasoactive intestinal peptide and noradrenaline exert long-term control on glycogen levels in astrocytes: blockade by protein synthesis inhibition. J Neurosci 12:4923-4931.

Specht CG, Schoepfer R (2001) Deletion of the alpha-synuclein locus in a subpopulation of C57BL/6J inbred mice. BMC Neurosci 2:11.

St George-Hyslop P, Haines J, Rogaev E, Mortilla M, Vaula G, Pericak-Vance M, Foncin JF, Montesi M, Bruni A, Sorbi S, et al. (1992) Genetic evidence for a novel familial Alzheimer's disease locus on chromosome 14. Nat Genet 2:330-334.

Stefanis L (2012) alpha-Synuclein in Parkinson's disease. Cold Spring Harb Perspect Med 2:a009399.

Steyaert A, Cisse S, Merhi Y, Kalbakji A, Reid N, Gauvreau D, Lacoste-Royal G (1990) Purification and polypeptide composition of corpora amylacea from aged human brain. J Neurosci Methods 31:59-64.

Stokin GB, Lillo C, Falzone TL, Brusch RG, Rockenstein E, Mount SL, Raman R, Davies P, Masliah E, Williams DS, et al. (2005) Axonopathy and transport deficits early in the pathogenesis of Alzheimer's disease. Science 307:1282-1288.

Stranahan AM, Haberman RP, Gallagher M (2011) Cognitive decline is associated with reduced reelin expression in the entorhinal cortex of aged rats. Cereb Cortex 21:392-400.

Strasser V, Fasching D, Hauser C, Mayer H, Bock HH, Hiesberger T, Herz J, Weeber EJ, Sweatt JD, Pramatarova A, et al. (2004) Receptor clustering is involved in Reelin signaling. Mol Cell Biol 24:1378-1386.

Szot P, White SS, Greenup JL, Leverenz JB, Peskind ER, Raskind MA (2006) Compensatory changes in the noradrenergic nervous system in the locus ceruleus and hippocampus of postmortem subjects with Alzheimer's disease and dementia with Lewy bodies. J Neurosci 26:467-478.

Szot P, White SS, Greenup JL, Leverenz JB, Peskind ER, Raskind MA (2007) Changes in adrenoreceptors in the prefrontal cortex of subjects with dementia: evidence of compensatory changes. Neuroscience 146:471-480.

Takahashi K, Agari M, Nakamura H (1975) Intra-axonal Corpora amylacea in ventral and lateral horns of the spinal cord. Acta Neuropathol 31:151-158.

Tanzi RE, Bertram L (2005) Twenty years of the Alzheimer's disease amyloid hypothesis: a genetic perspective. Cell 120:545-555.

Tatetsu M, Kim J, Kina S, Sunakawa H, Takayama C (2012) GABA/glycine signaling during degeneration and regeneration of mouse hypoglossal nerves. Brain Res 1446:22-33.

Tissari J, Siren J, Meri S, Julkunen I, Matikainen S (2005) IFN-alpha enhances TLR3-mediated antiviral cytokine expression in human endothelial and epithelial cells by up-regulating TLR3 expression. J Immunol 174:4289-4294.

Tomlinson BE, Irving D, Blessed G (1981) Cell loss in the locus coeruleus in senile dementia of Alzheimer type. J Neurol Sci 49:419-428.

Toussay X, Basu K, Lacoste B, Hamel E (2013) Locus coeruleus stimulation recruits a broad cortical neuronal network and increases cortical perfusion. J Neurosci 33:3390-3401.

Town T, Jeng D, Alexopoulou L, Tan J, Flavell RA (2006) Microglia recognize double-stranded RNA via TLR3. J Immunol 176:3804-3812.

Trommsdorff M, Borg JP, Margolis B, Herz J (1998) Interaction of cytosolic adaptor proteins with neuronal apolipoprotein E receptors and the amyloid precursor protein. J Biol Chem 273:33556-33560.

Trommsdorff M, Gotthardt M, Hiesberger T, Shelton J, Stockinger W, Nimpf J, Hammer RE, Richardson JA, Herz J (1999) Reeler/Disabled-like disruption of neuronal migration in knockout mice lacking the VLDL receptor and ApoE receptor 2. Cell 97:689-701.

Tuli JS, Smith JA, Morton DB (1995) Stress measurements in mice after transportation. Lab Anim 29:132-138.

Ueda K, Fukushima H, Masliah E, Xia Y, Iwai A, Yoshimoto M, Otero DA, Kondo J, Ihara Y, Saitoh T (1993) Molecular cloning of cDNA encoding an unrecognized component of amyloid in Alzheimer disease. Proc Natl Acad Sci U S A 90:11282-11286.

Usher M, Cohen JD, Servan-Schreiber D, Rajkowski J, Aston-Jones G (1999) The role of locus coeruleus in the regulation of cognitive performance. Science 283:549-554.

Utsunomiya-Tate N, Kubo K, Tate S, Kainosho M, Katayama E, Nakajima K, Mikoshiba K (2000) Reelin molecules assemble together to form a large protein complex, which is inhibited by the function-blocking CR-50 antibody. Proc Natl Acad Sci U S A 97:9729-9734.

Van Broeckhoven C, Haan J, Bakker E, Hardy JA, Van Hul W, Wehnert A, Vegter-Van der Vlis M, Roos RA (1990) Amyloid beta protein precursor gene and hereditary cerebral hemorrhage with amyloidosis (Dutch). Science 248:1120-1122.

Vilchez D, Ros S, Cifuentes D, Pujadas L, Valles J, Garcia-Fojeda B, Criado-Garcia O, Fernandez-Sanchez E, Medrano-Fernandez I, Dominguez J, et al. (2007) Mechanism suppressing glycogen synthesis in neurons and its demise in progressive myoclonus epilepsy. Nat Neurosci 10:1407-1413.

von Rotz RC, Kohli BM, Bosset J, Meier M, Suzuki T, Nitsch RM, Konietzko U (2004) The APP intracellular domain forms nuclear multiprotein complexes and regulates the transcription of its own precursor. J Cell Sci 117:4435-4448.

Vuillermot S, Joodmardi E, Perlmann T, Ogren SO, Feldon J, Meyer U (2012) Prenatal immune activation interacts with genetic Nurr1 deficiency in the development of attentional impairments. J Neurosci 32:436-451.

Vuillermot S, Weber L, Feldon J, Meyer U (2010) A longitudinal examination of the neurodevelopmental impact of prenatal immune activation in mice reveals primary defects in dopaminergic development relevant to schizophrenia. J Neurosci 30:1270-1287.

Walter J, Haass C (2000) Posttranslational modifications of amyloid precursor protein : ectodomain phosphorylation and sulfation. Methods Mol Med 32:149-168.

Weeber EJ, Beffert U, Jones C, Christian JM, Forster E, Sweatt JD, Herz J (2002) Reelin and ApoE receptors cooperate to enhance hippocampal synaptic plasticity and learning. J Biol Chem 277:39944-39952.

Whitehouse PJ, Martino AM, Marcus KA, Zweig RM, Singer HS, Price DL, Kellar KJ (1988) Reductions in acetylcholine and nicotine binding in several degenerative diseases. Arch Neurol 45:722-724.

Whitehouse PJ, Price DL, Struble RG, Clark AW, Coyle JT, Delon MR (1982) Alzheimer's disease and senile dementia: loss of neurons in the basal forebrain. Science 215:1237-1239.

Whitson JS, Selkoe DJ, Cotman CW (1989) Amyloid beta protein enhances the survival of hippocampal neurons in vitro. Science 243:1488-1490.

Willi R, Harmeier A, Giovanoli S, Meyer U (2013) Altered GSK3beta signaling in an infection-based mouse model of developmental neuropsychiatric disease. Neuropharmacology 73:56-65.

Wirths O, Weis J, Szczygielski J, Multhaup G, Bayer TA (2006) Axonopathy in an APP/PS1 transgenic mouse model of Alzheimer's disease. Acta Neuropathol 111:312-319.

Wolfman C, Abo V, Calvo D, Medina J, Dajas F, Silveira R (1994) Recovery of central noradrenergic neurons one year after the administration of the neurotoxin DSP4. Neurochem Int 25:395-400.

Wroblewska B, Spatz M, Merkel N, Bembry J (1984) Cerebrovascular smooth muscle culture. II. Characterization of adrenergic receptors linked to adenylate cyclase. Life Sci 34:783-791.

Xiao AW, He J, Wang Q, Luo Y, Sun Y, Zhou YP, Guan Y, Lucassen PJ, Dai JP (2011) The origin and development of plaques and phosphorylated tau are associated with axonopathy in Alzheimer's disease. Neurosci Bull 27:287-299.

Yankner BA, Duffy LK, Kirschner DA (1990) Neurotrophic and neurotoxic effects of amyloid beta protein: reversal by tachykinin neuropeptides. Science 250:279-282.

Yokokura M, Mori N, Yagi S, Yoshikawa E, Kikuchi M, Yoshihara Y, Wakuda T, Sugihara G, Takebayashi K, Suda S, et al. (2011) In vivo changes in microglial activation and amyloid deposits in brain regions with hypometabolism in Alzheimer's disease. Eur J Nucl Med Mol Imaging 38:343-351.

Young SZ, Taylor MM, Wu S, Ikeda-Matsuo Y, Kubera C, Bordey A (2012) NKCC1 knockdown decreases neuron production through GABA(A)-regulated neural progenitor proliferation and delays dendrite development. J Neurosci 32:13630-13638.

Yu AJ, Dayan P (2005) Uncertainty, neuromodulation, and attention. Neuron 46:681-692.

Yu JT, Tan L, Ou JR, Zhu JX, Liu K, Song JH, Sun YP (2008) Polymorphisms at the beta2-adrenergic receptor gene influence Alzheimer's disease susceptibility. Brain Res 1210:216-222.

Yu JT, Tan L, Song JH, Sun YP, Chen W, Miao D, Tian Y (2009) Interleukin-18 promoter polymorphisms and risk of late onset Alzheimer's disease. Brain Res 1253:169-175.

Yu WH, Cuervo AM, Kumar A, Peterhoff CM, Schmidt SD, Lee JH, Mohan PS, Mercken M, Farmery MR, Tjernberg LO, et al. (2005) Macroautophagy--a novel Beta-amyloid peptide-generating pathway activated in Alzheimer's disease. J Cell Biol 171:87-98.

Zaretsky MV, Alexander JM, Byrd W, Bawdon RE (2004) Transfer of inflammatory cytokines across the placenta. Obstet Gynecol 103:546-550.

Zigmond MJ, Abercrombie ED, Berger TW, Grace AA, Stricker EM (1990) Compensations after lesions of central dopaminergic neurons: some clinical and basic implications. Trends Neurosci 13:290-296.

Zorrilla EP (1997) Multiparous species present problems (and possibilities) to developmentalists. Dev Psychobiol 30:141-150.

Zuckerman L, Rehavi M, Nachman R, Weiner I (2003) Immune activation during pregnancy in rats leads to a postpubertal emergence of disrupted latent inhibition, dopaminergic hyperfunction, and altered limbic morphology in the offspring: a novel neurodevelopmental model of schizophrenia. Neuropsychopharmacology 28:1778-1789.

ABBREVIATIONS

Aβ	amyloid-β
ACh	acetylcholine
AD	Alzheimer's disease
AF	area fraction
AICD	APP intracellular domain
apoE	apolipoprotein E
ApoER2	Apolipoprotein receptor 2
APP	amyloid precursor protein
AUC	area under the curve
BBB	blood brain barrier
BSA	bovine serum albumin
CA1	cornu ammonis area 1
CA3	cornu ammonis area 3
CAm	corpora amylacea
ChAT	Choline acetyltransferase
COX2	cyclooxygenase
CD11b	part of the complement receptor 3 complex
CD45	lymphocyte common antigen
CD68	cluster of differentiation 68
CDK5	cyclin-dependent kinase 5
CNS	central nervous system
CSF	cerebrospinal fluid
CTF	C-terminal fragment
d	day
DAB	3,3-diaminobenzidine
DG	dentate gyrus
DSP-4	N-(2-chloroethyl)-N-ethyl-2-bromobenzylamine
EC	entorhinal cortex
EOAD	early-onset Alzheimer’s disease
FA	formic acid
FDG	Fluorodeoxyglucose

GABA	γ-aminobutyric acid
GD	gestational day
GFAP	glial fibrillary acidic protein
GL	granule layer (of the dentate gyrus)
GSK-3β	Glycogen synthase kinase 3β
GWAS	genome-wide association studies
h (rs)	hour (s)
Iba1	ionized calcium-binding adapter molecule 1
IgG	Immunoglobulin G
IHC	immunohistochemistry
IL	interleukin
IFN	interferon
IRF	interferon regulatory factor
i.p.	intraperitoneal
i.v.	intravenous
LC	locus coeruleus
LSD	least significant difference
DG (ML)	molecular layer (of the dentate gyrus)
LOAD	late-onset Alzheimer's disease
MAP2	microtubule-associated protein 2
MCI	mild cognitive impairment ("pre-stage" of AD)
MT	microtubule
N	NaCl
NA	noradrenaline, noradrenergic
NAT	NA transporter
NFT	neurofibrillary tangles
NR2	N-terminal cleaved Reelin fragment (180kDa)
NR6	C-terminal cleaved Reelin fragment (310 kDa)
OB	olfactory bulb
PBS	phosphate-buffered saline
P	PolyI:C
PD	Parkinson's disease
PET	positron emission tomography

PHF	paired helical filament
PolyI:C	polyriboinosinic-polyribocytidilic acid
pTau	phosphorylated Tau
REM	rapid eye movement
ROI	region of interest
SEM	standard error of the mean
SL	stratum lucidum
SLM	stratum lacunosum moleculare
SNP	single nucleotide polymorphism
SO	stratum oriens
SP	stratum pyramidale
SR	stratum radiatum
ssf	optical fractionator sampling fraction
SUV	standardized uptake value
S1	primary somatosensory cortex
TH	tyrosine hydroxylase
TLR	Toll-like receptor
TNF	tumor necrosis factor
VLDLR	very low density lipoprotein receptor
VOI	volume of interest
V1	primary visual cortex

CURRICULUM VITAE

PERSONAL DETAILS

Last name	Notter
First name	Tina
Middle name	Fabia
Address	Winterthurerstrasse 190, CH-8057 Zurich
Date of Birth	8th of July 1985
Nationality	Swiss

Education

Since 2011	**Ph.D. student** at the University of Zurich; International Program of Neuroscience (ZNZ); Supervision PD Dr. Irene Knuesel and Professor Dr. Jean-Marc Fritschy; Institute of Pharmacology and Toxicology, University of Zurich
2010 – 2011	**Degree: Master of Science UZH in Human Biology** University of Zurich, Switzerland; Institute of Pharmacology and Toxicology; Supervision PD Dr. Irene Knuesel Field of Master Thesis: Neuromorphology, Neurodegeneration; Average grade during studies: 6 (maximum 6; summa cum laude); Diploma thesis grade: 6 (maximum 6; summa cum laude)
2006 – 2009	**Degree: Bachelor of Science UZH in Biology** Faculty of Science; University of Zurich, Switzerland; Average grade during studies: 5.4 (maximum 6)
2002 – 2006	**Degree: Matura** (Major in: Biology and Chemistry); Kantonsschule Baden, Switzerland

PUBLICATIONS

Original Articles

Notter T, Panzanelli P, Pfister S, Mircsof D, Fritschy JM (2014). *A protocol for concurrent high-quality immunohistochemical and biochemical analyses in adult mouse central nervous system.* European Journal of Neuroscience 39(2):165-75.

Notter T and Knuesel I (2013) *Reelin immunoreactivity in neuritic varicosities in the human hippocampal formation of non-demented subjects and Alzheimer's disease patients.* Acta Neuropathologica Communication 1(1):27.

Krstic D, Pfister S, **Notter T**, Knuesel I (2013) *Decisive role of Reelin signaling during early stages of Alzheimer's disease.* J Neuroscience 246:108-16.

Krstic D, Madhusudan A, Doehner J, Vogel P, **Notter T**, Imhof C, Manalastas A, Hilfiker M, Pfister S, Schwerde1 C, Riether C, Meyer U, Knuesel I (2012) *Systemic immune challenges trigger and drive Alzheimer-like neuropathology in mice.* J Neuroinflammation 9:151.

Abstracts for Posters

Notter T, Fritschy JM, Knuesel I (2014). Chronic Inflammation Impairs the Regeneration Capacity of Locus Coeruleus (LC): Relevance for AD-like Pathogenesis. 9th Forum of European Neuroscience (FENS), Milano, Italy

Notter T, Knuesel I (2013). Reelin immunoreactivity in neuritic varicosities in the human hippocampus. Annual Meeting of the Society of Neuroscience (SfN), San Diego, CA, USA

Notter T, Knuesel I (2013). Reelin Deposits in the Human Brain – Relevance for Alzheimer's Disease. 11th International Alzheimer's Disease and Parkinson's Disease (AD/PD) Meeting, Florence, Italy

Notter T, Knuesel I (2013). Characterization of Reelin Deposits in the Human Postmortem Brain of Non-demented and AD Patients. Swiss Society for Neuroscience, SSN Annual Meeting, Geneva, Switzerland

Notter T, Knuesel I (2012). Characterization of Reelin deposits in the human postmortem brain of non-demented and AD patients. 8th Forum of European Neuroscience (FENS), Barcelona, Spain

APPENDIX

EJN European Journal of Neuroscience

European Journal of Neuroscience, Vol. 39, pp. 165–175, 2014 doi:10.1111/ejn.12447

TECHNICAL SPOTLIGHT
A protocol for concurrent high-quality immunohistochemical and biochemical analyses in adult mouse central nervous system

Tina Notter,[1,2,*] Patrizia Panzanelli,[3,*] Sandra Pfister,[1,2] Dennis Mircsof[1,2] and Jean-Marc Fritschy[1,2]
[1]Institute of Pharmacology and Toxicology, University of Zurich, CH-8057, Zurich, Switzerland
[2]Neuroscience Center Zurich, Federal Institute of Technology and University of Zurich, Zurich, Switzerland
[3]Department of Neuroscience Rita Levi Montalcini, University of Turin, Turin, Italy

Keywords: antibodies, immunofluorescence, RT-PCR, ultrastructure, Western blot

Abstract

Biochemical analysis of central nervous system proteins and nucleic acids requires fresh-tissue homogenates, whereas immunohistochemistry usually is performed in sections prepared from perfusion-fixed tissue. Post-mortem immersion-fixation is possible, but largely impairs morphological preservation and protein antigenicity. Here, we present a simple, fast and versatile protocol allowing concurrent biochemical and immunohistochemical analysis, including pre-embedding immunoelectron microscopy, using tissue from the same animal. The protocol includes a brief transcardiac perfusion with ice-cold, oxygenated and glucose-supplemented artificial cerebrospinal fluid to maintain brain tissue alive, prior to isolation of regions of interest, followed by homogenisation for biochemistry or immersion-fixation for immunohistochemistry. We provide several examples demonstrating that this protocol allows optimal biochemical and morphological analysis, characterised with optimal sensitivity and preservation of tissue structure, along with a reduction of artefacts typically seen in perfusion-fixed tissue. This protocol should find widespread applications for combining analytical methods in tissue from the same animal, thereby reducing the number of mice required for a given experiment.

Introduction

The structural complexity and heterogeneity of the nervous system requires sophisticated methods for morphological and biochemical analysis, with high selectivity and sensitivity. Immunohistochemistry allows the localisation of proteins (and other tissue constituents) with high spatial resolution; however, it is constrained by the need to protect tissue against degradation by chemical fixation. Aldehydes cross-link proteins, thereby immobilizing them in their native subcellular compartments but causing reduced antigenicity due to structural alterations. Biochemical analysis of proteins and nucleic acids typically is performed in extracts prepared from fresh tissue, following decapitation and rapid isolation of the region of interest. Among the methods for protein analysis, Western blotting allows the detection of proteins separated by gel electrophoresis. It lacks spatial resolution, but is highly sensitive and provides a semi-quantitative measure of protein abundance in samples of interest. It is therefore largely complementary to immunohistochemistry, and often performed with the same antibodies. However, both methods are not readily combined in the same brain due to different requirements for fixation.

Numerous experimental paradigms would greatly benefit from concurrent biochemical and immunohistochemical analysis of tissue samples from the same animals (e.g. left and right hemisphere of the brain), requiring a tissue preparation procedure compatible with all analytical methods to be used. While immunohistochemistry can be performed on fresh-frozen tissue (Fritschy *et al.*, 1998), for instance, it is suboptimal for cytoplasmic proteins, which are not immobilised in their native micro-environment and leak out of the cells because freezing damages the plasma membrane. Post-mortem immersion-fixation of tissue blocks is also suboptimal because of tissue degradation prior to fixation and possible differences in fixation strength between the surface and the depth of the tissue block. Under these conditions, the detection sensitivity of numerous neuronal proteins, notably in pre- and postsynaptic elements, is markedly reduced.

We have observed that immunohistochemistry performed in sections prepared from living tissue slices, briefly fixed by immersion in fixative solution, provides excellent detection sensitivity for synaptic proteins, and adequate tissue preservation (Schneider Gasser

Correspondence: Dr J.-M. Fritschy, [1]Institute of Pharmacology and Toxicology, as above.
E-mail: fritschy@pharma.uzh.ch

*T.N. and P.P. contributed equally to this study.

Received 15 October 2013, revised 6 November 2013, accepted 7 November 2013

et al., 2006), but the preparation of these sections is time-consuming and requires considerable experience with histology. Furthermore, following preparation with a sliding microtome, the tissue slices are no longer in optimal conditions for biochemical analysis. Here, we propose a much simplified variant of this approach, which is easy to apply, fast, and yields tissue that is optimal for both biochemistry and immunohistochemical analysis with high sensitivity and selectivity.

This protocol is based on perfusion of anesthetised mice with oxygenated artificial cerebrospinal fluid (ACSF) containing glucose in order to keep brain tissue alive until it is either frozen (for biochemistry) or immersion-fixed during a relatively short period of time (45 min – 6 h) for immunohistochemistry. The entire procedure is carried out at <4 °C to minimise excitotoxicity and enzymatic degradation of tissue constituents.

We provide proof-of-principle for the outstanding preservation of tissue structure and antigenicity compatible for both biochemistry and immunohistochemistry with antibodies against various types of proteins in adult and aged mouse brain. Further, we show that a large protein which undergoes complex proteolytic processing, such as Reelin, can be analysed satisfactorily by both methods. Finally, we demonstrate the superiority of this method over traditional fixation procedures for detection of low-abundance proteins, by describing with unprecedented sensitivity the cellular and subcellular distribution of the $GABA_A$ receptor ($GABA_AR$) α3 subunit in cerebellar cortex.

Materials and methods

Animals

Experiments were performed with adult C57Bl6/J mice purchased from Harlan Laboratories (Horst, the Netherlands) and bred in the animal facility of the Institute of Pharmacology and Toxicology, aged 6 weeks to 19 months. In addition, GAD67-GFP knock-in mice, expressing enhanced green fluorescent protein (eGFP) under the control of the GAD67 promoter to label the majority of GABAergic neurons (Tamamaki *et al.*, 2003), and GlyT2-GFP mice, carrying a BAC-transgene directing eGFP expression in glycinergic neurons (Zeilhofer *et al.*, 2005), were used to test the suitability of this protocol for detecting eGFP in tissue sections. Such experiments were also performed with mice injected in the dentate gyrus with a retrovirus encoding eGFP to label adult-born granule cells. The procedures followed are described in Duveau *et al.* (2011). All animal experiments were carried out in accordance with Swiss law on animal experimentation and approved by the cantonal veterinary office of Zurich.

Tissue preparation

ACSF perfusion and immersion-fixation

Mice were deeply anesthetised with sodium pentobarbital (Nembutal; 50 mg/kg; i.p.) and perfused intracardially with 15–20 mL ice-cold, oxygenated ACSF [containing (mM) NaCl 125, KCl 2.5, $CaCl_2$ 2.5, $MgCl_2$ 2, $NaHCO_3$ 26, NaH_2PO_4 1.25, glucose 25], pH 7.4, at a flow rate of 10–15 mL/min. Animals were decapitated on ice immediately thereafter, the brain extracted from the skull and cut either in two halves or in blocks containing the regions of interest for analysis (e.g. hippocampal formation, cerebellum). Tissue to be used for immunohistochemistry was plunged into ice-cold, freshly prepared fixative [4% paraformaldehyde dissolved in 0.15 M sodium phosphate buffer, pH 7.4 (for electron microscopy, 0.2% glutaraldehyde was added to the fixative)] and postfixed for the desired time (see Table 1), rinsed with phosphate-buffered saline (PBS), cryoprotected overnight in 30% sucrose in PBS, frozen with powdered dry ice and stored at –80 °C. Tissue for biochemistry and RNA analysis was immediately homogenised in buffer containing the appropriate enzyme inhibitors, frozen and stored in sealed containers at –80 °C.

Perfusion-fixation

Mice were anesthetised as above, and perfused transcardially with 20 mL PBS followed by 50–70 mL freshly prepared fixative (4% paraformaldehyde dissolved in 0.15 M sodium phosphate buffer, pH 7.4). The brain was extracted and postfixed for 3–4 h in the same fixative. It was then rinsed in PBS, cryoprotected in 30% sucrose in PBS and stored at –80 °C.

Fresh-frozen tissue preparation

Mice were decapitated and the brain immediately extracted on ice, cut in blocks containing the region of interest, homogenised frozen and stored in sealed containers at –80 °C.

Immunohistochemistry

Sections were cut from frozen blocks with a sliding microtome at a thickness of 40 μm and were collected free-floating in PBS. They were incubated under continuous agitation in primary solution [Tris buffer (pH 7.4) containing 0.2 Triton X-100, 2% normal serum and the primary antibodies of choice (see Table 1)] for 15–48 h at 4 °C, washed in Tris buffer and incubated for 30–60 min at room temperature in secondary antibodies coupled to biotin or to a fluorochrome. They were washed again, and either processed further for immunoperoxidase staining (Vectastain Elite kit; Vector Laboratories, Burlingham, CA, USA, following the manufacturer's instructions) or washed, mounted, coverslipped with Dako fluorescence mounting medium and stored in the dark. All antibodies tested have been extensively characterised for specificity (see Table 1). The comparison of staining patterns in perfusion-fixed and immersion-fixed tissue confirmed the specificity of the immunohistochemical reaction in the latter tissue.

Electron microscopy

After postfixation, tissue was rinsed several times in 0.1 M phosphate buffer, and cut into 100-μm-thick coronal slices with a vibrating microtome. Slices were processed for pre-embedding immunogold labeling as described (Fritschy *et al.*, 2006), using antibodies against gephyrin (Table 1) and secondary antibodies (Fab fragments) coupled to fluronanogold (1.4 nm), followed by gold intensification, using the manufacturer's kit (Nanoprobes Inc., Yaphank, NY, USA). Slices were then intensified with osmium tetroxide, dehydrated and flat-embedded in resin. Ultra-thin sections were examined with a Jeol JEM-1010 electron microscope and photographed with a digital camera.

Western blotting

Brain lysis and sample preparation, protein separation and immunoblotting of amyloid-precursor protein (APP) and Tau were performed as described (Krstic *et al.*, 2012a). Each lane was loaded with 90 μg protein and after blotting, the nitrocellulose membrane was directly blocked for 30 min with 1% solution of Western Blocking Reagent (Roche Applied Science, Indianapolis, US). Reelin Western blots were performed as described by Krstic *et al.* (2012b).

TABLE 1. List of antibodies tested

Target	Distributor	Description, catalog no.	Dilution	Application; immersion post-fixation time	Reference for specificity
APP	Millipore, Billerica, MA, USA	Mouse monoclonal, (A4), N-termimal, clone 22 C 11, MAB348	1 : 2000	WB	Krstic *et al.* (2012a)
CD68	AbD Serotec Ltd, Oxford, UK	Rat monoclonal, clone FA11, MCA1957GA	1 : 3000	IHC; 3–6 h	Ulvestad *et al.* (1994)
CD73	eBioscience Inc., San Diego, CA, USA	Rat monoclonal, IgG1; #16-0731	1 : 1000	IHC; 3 h	Pfister *et al.* (2012)
$GABA_AR$ α1 subunit	Fritschy lab	Guinea pig antiserum	1 : 10 000	IHC; 60–90 min	Fritschy *et al.* (2006)
$GABA_AR$ α2 subunit	Fritschy lab	Affinity purified guinea pig antiserum	1 : 1000	IHC; 60–90 min	Panzanelli *et al.* (2011)
$GABA_AR$ α3 subunit	Fritschy lab	Guinea pig antiserum	1 : 10 000	60–90 min	Studer *et al.* (2006)
Gephyrin	Synaptic Systems, Göttingen, Germany	Mouse monoclonal, clone 7a, 147021	1 : 1000 1 : 300	IHC;60–90 min IHC-EM; 2.5 h	Pfeiffer *et al.* (1984)
GFAP	Dako Schweiz AG, Baar, Switzerland	Rabbit antiserum, Z334	1 : 15 000	IHC; 3–6 h	Bignami *et al.* (1980)
GFP	Aves Labs Inc., Tigard, OR, USA	Chicken polyclonal, GFP-1020	1 : 10 000	IHC; 1–6 h	–
IP3R3	BD BioScience, Allschwil, Switzerland	Mouse monoclonal, IgG1, #610312	1 : 500	IHC; 3 h	Elsaesser *et al.* (2005)
Neuroligin-2	Peter Scheifele, University of Basel, Switzerland	Rabbit polyclonal	1 : 10 000	IHC; 60–90 min	Varoqueaux *et al.* (2004)
Parvalbumin	Swant, Bellinzona, Switzerland	Rabbit polyclonal, PV-28	1 : 10 000	IHC; 1–2 h	Chen *et al.* (2006)
Olfactory marker protein	Wako Chemicals, Richmond, VA, USA	Goat polyclonal, #544–10001	1 : 1500	IHC; 3 h	Baker *et al.* (1989)
PLC-β2	Santa Cruz Biotechnology, Dallas, TX, USA	Rabbit polyclonal, Q-15, #sc-206	1 : 500	IHC; 3 h	Elsaesser *et al.* (2005)
Reelin	Millipore	Mouse monoclonal, clone G10, MAB5364	1 : 1000	WB IHC; 1–3 h	Doehner *et al.* (2010)
Serotonin	Diasorin, Stillwater, MN, USA	Rabbit polyclonal, 20080	1 : 20 000	IHC; 1–3 h	Lidov *et al.* (1980)
Synapsin I	Molecular Probes, Eugene, OR, USA	Rabbit polyclonal, A-6442	1 : 1000	IHC; 3 h	Chi *et al.* (2001)
Tau	Thermo Fisher Scientific, Waltham, MA, USA	Mouse monoclonal, total Tau, clone Tau-5	1 : 4000	WB	Krstic *et al.* (2012a)
Tyrosine hydroxylase	Millipore	Rabbit polyclonal, AB152	1 : 3000	IHC; 1–3 h	Hökfelt *et al.* (1977)
VGAT	Synaptic Systems	Rabbit polyclonal, 131003	1 : 4000	IHC; 1–3 h	Dumoulin *et al.* (1999)

cDNA production and quantitative real-time PCR analysis

RNA was extracted using a GenElute Mammalian Total RNA Miniprep Kit (Sigma, St Louis, MO, USA) according to the manufacturer's instructions. Total RNA was quantified by absorbance spectroscopy and RNA integrity and quality was assessed by 1.0% agarose gel electrophoresis. Total RNA (1 μg) was transcribed to cDNA with SuperScript II (Invitrogen, Carlsbad, CA, USA) using random hexamer primers according to the manufacturer's instructions. For quantitative real-time PCR (qPCR), 20 ng of cDNA was used, and single transcript levels of genes were detected with the HOT FIREPol EvaGreen qPCR Mix (Solis BioDyne, Tartu, Estonia) and an AB7900 thermocycler. Primers used for detection of synaptic transcripts were as follows: β-actin, AGTGTGACGTTG ACAT CCGTA (sense), GCCAGAGCAGTAATCTCCTTCT (antisense); Gephn, GGCGACCGAGGGAATGAT (sense), CCACCCAACAAA GAAGGATCTT (antisense); Gabra1, GGTTGACCGTGAGAGCTG AA (sense), CTACAACCACTGAACGGGCT (antisense); Gabra2, CAGTGGCCCATAACATGACAAT (sense), GGACATTCGGCTT GGACTGT (antisense); CamKIIa, CCCCTTTCGCCTACATGTGA (sense), GGCTACAGTGGAGCGGCTTA (antisense). Data were analysed using the comparative C_T method (Schmittgen & Livak, 2008).

Microscopy and image processing

Images from immunoperoxidase staining were acquired with a color digital camera using either bright- or dark-field illumination (Zeiss Axioskop microscope, Jena, Germany) and assembled with Photoshop. A sharpening filter was applied to all images. Immunofluorescence images were captured by laser scanning confocal microscopy, using a 40 × lens, NA 1.4, 1024 × 1024 pixels (Zeiss LSM 700). Final illustrations were prepared from the maximal intensity projection of stacks of images spaced at 0.5 μm. Images were background-subtracted and filtered with a Gaussian filter, but no change in brightness and contrast was applied.

Results

Immunohistochemical detection of proteins from different classes

In this protocol, ACSF-perfused living tissue is fixed by immersion in aldehyde solution (4% paraformaldehyde dissolved in sodium phosphate buffer). We systematically tested the duration of fixation to determine the time required for entire blocks (hemi-brain cut sagitally along the midline or coronal block containing either the entire

hippocampal formation or the entire cerebellum) to be fixed while preserving optimal antigenicity of proteins of interest. For such tissue blocks (up to 2–3 cm^3), we saw no difference in staining quality/intensity at different tissue depths, suggesting that a homogeneous fixation was achieved even after a short fixation (60–90 min). However, fixation of entire brains was not appropriate, possibly because fixative did not penetrate through the ventricular system. No tissue block was fixed longer than 6 h, prior to washing and cryoprotection. Sections were then prepared with a freezing microtome and processed free-floating for immunohistochemistry, being transferred manually with a fine brush from bath to bath. The shortest fixation time allowing the maintenance of intact sections throughout the procedure was 45 min.

We tested a battery of antibodies against various classes of proteins, using tissue routinely fixed by transcardiac perfusion with a 4% paraformaldehyde solution as comparison. Using immunoperoxidase staining, all antibodies tested produced regional immunoreactivity patterns that were at least as well discernible, or better, in sections from immersion-fixed tissue as from perfusion-fixed tissue. Figure 1 depicts comparative immunostaining patterns of CD68, glial fibrillary acidic protein (GFAP), synapsin 1, tyrosine hydroxylase (TH) and serotonin (5-HT) in perfusion-fixed and immersion-fixed tissue. Optimal signal-to-noise ratio, as assessed qualitatively, was obtained in sections from blocks postfixed for 3 h, and this time-point was selected here for illustration. CD68 and GFAP were tested in sections prepared from adult (3 months; perfusion-fixed) and from old mice (19 months; immersion-fixed), but this difference in age had no influence on the quality of the staining.

As expected, staining of cytoskeletal proteins (e.g. GFAP) showed little influence from the duration of fixation, and a longer post-fixation either had no effect or led to a slight decrease in immunoreactivity (not shown). Abundant transmembrane proteins, such as CD68, myelin-basic protein or vesicular GABA transporter, likewise showed little dependence on post-fixation duration, and could be detected at high sensitivity in tissue fixed for 1–6 h. The same result was obtained with transmitter-synthesizing enzymes, for example

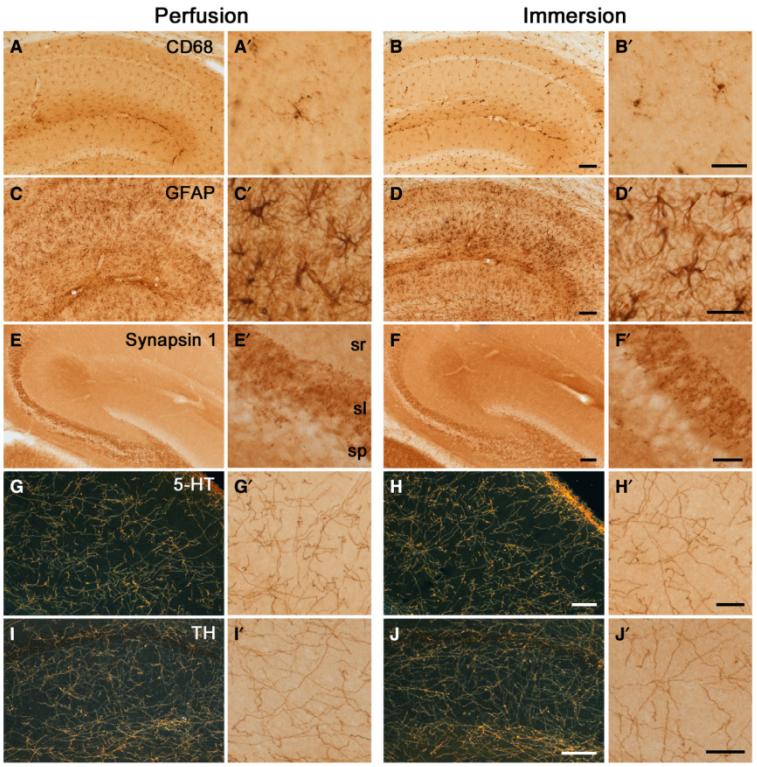

FIG. 1. Comparative immunoreactivity of a selected panel of antibodies in perfusion-fixed and immersion-fixed tissue. Immersion fixation was carried out immediately following perfusion with ACSF (see Methods). Images are from immunoperoxidase staining and photographed in bright-field (A–F; G′, H′, I′, J′) or dark-field (G, H, I, J) transmission microscopy. Each staining pattern is illustrated at two different magnifications to highlight the regional and cellular distribution of the markers investigated. The regions selected include the dorsal hippocampus (A–F; I–J) and the occipital cortex (G–H). (A, B) CD68 is a microglial cell marker, expressed at low levels in resting microglia; as seen in A′ and B′, both fixation methods are compatible with the staining of fine ramified processes of resting microglia. (C, D) GFAP is a marker of astrocytes, strongly expressed in the hippocampal formation, depicted in tissue from old mice (16 and 19 months) to illustrate that immersion-fixation is also suitable for tissue from aged mice. (E, F) Synapsin 1 is a presynaptic protein, strongly expressed in mossy fibers innervating CA3 pyramidal cells; the two fixation protocols provide similar results, with a clear distinction of these terminal in the stratum lucidum (sl) and a weaker staining in the stratum pyramidale (sp) and radiatum (sr). (G, H) Distribution of serotonergic (5-HT) axons in the neocortex, depicted in both bright- and dark-field to illustrate that a similar signal-to-noise ratio and morphology of axons is achieved with both fixation procedures. (I, J) Likewise, staining for tyrosine hydroxylase (TH) the rate-limiting enzyme for catecholamine synthesis in the hippocampus, detecting mainly noradrenergic axons, is qualitatively similar after perfusion-fixation and immersion-fixation. Scale bars: A–J, 100 μm; A′–J′, 25 μm.

TH, and with small molecules, such as 5-HT. A pretreatment of sections with pepsin to better expose fixation-sensitive epitopes yielded similar antigen-retrieving effects in immersion-fixed tissue and in perfusion-fixed tissue (not shown) and did not damage the tissue during handling of free-floating sections, indicating that such procedures are compatible with immersion-fixation of living tissue. In our protocol, there is no blocking step prior to incubation in primary antibodies, and endogenous peroxidase activity is not quenched with H_2O_2. These two steps were skipped, because they bring no improvement to the quality of immunoperoxidase staining in rodent tissue, when it is adequately fixed. Interanimal variability, reflecting the quality of perfusion, was low and comparable among perfusion-fixed and ACSF-perfused mice (not shown).

Immunofluorescence staining and imaging by confocal laser scanning microscopy was performed to assess subcellular distribution of neuronal markers, such as the calcium-binding protein parvalbumin (Fig. 2A) or the $GABA_AR$ α2 subunit (Fig. 2B and C), as well as eGFP in transgenic mice expressing GAD67-eGFP (Tamamaki *et al.*, 2003) (Fig. 2D and E) and in adult-born neurons labeled with a retrovirus encoding eGFP (Fig. 2F and G) (Duveau *et al.*, 2011). In perfusion-fixed tissue, immunostaining for parvalbumin is typically hampered by poor tissue penetration of the primary antibody. Tissue penetration was enhanced in immersion-fixed tissue (90 min) and, overall, the sensitivity of detection was increased compared with perfusion-fixed tissue (Fig. 2A and A′). With regard to $GABA_ARs$ (as well as other postsynaptic proteins), perfusion-fixation hampers their detection in postsynaptic densities, depending on the strength of fixation. The latter is determined by both concentration of aldehydes and duration of the fixation (perfusion-time, post-fixation or immersion of fresh tissue in fixative). The effect of time is illustrated in Fig. 2B and C, showing the staining pattern of the $GABA_AR$ α2 subunit in perfusion-fixed tissue with brief (2 h) and long (6 h) post-fixation, compared with immersion-fixed tissue (45 and 150 min). The marked differences in apparent distribution of the α2 subunit immunofluorescence among these four representative images underline the dependence of immunohistochemistry on tissue preparation procedures, and the enhanced sensitivity achieved in tissue briefly fixed by immersion in aldehyde solution.

Likewise, GFP immunofluorescence staining (superimposed to eGFP fluorescence) in immersion-fixed sections from GAD67-GFP mice yielded excellent structural preservation and a high signal-to-noise ratio, indicating that no leakage of GFP molecules occurred during tissue preparation (Fig. 2D and E). Finally, imaging eGFP-positive dendrites and axons in adult-born dentate gyrus granule cells likewise revealed very small structures, such as spine heads (Fig. 2F) and filopodia (Fig. 2G), even in tissue that was immersion-fixed for <2 h. Therefore, detection of eGFP-positive structures is feasible in weakly fixed tissue, compatible with the short post-fixation time needed to detect synaptic proteins (see below).

To determine whether this immersion-fixation is also applicable for epithelial-like tissues, which lose considerable antigenicity upon perfusion-fixation, we tested the ACSF perfusion protocol followed by 3 h of immersion-fixation on sections of the olfactory epithelium, decalcification in 5% EDTA for 7 days, cut with a cryostat and mounted on glass-slides prior to immunofluorescence staining. The markers selected for comparison with perfusion-fixation are olfactory marker protein (OMP) (Baker *et al.*, 1989) and three markers selective for microvillar cells, a specialised cell population expressing proteins of the PLCβ2/IP3R3 signaling cascade (Elsaesser *et al.*, 2005; Pfister *et al.*, 2012). As illustrated in Fig. 3A–D, a higher signal-to-noise ratio, due to increased sensitivity and epitope preservation, was obtained for these markers in the immersion-fixed tissue.

Finally, to determine the degree of ultrastructural preservation of immersion-fixed tissue, and its suitability for immunoelectron microscopy, we performed pre-embedding immunogold labeling for gephyrin in slices of the dorsal hippocampal formation, prepared from ACSF-perfused tissue blocks postfixed for 2.5 h, and examined the distribution of labeled profiles in relation to presynaptic terminals. The results show a good ultrastructural preservation of the tissue, notably membrane structures, allowing unambiguous recognition of pre- and postsynaptic density, synaptic vesicles, mitochondria, etc. (Fig. 3E), comparable with that seen after traditional tissue fixation (Panzanelli *et al.*, 2011). Gephyrin immunogold labeling was prominent in profiles forming symmetric synaptic contacts with axon terminals enriched in synaptic vesicles. This intense immunoreactivity points to excellent preservation of antigenicity owing to the brief post-fixation.

Gene expression analysis by qPCR analysis

We have assessed the suitability of the ACSF perfusion protocol for RNA purification compared with fresh-frozen tissue, and tested mRNA integrity by qPCR analysis. Experiments were performed in triplicate, using tissue from 2–3 mice per condition. Figure 3F illustrates that high-quality RNA can be purified from brain samples perfused with ACSF. Furthermore, the results demonstrate that RNA extracted from ACSF-perfused mice is compatible with qPCR analysis. By comparison with fresh brain samples, the expression level of four selected genes encoding synaptic proteins remained unaltered (Table 2), giving the opportunity to study brain morphology and gene expression in parallel.

Immunohistochemical and biochemical analysis of Reelin in the brain of adult mice

For proof-of-principle that optimal biochemical and immunohistochemical analyses can be performed using tissue blocks taken from the same brain following ACSF-perfusion, we performed Western blotting and immunohistochemistry with tissue from an ACSF-perfused mouse. Each method was compared with standard tissue preparations [fresh tissue for Western blotting and sections from perfusion-fixed brain (4% paraformaldehyde) for immunoperoxidase staining]. In Western blots, we investigated the expression of Tau, APP and Reelin in cerebral cortex and hippocampus. As illustrated in Fig. 4A–C, no difference in relative abundance of Tau, APP or Reelin was observed in fresh-frozen and ACSF-perfused tissue, and proteolytic fragments of Reelin were readily detected, with clear differences in abundance between cortex and hippocampus. In parallel, we stained for Reelin in the hippocampal formation in sections that were pretreated with pepsin, prior to incubation with primary antibodies (Doehner *et al.*, 2010). Immersion-fixation (3 h) of ACSF-perfused tissue allowed detection of Reelin immunoreactivity in hippocampal interneurons and neuropils with similar intensity and high signal-to-noise ratio as in perfusion-fixed tissue (Fig. 4D and E).

Cellular and subcellular distribution of the $GABA_A$ receptor α3 subunit in the cerebellum

We have shown previously that the detection of postsynaptic proteins of GABAergic synapses, in particular gephyrin and various $GABA_AR$ subunits, is markedly improved in weakly fixed tissue, in particular when derived from living brain slices (Schneider Gasser *et al.*, 2006). Under these conditions, postsynaptic localisation of these proteins becomes apparent as brightly stained puncta (clusters)

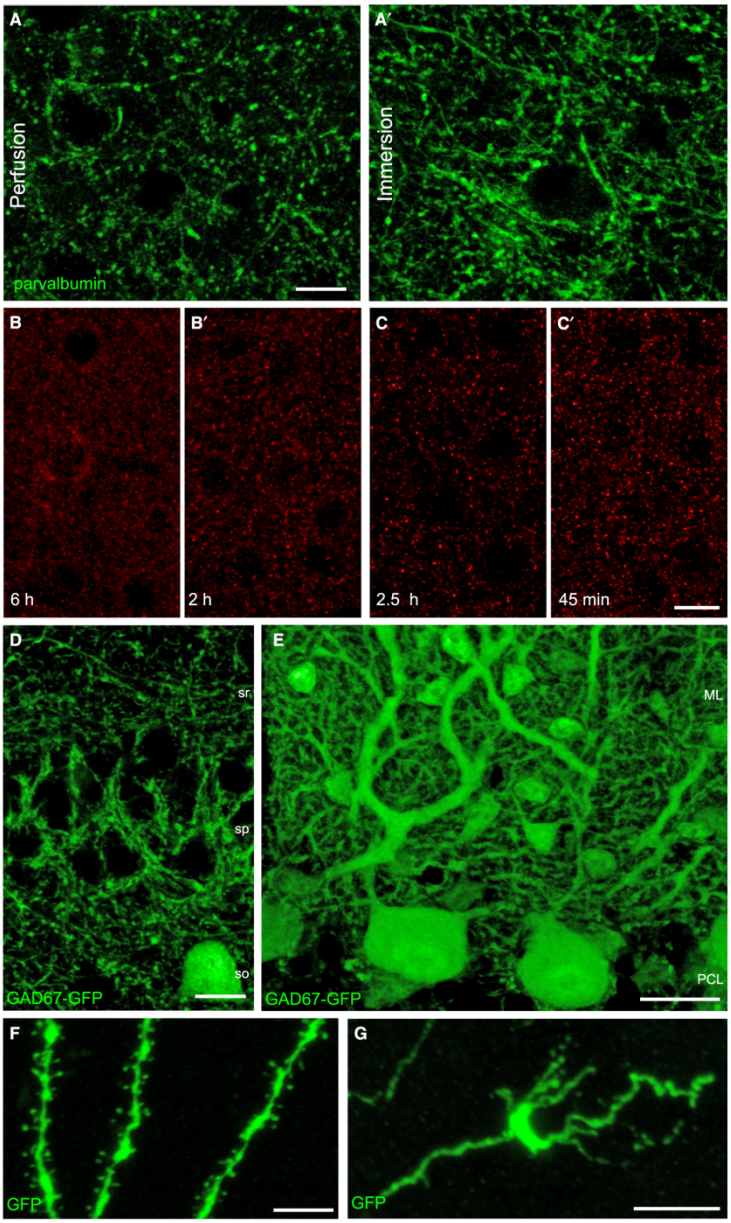

FIG. 2. Preservation of fine morphological structures and detection of postsynaptic proteins in immunofluorescence staining of immersion-fixed tissue. Images were captured by confocal laser scanning microscopy and depict maximal intensity projections of stacks of 3–10 images spaced by 0.5 μm. (A, A′) Comparative detection of parvalbumin-immunoreactivity in axon and axon terminals in layer III of somatosensory cortex in perfusion-fixed and immersion-fixed tissue. Note the stronger staining and higher density of immunoreactive structures in immersion-fixed tissue, primarily due to enhanced penetration of the primary antibody. (B, B′ and C, C′) Comparison of $GABA_AR$ α2 subunit immunofluorescence in perfusion-fixed (B) and immersion-fixed tissue (C), and effect of the duration of post-fixation as indicated on each panel; perfusion-fixation largely precludes detection of postsynaptic receptor clusters (which appear as bright aggregates) and the effect is dependent on the length of post-fixation; immersion-fixation allows improved detection of postsynaptic clusters, but their apparent density decreases after prolonged fixation. (D, E) Immunofluorescence for GFP in immersion-fixed sections from GAD67-GFP transgenic mice revealing, with high sensitivity and signal-to-noise ratio, the distribution of this marker in the hippocampus CA1 region (D) and cerebellum (E); in particular, note the high density of GABAergic terminals around CA1 pyramidal cells. (F, G) Immunofluorescence for GFP in sections of mice, injected 4 weeks previously, with a retrovirus encoding eGFP to label adult-born neurons in the dentate gyrus. F depicts the spiny dendrites of these neurons and G shows a mossy fiber terminal in the stratum lucidum of CA3. Both images reveal that fine dendritic and axonal structures can be detected with high resolution in immersion-fixed tissue. Scale bars: A–D, 20 μm; F and G, 5 μm.

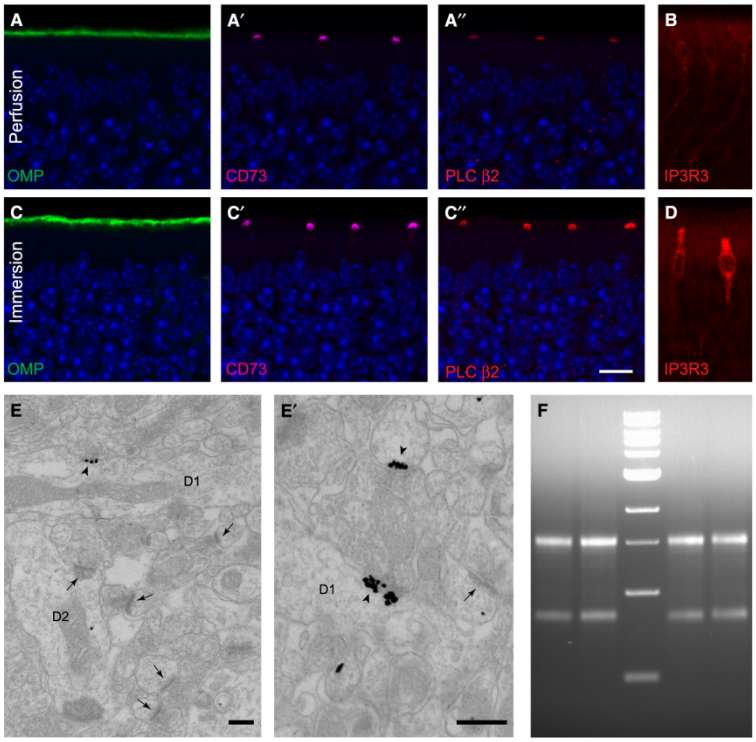

FIG. 3. Versatility of immersion-fixation and ACSF-perfusion for immunofluorescence analysis of olfactory epithelium, immunoelectron microscopy, and isolation of mRNA from brain tissue. (A–D) Comparative immunofluorescence staining for three markers of microvillar cells (CD73, PLCβ2, IP3R3), along with the olfactory marker protein (OMP) in the olfactory epithelium, as shown by triple immunofluorescence (A–A″; C–C″) in perfusion-fixed and immersion-fixed tissue (blue = nuclear dye, Dapi); B and D depict IP3R3-immunofluorescence in adjacent sections. Note the higher sensitivity and signal-to-noise ratio obtained in immersion-fixed tissue for all these markers. (E, E′) Pre-embedding staining for gephyrin using Fluoronanogold-conjugated antibodies and silver intensification in immersion-fixed hippocampal tissue. E depicts tissue ultrastructure, with a single gephyrin-positive GABAergic synapse on a dendrite (D1; arrowhead) and numerous unlabeled asymmetric, type 1, excitatory synapses on a dendrite (D2) and spines (arrows); E′ depicts the strong and selective staining of two postsynaptic densities of symmetric synapses (arrowheads) formed by a large terminal containing numerous presynaptic vesicles. Scale bars: A–D, 10 μm; E and E′, 100 nm. (F) Total RNA extracted from fresh (left) and ACSF-perfused (right) brain was fractioned in native 1% agarose gel and visualised by ethidium bromide. Approximately 500 ng of RNA was loaded in each lane. Intact 28S and 18S rRNA were observed in the absence of degraded molecules with lower molecular weight. The middle lane contains the 1-kb NEB DNA ladder.

TABLE 2. qPCR data

Gene	Fresh tissue	ACSF perfusion	Statistics
Gephn	100.0 ± 1.3	96.4 ± 5.1	$t_3 = 0.406$; $P = 0.712$
Gabra1	100.0 ± 5.5	98.5 ± 6.7	$t_3 = 0.21$; $P = 0.853$
Gabra2	100.0 ± 10.0	98.8 ± 4.3	$t_3 = 0.2$; $P = 0.855$
CamkIIa	100.0 ± 8.9	92.8 ± 4.4	$t_3 = 1.251$; $P = 0.299$

Values (mean ± SD) were normalised to β-actin mRNA and are calculated relative to fresh tissue.

apposed to GABAergic, vesicular GABA transporter (VGAT)-positive, axon terminals. To assess the sensitivity of immunofluorescence staining in sections briefly fixed by immersion after ACSF fixation, we investigated the distribution of the $GABA_AR$ α1 and α3 subunits in relation to neuroligin 2, gephyrin and VGAT in the cerebellum of adult mice. In addition, to determine which neuron type expresses the α3 subunit, we analysed sections from GlyT2-GFP mice (Zeilhofer *et al.*, 2005), in which a large subpopulation of Golgi cells are distinctly eGFP-positive.

The results, illustrated in Fig. 5, revealed that upon brief immersion-fixation (60–90 min), postsynaptic GABAergic markers exhibit a bright, punctate staining, with high signal-to-noise ratio, thereby precisely revealing the distribution of presumptive GABAergic synapses on the cell body of Purkinje cells and in the molecular layer. While the $GABA_AR$ α1 subunit was colocalised extensively with neuroligin 2 (Fig. 5A and A′), the α3 subunit was present in only a small subset of GABAergic synapses located on dendrites in the molecular layer (Fig. 5B). Co-staining with gephyrin confirmed the postsynaptic localisation of the α3 subunit (Fig. 5C and C′), whereas parvalbumin double-labeling a marker of both, Purkinje cells and molecular layer interneurons (Celio, 1990) confirmed that the α3 subunit-immunoreactivity was not located in parvalbumin-positive neurons (Fig. 5D). Examination of sections from GlyT2-GFP mice revealed that the α3 subunit clusters were present on the soma and dendrites of glycinergic Golgi cells (Fig. 5E and E′; Simat *et al.*, 2007), and their postsynaptic localisation was confirmed by staining with VGAT (Fig. 5F and F′).

As noted above for Fig. 2B and C, a longer immersion-fixation time (up to 3 h) was deleterious for the detection of synaptic

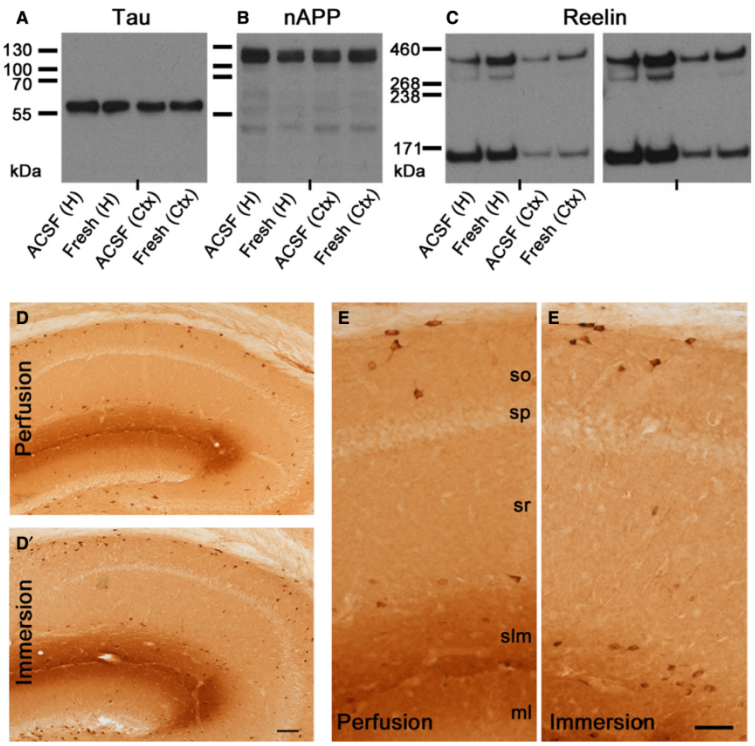

FIG. 4. Concurrent Western blot analysis and immunoperoxidase staining in tissue from the same mouse perfused with ACSF. (A–C) Comparison of Western blots for Tau, APP and Reelin performed with hippocampal and crude cortical tissue homogenates prepared from decapitated mice (fresh) and from ACSF-perfused mice. Bands of comparable intensity were obtained in all cases; there was no evidence of tissue degradation in ACSF-perfused tissue, and proteolytic fragments [N-terminal cleavage (160 kDa), C-terminal cleavage (380 kDa)] of Reelin were readily detectable. (D, E) Immunoperoxidase staining for Reelin in tissue from the same ACSF-perfused mouse as that used for Western blotting, and compared with a perfusion-fixed mouse, depicted at two different magnifications. The typical laminar distribution of Reelin immunoreactivity in the neuropil and in a subset of interneurons was evident in both cases. Scale bars: D and D′, 100 μm; E and E′, 25 μm.

proteins, albeit the effects were variable among the antibodies tested. Presynaptic markers, such as VGAT and VGluT1, showed little influence of fixation time, whereas postsynaptic proteins, such as neuroligin 2 and gephyrin, were highly sensitive to the duration of fixation. Therefore, in our hands, immersion-fixation for 60–90 min represented an optimal duration for good quality staining and preservation of sections after the staining procedure.

Taken together, these results underline the remarkable sensitivity of immunofluorescence staining and morphological preservation obtained in sections from ACSF-perfused mice, immersion-fixed for a short duration. Until now, the subcellular distribution of postsynaptic α3 subunit clusters could not be resolved satisfactorily in the cerebellum (Fritschy & Panzanelli, 2006), whereas here it is unambiguously demonstrated in a subpopulation of Golgi cells.

Discussion

Adequate tissue preparation is obviously a *sine qua non* prerequisite for biochemical and morphological analysis of cellular constituents, in particular in the central nervous system, where tissue heterogeneity is very high. It is particularly important to prevent activation of enzymes that modify proteins, lipids and nucleic acids, due to hypoxia and cellular stress. Likewise, preservation of membranes is essential to prevent dispersion of soluble proteins out of cells and organelles. Hypoxia can also dramatically increase exocytosis, in particular from presynaptic transmitter vesicles. For biochemical and neurochemical analyses, rapid dissection of the tissue of interest and cooling on ice, followed by homogenisation in the presence of enzyme inhibitors, is usually sufficient for yielding high-quality protein and nucleic acid preparations. For immunohistochemistry, chemical fixation, most commonly with aldehydes, is necessary to ensure preservation of histological sections throughout the staining procedure. We, and others, have shown extensively that chemical fixation markedly reduces antigenicity and/or accessibility of synaptic proteins, thereby impairing or preventing their characterisation by immunohistochemistry (Nusser *et al.*, 1995; Fritschy *et al.*, 1998; Watanabe *et al.*, 1998; Sassoè-Pognetto *et al.*, 2000; Lorincz & Nusser, 2008). Several antigen retrieval procedures have been proposed to circumvent these limitations. In particular, minimizing exposure to fixatives is a key factor for detecting synaptic proteins in brain tissue. Thus, using perfusion-fixation with low concentration of paraformaldehyde (1–2%) and skipping post-fixation also allows highly sensitive detection of pre- and postsynaptic proteins (Eyre *et al.*, 2012); alternatively, we have shown that immersion-fixation of living tissue slices allows detection of both transmembrane synaptic proteins and soluble neuronal markers, in particular eGFP (Schneider Gasser *et al.*, 2006, 2007).

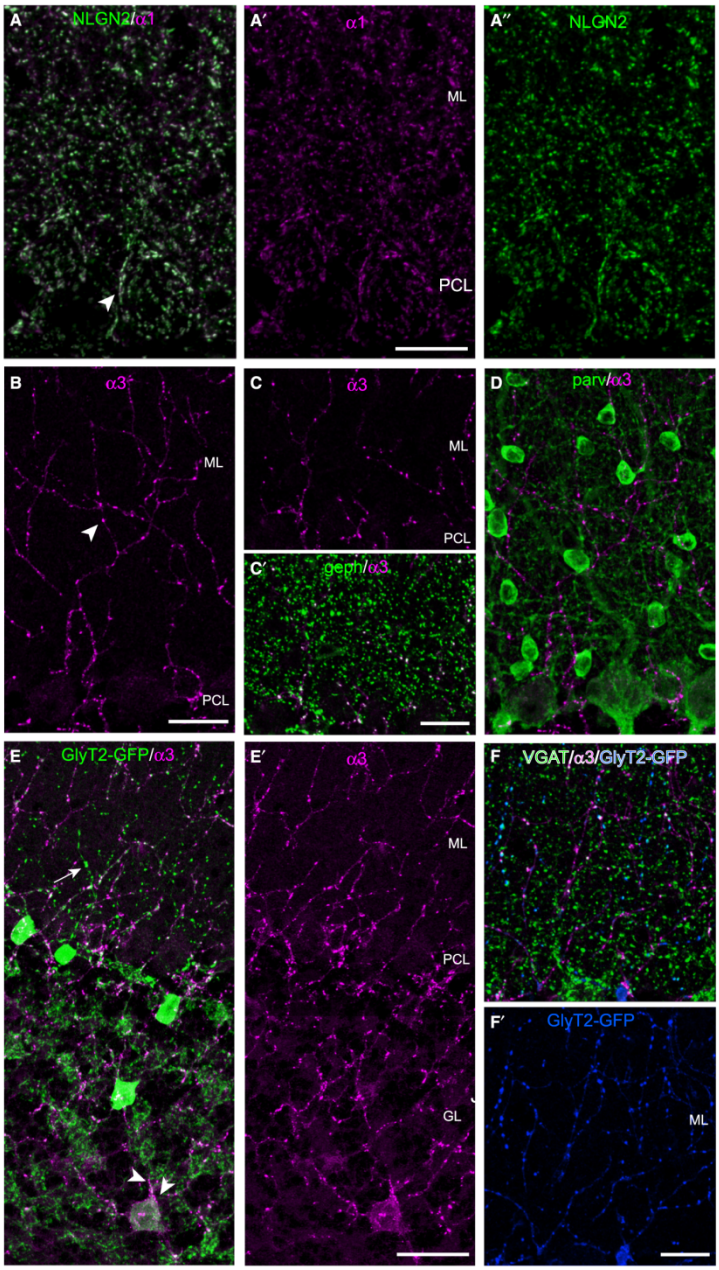

FIG. 5. Detection of synaptic markers and distribution of the $GABA_AR$ α3 subunit in cerebellum, as visualised by immunofluorescence in immersion-fixed tissue. (A, A″) Double staining for the α1 subunit (magenta) and neuroligin 2 (NLGN2, green), depicting the clustered distribution and extensive colocalisation of both markers at presumptive postsynaptic sites in the molecular layer (ML) and on Purkinje cell bodies (arrowhead in A). (B) Distribution of the α3 subunit-immunoreactivity in the molecular layer, forming strings of bright clusters on weakly stained processes (arrowhead). (C, C′) Colocalisation of α3 subunit-positive clusters (magenta) with gephyrin clusters (green), confirming their postsynaptic localisation (white); note the much higher density of gephyrin clusters, indicating the selective localisation of α3-$GABA_AR$ in a small subset of synapses. (D) Double staining for the α3 subunit (magenta) and parvalbumin (green), a marker of Purkinje cells and molecular layer interneurons; the two markers do not appear to be colocalised, indicating that the α3 subunit is present in a different cell type. (E, E′) Double staining for the α3 subunit (magenta) and GlyT2-eGFP (green) in the granule cell layer (GL) and molecular layer, demonstrating the presence of α3 subunit clusters on the soma (arrowheads) and dendrites of eGFP-positive Golgi cells; processes positive for eGFP-only in the molecular layer (arrow) represent the axons of Lugaro and globular cells. (F, F′) Triple staining for VGAT (green), the α3 subunit (magenta) and GlyT2-eGFP (blue), confirming the postsynaptic localisation of α3 subunit clusters in the molecular layer. Scale bars: 20 µm.

European Journal of Neuroscience, **39**, 165–175

Here, we show that it is possible, via a brief perfusion with ice-cold, oxygenated and glucose-supplemented ACSF, to keep brain tissue alive and in optimal conditions, suitable for both homogenisation for biochemical analysis and immersion-fixation for immunohistochemistry. The possibility to combine multiple analytical methods (qPCR, Western blotting, immunofluorescence/immunoperoxidase staining, immunoelectron microscopy) on brain tissue from the same animal represents a major advantage for correlative studies. In addition, it allows a marked reduction of the number of animals needed for studies requiring a combination of analytical methods. Although we did not attempt here to perform electrophysiology on slices prepared from ACSF-perfused mice, it is a routine procedure, in particular for preparing tissue for patch-clamp recordings. Therefore, we expect that this protocol is also suitable for concurrent (or sequential) functional and immunohistochemical/biochemical analysis of tissue from the same animal. A further benefit of immersion-fixation over perfusion-fixation is to minimise human exposure to aldehyde vapors, especially in laboratories devoid of a ventilated cabinet.

A key feature of this protocol is to ensure optimal tissue preservation, allowing the combination of methods without compromising the quality or sensitivity of each method taken separately. On the contrary, we demonstrate that immunofluorescence staining is rather improved when compared with perfusion-fixation, and even when compared with staining in sections prepared from living slices. There is a gain in sensitivity and signal-to-noise ratio, most probably explained by the strong reduction of fixation artifacts and loss of antigenicity due to protein dispersion through damaged membranes. We have also observed enhanced tissue penetration of antibodies (Fig. 2A and A′), yielding strong signals at a depth of 10–15 μm rather than 2–3 μm following overnight incubation with primary antibodies. A further advantage of the current protocol is that tissue is fixed immediately after dissection of blocks of interest, thereby minimizing remodeling of plastic structures, such as dendritic spines and synaptic contacts. In contrast, preparation of slices and their stabilisation in warm ACSF, as described by Schneider Gasser *et al.* (2006), requires more than 1 h, and this delay is highly propitious to changes in synaptic connectivity.

The duration of the immersion-fixation is a critical factor of this protocol. We were initially surprised to note that 3 h is sufficient for obtaining a degree of fixation of a mouse hemi-brain (or a tissue block containing the entire hippocampal formation or cerebellum/brainstem) comparable to that obtained by perfusion-fixation, based on tissue rigidity. Under these conditions, the detection of synaptic proteins, not surprisingly, was not optimal. Likewise, application of secondary anti-mouse IgGs to detect monoclonal primary antibodies yielded non-specific labeling of brain blood vessels. Reducing the duration of immersion-fixation to 1 h was sufficient to obtain sections that were fragile, but remained largely intact during the staining procedure. In this tissue, the detection of synaptic proteins was markedly improved, reaching a degree of sensitivity not yet observed in our laboratory, and the non-specific staining caused by mouse IgG was completely abolished. These observations underline the critical role of fixation for immunohistochemistry and indicate that most non-specific staining, which often limits the power of this technique, is due to hyper-fixation and poor tissue preservation.

In conclusion, besides opportunities afforded by novel tissue embedding techniques, such as the 'CLARITY' (Chung & Deisseroth, 2013), for multimodal imaging analyses, ACSF perfusion provides a fast, simple and versatile protocol for tissue preparation compatible with mRNA quantification, protein biochemistry and high-resolution immunohistochemistry.

Acknowledgements

This study was supported by the Swiss National Science Foundation (grant Nr. 31003A_130495 to J.M.F.) and the 'Forschungskredit' of the University of Zurich (fellowship to T.N.). We thank Prof. Peter Scheiffele (University of Basel) for a kind gift of antibodies to neuroligin 2, and are grateful to all lab members for discussions, technical advice and providing samples for analysis.

Abbreviations

ACSF, artificial cerebrospinal fluid; APP, amyloid-precursor protein; EGFP, enhanced green fluorescent protein; GFAP, glial fibrillary acidic protein; 5-HT, serotonin; OMP, olfactory marker protein; QPCR, quantitative real-time PCR; TH, tyrosine hydroxylase; VGAT, vesicular GABA transporter.

References

Baker, H., Grillo, M. & Margolis, F.L. (1989) Biochemical and immunocytochemical characterization of olfactory marker protein in the rodent central nervous system. *J. Comp. Neurol.*, **285**, 246–261.

Bignami, A., Dahl, D. & Rueger, D.C. (1980) Glial fibrillary acidic protein (GFA) in normal neural cells and in pathological conditions. *Adv. Cell. Neurobiol.*, **1**, 285–310.

Celio, M.R. (1990) Calbindin D-28k and parvalbumin in the rat nervous system. *Neuroscience*, **35**, 375–475.

Chen, G., Racay, P., Bichet, S., Celio, M.R., Eggli, P. & Schwaller, B. (2006) Deficiency in parvalbumin, but not in calbindin D-28k upregulates mitochondrial volume and decreases smooth endoplasmic reticulum surface selectively in a peripheral, subplasmalemmal region in the soma of Purkinje cells. *Neuroscience*, **142**, 97–105.

Chi, P., Greengard, P. & Ryan, T.A. (2001) Synapsin dispersion and reclustering during synaptic activity. *Nat. Neurosci.*, **4**, 1187–1193.

Chung, K. & Deisseroth, K. (2013) CLARITY for mapping the nervous system. *Nat. Methods*, **10**, 508–513.

Doehner, J., Madhusudan, A., Konietzko, U., Fritschy, J.M. & Knuesel, I. (2010) Co-localization of Reelin and proteolytic APP fragments in hippocampal plaques in aged wild type mice. *J. Alzheimers Dis.*, **19**, 1339–1357.

Dumoulin, A., Rostaing, P., Bedet, C., Lévi, S., Isambert, M.F., Henry, J.P., Triller, A. & Gasnier, B. (1999) Presence of the vesicular inhibitory amino acid transporter in GABAergic and glycinergic synaptic terminal boutons. *J. Cell Sci.*, **112**, 811–823.

Duveau, V., Laustela, S., Barth, L., Gianolini, F., Vogt, K.E., Keist, R., Chandra, D., Homanics, G.E., Rudolph, U. & Fritschy, J.M. (2011) Spatiotemporal specificity of $GABA_A$ receptor-mediated regulation of adult hippocampal neurogenesis. *Eur. J. Neurosci.*, **34**, 362–373.

Elsaesser, R., Montani, G., Tirindelli, R. & Paysan, J. (2005) Phosphatidylinositide signalling proteins in a novel class of sensory cells in the mammalian olfactory epithelium. *Eur. J. Neurosci.*, **21**, 2692–2700.

Eyre, M., Renzi, M., Farrant, M. & Nusser, Z. (2012) Setting the time course of inhibitory synaptic currents by mixing multiple GABA(A) receptor α subunit isoforms. *J. Neurosci.*, **32**, 5853–5867.

Fritschy, J.M. & Panzanelli, P. (2006) Molecular and synaptic organization of $GABA_A$ receptors in the cerebellum: effects of targeted subunit gene deletions. *Cerebellum*, **5**, 275–285.

Fritschy, J.M., Weinmann, O., Wenzel, A. & Benke, D. (1998) Synapse-specific localization of NMDA and GABA(A) receptor subunits revealed by antigen-retrieval immunohistochemistry. *J. Comp. Neurol.*, **390**, 194–210.

Fritschy, J.M., Panzanelli, P., Kralic, J.E., Vogt, K.E. & Sassoè-Pognetto, M. (2006) Differential dependence of axo-dendritic and axo-somatic GABAergic synapses on GABAA receptors containing the α1 subunit in Purkinje cells. *J. Neurosci.*, **26**, 3245–3255.

Hökfelt, T., Johansson, O., Fuxe, K., Goldstein, M. & Park, D. (1977) Immunohistochemical studies on the localization and distribution of monoamine neuron systems in the rat brain II. Tyrosine hydroxylase in the telencephalon. *Med. Biol.*, **55**, 21–40.

Krstic, D., Madhusudan, A., Doehner, J., Vogel, P., Notter, T., Imhof, C., Manalastas, A., Hilfiker, M., Pfister, S., Schwerdel, C., Riether, C., Meyer, U. & Knuesel, I. (2012a) Systemic immune challenges trigger and drive Alzheimer-like neuropathology in mice. *J. Neuroinflamm.*, **9**, 151.

Krstic, D., Rodriguez, M. & Knuesel, I. (2012b) Regulated proteolytic processing of Reelin through interplay of tissue plasminogen activator (tPA), ADAMTS-4, ADAMTS-5, and their modulators. *PLoS One*, **7**, e47793.

Lidov, H.G., Grzanna, R. & Molliver, M.E. (1980) The serotonin innervation of the cerebral cortex in the rat – an immunohistochemical analysis. *Neuroscience*, **5**, 207–227.

Lorincz, A. & Nusser, Z. (2008) Specificity of immunoreactions: the importance of testing specificity in each method. *J. Neurosci.*, **28**, 9083–9086.

Nusser, Z., Roberts, J.D., Baude, A., Richards, J.G. & Somogyi, P. (1995) Relative densities of synaptic and extrasynaptic GABAA receptors on cerebellar granule cells as determined by a quantitative immunogold method. *J. Neurosci.*, **15**, 2948–2960.

Panzanelli, P., Gunn, B.G., Schlatter, M.C., Benke, D., Tyagarajan, S.K., Scheiffele, P., Belelli, D., Lambert, J.J., Rudolph, U. & Fritschy, J.M. (2011) Distinct mechanisms regulate $GABA_A$ receptor and gephyrin clustering at perisomatic and axo-axonic synapses on CA1 pyramidal cells. *J. Physiol.*, **589**, 4959–4980.

Pfeiffer, F., Simler, R., Grenningloh, G. & Betz, H. (1984) Monoclonal antibodies and peptide mapping reveal structural similarities between the subunits of the glycine receptor of rat spinal cord. *Proc. Natl. Acad. Sci. USA*, **81**, 7224–7227.

Pfister, S., Dietrich, M., Sidler, C., Fritschy, J., Knuesel, I. & Elsaesser, R. (2012) Characterization and turnover of CD73/IP(3)R3-positive microvillar cells in the adult mouse olfactory epithelium. *Chem. Senses*, **37**, 859–868.

Sassoè-Pognetto, M., Panzanelli, P., Sieghart, W. & Fritschy, J.M. (2000) Co-localization of multiple GABA(A) receptor subtypes with gephyrin at postsynaptic sites. *J. Comp. Neurol.*, **420**, 481–498.

Schmittgen, T. & Livak, K. (2008) Analyzing real-time PCR data by the comparative CT method. *Nat. Protoc.*, **8**, 1101–1108.

Schneider Gasser, E.M., Straub, C.J., Panzanelli, P., Weinmann, O., Sassoè-Pognetto, M. & Fritschy, J.M. (2006) Immunofluorescence in brain sections: simultaneous detection of presynaptic and postsynaptic proteins in identified neurons. *Nat. Protoc.*, **1**, 1887–1897.

Schneider Gasser, E.M., Duveau, V., Prenosil, G.A. & Fritschy, J.M. (2007) Reorganization of GABAergic circuits maintains GABAA receptor-mediated transmission onto CA1 interneurons in α1-subunit-null mice. *Eur. J. Neurosci.*, **25**, 3287–3304.

Simat, M., Parpan, F. & Fritschy, J.M. (2007) Heterogeneity of glycinergic and GABAergic interneurons in the granule cell layer of mouse cerebellum. *J. Comp. Neurol.*, **500**, 71–83.

Studer, R., von Boehmer, L., Haenggi, T., Schweizer, C., Benke, D., Rudolph, U. & Fritschy, J.M. (2006) Alteration of GABAergic synapses and gephyrin clusters in the thalamic reticular nucleus of $GABA_A$ receptor α3 subunit-null mice. *Eur. J. Neurosci.*, **24**, 1307–1315.

Tamamaki, N., Yanagawa, Y., Tomioka, R., Miyazaki, J., Obata, K. & Kaneko, T. (2003) Green fluorescent protein expression and colocalization with calretinin, parvalbumin, and somatostatin in the GAD67-GFP knock-in mouse. *J. Comp. Neurol.*, **467**, 60–79.

Ulvestad, E., Williams, K., Bjerkvig, R., Tiekotter, K., Antel, J. & Matre, R. (1994) Human microglial cells have phenotypic and functional characteristics in common with both macrophages and dendritic antigen-presenting cells. *J. Leukocyte Biol.*, **56**, 732–740.

Varoqueaux, F., Jamain, S. & Brose, N. (2004) Neuroligin 2 is exclusively localized to inhibitory synapses. *Eur. J. Cell Biol.*, **83**, 449–456.

Watanabe, M., Fukaya, M., Sakimura, K., Manabe, T., Mishina, M. & Inoue, Y. (1998) Selective scarcity of NMDA receptor channel subunits in the stratum lucidum (mossy fibre-recipient layer) of the mouse hippocampal CA3 subfield. *Eur. J. Neurosci.*, **10**, 478–487.

Zeilhofer, H.R., Studler, B., Arabadzisz, D., Schweizer, C., Ahmadi, S., Layh, B., Bösl, M.R. & Fritschy, J.M. (2005) Glycinergic neurons expressing enhanced green fluorescent protein in bacterial artificial chromosome transgenic mice. *J. Comp. Neurol.*, **482**, 123–141.

University of Zurich[UZH]

Institute of Pharmacology and Toxicology

Declaration of originality

The signed declaration of originality is a component of every Master's thesis, PhD thesis and any other degree paper undertaken during the course of studies, including the respective electronic versions.

Lecturers may also require a declaration of originality for other written papers compiled for their courses.

I hereby confirm that I am the sole author of the written work here enclosed and that I have compiled it in my own words. Parts excepted are corrections of form and content by the supervisor.

Title of work (in block letters):

EVALUATION OF THREE RISK FACTORS FOR SPORADIC ALZHEIMER'S DISEASE IN HUMAN AND IN IMMUNE-CHALLENGED WILD TYPE MICE

Authored by (in block letters):

For papers written by groups the names of all authors are required.

Name(s):	First name(s):
NOTTER	TINA

With my signature I confirm that

- I have committed none of the forms of plagiarism described in the information sheet issued on 30 April 2007 by the Teaching Committee of the University of Zurich (http://www.lehre.uzh.ch/plagiate/20110314_LK_Plagiarism.pdf)
- I have documented all methods, data and processes truthfully.
- I have not manipulated any data.
- I have mentioned all persons who were significant facilitators of the work.

I am aware that the work may be screened electronically for plagiarism.

Place, date	Signature(s)
ZURICH, 6.3.2015	

For papers written by groups the names of all authors are required. Their signatures collectively guarantee the entire content of the written paper.

Adapted from the Declaration of originality of the ETH Zürich